THE MARINE GEOLOGY OF WALKER BAY, OFF HERMANUS, SW CAPE, SOUTH AFRICA

by

Louis Lenhoff

Thesis presented in fulfillment of the requirements for the degree of Master of Science in Geology at the University of Cape Town.

1995

ABSTRACT

The seafloor geology of Walker Bay on the southern Cape coastline is described by making use of geophysical information obtained over a period of 4 years, between 1986 and 1990. The data include side-scan sonar images, seismic profiles, seabed samples and observations by a Remotely Operated underwater Vehicle (ROV).

Four sonograph facies were identified, based on their distinctly different reflectivity patterns. Using the seabed samples and R.O.V. observations, the physical characteristics of these facies are determined and presented in map format.

Facies 1 consists of Bokkeveld Group rock outcrops with relatively high relief, occupying approximately 45 percent of the study area. Facies 2 represents similar outcrops but with low relief and partially covered by a thin veneer of unconsolidated sediment, including localized occurrences of loose cobbles and boulders. Facies 3 and 4 relate to sediment-covered areas displaying different bedform types. Facies 3 is dominated by well-defined patches of megarippled gravelly sand, whereas Facies 4 consists of small-scale rippled sand. The characteristics of the Facies 3 megarippled patches are discussed in detail and their relationships with the local wave pattern and nearby Facies 1 and 2 rock outcrops are investigated.

ACKNOWLEDGEMENTS

I wish to thank the management of the Division of Earth, Marine and Atmospheric Science and Technology (EMATEK) in Stellenbosch for their financial support and approval of study leave to complete this project. Their commitment to expertise enhancement and career development makes me proud to be associated with the organization.

I thank my colleague, Mr C (Kriek) Roux and the rest of the EMATEK Survey Team for their tireless assistance on the numerous field excursions, often under difficult circumstances. I also appreciate the consistent support of all my other colleagues at EMATEK, who never hesitated to make time available for discussions and suggestions.

Mrs Juanita van Heerden and Mr Gregory Davids deserve thanks for typing the manuscript and draughting assistance, respectively. A special thank you to Monique Knoetze for all her assistance in the production of the colour prints accompanying this thesis.

Finally, I sincerely thank my supervisor, Dr John Rogers, for all his assistance, his patience and his personal interest in the project.

CONTENTS

LIST OF FIGURES

LIST OF TABLES

1. INTRODUCTION

In 1985 the Coastal Processes Committee of the South African National Committee for Oceanographic Research (SANCOR) identified Walker Bay, off Hermanus in the South-western Cape, as a regional site for coastal-process research in the Western Cape. (Figure 1). This implied that physical and biological coastal research would be funded and encouraged at the site. The then Sediment Dynamics Division of the Council for Scientific and Industrial Research (CSIR) consequently embarked on a research programme to obtain a better understanding of the fundamentals of nearshore wave, current and sediment movement and the interactions between them. This would allow the division to develop better predictive techniques which could be used to predict nearshore processes and thus to assist in the design of nearshore structures (Swart, 1986).

To date, a number of major field experiments have been carried out by the Sediment Dynamics Division, during which routine measurements were made at selected stations on the beach and in the surf zone. These included beach profiling, current and suspended-sediment measurements in the water column, wave characteristics and aeolian sand transport.

As indicated above, all these measurements were limited to the beach and the inshore area only. In order to broaden the foundation for future process/response research in the area, the Marine Geoscience Division initiated a study of the greater Walker Bay seafloor characteristics, which would contribute largely to the understanding of the complex interactions between modern-day coastal processes and the driving mechanisms behind them. This report contains the result of seafloor investigations conducted over a period of 4 years, using seismic profiling, sidescan sonar, underwater photography and seabed sampling.

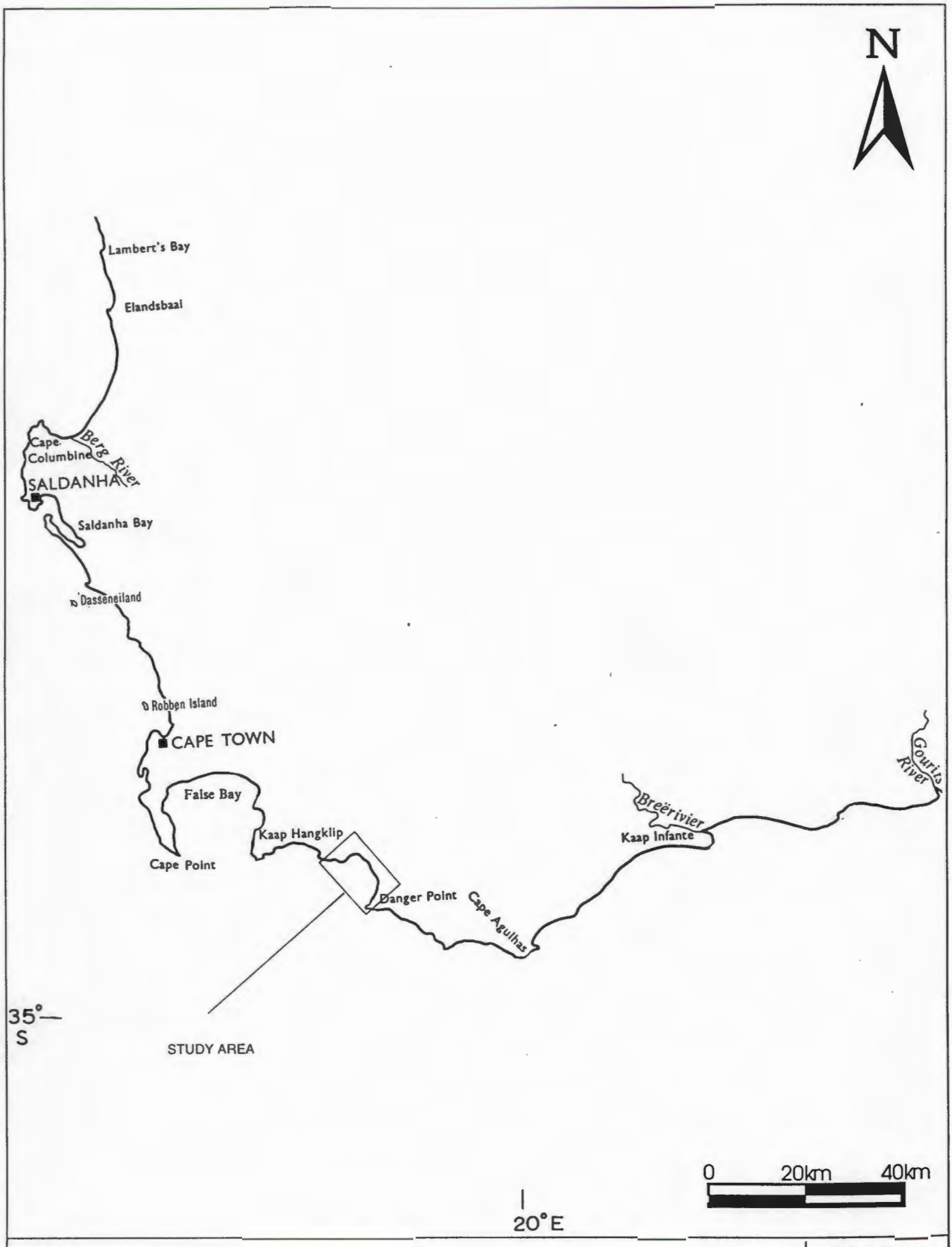

WALKER BAY

LOCATION OF STUDY AREA

FIGURE 1

2. REGIONAL SETTING

2.1 Onshore Geology and Geomorphology

2.1.1 Introduction

Coastal features are constructed and destroyed by processes which operate at different scales in time and space. Large features such as mountain ranges, deltas and continental shelves are strongly influenced by crustal plate movements and develop over millions of years. Intermediate features such as estuary spits and barrier islands are more closely related to changes in sea level caused by tectonic processes and glaciation and may be formed in 100s or 1 000s of years. Small-scale features such as beach profiles, ridge-and-runnel topography and nearshore bars are controlled by waves and tides. The waves and currents which control beach and nearshore topography are strongly influenced by local weather patterns and major storm tracks. Small-scale features are often formed and destroyed in a few days or by a single storm event. On some beaches oscillations in the profile can even be detected which have frequencies of 120 seconds and less (Waddel, 1973). In unravelling the geomorphologic and sedimentary history of a coastal area it is therefore necessary to consider all these processes operating at different scales with the smaller features superimposed on the larger features (Fox and Davies, 1976).

2.1.2 Subcontinental setting

Dingle and Scrutton (1974) subdivided the continental margin around Southern Africa into three different sections, each dominated by a particular tectonic style. These styles (Figure 2) are reflections of the dominant tectonic processes operative at the time of the breakup of Gondwanaland approximately 180 m.y. Before Present (B.P), namely (a) the northeastern margin (Mozambique and North Zululand) - tensional faulting; (b) eastern and southern margin (eastern Agulhas Bank, Transkei and Natal) - transform faulting; and (c) western margin (western Agulhas Bank to Walvis Bay) - tensional faulting. These tectonic styles are also reflected in the margins' different morphological features and as such have a direct bearing on the present-day shape of the coastline.

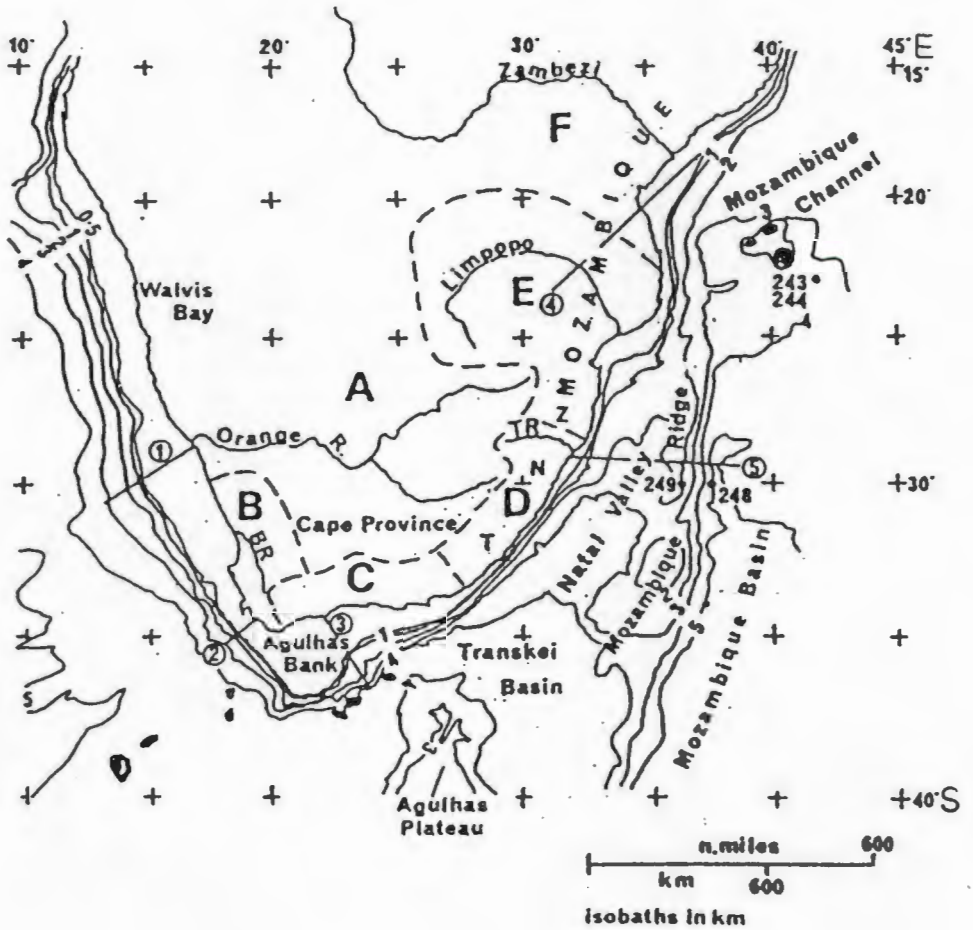

Key: Z, Zululand; N, Natal; T, Transkei; TR, Tugela River; BR, Berg River. Drainage areas: A, Orange River; B, southwest Cape; C, southern Cape; D, Transkei and Natal; E, Zululand and River Limpopo; F, River Zambezi.

WALKER BAY

MAIN BATHYMETRIC FEATURES OF THE OCEANS AROUND SOUTHERN AFRICA

(FROM DINGLE AND SCRUTTON, 1974)

FIGURE

2

The large east-west trending faulted folds of the Cape Supergroup rocks in the Southern Cape are the result of the second and major phase of the Cape Orogeny, 235 to 200 m.y. B.P. When West Gondwanaland separated, 125 to 130 m.y. B.P, through a process of transform faulting, the Southern Cape continental margin was left with a mountainous coastal terrain and a predominantly rocky inner shelf. Numerous rocky headlands were formed of which Danger Point and Cape Agulhas (Figure 1) are large-scale examples, giving rise to the distinctive irregular shape of this stretch of coastline. Log-spiral beaches are located between these headlands, Walker Bay being a typical example.

In contrast to the above scenario, the northwest-southeast-trending folded rocks of the west coast, together with tensional faulting during breakup, gave rise to the relatively straight and predominantly sandy coastline between Cape Town and Walvis Bay.

2.1.3 Local setting

For the purpose of this study, the Walker Bay area is defined as the seafloor environment landward of a line, approximately 19 km long drawn between Danger Point and a point 5 km off Mudge Point (Figure 3). In this section, a brief summary of the onshore geological setting of the area is given. The information was obtained during site visits and by referring to published geological maps of the Geological Survey, in particular the map of Bremner and Malan (1990) (Figure 3) which depicts the onshore/offshore geology of the Hermanus area.

In the Gansbaai area, between Die Kelders and Danger Point, the onshore topography reflects a flat, undulating surface at an elevation of approximately 20 m, extending approximately 2 km inland, from where it rises to more than 500 m in the Franskraal Mountains. This surface is clearly wave-cut, since no major present-day rivers or palaeo-drainage channels are evident in the area. Surface deposits on this wave-cut coastal plain consist of Cenozoic marine sands and limestones, overlying Palaeozoic Table Mountain Group (TMG) sandstones (Malan, 1989). Between Danger Point and Die Kelders (Figure 3) continuous outcrops of T.M.G sandstones occur along the

STRUCTURE SYMBOLS
STRUKTUURSIMBOLE

- Actual geological contact / Werklike geologiese kontak
- Inferred geological contact / Afgeleide geologiese kontak
- Fault / Verskuiwing
- Inferred fault / Afgeleide verskuiwing
- Anticline / Antiklien
- Inferred anticline / Afgeleide antiklien
- Syncline / Sinklien
- Inferred syncline / Afgeleide sinklien

GEOLOGICAL LEGEND
GEOLOGIESE LEGENDE

CAINOZOIC / SENOSOÏKUM		Quaternary / Kwaternêr
		Bredasdorp Group / Bredasdorp Groep
CRETACEOUS / KRYT		Dolerite / Doleriet
DEVONIAN / DEVOON		Bokkeveld Group / Bokkeveld Groep
SILURIAN – ORDOVICIA / SILUUR – ORDOVISIUM		Table Mountain Group / Tafelberg Groep
CAMBRIAN / KAMBRIUM		Cape Granite Suite / Kaap Granietsuite
NAMIBIAN / NAMIBIUM		Malmesbury Group / Malmesbury Groep

OFFSHORE DREDGE-SAMPLE POSITIONS
AFLANDIGE DREGMONSTERPOSISIES

- ⊖ Bokkeveld Shale/Skalie (Gentle, 1987)
- ⊙ Table Mountain Quartzite / Tafelberg Kwartsiet
- ⊕ Cape Granite / Kaap Graniet

Δ Navigation beacon

Sidescan Sonar Traverse (Gentle, 1987)

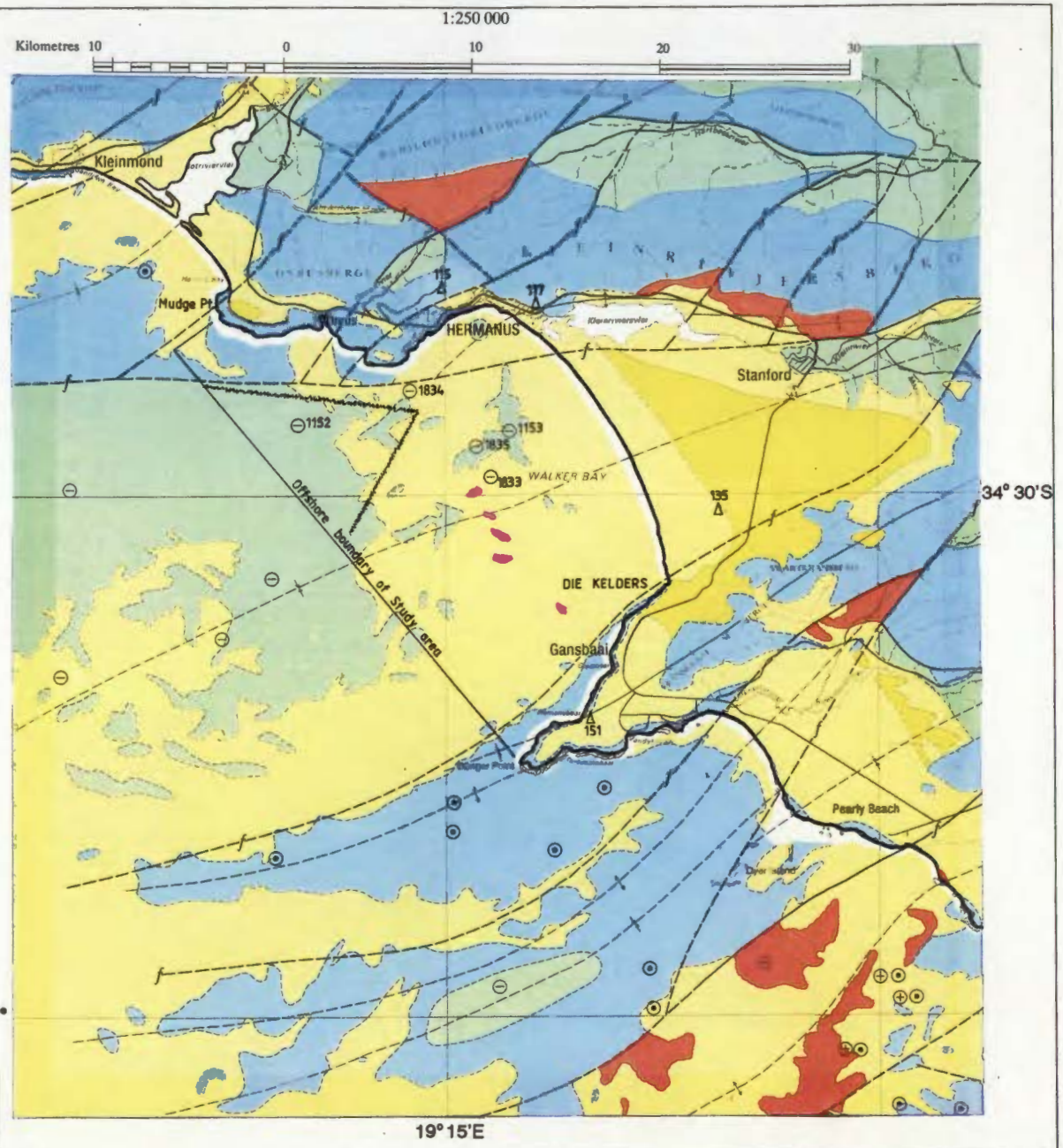

WALKER BAY

Onshore - offshore Geology (From Bremner & Malan, 1990)

FIGURE **3**

coastline and extend as far as 5 km west of Die Kelders, towards Stanford, where the coastline changes into a sandy beach, stretching all the way to the eastern edge of Hermanus, backed by frequent occurrences of aeolianites of the Pleistocene Waenhuiskrans Formation (Malan, 1989), above and below the present high-water line.

Caves, eroded in the Waenhuiskrans Formation containing well-rounded wave-abraded pebbles and cobbles, occur in the overlying limestones at an elevation of approximately 6 m above present sea level and they are indicative of a sea-level highstand after deposition of the Waenhuiskrans Formation. This is particularly evident in the immediate vicinity of Die Kelders (Tankard and Schweitzer, 1976).

The Waenhuiskrans Formation displays prominent aeolian crossbedding, dipping to the southeast and to the northwest. The northwesterly and southeasterly winds responsible for the crossbedding still prevail today, as is manifested by the southwest-northeast orientated crests of the modern dunefield between the coastline and the Klein River (Figure 4). This coastal dunefield underwent some dramatic geomorphological changes in terms of vegetation cover over the past 150 years, mainly due to man's influence (Munro, 1988). Before 1830, the entire area was covered with vegetation, after which veld fires and farming malpractices led to the destruction of almost all the stabilizing vegetation by 1853. Only after 1973 has an effective stabilizing programme again been applied and at present aeolian sediment transport is limited to the beach itself, an area near Die Kelders and a small area at Wolwefontein se Duine (Figure 4).

North of the Klein River the topography rises rapidly to an elevation in excess of 1 000 m above sea level to form the Kleinriviersberge (Klein River Mountain) with folded Table Mountain Group sandstones well exposed on the southern flank.

From Hermanus to Mudge Point the coastline is again rocky, with the clearly visible + 6 m and + 20 m platforms (Figure 5) cut into Table Mountain Group sandstones, which dip gently northward (Figure 3).

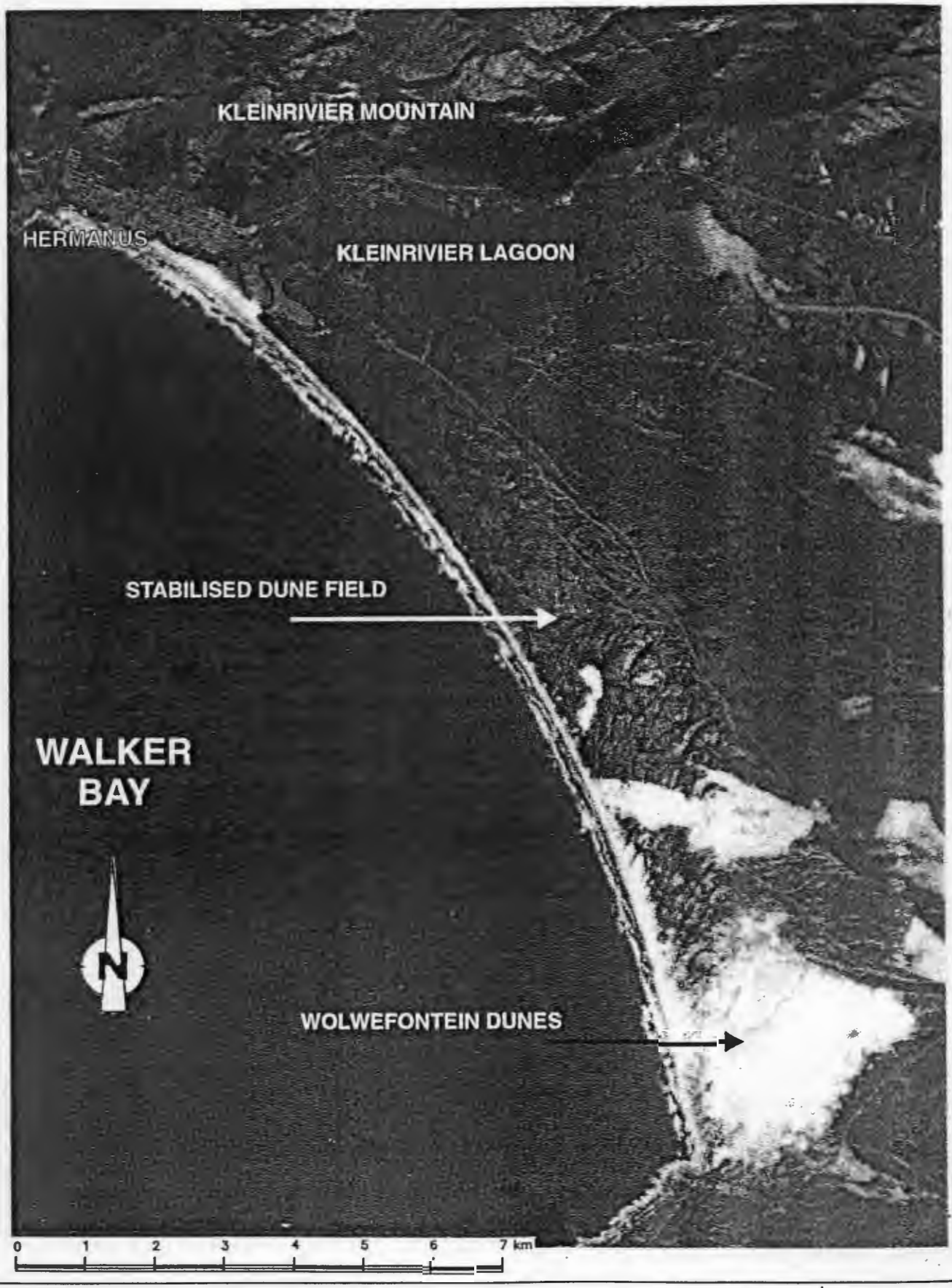

WALKER BAY

AERIAL VIEW OF WALKER BAY
SCALE 1: 75 000

FIGURE

4

WALKER BAY

20m WAVE-CUT PLATFORM, HERMANUS
(PHOTO: DR J ROGERS)

FIGURE

5

2.2 Climate

2.2.1 Weather patterns and wave climate

As indicated before, local weather patterns have a direct influence on wave and current conditions offshore and in the littoral zone. In turn, waves and currents are the chief creators and destroyers of small-scale morphological features.

The relationships between weather patterns and coastal processes have been studied by Fox and Davies (1970) at three coastal areas in the USA, namely, the eastern shore of Lake Michigan, Mustang Island on the coast of Texas in the sheltered Gulf of Mexico and the exposed central Oregon coast. Time-series analyses of weather patterns, wave data and current data were used in conjunction with topographical beach surveys to develop a model for predicting the relationships between weather patterns and coastal processes. Despite the varying sizes of the areas and the different energy levels encountered, definite similarities emerged for the relationships between weather patterns and coastal processes.

Weather-related parameters, which were directly measured during their field studies, included barometric pressure, wind speed and direction, air temperature and cloud cover. Wave measurements were made in the offshore area, the breaker zone and the plunge zone and included offshore wave height and period, breaker height and period, angle of incidence and breaker height and depth in the plunge zone. The direction and speed of the longshore currents were also measured. On the eastern shore of Lake Michigan, the longshore current velocity is a function of the first derivative of the barometric pressure, whereas breaker height is a function of the second derivative.

In the South African context, wave patterns along the southern Cape coastline are influenced by a number of dominant meteorological features (Rossouw, 1989). Heated air which rises in the tropics near the equator moves poleward and descends in the vicinity of 30°S to form the so-called Hadley cell. This process causes two semi-permanent high pressure systems, the South Atlantic High and the South Indian High,

with the air rotating anti-clockwise around the centre of the high-pressure system. South of the Hadley cell, the Ferrel westerlies spiral eastwards around the globe. The low-pressure systems of the South Atlantic are caused by disturbed air in the Ferrel westerlies. Once formed, these depressions move from west to east and are, together with their associated cold fronts, responsible for the waves affecting the South African coastline. In winter, the paths of these cold fronts frequently cross the southern tip of Africa, but in summer they shift farther south to pass south of the continent. The wind direction normally swings from NW through SW to SE during each eastward passage of a cold front.

More detailed statistics for the wind regime in the Walker Bay area are given in Figure 6. This wind rose was compiled from Voluntary Observations made by passing merchant Ships, the so-called VOS-data. Also incorporated in these statistics are data recorded *in-situ* for 18 months during the period June 1985 to December 1986 by means of a wind recorder in the stabilised dune field (Figure 4). Figure 6 shows that wind from the SE sector (ESE to SSE) occurs for 32 percent of the time, whereas wind from the NW sector (WNW to NNW) prevails for 18 percent of the time.

The best available offshore wave-climate information for the southern coast consists of a combination of simultaneous wave-height, wave-period and wave-direction measurements, recorded by means of "Waverider" buoys between Cape Point and Mossel Bay (just east of the Gouritz River, Figure 1) (Rossouw, 1989) and visual estimates of the wave direction at oil rigs off Mossel Bay (CSIR 1986, 1990). Rossouw (1989) has shown that the offshore wave climate varies little along the south and south-eastern Cape coastline and the data would therefore be applicable to Walker Bay.

Figure 7 and Table 1 give the details of the deep-sea wave climate off the southern Cape coast. Figure 7 shows the wave directions from 180°(S), 202,5°(SSW), 225°(SW), 247,5°(WSW) and 270°(W), clockwise from true north and their percentage occurrences. Also shown on Figure 7 is a "swell rose" displaying the relevant statistics. Table 1 shows combinations of wave period, significant deep-sea wave height and frequency and number of occurrences for each wave direction.

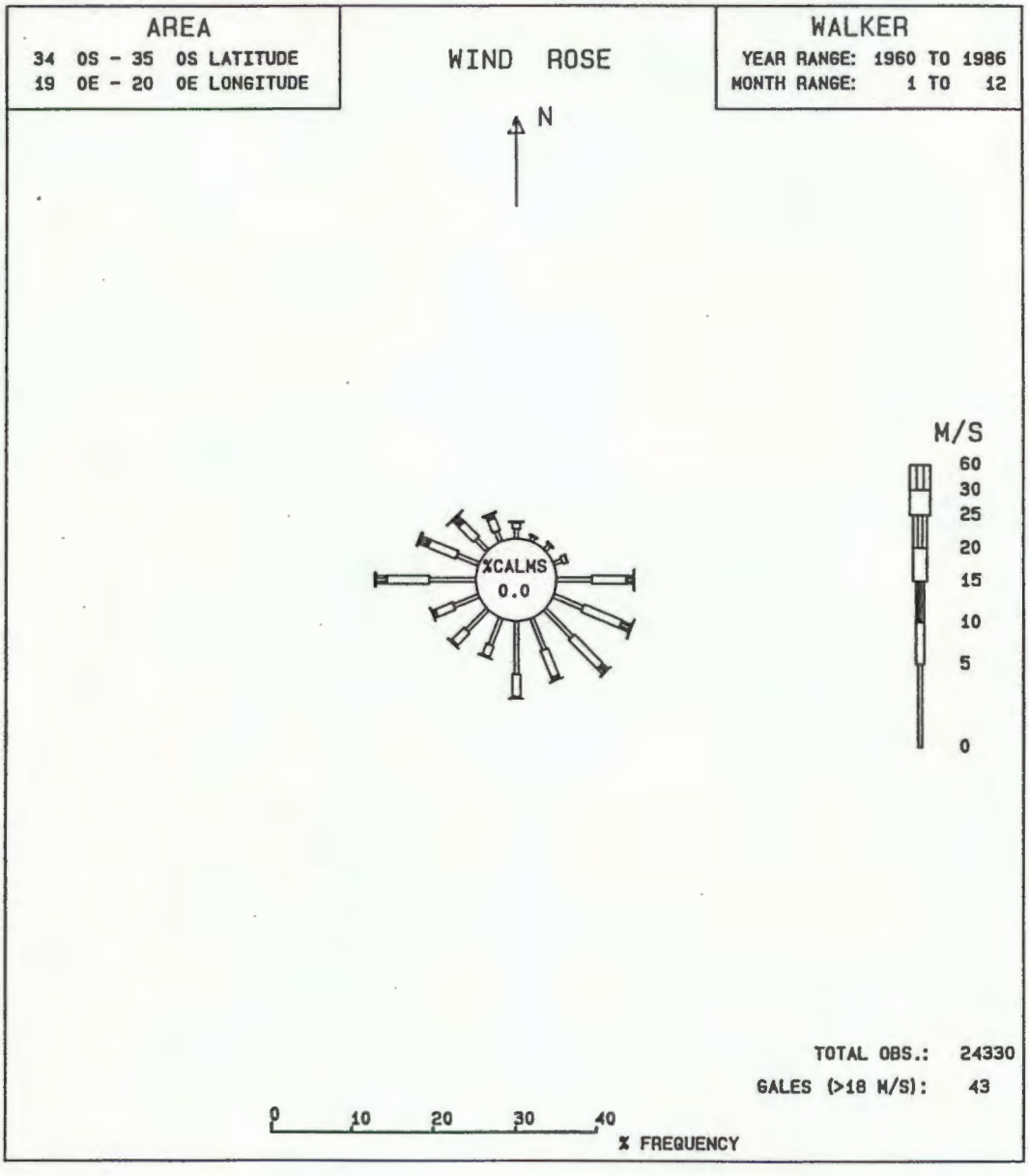

WALKER BAY

WIND DATA (UNPUBLISHED CSIR DATA)

FIGURE

6

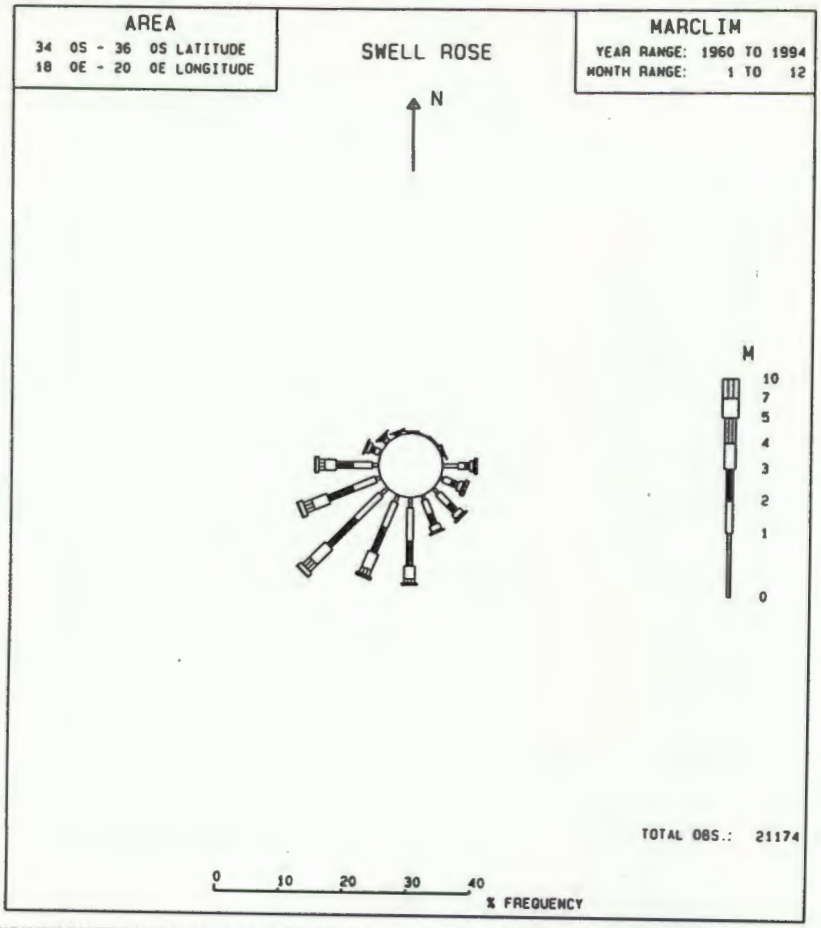

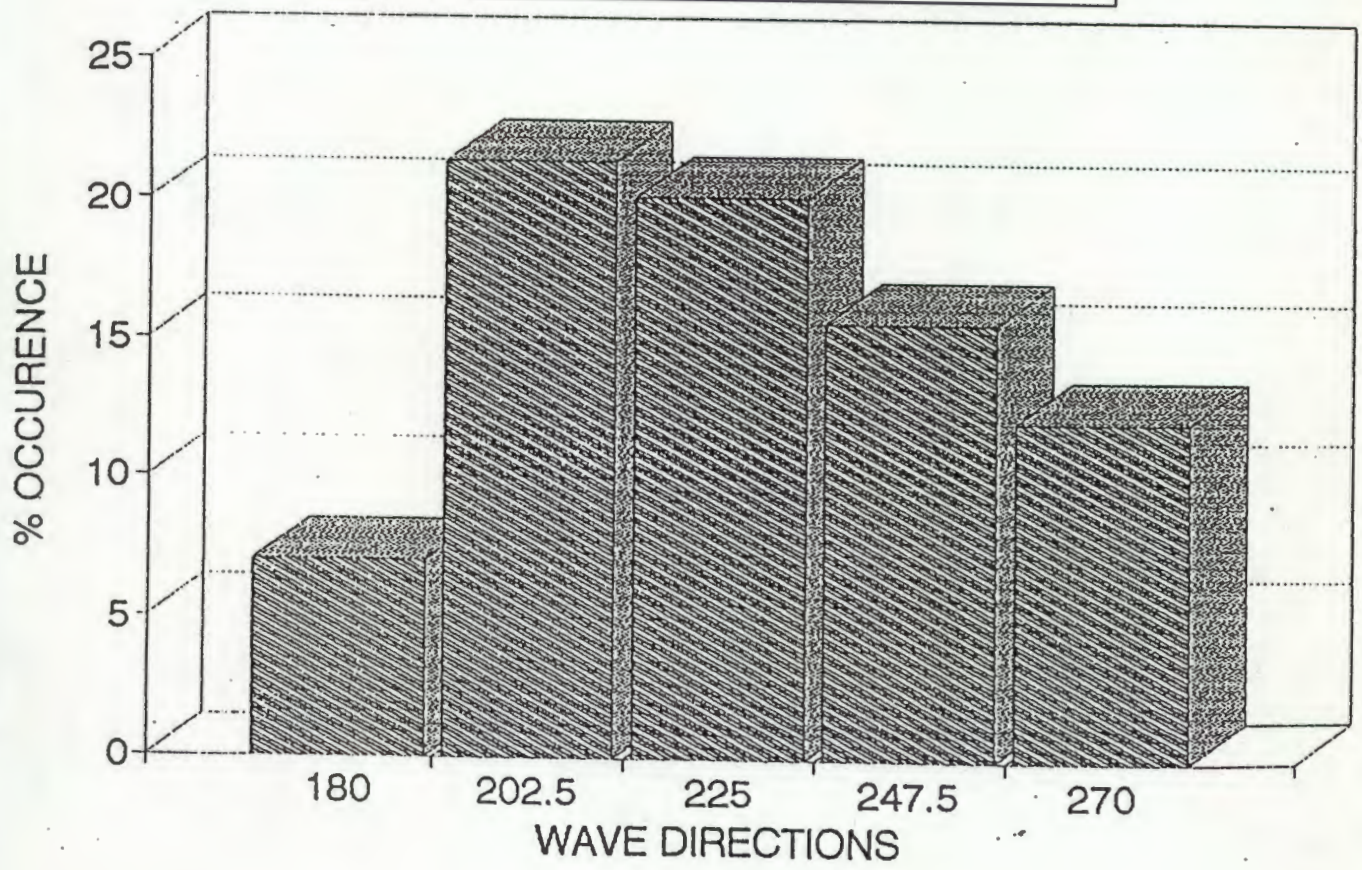

WALKER BAY

DEEP-SEA WAVE DIRECTIONS AND OCCURRENCES FOR THE SOUTHERN CAPE COASTLINE. (DATA FROM ROSSOUW, 1989 AND CSIR, 1986 AND 1990)

FIGURE 7

TABLE 1
DEEP-SEA WAVE CHARACTERISTICS

180° (48°)

Tp	Ho	f	n
8,0	2,4	0,007	20
10,2	2,2	0,0258	74
11,9	2,3	0,0171	49
13,5	2,5	0,0140	40
15,5	1,9	0,0059	17

202,5° (25,5°)

Tp	Ho	f	n
8,0	1,6	0,0153	44
10,2	2,3	0,0531	152
11,9	2,6	0,0702	201
13,5	2,9	0,0513	147
15,5	3,2	0,0203	58
18,3	3,5	0,0035	10

225° (3°)

Tp	Ho	f	n
8,0	2,1	0,0129	37
10,2	2,4	0,0608	174
11,9	2,7	0,0629	180
13,5	2,9	0,0119	134
115,5	3,2	0,0178	51

247,5° (-19,5°)

Tp	Ho	f	n
8,0	2,5	0,0150	43
10,2	2,6	0,0374	107
11,9	3,1	0,0461	132
13,5	3,3	0,0388	111
15,5	3,3	0,0189	54

270° (42,0°)

Tp	Ho	f	n
8,0	2,7	0,0119	34
10,2	2,7	0,0304	87
11,9	3,1	0,0328	94
13,5	3,6	0,0353	101
15,5	3,5	0,0112	32

Key: T_p = peak period
H_o = representative deep-sea significant wave height
f = frequency of occurrence
n = number of occurrences

2.2.2 Temperature, rainfall and drainage

The climate in the study area is described as Mediterranean with no extremes (Tyson 1969). The mean annual temperature is 17 °C and the mean rainfall is approximately 738 mm per annum. Rainfall measurements at the Walker Bay Forestry Station indicate that the highest rainfall is recorded during the austral winter months of June, July and August, with an average of approximately 90 mm per month.

Drainage of surface water into Walker Bay is channelled almost exclusively through the Kleinrivier (Figure 3) with a catchment area of 750 km² (Heydorn and Tilley, 1980). Rocks in the catchment area consist mainly of the Table Mountain Group and the overlying, younger Bokkeveld Group with limited outcrops of the underlying Cape Granite (Figure 3). Numerous streams from the slopes of the Kleinriviersberge flow directly into the normally closed Kleinrivier (Klein River) estuary, which is situated east of the town of Hermanus and is approximately 10 km long and 2 km across at its widest point (Figure 3). During periods of high monthly rainfall, in the austral winter, the mouth of the estuary is normally open to the sea, but for the remainder of the year it stays closed. Between August 1979 and February 1985 the estuary was open for 32 months out of 67 (Waldron, 1986).

3. PREVIOUS RESEARCH

3.1 Structural Geology

A structural analysis of the coastal area between Danger Point and Struisbaai, immediately east of the study area (Figure 8a), was performed by the Atomic Energy Corporation of South Africa (AEC) for the purpose of siting one of South Africa's future nuclear power stations. The findings of this study are reviewed by Andersen and Andreoli (1990) and comprise the most up-to-date account of both the onshore and offshore structural features of the area. A closely spaced airborne magnetic survey was flown, which enabled a detailed structural analysis to be carried out, backed by field mapping and existing maps of the Geological Survey of South Africa. Although west of their study area, a part of Walker Bay was nevertheless covered by the magnetic survey and the results provide some previously unknown information on the structure of pre-Mesozoic rocks in the bay. The regional structural development of the area is typical of the Cape Fold Belt as described by Hälbich (1983) and Söhnge (1983). Most of the structures can be related to the east-west trending deformational phase (D_1^{E-W}) caused by northward-directed compression of the Cape Orogeny, although some minor folding associated with the north-south syntaxis phase (D^{N-S}) occurs in the Romansbaai area (Figure 8b). Here the main southward-dipping F_1 cleavage overprints the F_1^{N-S} folds, but is affected by them elsewhere (Von Veh, 1988). Andersen and Andreoli (1990) therefore suggest that the two phases occurred coevally and that the southeastern boundary of the Syntaxis Zone, as proposed by Söhnge (1983), be moved from east of Quoin Point to south of Danger Point (Figure 8b).

Two major structural features were located in Walker Bay by the AEC aeromagnetic survey. These are the NE-SW trending Walker Bay (WB) fault (Figure 8b) and a northwest-southeast trending magnetic anomaly interpreted as a dolerite dyke (Figures 3 and 9). The Walker Bay fault is considered to be a normal fault of Gondwana age (Andersen and Andreoli, 1990). The northerly downthrow was inferred from dredging of younger Bokkeveld Group strata (Gentle, 1987) to the north in Walker Bay (Figure 3).

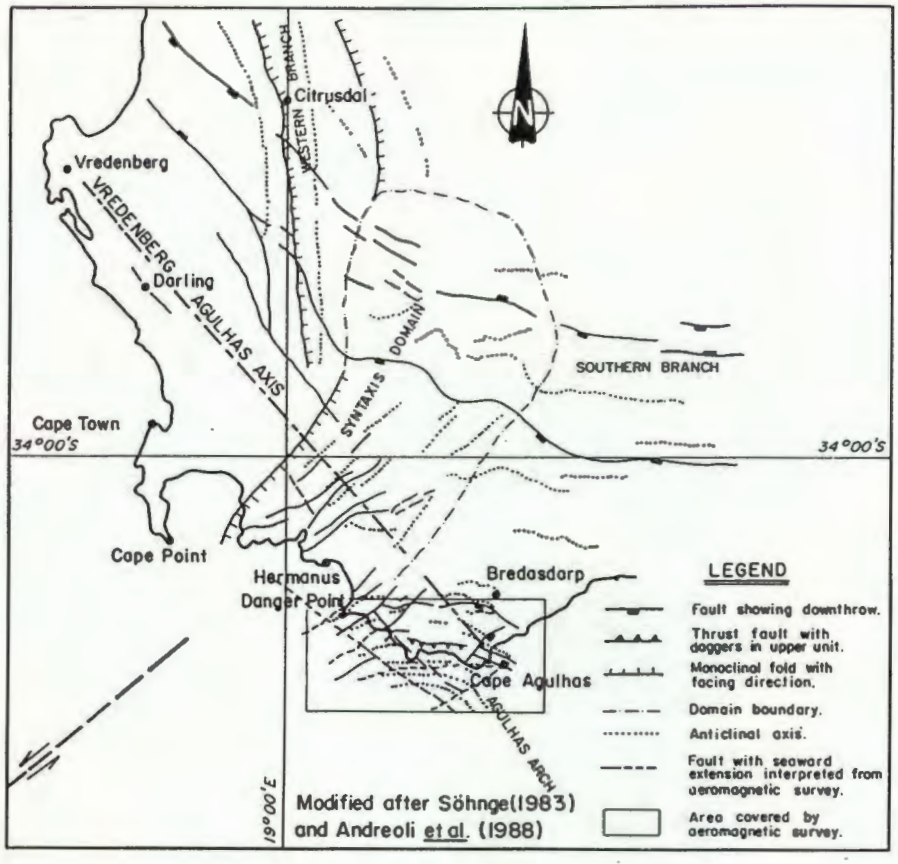

(a)

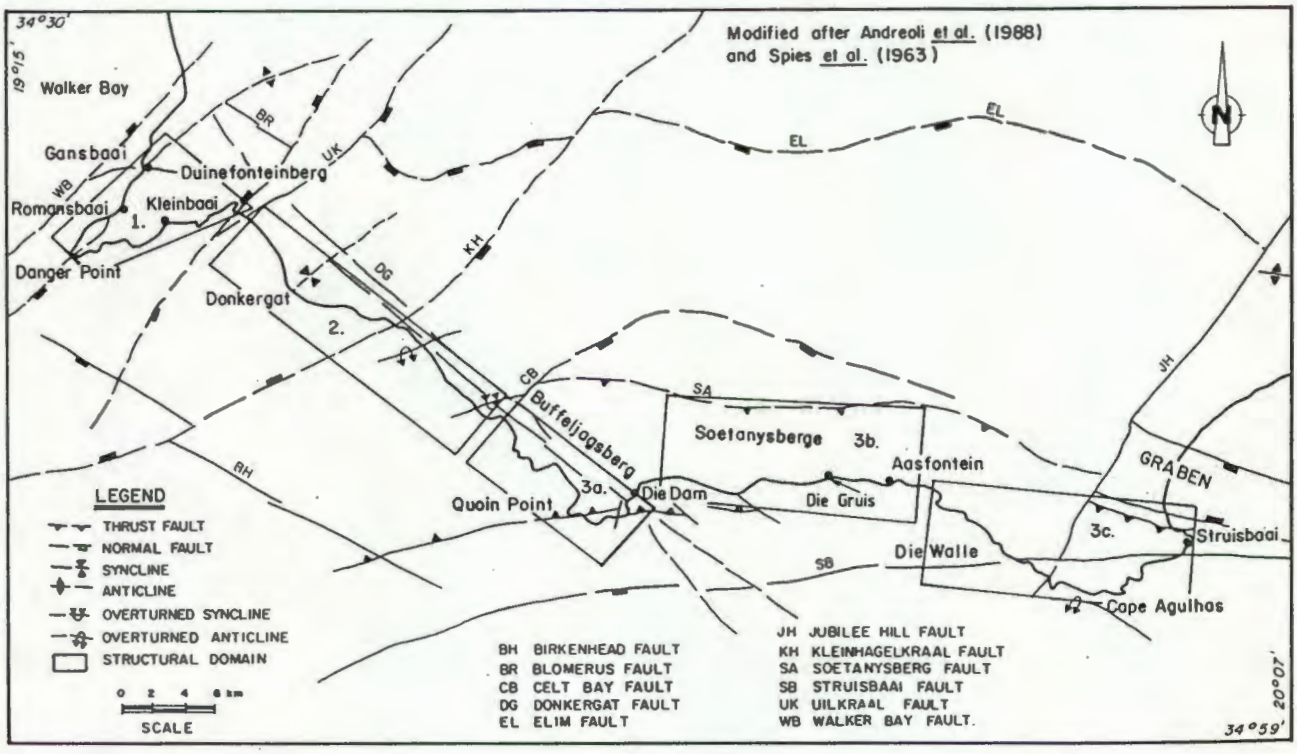

(b)

WALKER BAY

TECTONIC DOMAINS OF THE CAPE FOLD BELT (a) AND LOCATION OF MAJOR FAULTS (b) (FROM ANDERSEN & ANDREOLI, 1990)

FIGURE

8

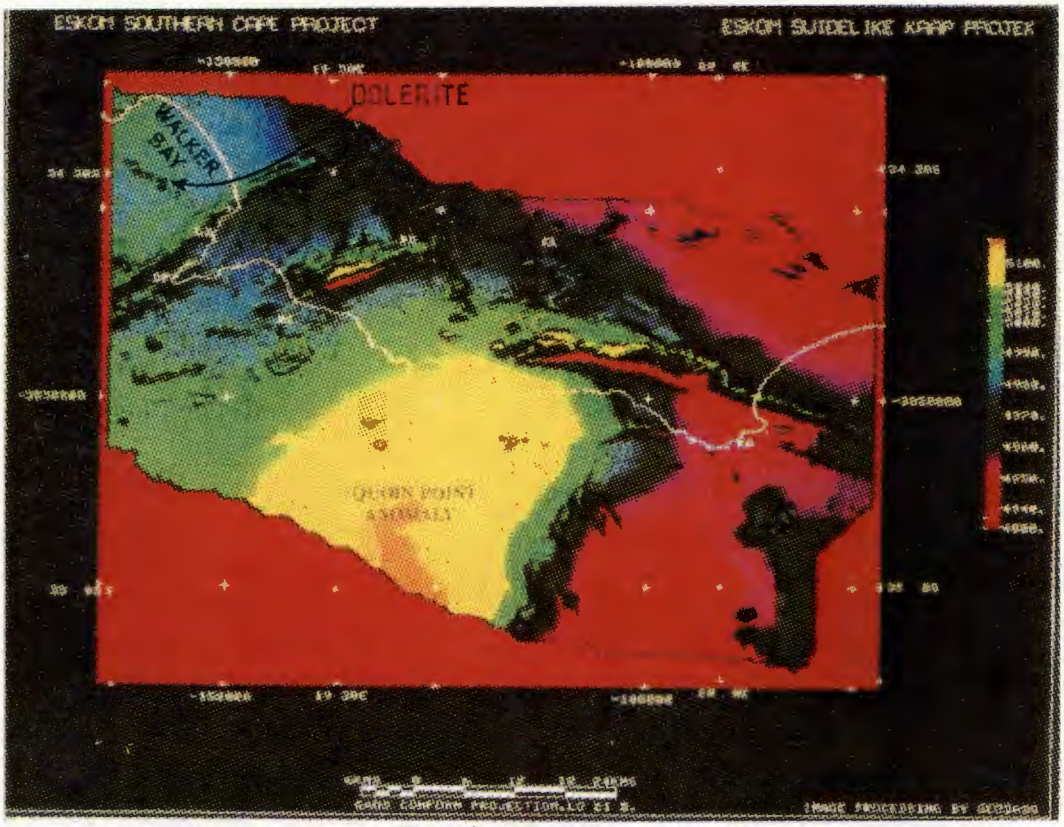

Total field image

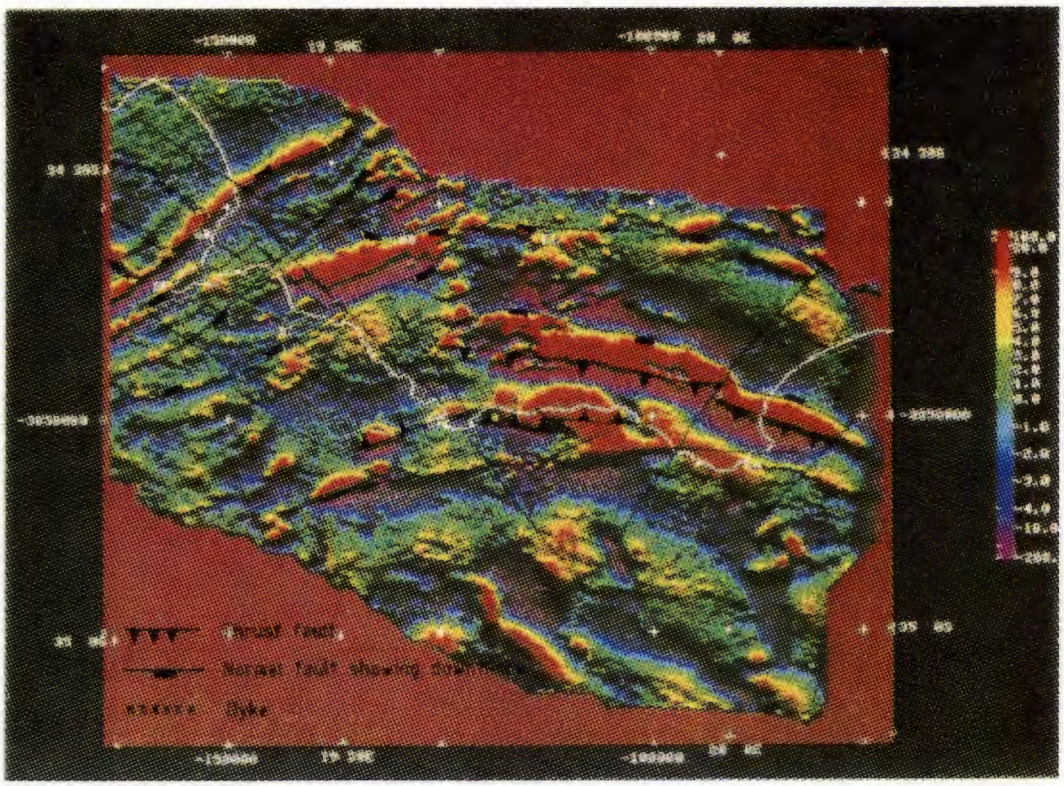

Filtered image with overlay

WALKER BAY

COMPUTER GENERATED MAPS OF MAGNETIC INTENSITIES.

(FROM ANDERSON & ANDREOLI, 1990)

FIGURE

9

Gentle (1987) further suggests that a major fault passes through between his sample position 1834 and the coastline (Figure 3). This is based on the fact that samples of Bokkeveld siltstone and sub-graywacke were retrieved less than 4 km from Peninsula Formation outcrops onland to the north. This fault is believed to have a downthrow of several thousand metres to the south (Gentle, 1987).

3.2 Bathymetry and Shoreface Geology

3.2.1 Bathymetry

Bremner (1987) produced a detailed bathymetric chart at 1 m contour intervals (Figure 10) of the Walker Bay area. As pointed out by Du Plessis and Glass (1991), the contour interval of a bathymetric map is usually chosen so that it is greater than (a) inaccuracies associated with measurement and (b) the variation in depth that may reasonably occur between lines. Based on these criteria, Figure 10 would not reflect true 1 m depth variations accurately, as the original data do not warrant a 1 m contour interval. The rationale behind the choice of a 1 m contour interval, however, was that the contour pattern may be used to map rock exposures on the seabed. Smooth parallel depth contours are normally indicative of relatively smooth sediment-covered seafloor, whereas high-relief rocky areas give rise to complex contour patterns. Such patterns are clearly distinguishable in Walker Bay (Figure 10). Towards the east of the bay, west of Danger Point, and along most of the shallow nearshore areas, the seabed is clearly mantled with sediment as reflected by the regular contour pattern. The few irregularities are most likely indicative of isolated rock outcrops. In the west and southwestern parts of the bay, the complex contour pattern suggests a predominantly rocky bottom.

3.2.2 Shoreface geology

Using the depth-contour principle described above, Bremner and Malan (1990) mapped the seabed geology of Walker Bay as part of an onshore/offshore mapping project for the South African coastline launched by the Geological Survey (now the Council for

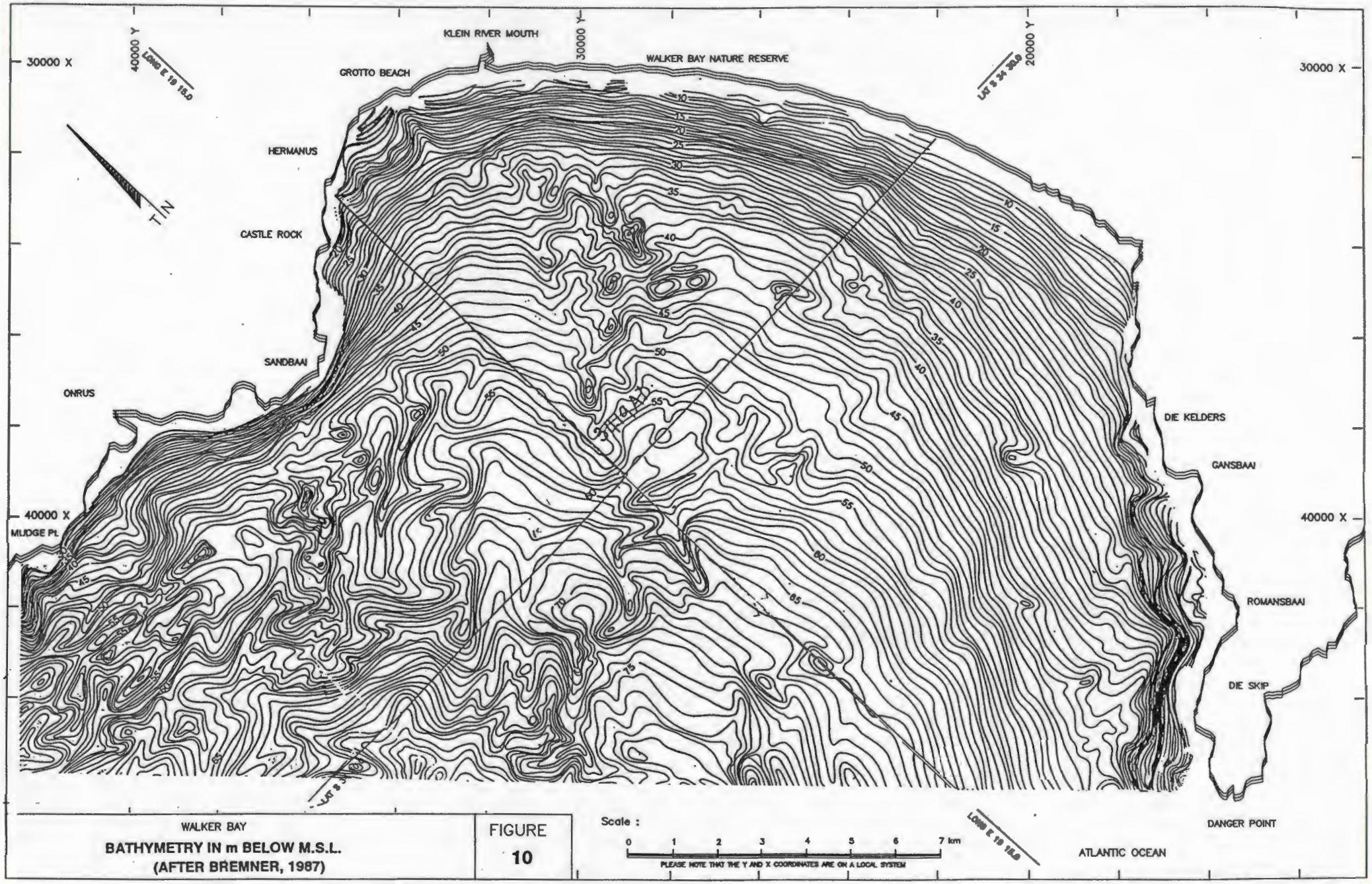

WALKER BAY

BATHYMETRY IN m BELOW M.S.L.
(AFTER BREMNER, 1987)

FIGURE
10

Geoscience). They were assisted in their stratigraphic interpretation by a number of dredged samples obtained and described by Gentle (1987), who mapped the pre-Quaternary geology of the inner continental shelf between Cape Town and Port Elizabeth. The geology of the study area, as interpreted by Bremner and Malan (1990), together with the locations of the dredged samples are shown in Figure 3. The correlation between depth contour pattern and seabed geology (Figures 10 and 3) clearly illustrates the mapping technique that was used.

As shown on Figure 3, rocks from both the Bokkeveld and Table Mountain Groups are exposed on the seabed in the study area. Table Mountain Group sandstones are exposed along the coast and in the nearshore areas at Hermanus and Gansbaai, whereas the exposures in the centre of the bay are composed of Bokkeveld strata. Five isolated dolerite outcrops of a dyke of presumed Cretaceous age are mapped (Figure 3) along a NW-SE orientated line in the bay. The existence of such a dolerite dyke was suggested by the detailed airborne magnetic survey, which was flown under the joint supervision of the Geological Survey and the Atomic Energy Corporation (Figure 9). No ground truth control in terms of dredged samples exists to verify these exposures.

As can be seen on Figure 3, the pre-Mesozoic basement rocks in Walker Bay are mostly covered by unconsolidated sediments. Gentle (1987) mapped the pre-Mesozoic geology of the area and his interpretation of the geological contacts between the TMG and the Bokkeveld strata are also indicated on Figure 3. Data from Gentle (1987), pertaining to the study area, consist of limited sidescan-sonar traverses into Walker Bay (Figure 3), totalling approximately 10 line-kilometres, and 4 dredged bottom samples collected on Cruise TBD 233 (1970) with the University of Cape Town's former research vessel *Thomas B Davie* (TBD). The approximate positions of these samples are shown in Figure 3. Gentle (1987 pages 114, 115 and 122) describes these samples as follows:

#1152 (Figure 11):
"One large boulder (60 cm x 40 cm x 17 cm) and other smaller pieces of black, micaceous fine grained shale. Thin section: quartz-rich and clay-rich areas occur. The

Whole sample

Thin section 1mm

WALKER BAY

DREDGED BOKKEVELD SHALE - GENTLE, 1987
SAMPLE # 1152

FIGURE

11

quartz is < 0,05 mm across and is angular and unstrained. Some of the clay layers are extremely iron rich and show marked boundaries with the quartz layers. Angular rock fragments also occur throughout the rock < 0,3 mm across in size."

1153 (Figure 12):
"Angular piece of black subgraywacke." (No thin section is available.)

1833 (Figure 13):
"Greenish micaceous graywacke with attached hydrozoan *Alveopora* sp. In thin section the quartz-rich areas contain angular grains up to 0,2 mm across, but in the pyrite/clay layers they are smaller."

1834 (Figure 14):
"Angular and sub-rounded chips of grey siltstone the largest of which is 5 cm across. In this section they are even-grained, pyritous, clay-rich, with only a little detrital quartz and some specks of iron ore."

#1835 (Figure 15):
"Three greenish angular pieces of slightly micaceous subgraywacke with black streaks. In thin section it is fine-grained with black highly pyritous streaks. It is rich in clay minerals and detrital quartz (0,1 mm across), constituting approximately 25% of the rock. Iron ore specks occur throughout the rock and occasional white mica and plagioclase."

All the above samples were assigned to the Bokkeveld Group.

The only sidescan traverse described, by Gentle (1987) from the study area, is situated 15 km northwest of Danger Point in water depths ranging from 74 to 90 metres and in an area where samples of Bokkeveld strata were dredged (Figure 3). The record shows linear, strike-parallel outcrops that vary from 50 metres to less than 10 metres in width. The bottom is uneven with a maximum height between ridges and gullies of 6 metres. Lineaments representing bedding strike is the main feature of Bokkeveld strata, with changes in strike showing up well on sonar images.

WALKER BAY

DREDGED BOKKEVELD SHALE - GENTLE, 1987
SAMPLE # 1153

FIGURE

12

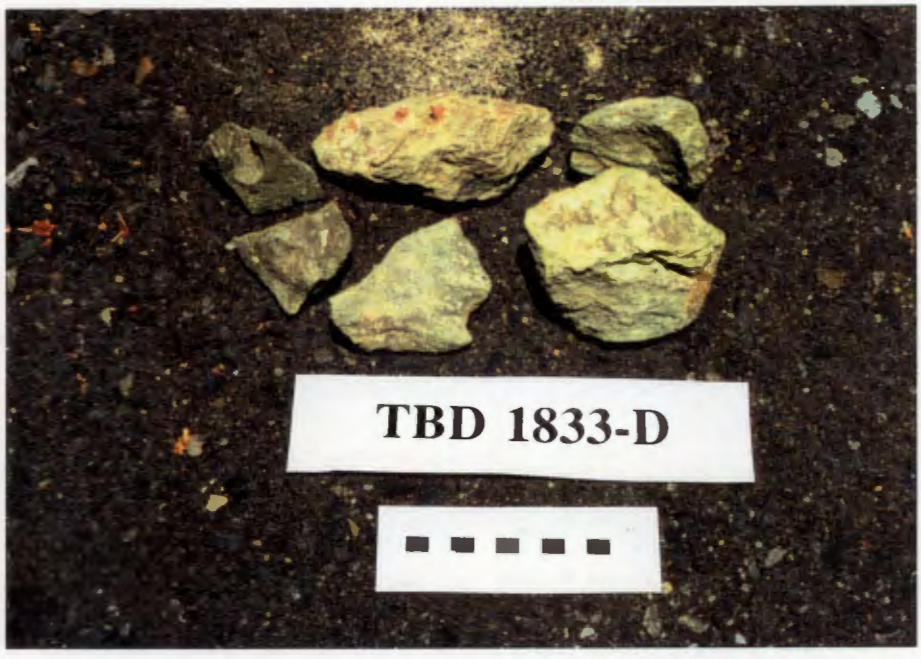

Whole sample

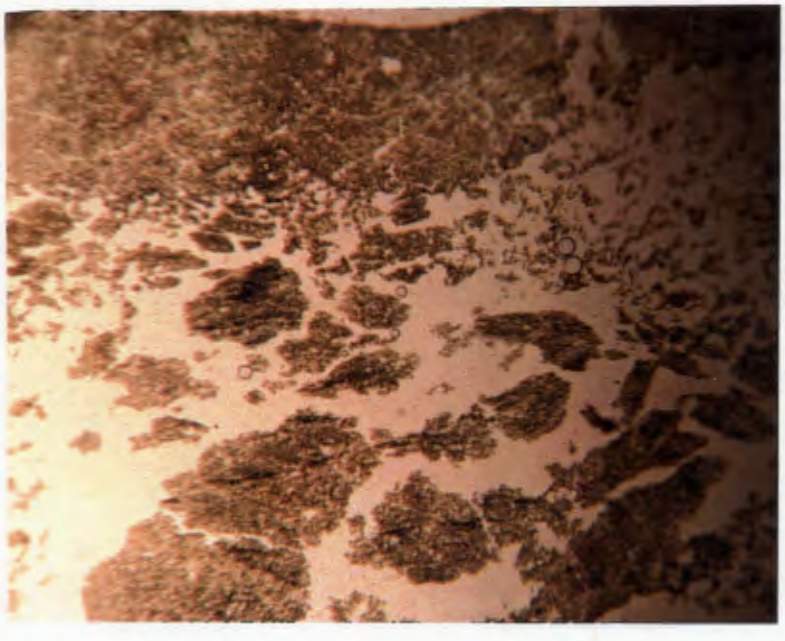

Thin section

WALKER BAY

DREDGED BOKKEVELD SHALE - GENTLE, 1987
SAMPLE # 1833

FIGURE

13

Whole sample

Thin section 1mm

WALKER BAY

DREDGED BOKKEVELD SHALE - GENTLE, 1987
SAMPLE # 1834

FIGURE

14

Whole sample

Thin section

WALKER BAY

DREDGED BOKKEVELD SHALE - GENTLE, 1987
SAMPLE # 1835

FIGURE

15

1) oscillatory flows related directly to incident waves

2) oscillatory or quasi-oscillatory flows corresponding to standing waves and edge waves at frequencies lower than the incident wave frequency

3) wave-generated nearshore currents

4) non-wave-generated currents.

Wind-generated incident waves, together with the resultant wave-generated nearshore currents, are the main source of energy in the littoral zone. The main onshore-offshore shift in beach and nearshore sediments, due to incident wave attack, is an annual change which is commonly referred to as the summer and winter profiles. Offshore shift of sand takes place during storm-wave attacks, whereas the reverse is true for periods of relatively calm wave conditions. In order to eliminate the seasonality, Komar (1976) suggested the descriptive terms "storm profile" and "swell profile". Beach-profile changes from storm to swell conditions are normally related to the wave steepness, which is the ratio of the deep water wave height H_0 to the deep water wave length L_0 (Komar, 1976). Within log-spiral beaches, such as Walker Bay, a shift in the direction of the wave-induced longshore current will re-orientate the shoreline, so that the shoreline retreats along the updrift side and progrades along the downdrift side. This is demonstrated best by the behaviour of Boomer Beach, La Jolla, California, where, within 24 hours after a change in wave direction, the sand shifted to the opposite end of the pocket beach with up to 3 m of sand disappearing from the updrift end (Shepard, 1950; Komar, 1976).

3.3.3 Local nearshore profiles

Between September 1986 and February 1990, nearshore profiles were measured along a distance of 2,7 km on the eastern side of the Kleinrivier Mouth in Walker Bay (Figure 4) (Unpublished CSIR data). The surveyed area is shown on Figure 16. Thirteen profiles, extending to approximately 25 metres water depth and 250 metres

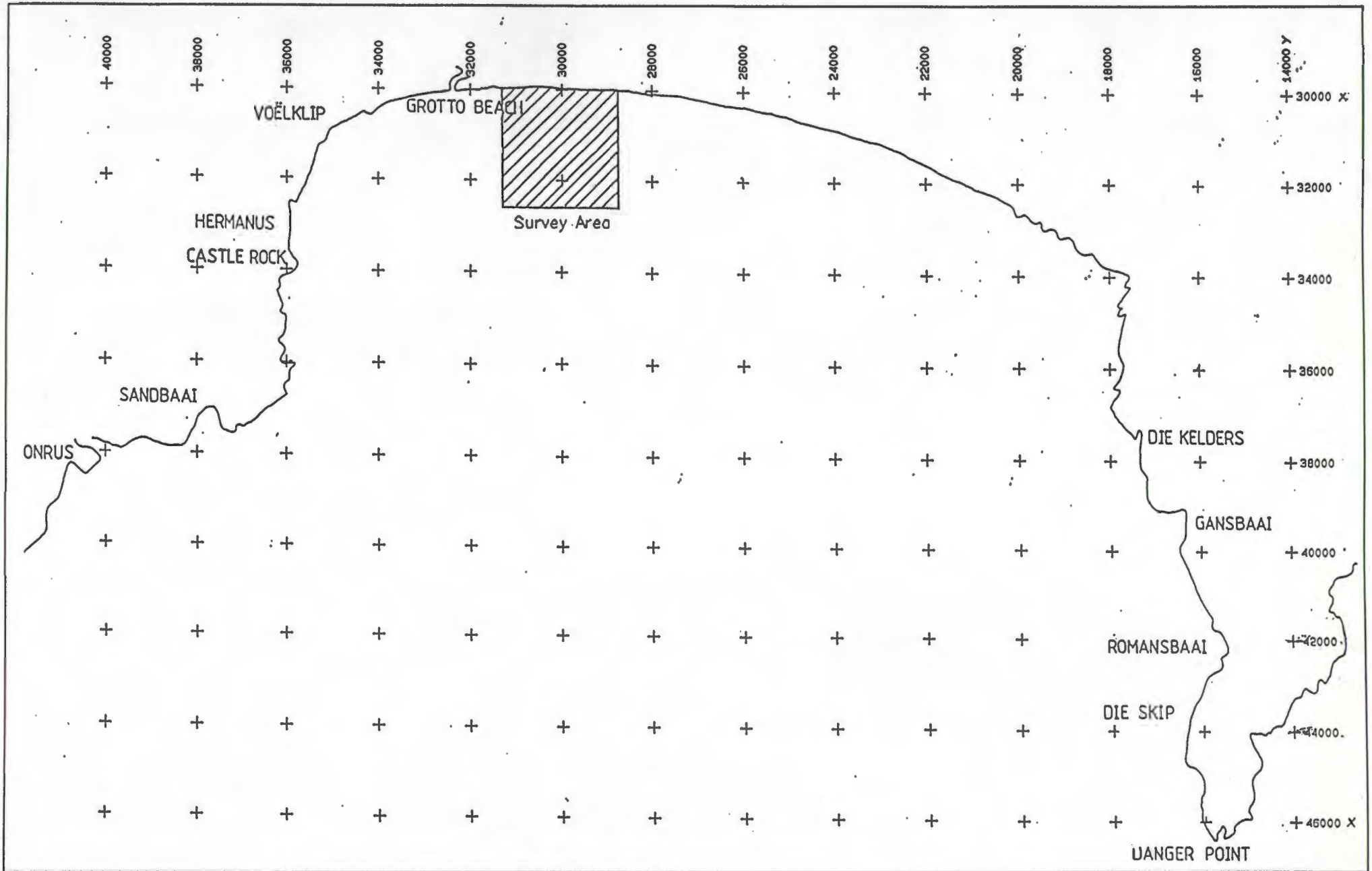

WALKER BAY

SURVEYED AREA - NEARSHORE PROFILES

FIGURE 16

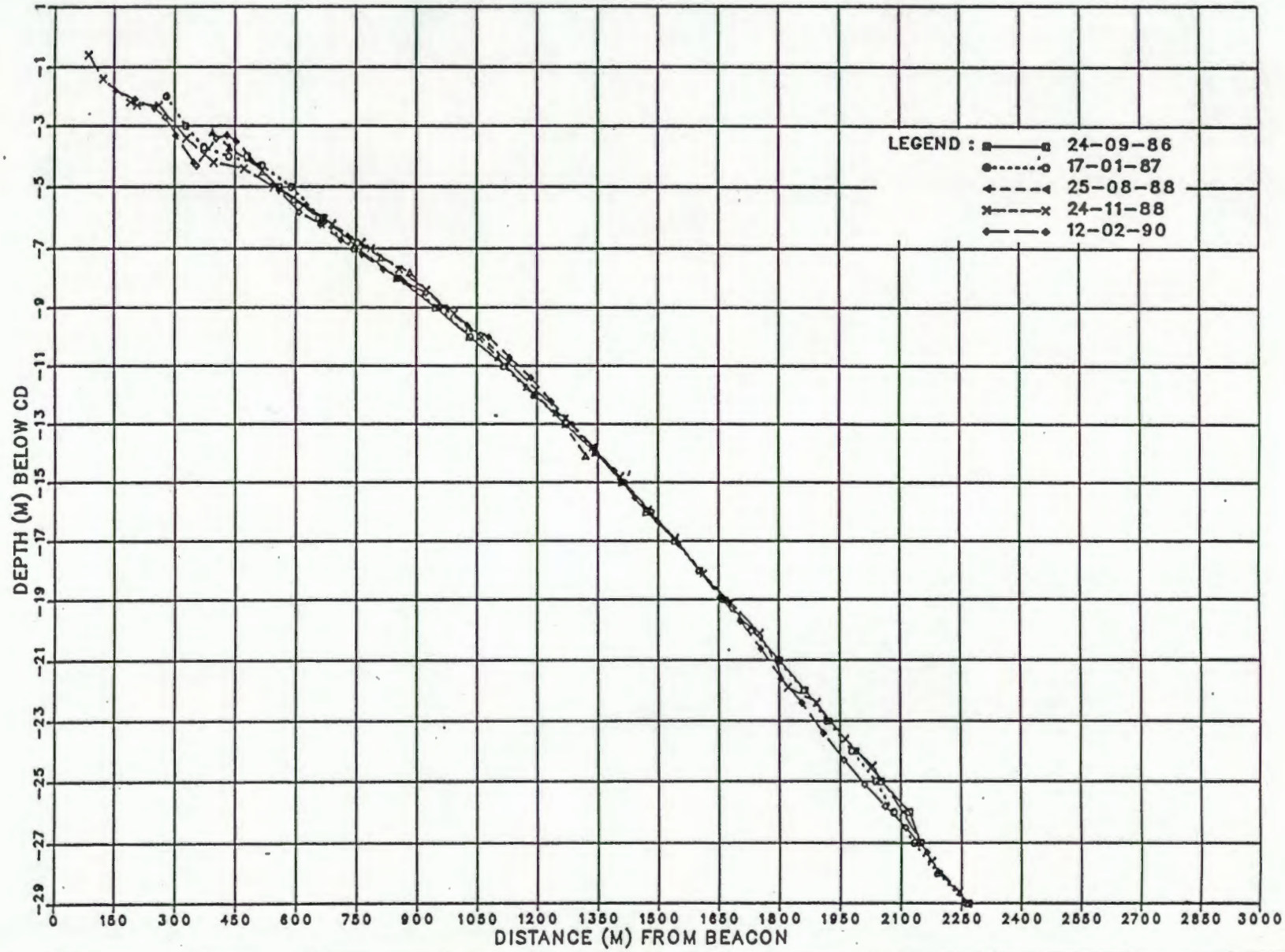

WALKER BAY

NEARSHORE PROFILES, PROFILE 7 (UNPUBLISHED CSIR DATA)

FIGURE 17

apart, were surveyed on each occasion, using a dedicated ski-boat and echo-sounder. The results obtained from the total number of profiles are very similar and the data for Profile 7, which is in the centre of the surveyed area, are shown in Figure 17. Seaward of the 5 metre depth contour, no significant changes in the sediment level occurred over the survey period. In the area landward of the 5 metre contour, which constitutes the surf and swash zones, sediment-level variations of between 1 and 2 metres occurred. This demonstrates the relatively high mobility of sediment in the littoral zone as opposed to the more stable seabed configuration of the shoreface.

4. METHODOLOGY

4.1 Introduction

The data used in this study were collected over a period of 4 years, from November 1986 to September 1990. The first survey, in November 1986, was carried out aboard the CSIR's research vessel *RV Meiring Naudé* and the data from this cruise, consisting of seismic profiling, sidescan sonography and seabed grab-sampling form the basis of this study. A follow-up survey was conducted in October, 1987, using a smaller chartered vessel with the purpose of filling in the gaps in the sidescan-sonar data set and to resurvey lines where the quality of the 1986 data was considered unacceptable. In August, 1988, a third survey was conducted to obtain detailed seismic and sidescan data, as well as bottom samples, in areas of specific interest. In January, 1990, the site was revisited to obtain a second set of bottom samples from selected areas to serve as groundtruth for sidescan-sonar interpretation and for further sedimentological information. A final survey was performed in September 1990, when sidescan-sonar data were collected in order to investigate possible temporal changes in the seabed configuration by resurveying specific areas. During this exercise, a remotely operated underwater vehicle (ROV) was also deployed at a number of locations to record video footage, in colour, of the seabed within the acoustic facies identified on the sidescan sonar records.

4.2 Navigation and Position Fixing

Navigation and position-fixing on all data-collection exercises were controlled by means of a Plessey MRD1 Tellurometer, a radio-wave positioning system, which uses simultaneous ranges from three remote stations on shore. The successive positions of the survey vessel, along each pre-determined track were regularly logged on a personal computer on board, at a time interval of 1 minute. The logged co-ordinates corresponded with synchronized event marks (fixes) on the analogue seismic and sidescan records, enabling a direct correlation between the recorded geophysical data and the ship's position at the time.

3.3 Beach and Nearshore Geomorphology

3.3.1 General

Although this study is mainly concerned with the shoreface geology in Walker Bay (ie the area from the outer reaches of the surf zone seawards across the inner continental shelf), some consideration must be given to the fact that there is a direct link between morphological changes on the beach and in the surf zone and the sedimentological processes in the deeper water of the shoreface. A better understanding of shoreface processes will therefore undoubtedly make a valuable contribution towards better shoreline management and development.

Marine-geological research in South Africa will in future largely be driven by problems arising from coastal-zone management and offshore mining activities. The reasons for this are man's increasing involvement in the coastal zone and the need for interdisciplinary research and co-operation with coastal engineers in order to supply answers to coastal developers. As such, marine geologists will play a major role in outlining and identifying the natural processes which govern the movement of sediments in the beach and nearshore zones.

3.3.2 Nearshore-profile changes

The morphological behaviour of a beach and the nearshore seabed depends on local environmental factors, the characteristics of the available sediments and the antecedent wave and tide conditions. In this respect, beaches and surf zones are generally considered to be dissipative, reflective or in any of a number of four intermediate states (Wright and Short, 1983). The four intermediate states are characterized, respectively by the longshore-bar-trough system, the rhythmic-bar-and-beach system, the transverse-bar-and-rip system and the low-tide-terrace system. The distinguishing features of the six major beach states are reviewed by Wright, *et al.* (1985). Wright and Short (1983) grouped the different modes of fluid motion contributing to the movement of beach and nearshore sediments into four broad categories, namely:

The 1986 and 1987 surveys were carried out along parallel NW-SE lines across the Bay at 400 m intervals (Figure 18). The lines were terminated inshore at a water depth of approximately 15 m, which was the minimum, safe, navigable depth for the survey vessel. A left-right indicator was installed on the bridge to assist the helmsman in keeping the line and only minor deviations from the line occurred occasionally during the survey. An accuracy of 2 to 3 metres in the recorded position of the vessel was maintained throughout the first and subsequent follow-up surveys. Note that the 1988 and 1990 survey lines are not shown on Figure 18 as they co-incided with existing 1986 and 1987 lines and were used for comparison purposes only.

To simplify the compilation of maps and charts for the study area, a local x-y grid system was designed, where the y-axis parallels the survey lines and the x and y values increase towards the south and east respectively.

Table 2 in both the Lo19° and local grid systems, gives the co-ordinates and elevations of the four remote stations used onshore and the navigational waypoints, which were used to define the survey lines. The positions of the remote stations are indicated on Figure 3.

As can be seen from Table 2, the X and Y axes of the local system are not parallel to the X and Y axes of the standard Lo 19° system. The local system was rotated through 21° with respect to the Lo 19° system in order to bring the Y-axis into a northwest-southeast orientation, which was better suited for navigational control in the area.

Figure 18 shows the sidescan sonar and seismic traverses of the 1986 and 1987 surveys, together with the designated line numbers (lines 1 to 44).

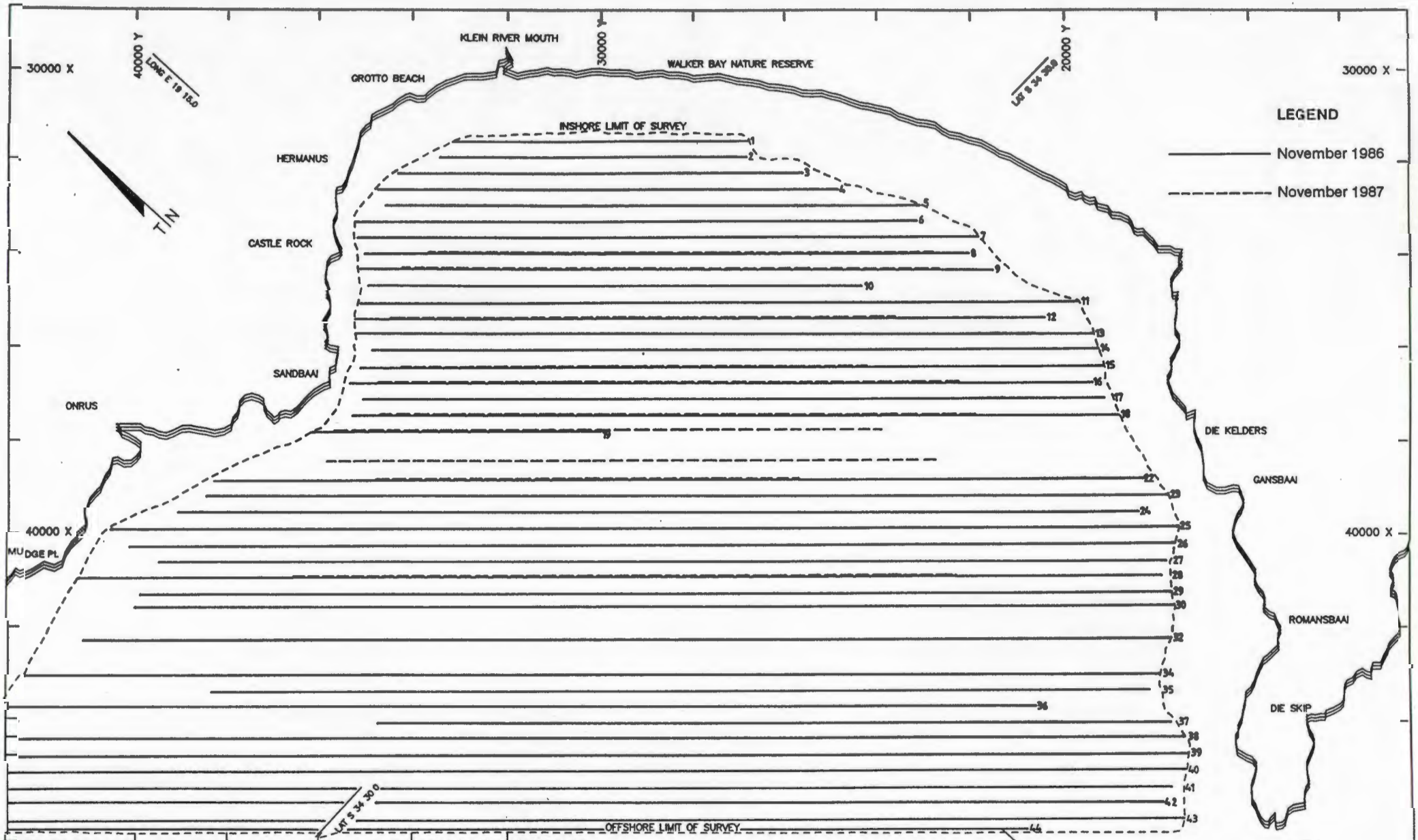

WALKER BAY
SURVEY TRACK CHART
NOVEMBER 1986 AND NOVEMBER 1987

FIGURE
18

TABLE 2: CO-ORDINATES OF REMOTE STATIONS AND NAVIGATIONAL WAYPOINTS

REMOTE STATIONS			
Lo 19°			
Trig. Beacon Id	**Y**	**X**	**Z**
Δ115, Hermanus C	- 20 442,61	+ 3 809 255,04	234,6
Δ117, Mossel River	- 27 423,07	+ 3 809 535,62	12,4
Δ135, Hattingsbosch	- 37 722,07	+ 3 820 456,96	163,0
Δ151, Romansbaai	- 30 887,21	+ 3 830 719,60	67,9
LOCAL SYSTEM			
Δ115, Hermanus C	+ 38 233,6	+ 34 932,2	234,6
Δ117, Mossel River	+ 33 376,2	+ 29 911,3	12,4
Δ135, Hattingsbosch	+ 18 370,3	+ 29 499,9	163,0
Δ151, Romansbaai	+15 264,99	+ 41 432,8	67,9
NAVIGATIONAL WAYPOINTS			
LOCAL SYSTEM			
P_o	+ 16 000	+ 48 000	0
P_1	+ 40 000	+ 48 000	0

4.3 Marine Geophysical Data

4.3.1 Seismic profiling

Most of the seismic data were obtained using an EG + G Boomer system with the sound source mounted on a surface-tow vehicle. The reflected signals were filtered by a Krohn-Hite bandpass filter, amplified by a CSIR-developed amplifier system and recorded on an EPC 3200 graphic recorder, which was normally set on a 500 millisecond (ms) sweep.

The Boomer is a medium-resolution (0,5 - 1,0 m) seismic source with an effective frequency of between 400 and 5 000 Hz, capable of penetrating unconsolidated sediments up to a depth of 50 m, depending on local conditions. Over most of the study area the system was able to penetrate unconsolidated sediments down to the underlying bedrock.

A limited number of traverses were also surveyed using a CSIR-built 20-electrode sparker sound source, in conjunction with the recording facilities mentioned above. With its lower frequency and higher energy output, typically 500 joules per pulse, the Sparker has superior penetrating capabilities, compared to the Boomer, with the sacrifice of profile resolution. The Sparker was used for comparison purposes only and it was found that the Boomer was the more suitable instrument for this study area.

In detailed follow-up surveys, a high-resolution Pinger system was used in an attempt to obtain detailed information on specific sedimentological features. The system uses two MASSA model TR 1061A piezo-electric transducers, mounted on a float, and is driven by a CSIR-built pinger driver. The reflected signals were filtered in the range 2800 - 4200 Hz and a maximum penetration of 8,0 metres was achieved. The resolution of the system varied between 0,5 and 1,0 metres, depending on the circumstances.

A surface - towed seismic source, as described above, is extremely sensitive to sea conditions and the quality of the recordings can deteriorate rapidly under adverse weather conditions. A deep-tow system is advisable under open-sea conditions. The present survey was, however, done under fairweather conditions in the austral spring or summer months of September, October, November and December, and the seismic data are generally considered to be of good quality.

All the seismic records were electronically marked in synchronization with the sidescan and navigational data. A towfish layback of 20 metres was maintained throughout the survey.

The speed of the survey vessel was kept as constant as possible (approximately 6 knots i.e. 180 m/minute).

4.3.2 Side-scan sonar

A Klein Model 520 sidescan-sonar system was used to obtain sonographs of the seabottom along the lines shown in Figure 18. The 100 kHz-towfish was towed behind the vessel by means of a 600 m-long armoured transmission cable on a slipring winch. A scanning range of 200 m to either side of the ship was used in order to obtain total coverage of the areas between adjacent lines. The towfish was kept at the optimum height above the bottom (10 - 20% of the scanning range) by using a dead-weight depressor of 40 kg, tied to the tow cable approximately 7 m from the towfish.

The sidescan records were manually tuned, whenever necessary, to ensure that good-quality records were obtained throughout the survey. Marking of the sonographs at 1-minute intervals, was achieved electronically and was synchronised with the computer logging of navigational data. The towfish layback was read off a calibrated metre-wheel and regularly noted on the records.

4.3.3 ROV observations

Underwater video footage of the seabed was obtained by means of a Phantom Remotely controlled Underwater Vehicle (ROV) equipped with a colour video camera (Figure 19). The recordings were monitored in real time on a screen and simultaneously taped on VHS casette-tape.

The same navigation system described earlier was used to position the vessel on the preselected deployment sites. The sites were chosen to be representative of the different reflective patterns observed on the sidescan records and the observations therefore provided valuable groundtruth for sidescan-sonar interpretations. The 8 recording sites are shown in Figure 20.

4.4 Seabed Sampling

4.4.1 Unconsolidated sediment

Sediment samples were collected in the study area on 3 different occasions, namely November 1986, October 1987 and January 1990.

The 1986 sample suite was obtained during the initial 100%-coverage geophysical survey, using a Shipek grab (Figure 21a) deployed via a hydraulic winch. The samples were taken on an evenly spaced grid and therefore covered the entire survey area at regular intervals of about 3 km. This was done because no knowledge of the sediment distribution was available at the time of the initial survey.

Once on deck, the samples were placed in plastic jars, which were numbered and sealed with a lid. The numbering system used was 1/86 through 44/86. Figure 22 shows the relative positions of the sample sites in the study area and their coordinates, in terms of the local xy grid system, are given in Table 3.

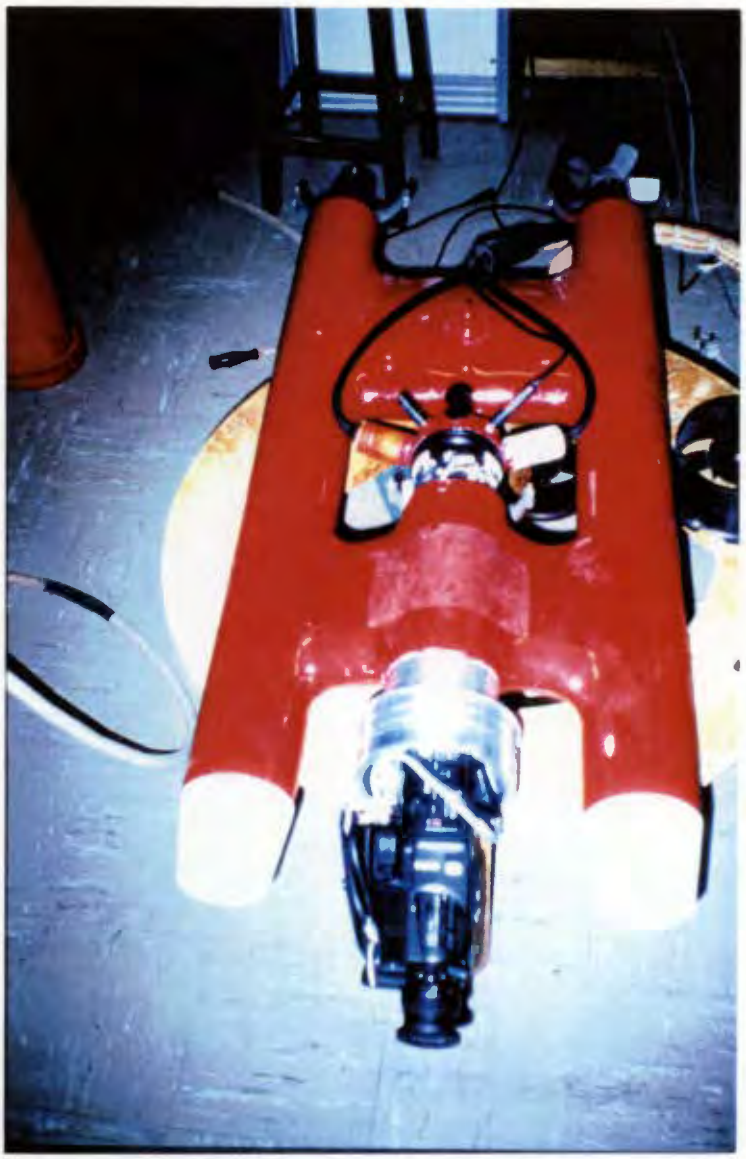

WALKER BAY

"PHANTOM" REMOTELY CONTROLLED UNDERWATER VEHICLE

FIGURE

19

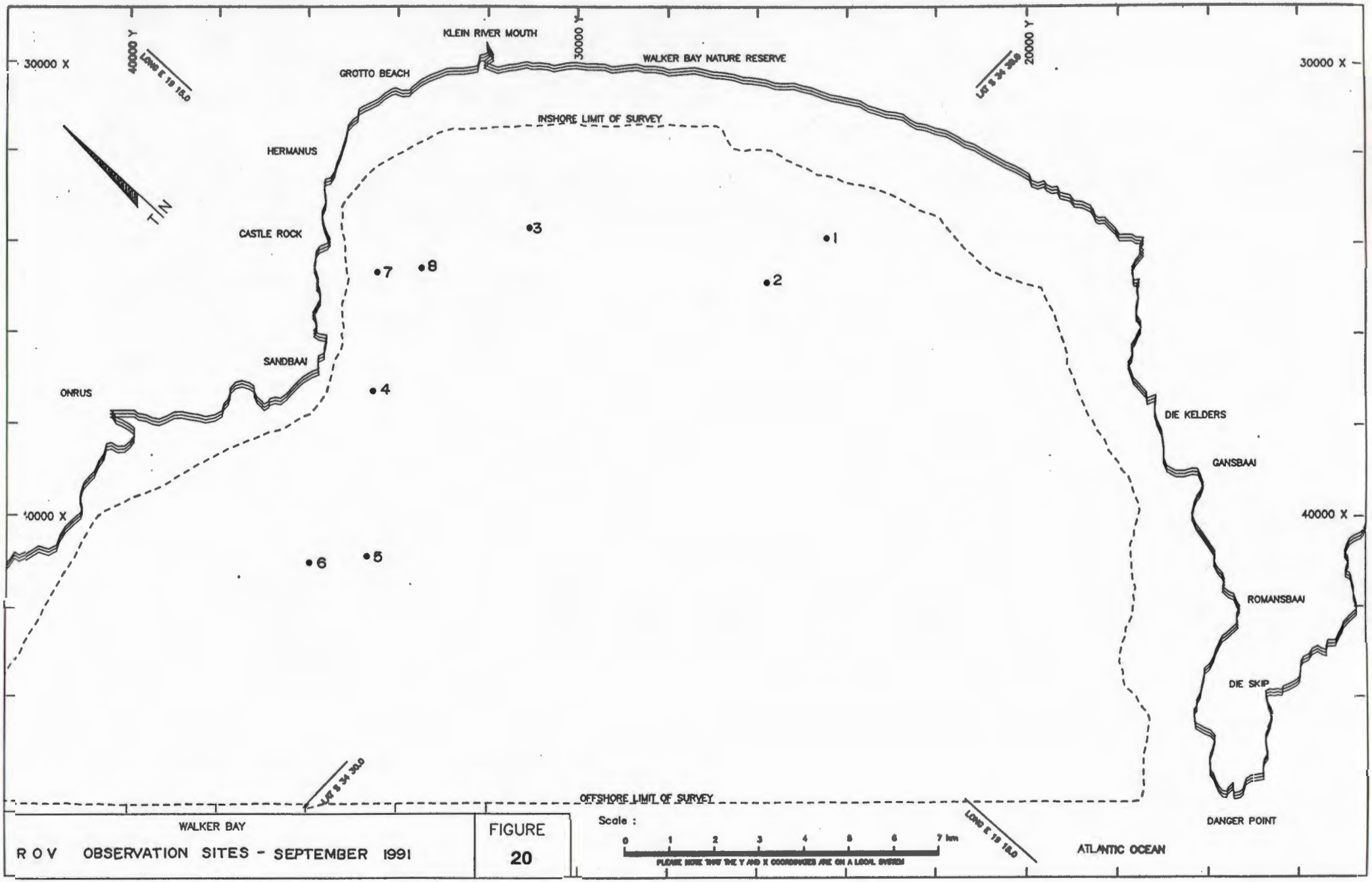

WALKER BAY

R O V OBSERVATION SITES - SEPTEMBER 1991

FIGURE 20

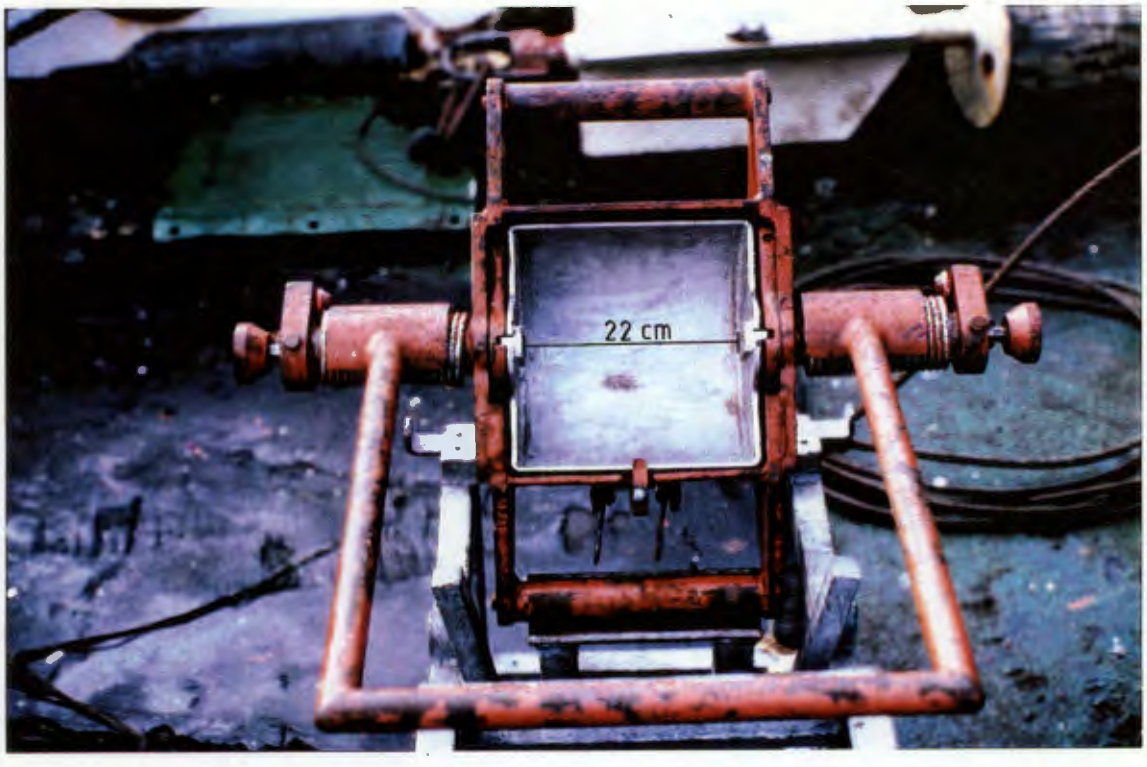

(a)

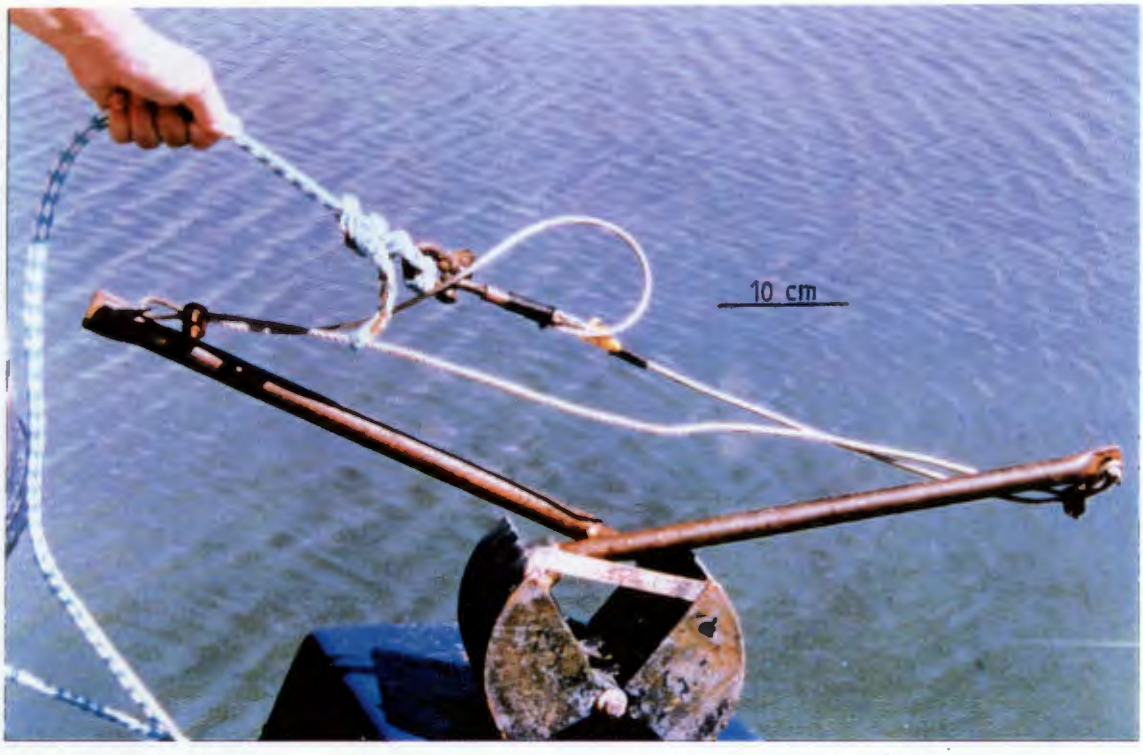

(b)

WALKER BAY

SEDIMENT SAMPLERS

(a) SHIPEK GRAB (Photo: Dr J Rogers)

(b) VAN VEEN GRAB (Photo: Dr J Rogers)

FIGURE

21

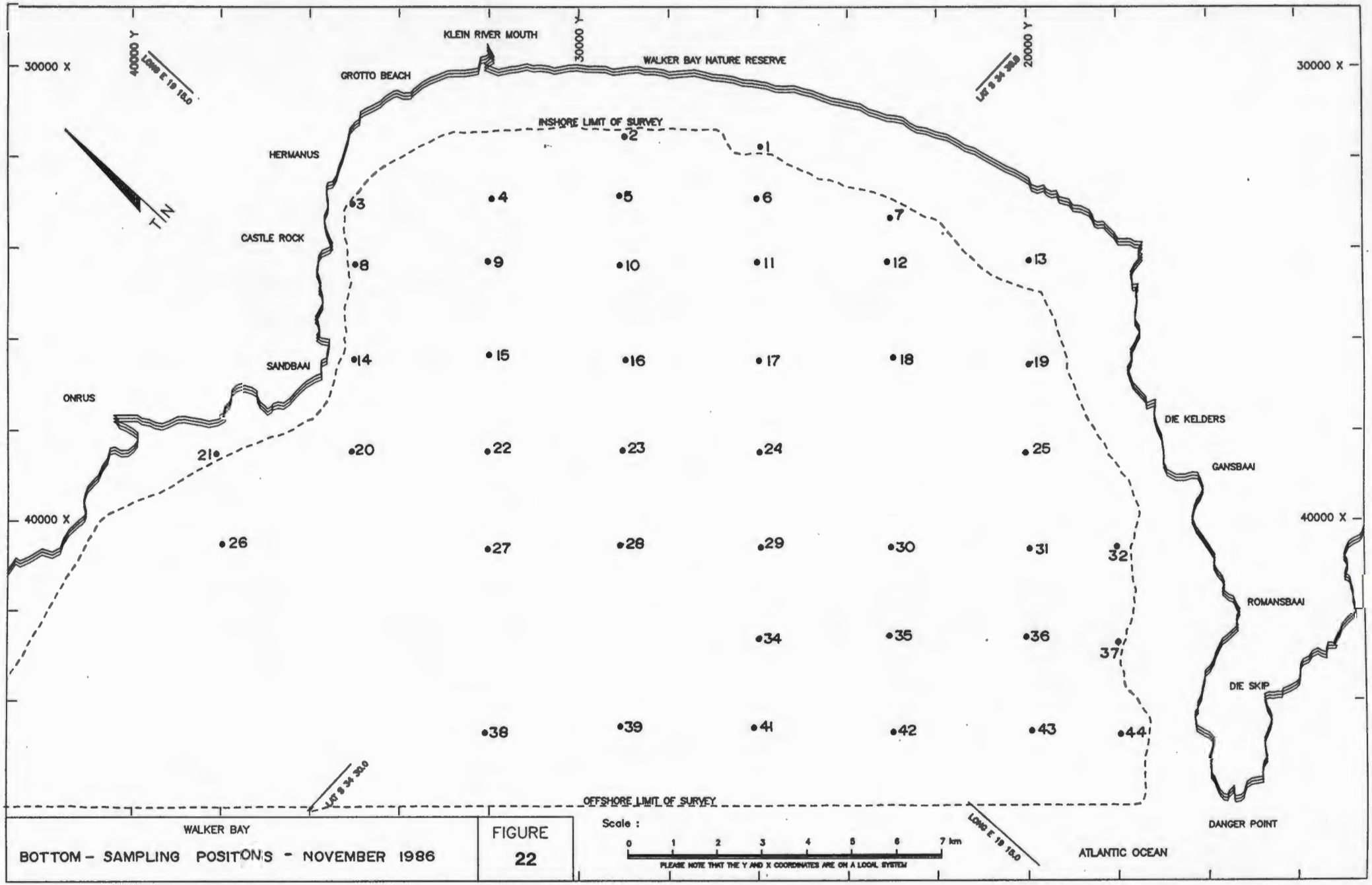

WALKER BAY

BOTTOM - SAMPLING POSITIONS - NOVEMBER 1986

FIGURE 22

TABLE 3: WALKER BAY: SAMPLE POSITIONS, NOVEMBER 1986

Sample No	Y-Co-ord.	X-Co-ord.	Sample No	Y-Co-ord.	X-Co-ord.
1/86	25958	31757	23/86	29002	38500
2/86	29021	31541	24/86	25965	38507
3/86	35010	32974	25/86	20007	38532
4/86	31940	32878	26/86	37979	40540
5/86	29114	32869	27/86	31992	40592
6/86	26011	32929	28/86	29043	40570
7/86	23032	33304	29/86	25960	42717
8/86	34965	34332	30/86	22972	40637
9/86	32008	34268	31/86	19987	40639
10/86	29050	34367	32/86	18010	40606
11/86	26034	34329	33/86	No position fix	
12/86	23067	34234	34/86	25960	42717
13/86	19936	34276	35/86	22996	42697
14/86	34940	36402	36/86	20015	42711
15/86	31948	36380	37/86	17985	42813
16/86	28961	36439	38/86	41060	44776
17/86	25968	36433	39/86	29043	44755
18/86	22968	36384	40/86	44054	44769
19/86	19979	36485	41/86	26051	44742
20/86	35027	38521	42/86	23007	44821
21/86	38018	38479	43/86	19978	44857
22/86	32005	38496	44/86	17940	44895

The smaller survey vessel, used during the 1987 follow-up survey necessitated the deployment of a manually operated, small Van Veen grab (Figure 21b) for the collection of the second sample suite. Since the Shipek and Van Veen grabs are similar in terms of sample volume it was assumed that the results would be comparable, although there may be a small discrepancy as far as depth of sampling is concerned. The Van Veen grab, because of its smaller mass, tends to scrape the material from the upper few centimetres, whereas the heavier, spring-loaded, Shipek grab takes a less disturbed sample to a deeper depth (approximately 10 cm). Should significant textural changes therefore occur within the upper few centimetres of the seafloor, the two techniques could yield different results.

At the time that the 1987 sample suite was collected, the surficial seafloor geology was known to a large extent and the sample locations could therefore be selected to provide optimum information. The samples were numbered 1/87 through 30/87 and Figure 23 shows their relative locations in the survey area. The corresponding x-y coordinates are given in Table 4.

The January 1990 sample suite was again obtained with a small Van Veen grab, with the purpose of obtaining additional coverage in certain areas of interest and to detect possible textural changes in time. They were numbered 1/90 through 51/90 and their positions and co-ordinates are shown in Figure 24 and Table 5 respectively.

In October 1988, 11 very closely spaced Van Veen grab samples were collected along a short traverse across a boundary between megarippled and rippled sediment. They were numbered 1/88 through 11/88, but were not treated as part of the overall sample suite from the area.

4.5 Sediment Sample Analyses

4.5.1 Grain size and carbonate content

The following is a description of the procedures followed in the analyses of the seabed

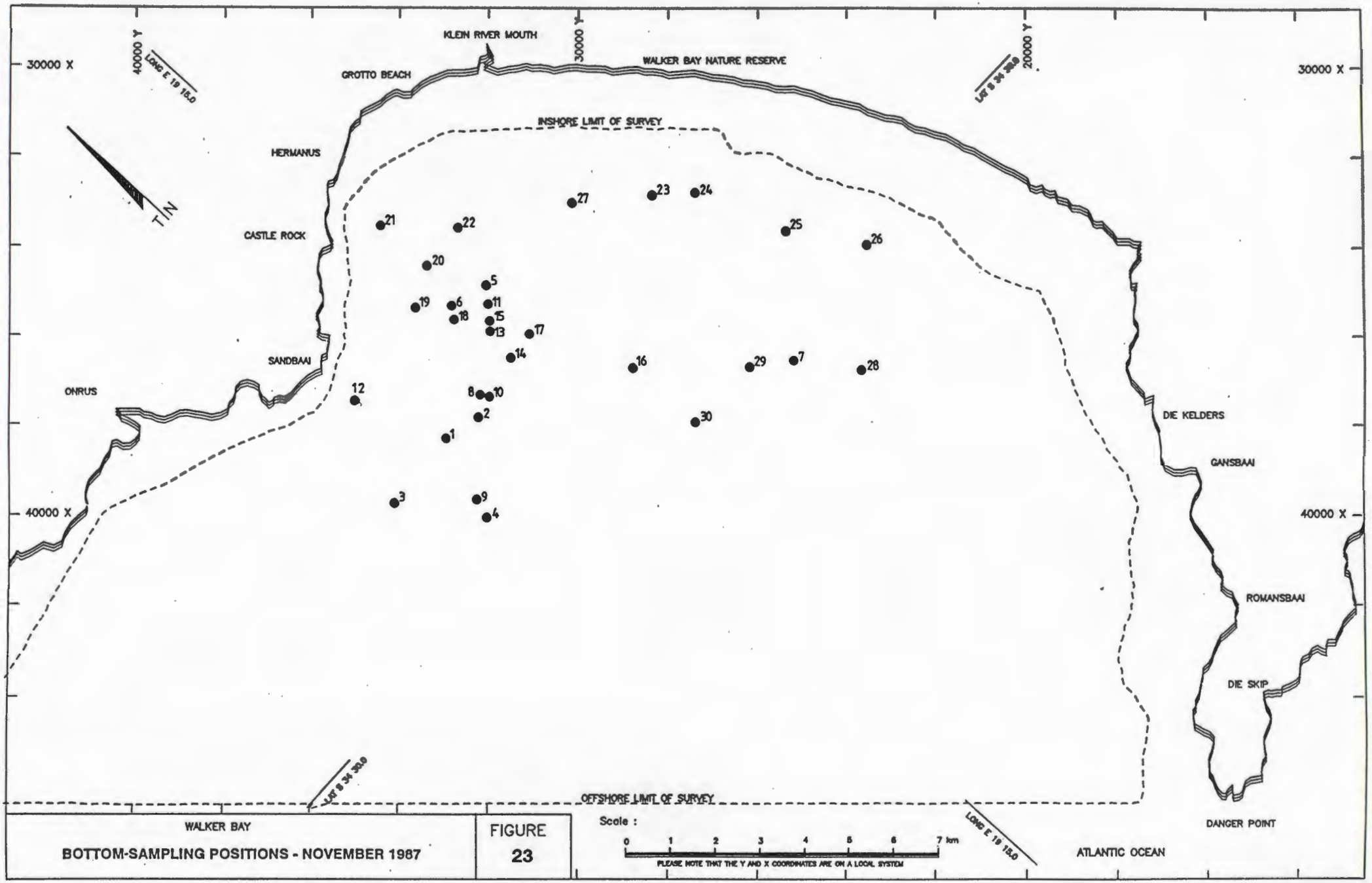

WALKER BAY

BOTTOM-SAMPLING POSITIONS - NOVEMBER 1987

FIGURE **23**

TABLE 4: WALKER BAY: SAMPLE POSITIONS, OCTOBER 1987

Sample No	X-Co-ord.	Y-Co-ord.
1/87		
2	37800	32200
3	39900	34000
4	40250	32000
5	35000	32000
6	35500	33000
7	36550	25300
8	37400	32200
9	39800	32300
10	37450	32100
11	35500	32100
12	37100	35000
13	36750	32000
14	36750	31500
15	35700	32000
16	36750	28700
17	36050	31000
18	35700	32700
19	35350	33500
20	34650	33300
21	33600	34300
22	33600	32700
23	32900	28300
24	33250	27000
25	33600	25300
26	33950	23500
27	33150	30000
28	36750	23500
29	36750	26000
30	38000	27000

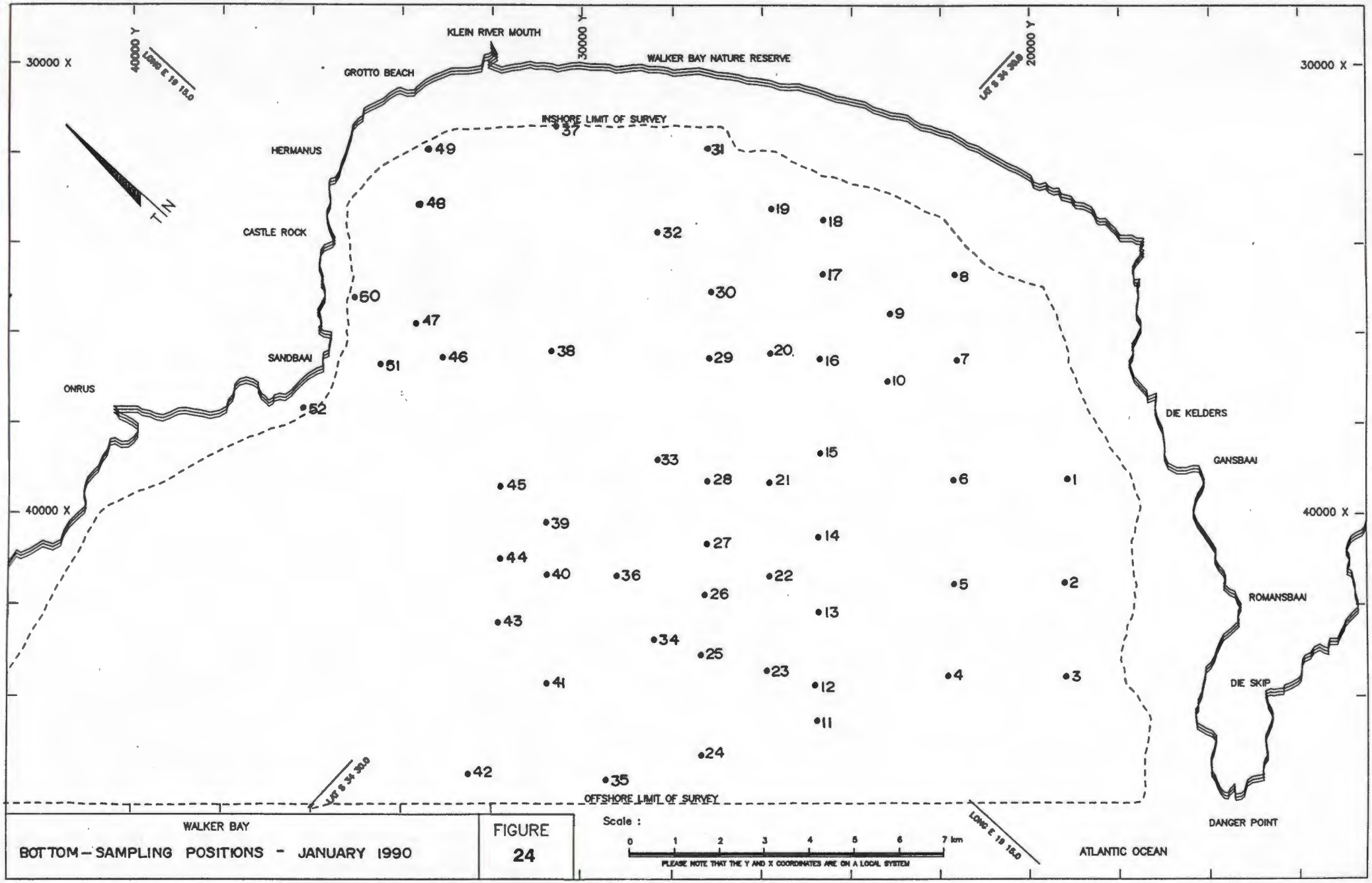

WALKER BAY

BOTTOM – SAMPLING POSITIONS - JANUARY 1990

FIGURE 24

TABLE 5: WALKER BAY: SAMPLE POSITIONS, JANUARY 1990

Sample No	X-Co-ord.	Y-Co-ord.	Sample No	X-Co-ord.	Y-Co-ord.
1/90	39400	19000	27	40850	27000
2	41700	19000	28	39500	27000
3	32800	19000	29	36750	27000
4	43800	21550	30	33250	27000
5	41700	21550	31	23000	27000
6	39400	21550	32	33900	28250
7	36700	21550	33	39000	28250
8	34800	21550	34	43000	28250
9	35700	23000	35	46100	29150
10	37500	23000	36	41100	29150
11	44800	24500	37	31450	30550
12	44000	24500	38	36600	30550
13	42300	24500	39	40500	30550
14	40650	24500	40	41600	30550
15	38850	24500	41	44000	30550
16	36700	24500	42	46100	32350
17	34800	24500	43	42600	31650
18	33600	24500	44	41400	31650
19	33300	25700	45	39700	31650
20	36600	25700	46	36750	33000
21	39500	25700	47	36000	33600
22	41500	25700	48	33550	33550
23	43650	25700	49	32000	33500
24	45550	27000	50	35400	35000
25	43300	27000	51	36900	34400
26	42000	27000			

surface samples that were collected in the course of the study as outlined in Section 4.4.1. A flowchart summarizing these procedures is given in Figure 25.

The wet sample was firstly oven-dried (at 100°C) and weighed, after which the complete sample was sieved through a 2mm screen to separate the mud and sand fraction from the gravel fraction. A representative subsample of the mud and sand fraction was subsequently obtained by splitting through a riffle splitter. To separate the mud fraction, the subsample was wet-sieved through a 63µm sieve and it was assumed that this process would also suffice in desalinating the sand fraction. The remaining sand fraction was again oven-dried and split to obtain a final sample of approximately 2g, while the remaining mud suspension was filtered, oven-dried and weighed to obtain the mud content as a percentage of the total weight of the sample. The gravel component was similarly weighed and expressed as a percentage of the total dry weight of the sample. The unleached sand fraction was settled through a settling tube to obtain the grain-size distribution of the sand fraction.

To obtain the percentage carbonate in the sand fraction, a weighed representative subsample was subjected to a leaching process, using dilute hydrochloric acid. The acid-insoluble residue was oven-dried and weighed and the carbonate fraction calculated by subtraction.

The use of a settling tube for textural analyses is described e.g. by Flemming (1976), Fromme (1977) and Brink and Rogers (1985), . Discrepancies do, however, often occur between the results obtained by different settling tubes and the reason can almost always be traced to the different calibration methods used, i.e. the relationship between settling velocity and grain size. In most cases, the calibration is based on the settling velocity of perfect glass spheres with a specific gravity of 2,65 and a shape factor of 1,0. The grain sizes obtained in such a case can be seen as "hydraulic grain diameters" and would not be similar to the results obtained by conventional sieving of the same sample. Studies by the writer (Lenhoff, 1981) have shown, however, that most settling tubes will give results comparable to sieving for the smaller grain sizes, but a significant deviation may be expected for the coarser fraction. This is mainly due to the slow settling rate of the coarser skeletal material with a low shape factor, giving rise to grain sizes which are smaller than would have been obtained by sieving. It must also be noted that fresh

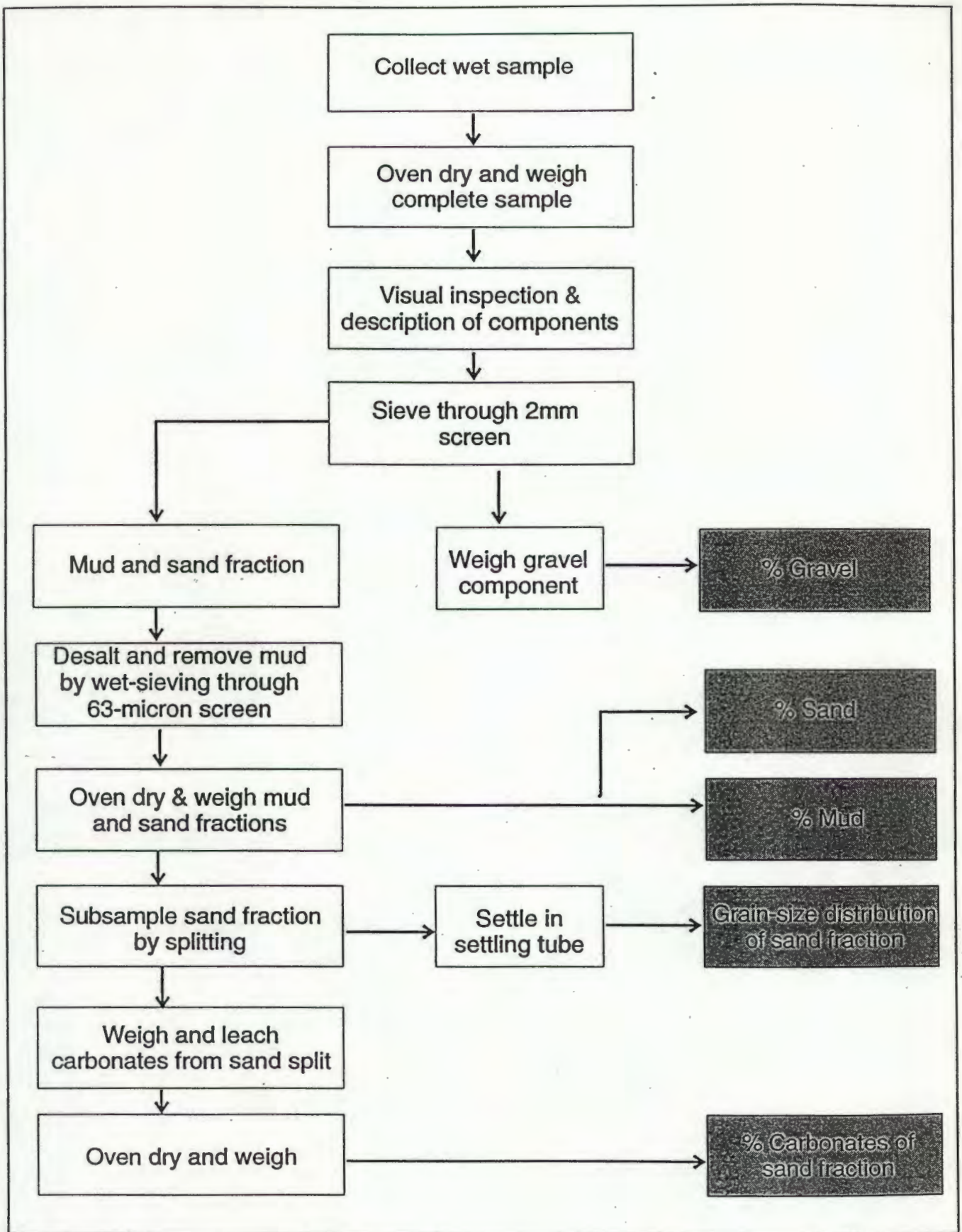

WALKER BAY

SEDIMENT SAMPLE ANALYSIS PROCEDURE

FIGURE 25

water at room temperature is normally used in a settling tube, resulting in a significantly higher effective density compared to the effective density in the low temperature/high salinity water of the marine environment. Settling-tube analyses therefore lead to mean grain sizes which are greater than those obtained by conventional sieving. For the purpose of this study it is assumed, however, that the nett effect of low shape factors and fluid density discrepancies on the settling tube results is insignificant, considering the fact that the expected errors may cancel each other out.

For this study, the settling tube in the Department of Geological Sciences at UCT was used. Grain-size data are provided in terms of hydraulic grain diameters (Equivalent Spherical Diameters). The settling-tube is computer linked and Figure 26 is an example of the printed output. The linear vertical scale (0 to 100%) only applies to the arithmetic cumulative curve. The 0%, 50% and 100% levels, however, also apply to the probability plot. Note that the frequency curve has been arbitrarily replotted, so that the major mode reaches the 50% level to aid inter-curve comparisons.

The settling curves for all the analysed sand fractions of Facies 3 and 4 are given in Appendices A and B respectively.

4.5.2 Component analysis of coarse fraction

The gravel fractions of the samples were visually inspected with the naked eye and the components noted. The sand fractions were analysed under a binocular microscope in order to identify the major and minor components, but no attempt was made to perform detailed counts. The results will be briefly discussed later.

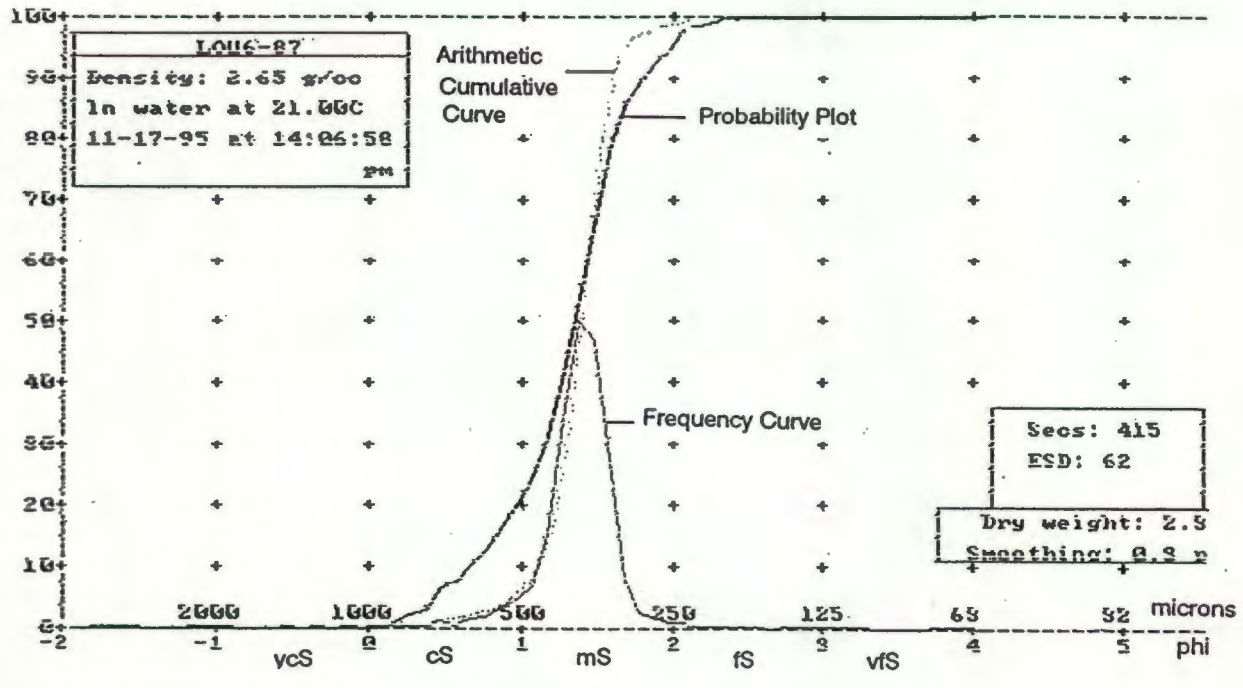


```
Moment statistics:
  Mean =  1.34 phi = 394.59u
  Std dev = 0.33 phi    Skewness = -3.11    Kurtosis = 37.82

Graphical values (F&W):
  Mean =  1.36 phi = 389.07u
  Median ( phi50) =  1.37 phi = 386.95u
  Sorting = 0.20 phi    Skewness = -0.14    Kurtosis =  1.32
```

ESD = Equivalent Spherical Diameter

WALKER BAY

EXAMPLE OF SETTLING TUBE COMPUTER OUTPUT

FIGURE

26

5. DATA PROCESSING

5.1 Navigational Data

The logged coordinates of the individual event marks were plotted on a scale of 1:80 000 and the resulting survey track chart was then used to compile the subsequent seismic and sidescan-sonar maps.

5.2 Marine Geophysical Data

5.2.1 Seismic Profiling

The transformation of seismic sub-bottom information from the analogue profiles into standard geological maps was done by using the survey track chart and the synchronized event marks on the records.

Penetration of up to 18 m into unconsolidated sediment in parts of the study area was achieved, using the Boomer sound source. Along most of the profiles, however, a continuous but irregular acoustic basement reflector can be followed at a depth well within the penetrative power of the profiler. This reflector was found to be impenetrable, even with the low-frequency Sparker system. The acoustic-basement reflector commonly crops out on the seafloor and clearly represents the upper surface of hard consolidated bedrock. No unconsolidated sediment is therefore likely to occur below the acoustic basement and any sediment-volume calculations from the seismic data can therefore be considered as a true reflection of the total sediment budget of the bay.

Values for the sediment thickness above the acoustic basement were measured at every event mark along each profile and plotted on the track chart. In the calculations, the speed of sound through unconsolidated sediments was assumed to be 1 500 m/s, as is generally accepted (McQuillin, 1979). These spot thicknesses were then manually contoured to obtain an isopach map of unconsolidated sediment thickness for the area.

Using the detailed bathymetric map of the area (Figure 10) and the sediment-thickness values, it was possible to compile a map showing the elevation of the acoustic basement reflector relative to Mean Sea Level. Since it was found that the acoustic basement represents the upper surface of the bedrock in the area, this map will be referred to as a "depth-to-bedrock" presentation.

5.2.2 Side-scan sonar

Analogue sidescan sonographs can either be of the "uncorrected" type or they can be "image corrected". In the former instance, the paper-drive speed of the recorder operates independently of the survey vessel's ground speed and the images are therefore normally compressed in the line of travel (Flemming 1976). Perpendicular to the line of travel a second distortion effect occurs, because the slant distance (i.e. the direct distance from the towfish to a specific seabed feature) is recorded, rather than the true horizontal distance from the ship's track to the object. As a result, the images of objects closer to the towfish are more compressed than the images of objects at the outer slant distances. The sidescan-data collected for the present study are of the uncorrected type. All measurements and information taken from the sonographs, therefore, had to be manually corrected for mapping purposes.

In image-corrected systems the paper speed is continually adjusted according to the vessel's speed-over-the-ground and it is also a function of the slant-range setting (normally 200 m). Perpendicular-to-the-line-of-travel corrections are also made, depending on the height of the towfish above the bottom and the slant distance of the specific object. It is therefore possible to obtain isometric images, having the same scale in all directions. If the images along adjacent lines overlap it is possible to construct a sidescan mosaic of the surveyed area. Having a mosaic as a base map, the mapping procedures are greatly simplified.

Using the event marks on the sonographs and applying the necessary corrections outlined above, the acoustic images along each survey line were mapped out on the survey track chart. Object height-estimations from the side-scan records were done by

directly observing the first bottom return signal and by using the direct relationship between object height, length of acoustic shadow, towfish-height and slant distance. The former method was useful in determining the general scale of bed roughness, i.e. relief, whereas the acoustic shadow method was used for calculating the height of specific objects not directly under the towfish but within the slant range used.

The data showed that the seafloor in the study area can be described in terms of four different sonograph facies, hereafter referred to as Facies 1, 2, 3 and 4, each displaying very characteristic reflective properties. Facies 1 and 2 represent rock outcrops of different relief characteristics, whereas Facies 3 and 4 represent sediment-covered areas with different bedform and grain-size characteristics. These facies will be discussed in detail in the next chapter.

The examples of sidescan images accompanying this report were computer generated by digitizing the original record with an optical scanner and printing on a high-resolution colour printer.

5.2.3 ROV observations

Still photographs were produced from the video recordings by means of a frame-grabbing technique, which resulted in an inevitable loss of resolution when compared to the original recording. They are nevertheless still of acceptable quality and will be used in this report to illustrate the different sonograph facies. Unfortunately no indication of scale was shown on the video footage. In estimating physical dimensions, the writer used objects of known sizes such as shell-debris and other marine organisms for scale purposes wherever they occurred on the video recordings.

5.3 Sedimentological Data

As shown on Figures 22, 23 and 24, seabed sampling was attempted at a total of 125 locations during the course of this study; 44 in 1986, 30 in 1987 and 51 in 1990. The main objective of the sampling exercises was to provide groundtruth for the

interpretation of the different sonograph facies, which explains why the samples were collected on 3 different occasions. The sidescan-sonar results from the 3 surveys have shown that the facies patterns were unaltered between 1986 and 1990 - an aspect that will be discussed in more detail in Chapter 7. Against this background, it was decided to treat the seabed samples from the 3 surveys as one suite and to assume that they are generally representative of the seabed materials in the area. A direct comparison of sediment samples taken at different times in the same general area has shown that such an assumption is justified.

Since the boundaries between Facies 3 and 4 are generally gradational and not clear-cut, only samples that originate from well within the boundaries of each facies were used in this study. This was done to eliminate possible spurious statistical results caused by border-line samples.

Tables 6 and 7 show the percentages of gravel, sand and mud and the textural class after Folk (1968) for the Facies 3 and 4 samples respectively.

Tables 8 and 9 show the carbonate content and the settling-tube results for the unleached sand fractions of the Facies 3 and 4 samples, respectively.

TABLE 6: TEXTURAL CLASS ANALYSIS OF FACIES 3 SAMPLES

Samples No	% Gravel	% Sand	% Mud	Textural class (Folk, 1968)
06/86	0	100	0	G
09/86	18	82	0	gS
14/86	9	91	0	gS
15/86	40	60	0	sG
17/86	0	100	0	G
18/86	0	100	0	S
22/86	34	66	0	sG
26/86	21	79	0	gS
27/86	33	67	0	sG
28/86	0	100	0	S
5/87	47	53	0	sG
6/87	3	97	0	S
7/87	0	100	0	S
8/87	6	94	0	gS
10/87	1	99	0	S
13/87	77	23	0	sG
14/87	0	100	0	S
15/87	18	82	0	gS
23/87	45	55	0	sg
25/87	9	91	0	gS
26/87	24	76	0	gS
28/87	57	43	0	sG
29/87	1	99	0	S
30/87	60	40	0	sG
09/90	0	100	0	S
10/90	24	76	0	gS
12/90	62	38	0	Sg

TABLE 6: (continue)

Samples No	% Gravel	% Sand	% Mud	Textural class (Folk, 1968)
13/90	0	100	0	S
14/90	0	100	0	S
14/86	0	100	0	S
16/90	3	97	0	(g)S
18/90	9	91	0	gS
19/90	0	100	>0,5	S
20/90	0	100	>0,5	S
23/90	0	100	>0,5	S
33/90	0	100	0	S
34/90	42	58	0	sG
36/90	0	100	0	S
38/90	55	45	0	sG
39/90	0	100	0	S
40/90	47	53	0	sG
41/90	5	95	0	gS
43/90	66	34	0	sG
45/90	33	67	0	sG
46/90	26	74	0	gS
48/90	16	84	0	gS
51/90	8	92	0	gS

S = Sand
(g)S = Slightly gravelly sand
gS = Gravelly sand
sG = Sandy gravel
G = Gravel

TABLE 7: TEXTURAL CLASS ANALYSIS OF FACIES 4 SAMPLES

Samples No	% Gravel	% Sand	% Mud	Textural class (Folk, 1968)
01/86	0	100	<0,5	S
02/86	0	100	<0,5	S
03/86	0	100	<0,5	S
04/86	0	100	<0,5	S
07/86	0	100	<0,5	S
08/86	0	100	<0,5	S
11/86	0	100	<0,5	S
12/86	0	100	<0,5	S
13/86	0	100	<0,5	S
19/86	0	100	<0,5	S
24/86	0	100	<0,5	S
25/86	0	100	<0,5	S
29/86	0	100	<0,5	S
30/86	0	100	<0,5	S
31/86	0	100	<0,5	S
32/86	0	100	<0,5	S
34/86	0	100	<0,5	S
35/86	0	100	<0,5	S
36/86	0	100	<0,5	S
37/86	0	100	<0,5	S
41/86	0	100	<0,5	S
42/86	0	100	<0,5	S
43/86	0	100	<0,5	S
44/86	0	100	<0,5	S
12/87	23	77	<0,5	gS
01/90	0	100	<0,5	S

TABLE 7: (continue)

Samples No	0% Gravel	% Sand	% Mud	Textural class (Folk, 1968)
02/90	0	100	<0,5	S
03/90	0	100	<0,5	S
04/90	0	100	<0,5	S
06/90	0	100	<0,5	S
07/90	0	100	<0,5	S
08/90	6	94	<0,5	S
11/90	0	100	<0,5	S
15/90	0	100	<0,5	S
17/90	0	100	<0,5	S
21/90	0	100	<0,5	S
24/90	0	100	<0,5	S
27/90	0	100	<0,5	S
29/90	0	100	<0,5	S
30/90	0	100	<0,5	S
31/90	0	100	<0,5	S
32/90	0	100	<0,5	S
37/90	0	100	<0,5	S
47/90	0	100	<0,5	S
49/90	0	100	<0,5	S
50/90	0	100	<0,5	S

S = Sand
gS = Gravelly sand

TABLE 8: SAND-FRACTION ANALYSIS OF FACIES-3 SAMPLES

Sample No	% $CaCo_3$	Moment Statistics				Graphical Statistics					Mode	
		Mean (phi)	St Dev (phi)	Skew	Kurt	Mean (phi)	Median (phi)	Sort (phi)	Skew	Kurt	Primary (phi)	Second (phi)
6/86	71	2,15	0,63	-2,08	13,00	2,18	2,28	0,54	-0,32	1,13	2,4	1,8
9/86	71	0,91	0,50	1,64	10,89	0,87	0,79	0,40	0,43	1,45	0,7	
14/86	47	1,43	0,42	-1,05	17,03	1,44	1,47	0,32	-0,16	1,28	1,6	
15/86	5	0,25	0,27	1,22	30,77	0,28	0,29	0,21	-0,22	1,29	0,3	
17/86	65	1,32	0,33	-1,37	39,07	1,31	1,30	0,21	0,11	1,25	1,3	
18/86	71	1,97	0,42	-1,47	19,74	1,97	1,99	0,35	-0,08	1,16	2,1	
22/86	4	0,01	0,30	5,27	69,42	0,01	0,02	0,22	-0,05	1,01	0,0	
26/86	100	0,90	0,46	2,86	18,35	0,84	0,85	0,18	-0,02	1,22	0,9	
27/86	10	0,01	0,30	5,21	75,00	0,02	0,01	0,26	0,06	1,08	0,0	0,6
28/86	75	2,06	0,59	-0,98	8,50	2,07	2,11	0,56	-0,09	1,01	2,2	
5/87	66	0,77	0,44	1,77	16,03	0,75	0,72	0,28	0,19	1,11	0,7	
6/87	45	1,34	0,33	-3,11	37,82	1,36	1,37	0,20	-0,14	1,32	1,3	
7/87	38	1,18	0,32	-0,21	34,70	1,18	1,18	0,20	0,02	1,27	1,2	
8/87	4	0,04	0,28	0,53	23,98	0,04	0,04	0,23	0,08	1,26	0,1	
10/87	33	1,02	0,37	-1,13	19,52	1,04	1,04	0,27	-0,01	1,40	1,1	
13/87	5	-0,09	0,15	-2,05	234,59	-0,05	-0,05	0,20	-0,01	1,07	0,0	
14/87	20	1,19	0,34	-0,52	22,36	1,20	1,21	0,24	-0,13	1,44	1,2	0,3
15/87	32	0,52	0,37	4,00	39,46	0,50	0,50	0,21	0,0	1,27	0,5	
23/87	52	0,00	0,35	6,56	73,80	0,0	-0,01	0,24	0,07	0,94	0,0	
25/87	74	0,64	0,37	2,36	40,30	0,63	0,64	0,19	-0,03	1,04	0,7	
26/87	100	0,74	0,35	2,11	35,70	0,73	0,74	0,22	-0,03	1,08	0,8	
28/87	71	0,54	0,32	3,12	43,39	0,54	0,54	0,17	-0,09	1,04	0,5	
29/87	72	1,42	0,39	-0,56	20,58	1,42	1,38	0,28	0,18	1,13	1,3	
30/87	67	0,69	0,37	3,71	37,44	0,65	0,65	0,16	0,08	1,16	0,6	
9/90	69	1,14	0,45	1,25	17,75	1,11	1,08	0,32	0,19	1,20	1,0	
10/90	32	0,30	0,36	5,91	59,67	0,29	0,29	0,16	-0,03	1,10	0,3	
12/90	16	0,20	0,50	3,06	21,02	0,16	0,17	0,34	-0,01	1,30	0,2	-0,4

TABLE 8: (continue)

Sample No	% $CaCo_3$	Moment Statistics				Graphical Statistics					Mode	
		Mean (phi)	St Dev (phi)	Skew	Kurt	Mean (phi)	Median (phi)	Sort (phi)	Skew	Kurt	Primary (phi)	Second (phi)
13/90	83	0,75	0,39	4,01	32,46	0,71	0,72	0,20	0,01	1,20	0,7	
14/90	78	0,95	0,40	2,54	26,15	0,93	0,90	0,25	0,21	1,24	0,8	
16/90	57	0,92	0,25	-3,65	42,16	0,92	0,92	0,18	0,03	1,22	0,9	
18/90	87	0,78	0,34	1,02	20,31	0,77	0,77	0,23	-0,07	1,22	0,8	
19/90	82	0,62	0,34	2,74	30,26	0,61	0,62	0,19	-0,12	1,11	0,7	
20/90	67	1,35	0,35	-0,84	20,13	1,34	1,32	0,26	0,20	1,50	1,3	
22/90	70	0,90	0,41	2,57	21,05	0,85	0,84	0,26	0,21	1,55	0,8	
23/90	85	2,20	0,56	-1,29	10,13	2,23	2,25	0,49	-0,11	1,36	2,3	
33/90	82	1,66	0,43	-1,13	22,13	1,65	1,64	0,30	0,04	1,22	1,6	
34/90	70	0,73	0,48	1,10	15,99	0,75	0,78	0,33	-0,30	1,37	0,8	0,0
36/90	73	1,36	0,46	0,28	8,75	1,35	1,31	0,41	0,18	1,02	1,2	
38/90	26	0,51	0,37	4,06	42,32	0,48	0,48	0,16	0,04	1,11	0,4	
39/90	53	1,92	0,52	-1,12	12,29	1,92	1,94	0,43	-0,05	1,07	2,0	
40/90	9	-0,04	0,44	4,60	40,40	-0,07	-0,10	0,30	0,21	1,35	-0,2	0,1
41/90	80	0,94	0,40	2,28	27,77	0,92	0,94	0,23	-0,10	1,10	1,0	
43/90	29	1,67	0,89	-0,40	2,94	1,64	1,90	0,89	-0,36	0,97	2,2	0,4
45/90	4	0,25	0,45	2,94	21,76	0,22	0,23	0,31	-0,02	1,14	0,2	
46/90	71	0,83	0,44	1,88	21,16	0,90	0,91	0,26	-0,03	1,22	0,9	
48/90	61	2,49	0,49	-2,80	21,52	2,52	2,58	0,39	-0,34	1,52	2,6	
51/90	78	0,96	0,39	1,69	24,44	0,94	0,95	0,23	-0,04	1,22	1,0	

TABLE 9: SAND-FRACTION ANALYSIS OF FACIES-4 SAMPLES

Sample No	% $CaCo_3$	Moment Statistics				Graphical Statistics					Mode	
		Mean (phi)	St Dev (phi)	Skew	Kurt	Mean (phi)	Median (phi)	Sort (phi)	Skew	Kurt	Primary (phi)	Second (phi)
1/86	83	2,49	0,33	-3,18	44,80	2,50	2,49	0,25	0,04	1,08	2,4	
2/86	80	2,54	0,37	-4,19	45,29	2,57	2,56	0,25	0,00	1,33	2,5	
3/86	54	1,38	0,58	-0,99	7,19	1,41	1,42	0,49	-0,10	1,41	1,4	
4/86	91	0,79	0,32	1,96	33,80	0,78	0,78	0,21	-0,01	1,16	0,8	
7/86	72	2,40	0,60	-2,10	11,87	2,40	2,55	0,54	-0,45	1,70	2,6	1,5
8/86	49	2,17	0,47	-1,41	15,27	2,17	2,19	0,41	-0,05	1,12	2,2	
11/86	74	2,69	0,56	-3,38	19,92	2,79	2,78	0,39	-0,18	2,15	2,8	
12/86	78	0,66	0,28	0,42	23,41	0,65	0,66	0,19	-0,04	1,10	0,7	
13/86	80	2,69	0,35	-6,25	78,60	2,71	2,70	0,22	0,08	1,06	2,7	
19/86	73	2,66	0,46	-4,54	38,83	2,72	2,72	0,30	-0,16	1,60	2,7	
24/86	75	2,00	0,49	-2,07	14,18	2,04	2,04	0,36	-0,03	1,29	2,1	
25/86	73	2,22	0,64	-1,02	5,23	2,24	2,39	0,61	-0,35	0,85	2,6	1,7
29/86	88	1,41	0,36	0,03	33,60	1,40	1,40	0,22	0,05	1,29	1,4	
30/86	89	2,20	0,45	-1,35	15,77	2,21	2,21	0,40	0,02	1,21	2,2	
31/86	67	2,73	0,44	-4,65	48,83	2,75	2,74	0,25	0,03	1,33	2,8	
32/86	74	2,80	0,38	-5,64	65,01	2,81	2,79	0,21	0,15	1,13	2,8	
34/86	81	2,35	0,73	-1,19	6,79	2,36	2,46	0,68	-0,25	1,40	2,4	1,3
35/86	84	2,47	0,47	-2,31	22,90	2,48	2,49	0,37	-0,05	1,16	2,5	
36/86	63	2,72	0,43	-3,54	32,75	2,76	2,77	0,30	-0,22	1,82	2,8	
37/86	74	2,79	0,45	-5,54	50,40	2,83	2,82	0,23	-0,01	1,25	2,8	
41/86	84	2,06	0,64	-0,58	5,53	2,06	2,09	0,62	-0,07	0,95	2,2	
42/86	89	2,42	0,64	-2,32	13,43	2,49	2,51	0,49	-0,18	1,51	2,5	2,1
43/86	71	2,65	0,46	-2,95	28,04	2,63	2,67	0,36	-0,20	1,40	2,7	
44/86	71	2,81	0,42	-5,67	55,92	2,84	2,84	0,23	-0,03	1,15	2,8	
12/87	70	0,74	0,38	3,32	33,95	0,73	0,74	0,22	-0,10	1,16	0,8	
1/90	69	2,52	0,66	-2,44	10,62	2,66	2,69	0,48	-0,41	2,60	2,8	
2/90	64	2,82	0,38	-7,27	92,28	2,83	2,82	0,19	0,07	1,09	2,8	

TABLE 9: (continue)

Sampie No	% $CaCo_3$	Moment Statistics				Graphical Statistics					Mode	
		Mean (phi)	St Dev (phi)	Skew	Kurt	Mean (phi)	Median (phi)	Sort (phi)	Skew	Kurt	Primary (phi)	Second (phi)
3/90	71	2,83	0,31	-6,63	100,07	2,84	2,83	0,19	0,13	1,06	2,8	
4/90	80	2,77	0,38	-4,19	54,47	2,77	2,76	0,27	0,09	1,15	2,7	
6/90	63	2,49	0,55	-2,69	22,57	2,50	2,55	0,41	-0,17	1,14	2,6	
7/90	70	2,65	0,45	-3,29	31,13	2,69	2,69	0,32	-0,11	1,49	2,7	
8/90	75	0,67	0,42	3,70	33,07	0,63	0,64	0,19	-0,03	1,03	0,6	
11/90	87	2,40	0,71	-1,02	5,63	2,42	2,53	0,70	-0,27	1,17	2,6	1,0
15/90	83	1,69	0,36	-0,71	23,72	1,69	1,70	0,25	-0,08	1,27	1,8	
17/90	77	2,51	0,50	-2,50	19,72	2,53	2,63	0,43	-0,34	1,12	2,7	1,3
21/90	80	2,27	0,45	-1,79	21,86	2,27	2,26	0,37	0,07	1,18	2,2	
24/90	79	2,45	0,71	-1,50	7,46	2,50	2,56	0,65	-0,23	1,34	2,6	0,2
27/90	83	1,37	0,42	-0,39	13,57	1,36	1,37	0,35	-0,02	1,23	1,4	
29/90	78	1,99	0,35	-1,55	33,37	1,99	1,99	0,24	0,01	1,22	2,0	
30/90	76	2,82	0,39	-5,38	60,33	2,85	2,85	0,25	-0,04	1,26	2,8	
31/90	80	2,57	0,42	-4,96	47,98	2,61	2,61	0,24	-0,07	1,26	2,6	
32/90	65	2,75	0,42	-5,79	61,47	2,79	2,78	0,26	-0,01	1,28	2,8	
37/90	84	2,56	0,34	-5,24	70,21	2,58	2,57	0,22	0,04	1,11	2,5	
47/90	43	1,35	0,34	-0,81	37,80	1,35	1,36	0,21	-0,11	1,22	1,3	
49/90	61	0,74	0,43	3,46	27,90	0,71	0,71	0,22	-0,02	1,10	0,8	
50/90	50	2,03	0,48	-0,91	10,51	2,04	2,02	0,44	0,06	1,15	2,0	

6. RESULTS

6.1 Seismic Profiling

The seismic-profiler data were primarily used to obtain the thickness of the overlying unconsolidated sediments. The resolution of the profiler (0,5 to 1,0 m) was not sufficient to detect any details of possible small-scale sedimentological structures within the overlying succession, other than the occasional occurrence of discontinuous internal reflectors indicating possible textural changes in depth. As indicated in Section 3.2.2, the acoustic basement was correlated with the upper surface of the pre-Mesozoic Bokkeveld strata. This basement reflector could be followed almost continuously, along all the lines and the isopach values are considered to be accurate. Figure 27 shows a typical example of the seismic profiles.

Figure 28 shows the variation in sediment thickness over the area, together with a swell rose indicating the dominant wave parameters. The thickness values range between 0 metres and in excess of 18 metres, with the thickest accumulation of unconsolidated sediment occurring towards the east in the shallower water off Gansbaai. The headland at Danger Point shelters this area from waves coming from the south-eastern quadrant.

The central and northern sections of the bay are dominated by rock outcrops and relatively thin sediment cover. Off Hermanus a localized thick deposit (15-18 m) occurs which most likely belongs to the nearshore sand prism not surveyed along the rest of the coastline.

According to Birch (1978), the nearshore sediment wedge between Cape Town and Cape Agulhas (Figure 1) is poorly developed due to minor fluvial supply and the predominance of closed estuaries. The Klein River is a prime example of insignificant sediment supply as will be discussed later. The relatively high biogenic content of the Walker Bay sediments which will be illustrated later, also indicates the low fluvial input of terrigenous material to the sediment budget of the area.

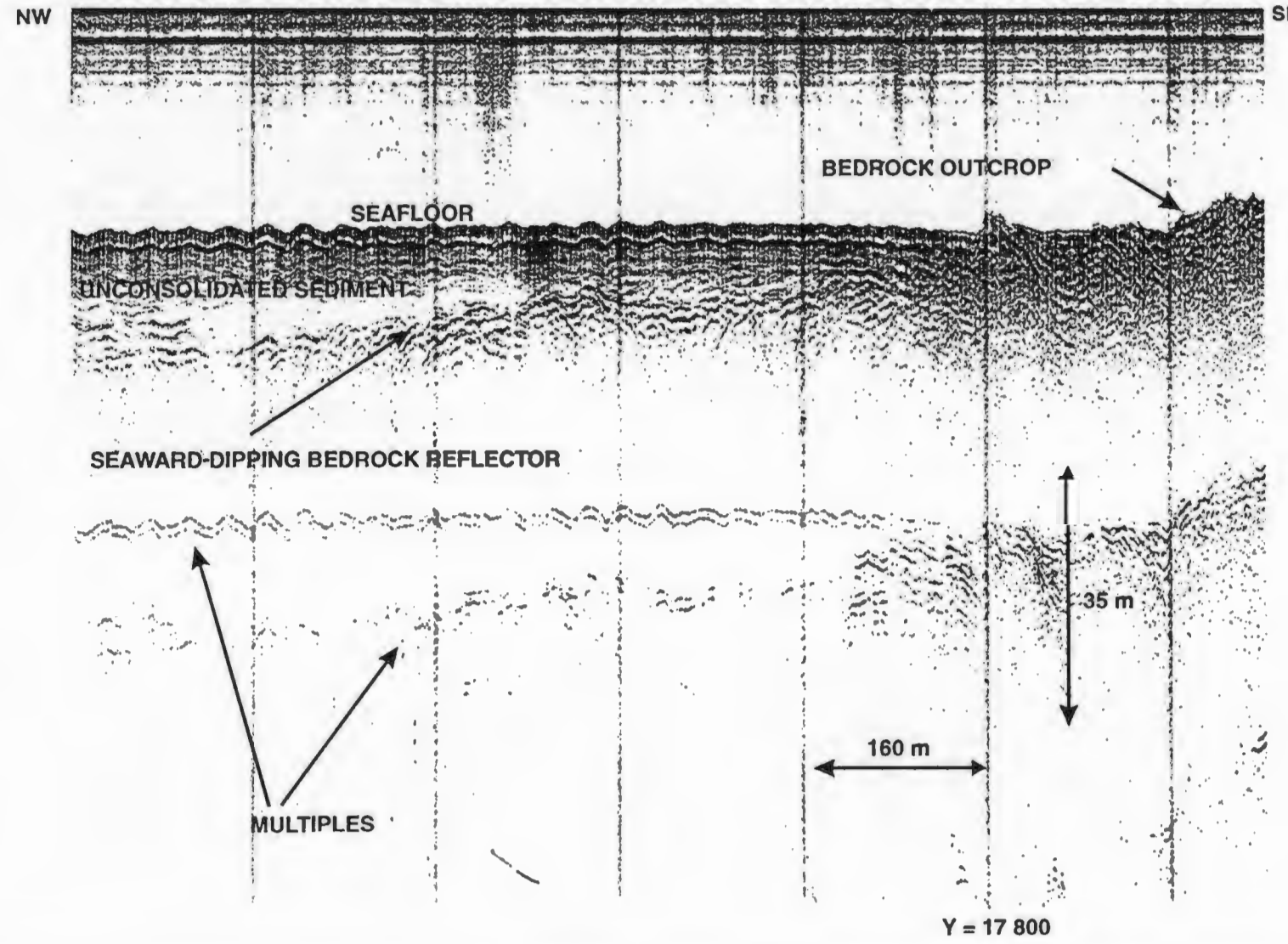

WALKER BAY
BOOMER PROFILE - LINE 38 (OFF DANGER POINT)
SWEEP = 500ms

FIGURE
27

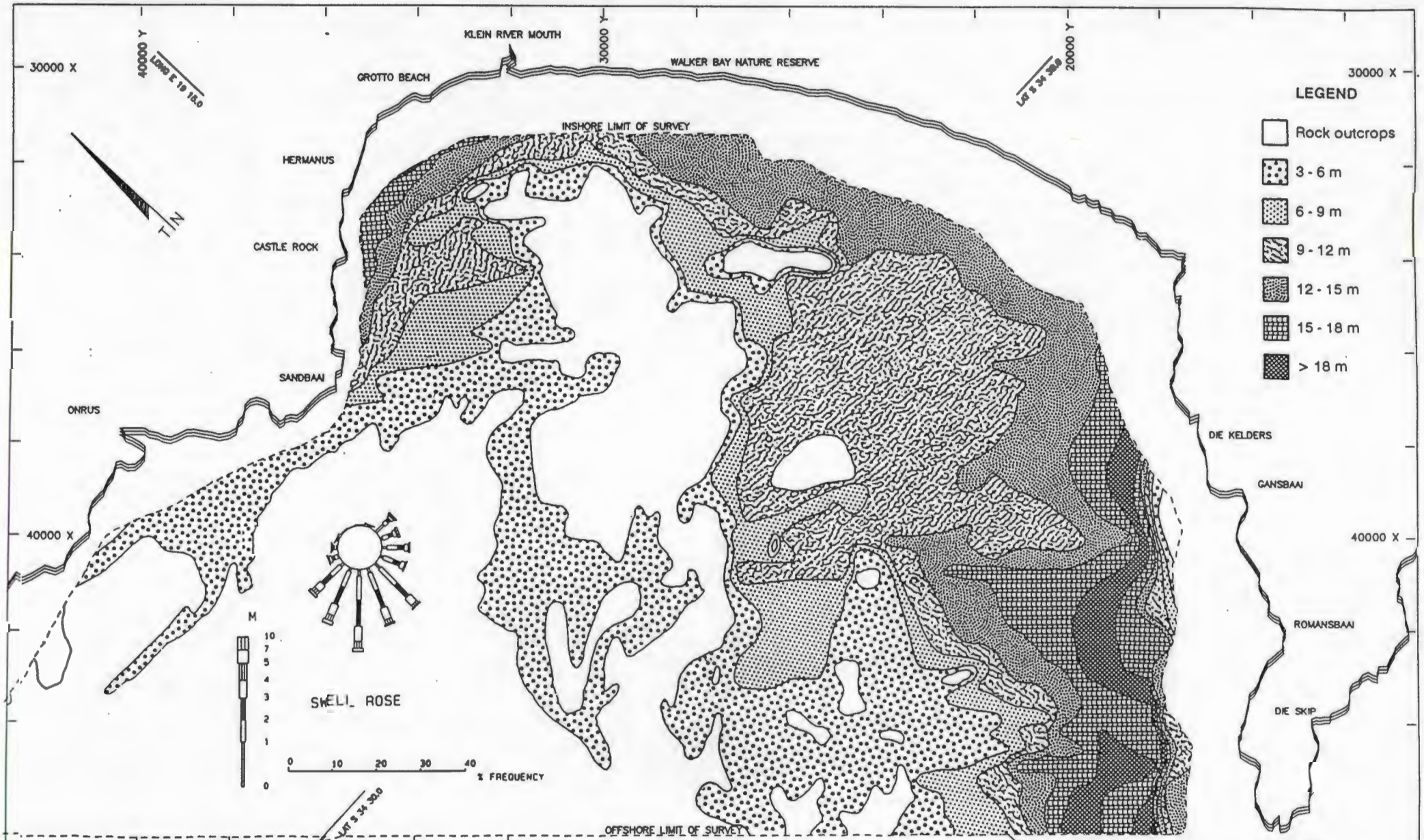

WALKER BAY

ISOPACHS OF UNCONSOLIDATED SEDIMENT COVER

FIGURE **28**

To the northwest and southeast of Walker Bay minor quantities of unconsolidated sediment occur in a narrow zone, approximately 5 km wide (Birch, 1978). The swell driven longshore drift on the Cape south coast is generally considered to be east-moving (Birch, 1978). In Walker Bay, however, wave directions covering the full southwestern quadrant commonly occur (Figure 28) which could result in frequent changes in the nett direction of longshore drift. It was stated earlier that Walker Bay approaches a log spiral shape, typical of many embayments on the south coast . Ideally a log spiral bay in equilibrium would have zero nett longshore sediment transport (Bremner, 1978). The relatively thick accumulation of sediment off the Gansbaai coast (Figure 28), however, suggests that the nett longshore sediment movement in Walker Bay is towards the east. The rocky headland at Danger Point appears to offer a low energy environment on its western, wave-sheltered side, resulting in an accumulation of nearshore transported sediment.

By adding the sediment-thickness value to the water depth (Figure 10), the elevation of acoustic basement relative to Mean Sea Level (MSL) was also calculated. Figure 29 shows these values as a depth-to-basement map, contoured at 10 m intervals, revealing the bedrock topography over the entire area. As can be expected, the bedrock contours generally follow the shape of the coastline, forming an embayment cut into relatively soft shales of the Bokkeveld Group (Figure 3). The northwestern and southeastern flanks of the bay closely coincide with geological contacts between Bokkeveld Group shales and the more resistant Table Mountain Group sandstones. These contacts extend for considerable distances both onshore and offshore and are the major factors controlling the bedrock topography and the shoreline configuration of the area. Figure 29 also shows a local 3 km wide valley-like depression in the bedrock, orientated in a NE-SW direction and situated off the present Klein River mouth. This feature is interpreted as a submarine extension of the Klein River valley, cut into bedrock at times of lower sea-levels. The channel can be followed for a distance of approximately 8 km seaward of the present mouth with the channel floor reaching a depth of 20 m below the surrounding seafloor off Sandbaai. Sediment up to 9 metres thick partially cover the channel floor. Birch (1979) surveyed a relict sediment-filled channel cut into similar bedrock off the Breede River mouth, approximately 60 km to the east of Walker Bay.

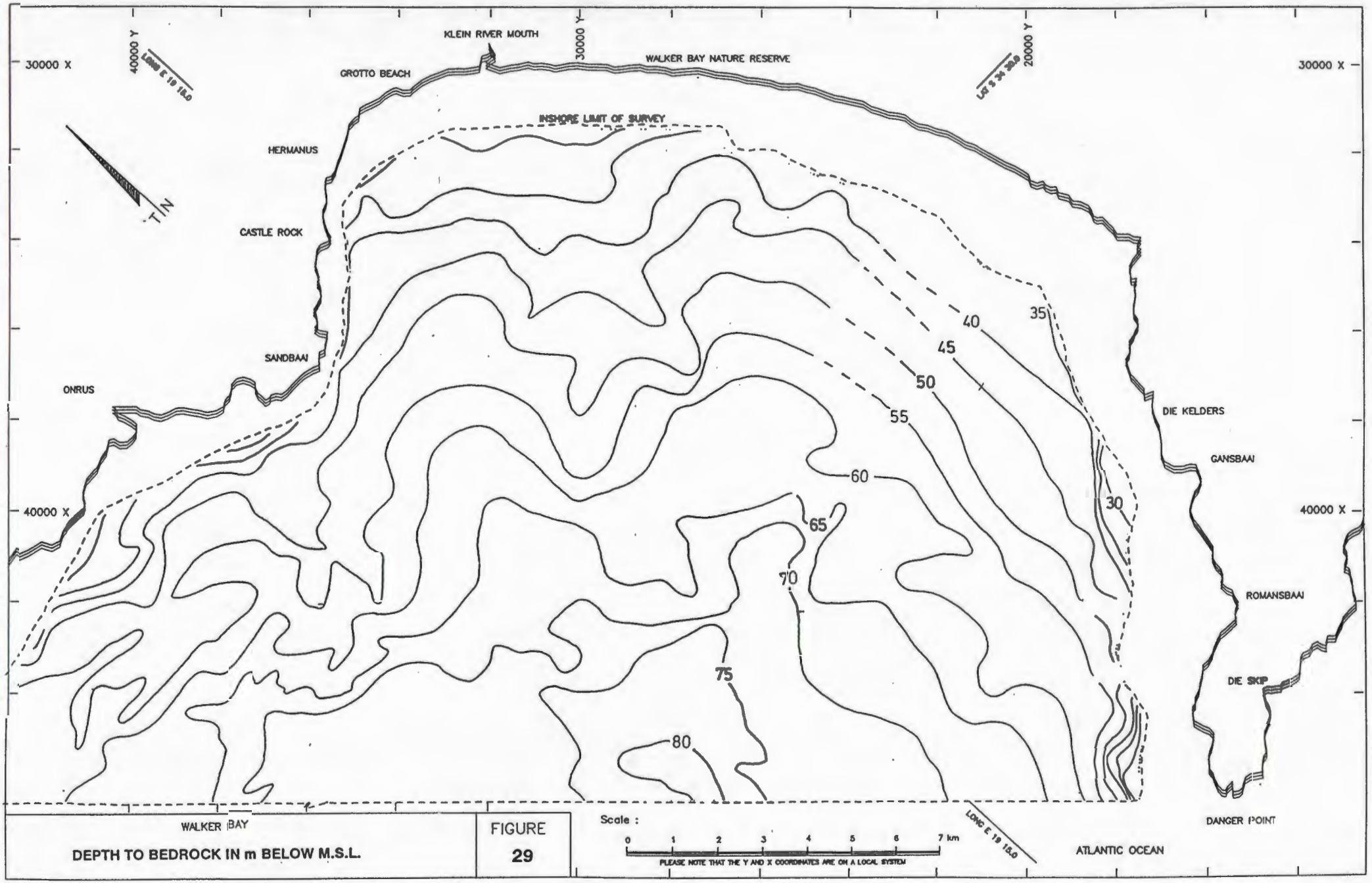
KLEIN RIVER MOUTH
WALKER BAY NATURE RESERVE
GROTTO BEACH
INSHORE LIMIT OF SURVEY
HERMANUS
CASTLE ROCK
SANDBAAI
ONRUS
DIE KELDERS
GANSBAAI
ROMANSBAAI
DIE SKIP
DANGER POINT
ATLANTIC OCEAN
WALKER BAY
30000 X
40000 X
30000 Y
40000 Y
20000 Y
35
40
45
50
55
60
65
70
75
80
30
Scale :
0 1 2 3 4 5 6 7 km
PLEASE NOTE THAT THE Y AND X COORDINATES ARE ON A LOCAL SYSTEM
FIGURE
29
DEPTH TO BEDROCK IN m BELOW M.S.L.

Here the 5 km wide, 50 m deep channel was traced to a point 20 km offshore, indicating a much larger-scale feature than the present one in Walker Bay.

At the mouth of the Bot River Lagoon, 10 km west of Walker Bay, Rogers (1985) located a palaeo-valley incised in similar bedrock to a depth of 51 m below sea level. Compared to both the examples cited above, the Klein River palaeo-valley in Walker Bay appears to be of relatively small dimensions. Considering the similar bedrock characteristics at the three locations i.e. Bokkeveld Group strata, it is evident that the catchment area and flow rate of the Klein River have been significantly smaller than that of the Breede and Bot Rivers during the times following the Würm IIb glacial period, 18 to 20 thousand years ago when sea level dropped to about 130 m below present MSL.

6.2 Seafloor Sedimentology

6.2.1 General

The Walker Bay seafloor was described in terms of 4 different reflectivity patterns or sonograph facies. Once identified, these facies were mapped in order to show their configuration in the study area.

The geological interpretation of sonograph facies on sidescan sonar records is often speculative and relies to a large extent on past experience. In this respect the video recordings and seabed samples greatly assisted in deducing the true nature of the different sonograph facies observed.

The specific locations of all the examples cited below are indicated on Figure 30 which forms an overlay for Figure 31.

Figure 31 shows the interpreted sidescan-sonar results in the form of a sonograph facies map of the study area. In the following paragraphs, the main features of the different seabed materials are discussed in some detail, making use of all the available data, i.e. sonograph images, ROV recordings and seabed-sampling results.

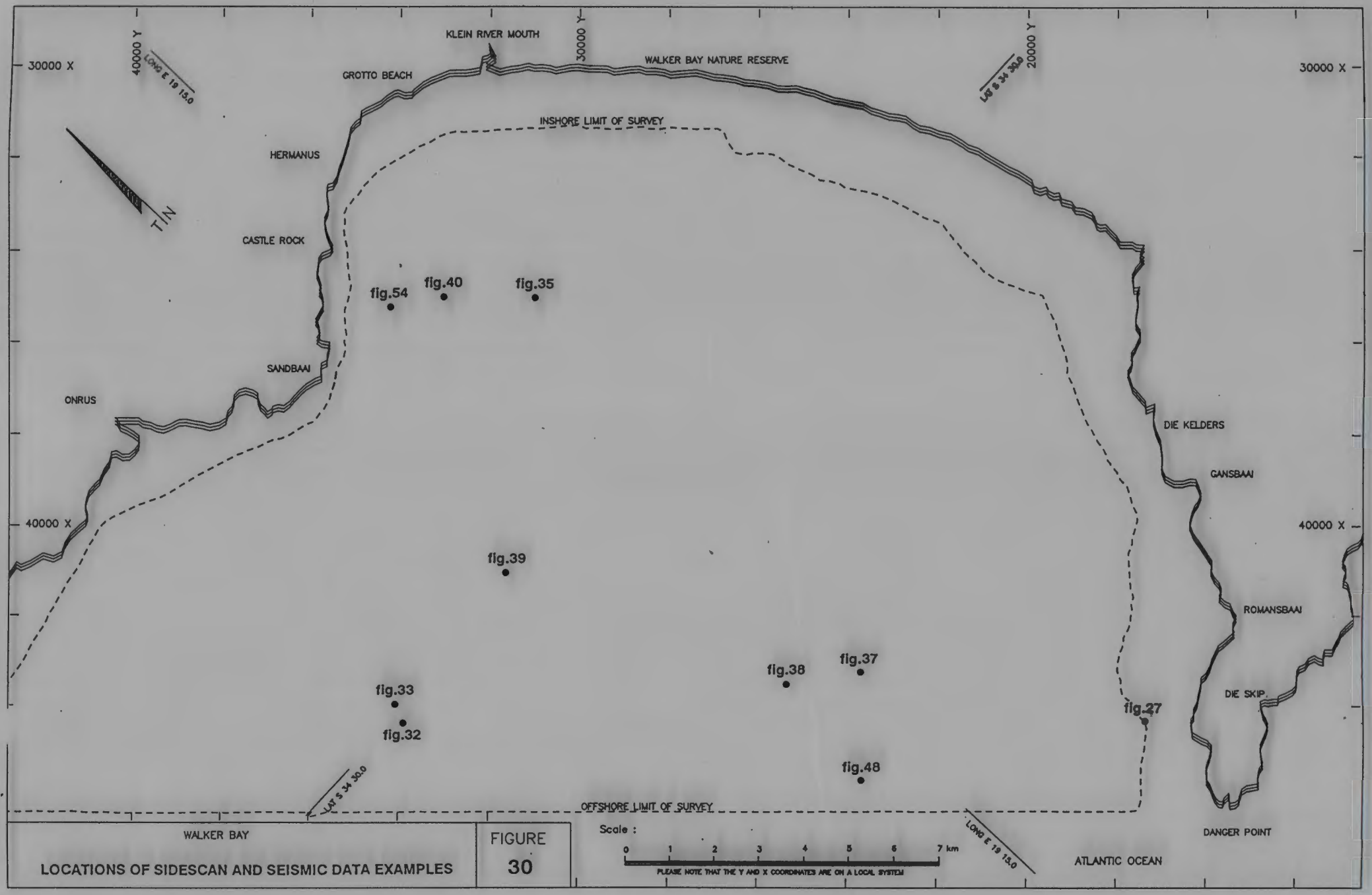

WALKER BAY

LOCATIONS OF SIDESCAN AND SEISMIC DATA EXAMPLES

FIGURE 30

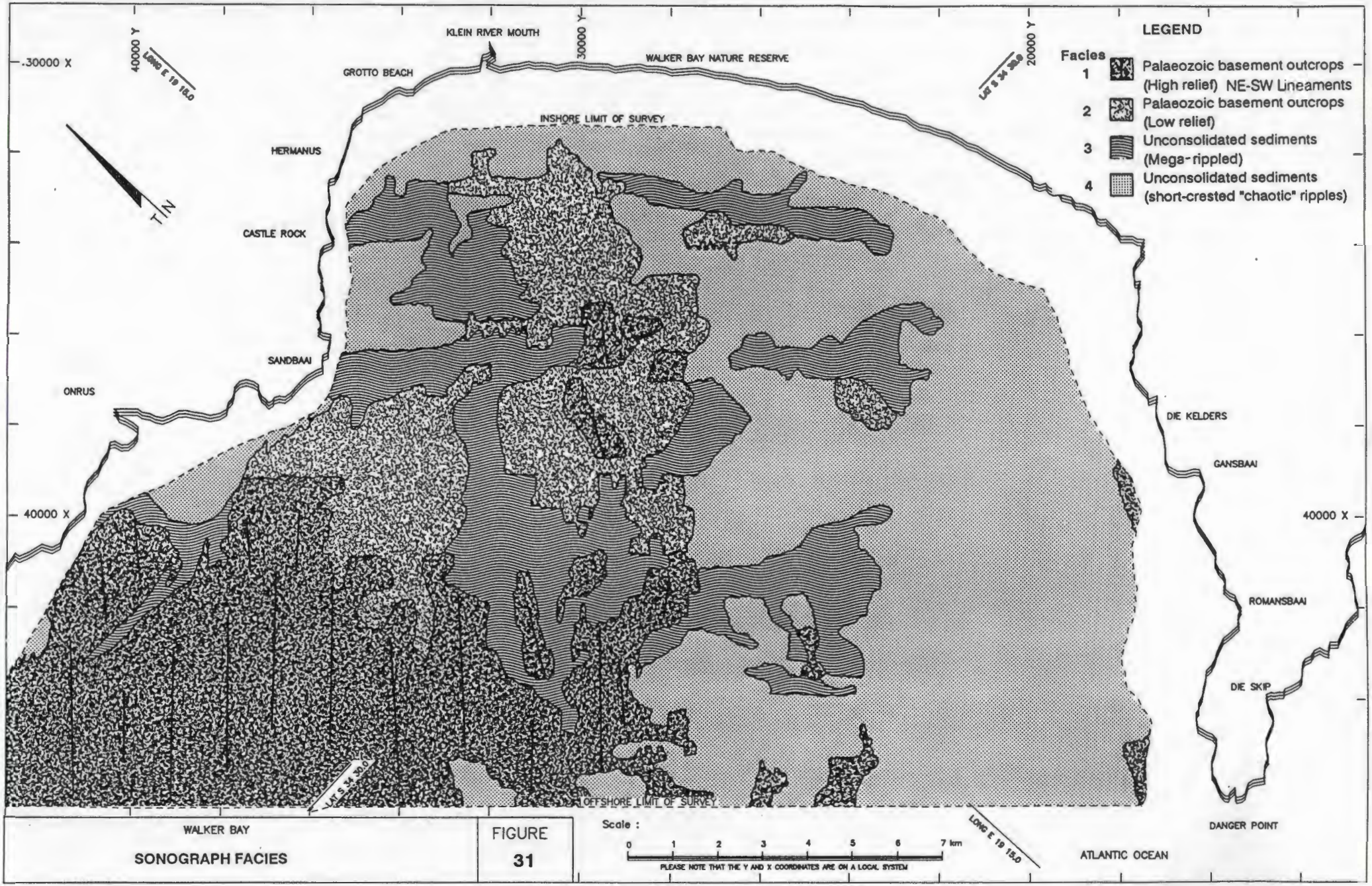

WALKER BAY

SONOGRAPH FACIES

FIGURE **31**

6.2.2 Description of facies

Facies 1 (High-relief bedrock outcrops)

Facies 1 accounts for approximately 25 percent of the surveyed seafloor and is mainly found in the western corner of the study area. Its image on the sonographs is typically that of a highly reflective rocky seafloor with a rugged relief. Prominent lineaments on the records clearly represent primary bedding, striking NE-SW with a large variation in thickness. Sediment-filled strike gullies, up to 100 m in width, commonly occur, with well-developed sedimentary bedforms on the floor of the gullies (cf. Ramsay and Mason, 1990). This is well illustrated by Figure 32. Large-scale jointing of the rocks is not evident from the records. A joint set does, however, show up occasionally, intersecting the primary bedding lineaments with their northeast-southwesterly orientation (Figure 33).

The high relief of the Facies 1 rocks is controlled by the primary bedding. Peaks often rise almost vertically up to 10 metres above the average elevation of the surrounding seafloor.

The video recordings at locations 5 and 6 off Onrus (Figure 20) confirmed the above sonograph interpretation. Figure 34(a) shows a prominent ripple crest in one of the strike-gullies at site 6 and Figure 34(b) is testimony to the abundant marine growth covering the high-relief rocks of Facies 1 at the same site.

Facies 2 (Low-relief bedrock outcrops)

Figure 31 shows that Facies 2 occupies approximately 20 percent of the surveyed seafloor and occurs as an eastward and shallower landward extension of Facies 1. In contrast with Facies 1, the sonograph images of Facies 2 indicate significantly lower relief and close examination of this sonograph facies suggests a thin veneer of unconsolidated sediment cover in many places. Lineaments are rarely recognisable and rock pinnacles only occasionally protrude more than 2 metres above the surrounding seafloor. Figure 35 shows a typical example of Facies 2.

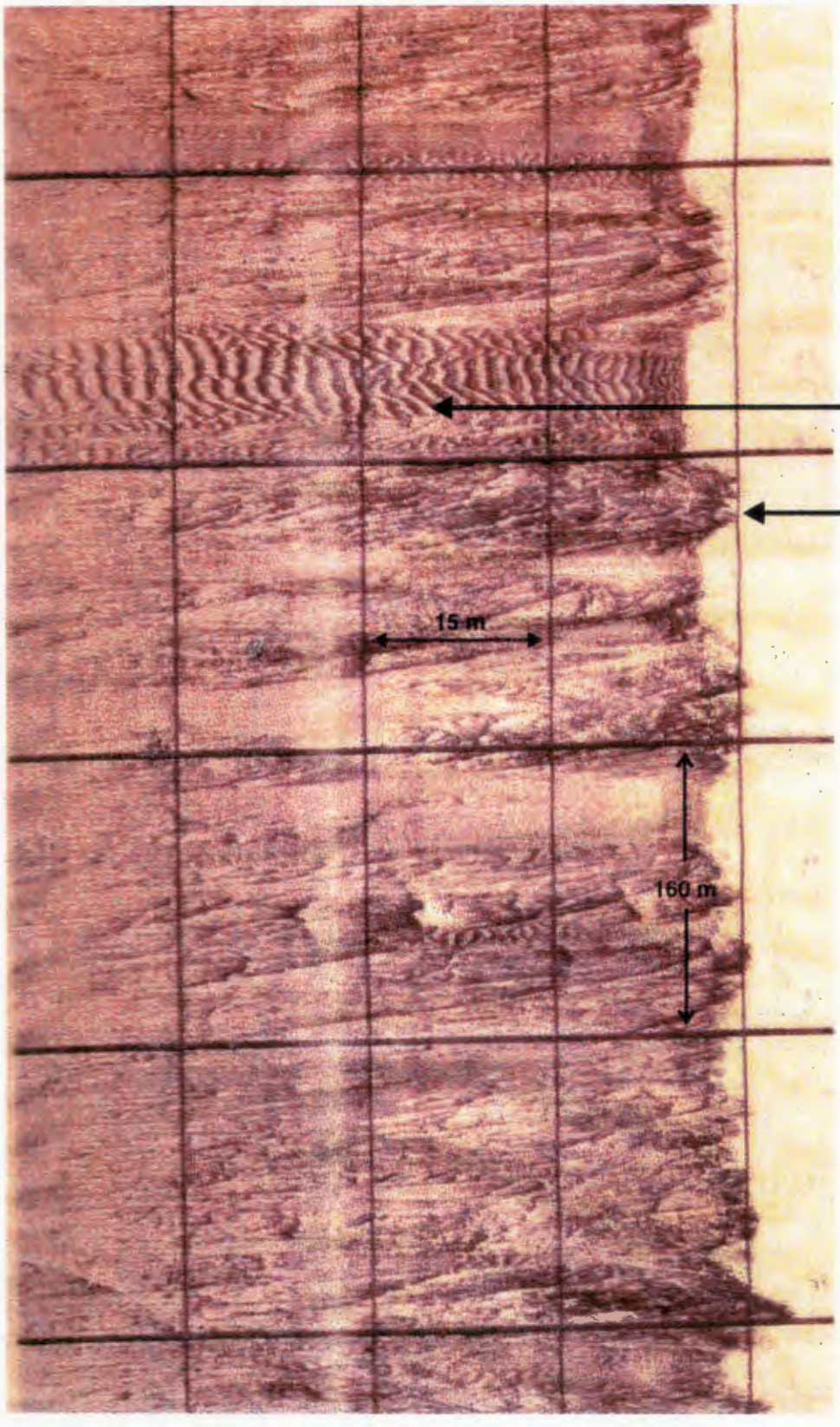

WALKER BAY

SONOGRAPH EXAMPLE - FACIES 1
LOCATION 44400 X; 34000 Y. LINE 39
500kHz

FIGURE

32

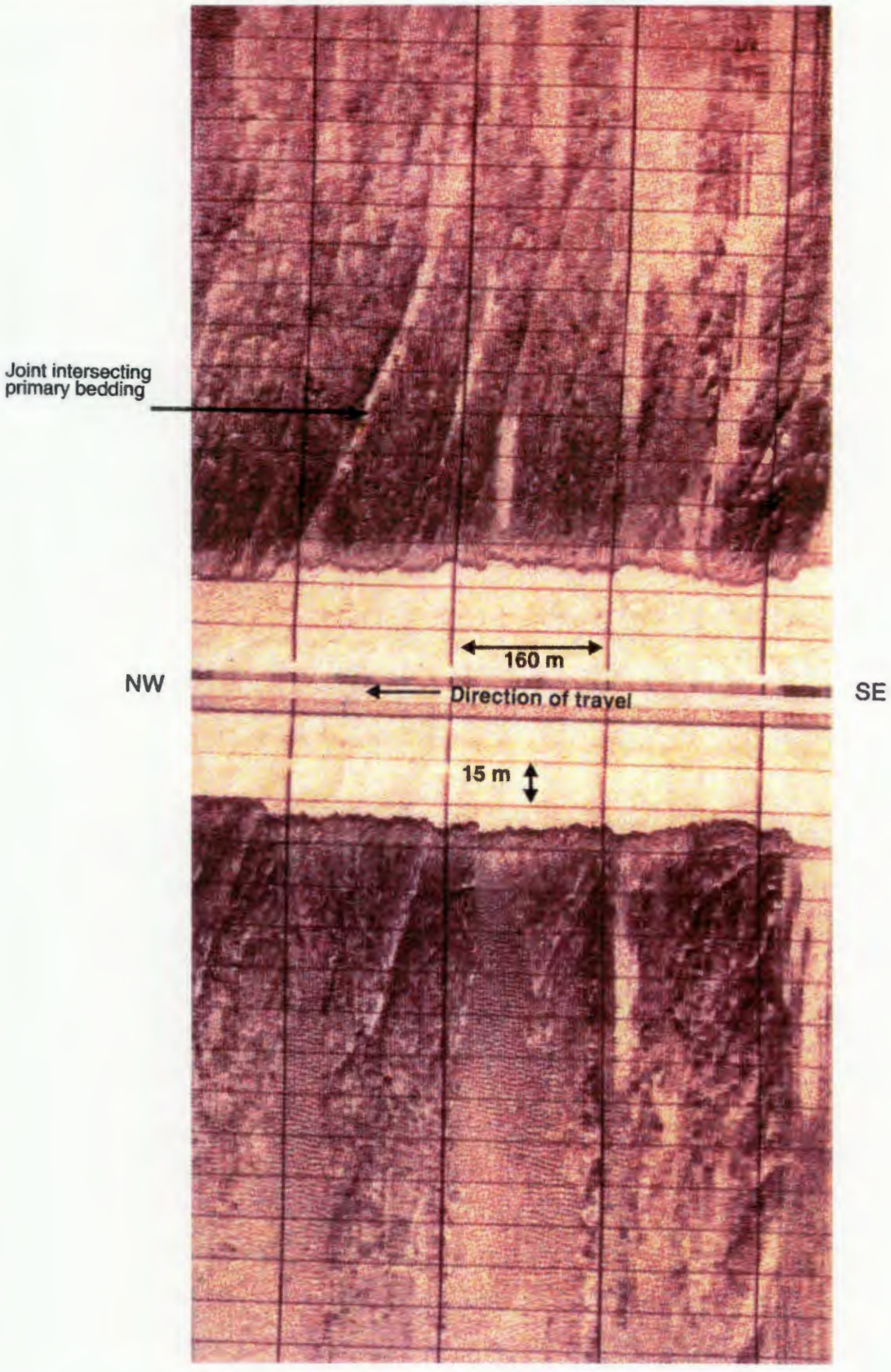

WALKER BAY

SONOGRAPH EXAMPLE - FACIES 1
LOCATION 46000 X; 34000 Y. LINE 42
100kHz

FIGURE

33

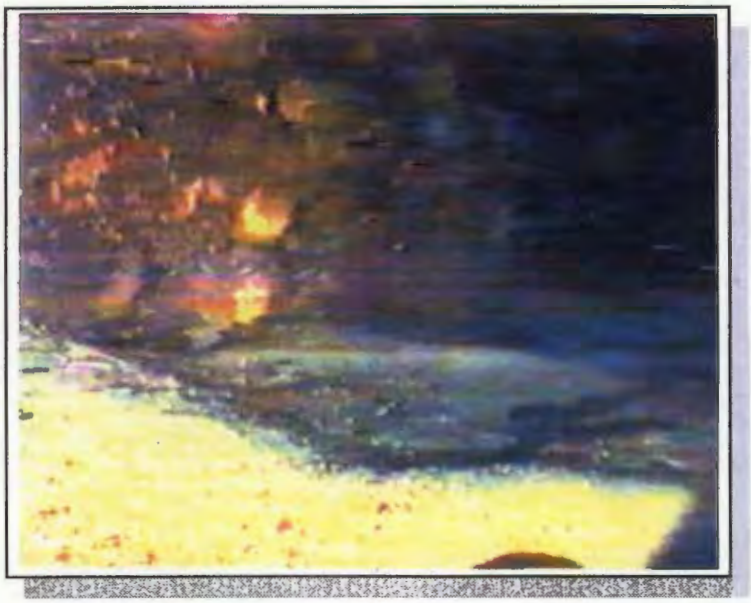

(a)

(b)

WALKER BAY

UNDERWATER PHOTOGRAPHS - FACIES 1
ROV DEPLOYMENT SITE 6

FIGURE

34

WALKER BAY

UNDERWATER PHOTOGRAPH - FACIES 2
ROV SITE 3

FIGURE

36

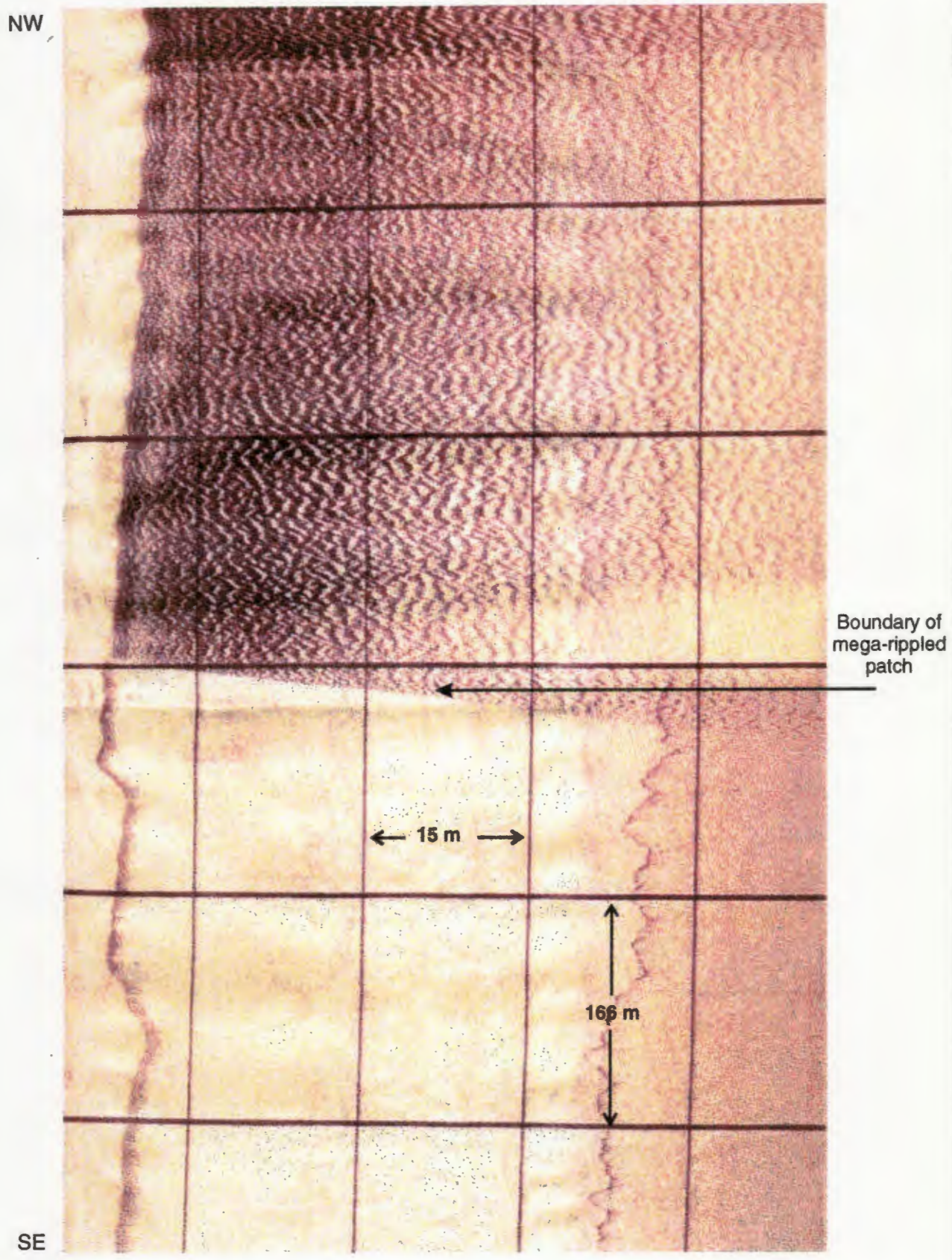

WALKER BAY

SONOGRAPH EXAMPLE - FACIES 3

LOCATION 43394 X; 23795 Y. LINE 35

FIGURE

37

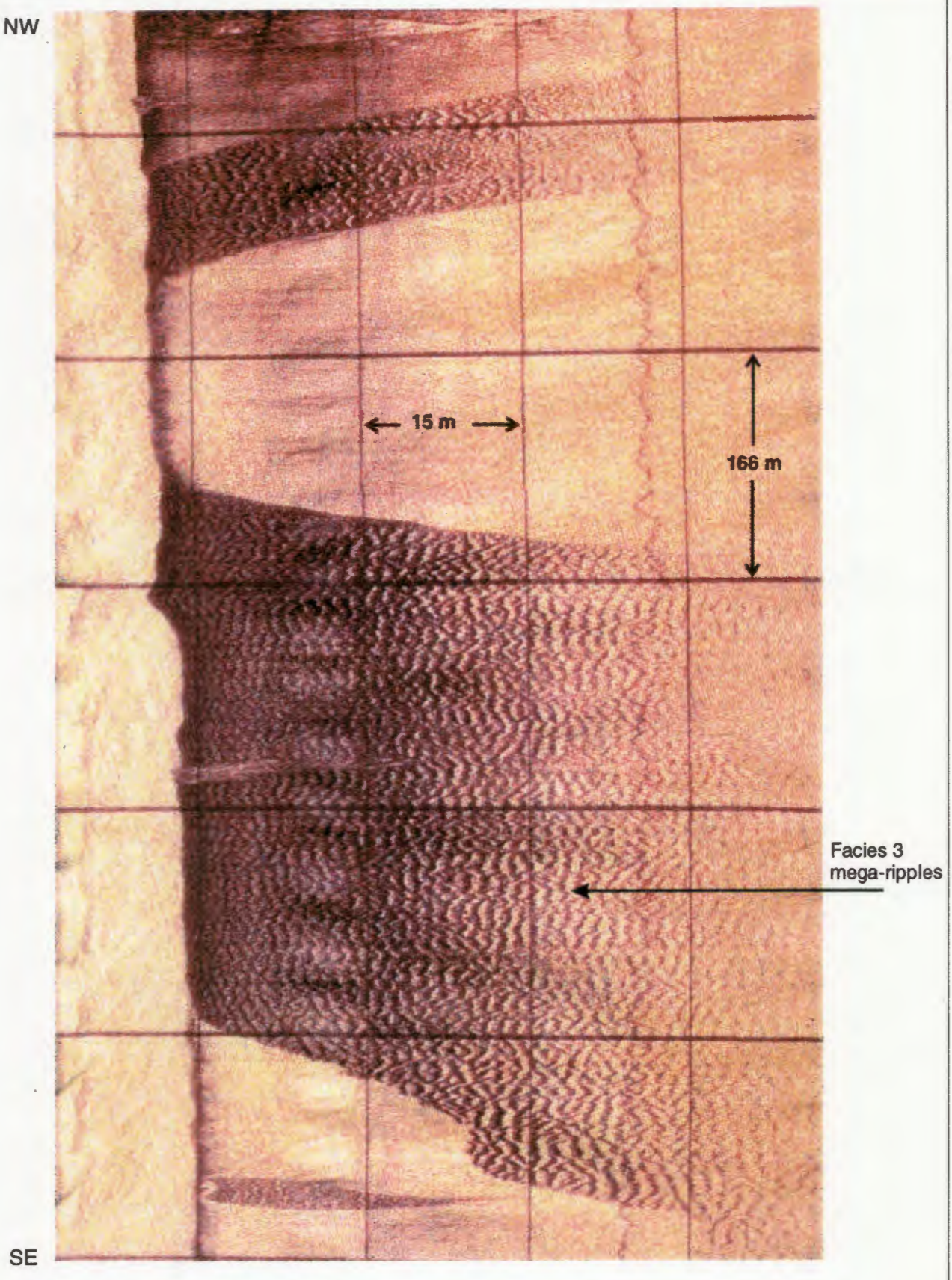

WALKER BAY

SONOGRAPH EXAMPLE - FACIES 3

LOCATION 43407 X; 25258Y

FIGURE

38

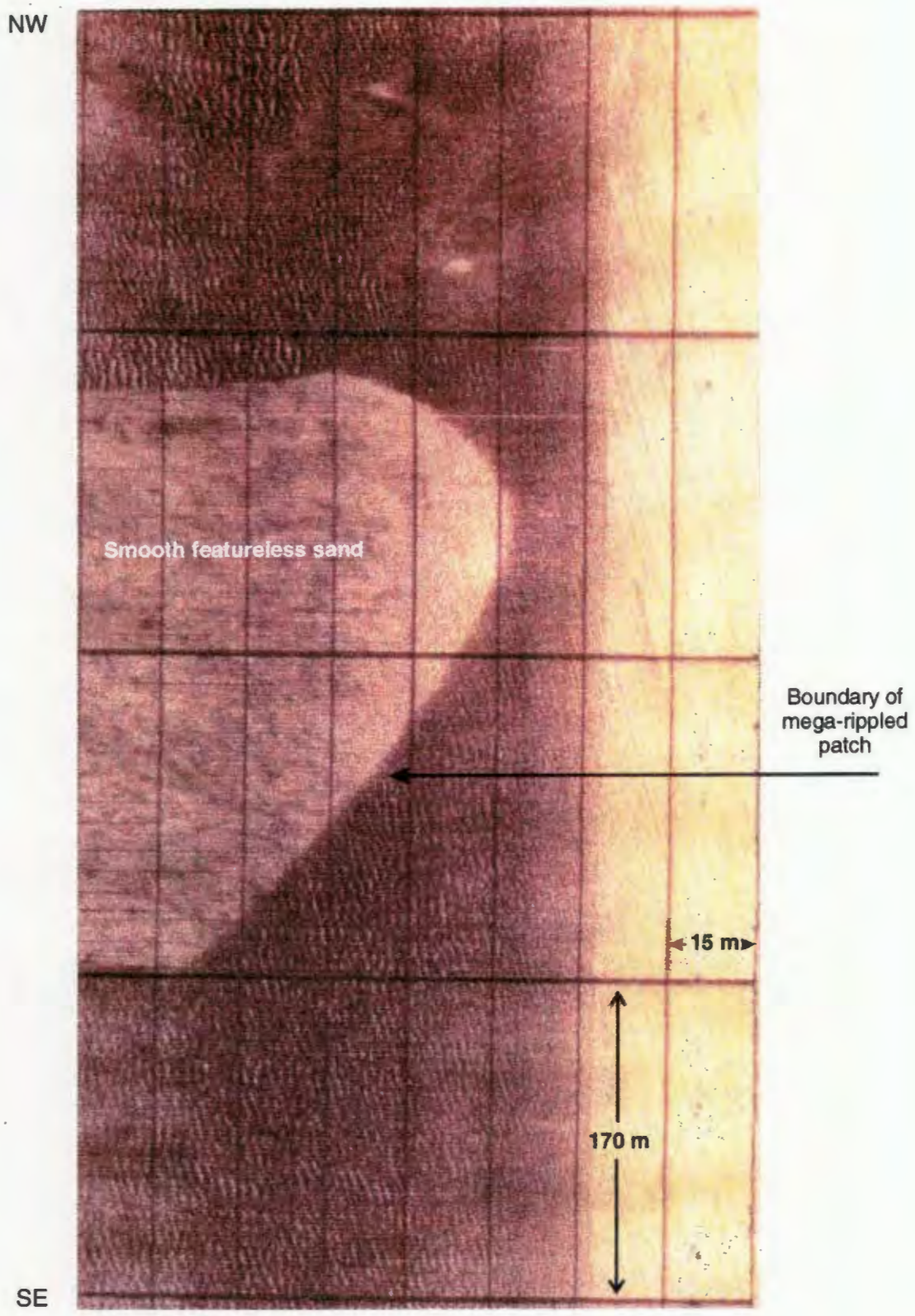

WALKER BAY

SONOGRAPH EXAMPLE - FACIES 3
LOCATION 40954 X; 31277 Y. LINE 28
100kHz

FIGURE

39

NW

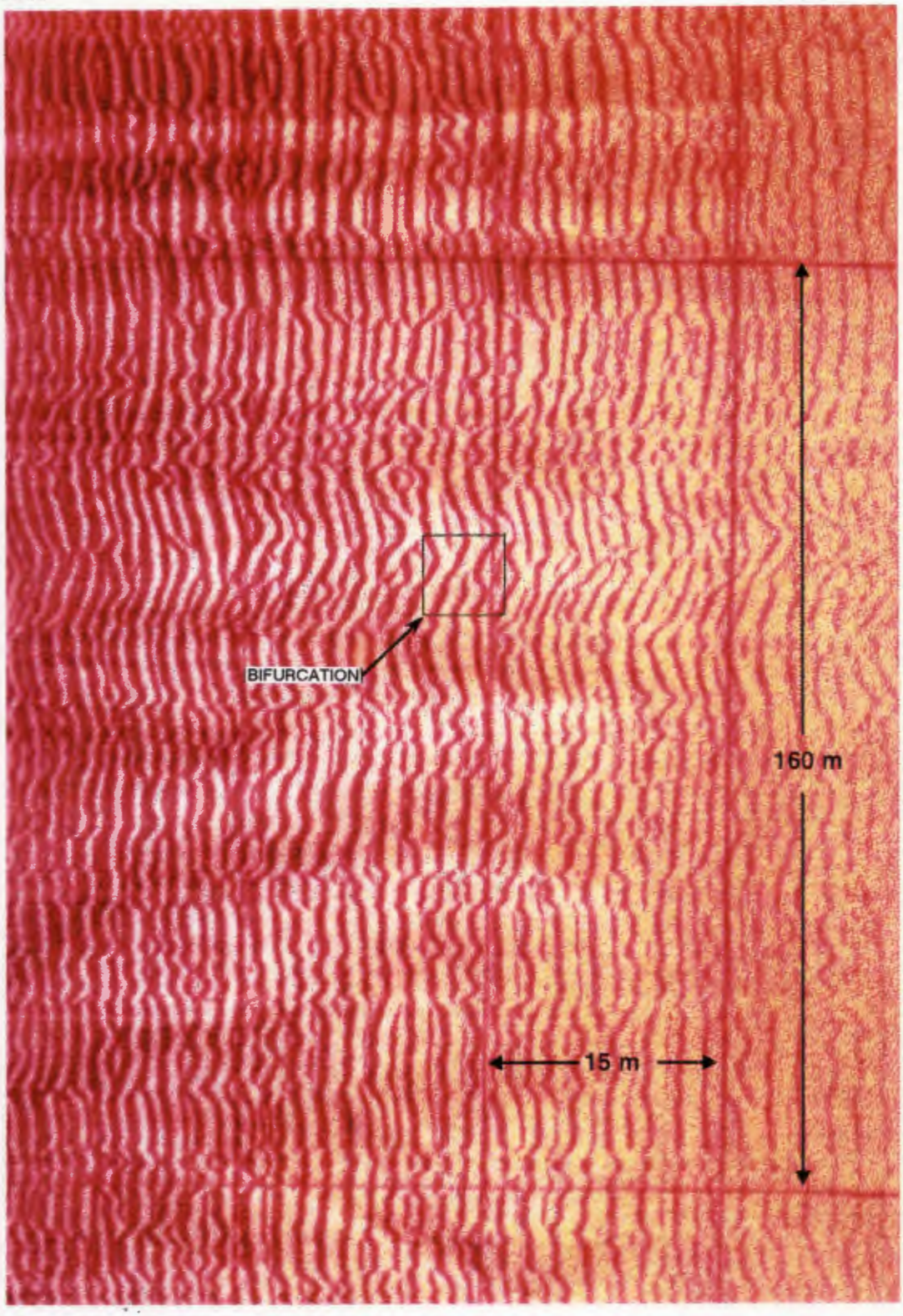

SE

WALKER BAY

SONOGRAPH EXAMPLE - FACIES 3 MEGARIPPLES

LOCATION 34500 X; 33000 Y. LINE 10

500kHz

FIGURE

40

generally symmetrical, with crest heights of between 30 and 40 centimetres and wavelengths of between 1,0 and 2,0 metres. Examples of Facies 3 megaripples are shown in Figures 41 and 42. Note the difference in ripple shape between Figures 41 (a) and (b). The megaripples in Figure 41(a) occur in approximately 30 m water depth and those in Figure 41(b) in 40 m water depth. The ripples in the shallower water appear to be sinusoidal in nature, whereas those in deeper water tend to be sharp-crested. Both shapes, however, are symmetrical, suggesting oscillatory flow as the common controlling mechanism Figure 42(a) shows the termination of an individual ripple with the ripple crest diminishing in height towards the viewer. Small interference ripples on the flank of the main ripple are visible in the background.

Figure 42(b) illustrates how coarse material, mostly shells and shell fragments, tends to accumulate in the ripple troughs. Figure 43 shows similar material obtained by dredging off Sandbaai (Figure 3), in a water depth of approximately 50 metres (Gentle, 1987). The presence of intertidal species such as Patella granularis, Patella compressa, Donax serra, Venus verrucosa and Burnupena sp. indicates that the shell assemblage does not represent the marine environment in which it was found. The dull, bored surfaces of the shells suggest that they were drowned by a rising sea-level in the recent geological past, rather than being transported into deeper water from the present-day shoreline and are therefore relict shells.

In the next chapter it will be shown that the sediment within individual megarippled patches is generally much coarser than that of the apparently smooth seabed separating them. When sampling Facies 3 sediments, it was therefore not possible to assess whether a specific sample was taken from a megaripple crest, from a trough or from the areas between the megarippled patches. Since the sediment texture appears to differ considerably between these environments within Facies 3, sedimentological trends are unlikely to emerge from the overall sample suite.

The expected large textural variation within the Facies 3 sample set is obvious from Table 6 which shows that the textures range between sandy gravel (sG) and sand (S).

The distribution of the mean size of the sand fraction, as obtained by the moment statistics from the settling-tube data (Table 8), is illustrated in Figure 44. The mean

(a) ROV Site 1

(b) ROV Site 8

WALKER BAY

UNDERWATER PHOTOGRAPHS - FACIES 3

FIGURE

41

(a)

(b)

WALKER BAY

UNDERWATER PHOTOGRAPHS - FACIES 3

ROV Site 4

FIGURE

42

WALKER BAY

DREDGED SHELLS - GENTLE, 1987
SAMPLE # 1834

FIGURE

43

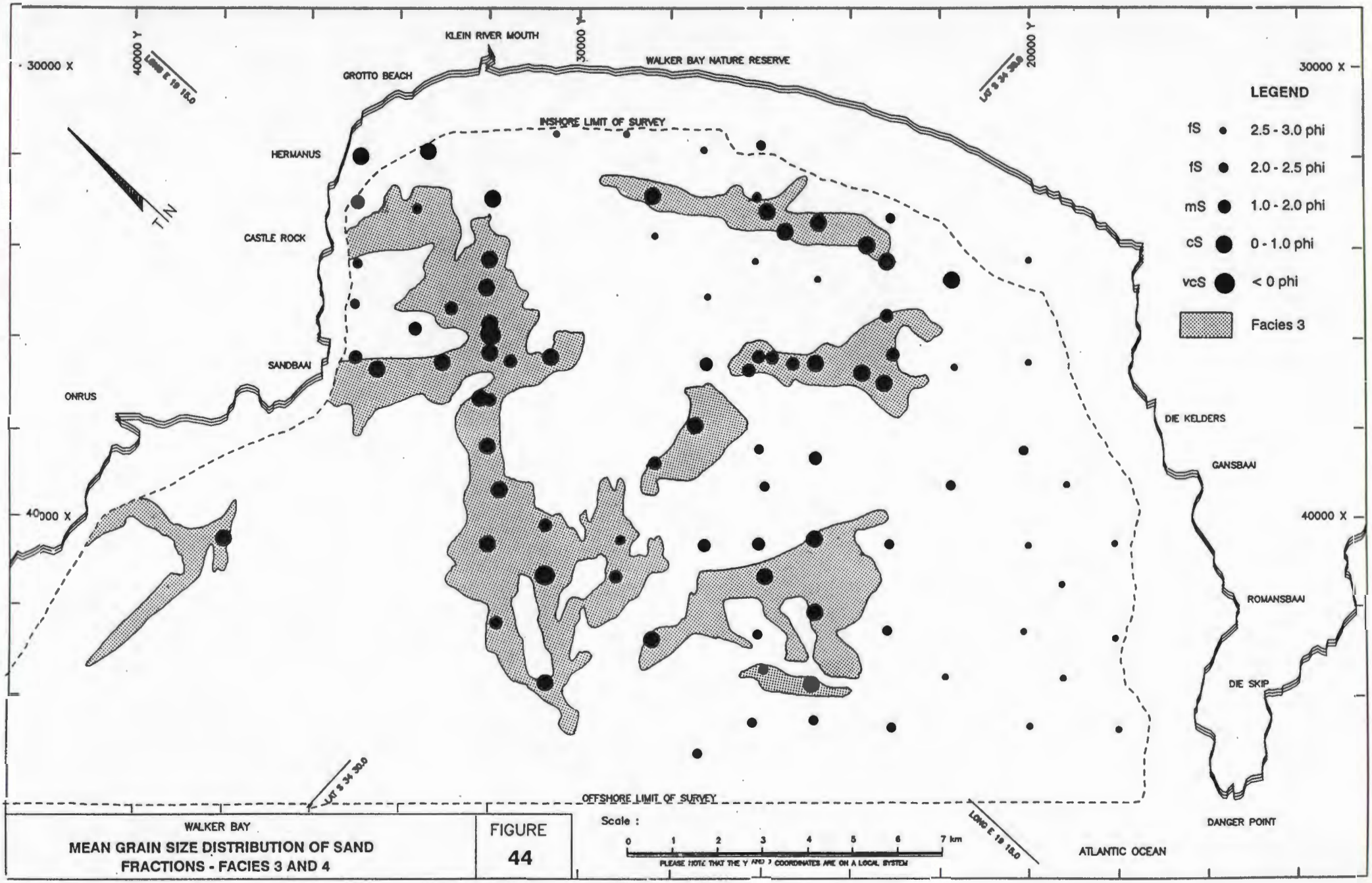

WALKER BAY

MEAN GRAIN SIZE DISTRIBUTION OF SAND FRACTIONS - FACIES 3 AND 4

FIGURE **44**

sizes within the outlined Facies 3 areas vary, with few exceptions, between 0 and 2,0 phi, i.e. coarse to medium sand according to the Wentworth grade scale.

The distribution of the percentage carbonate in the sand fraction is shown in Figure 45. Over most of the outlined Facies 3 areas the carbonate content generally varies between 40 and 100 percent with no general trend. A significant anomaly, however, occurs toward the west where the values are consistently low (between 0 and 40 percent) along a line trending NE-SW, southeast of Sandbaai and Onrus. The Facies 3 sediment in this area is almost surrounded by rock outcrops of both Facies 1 and Facies 2 (Figure 31). As discussed in Section 6.1, the depth-to-basement map (Figure 29) shows that the bedrock surface in this area is trough-shaped, closely aligned with the occurrences of low carbonate content sediment. A visual examination of these particular samples showed that they can generally be classified as lithic sandy gravel, dominated by shale fragments (Figure 46). They are most likely of fluvial origin, deposited in a paleo-channel of the Kleinrivier during sea-level lowstands.

The gravel component of the Facies 3 sediments generally consists of bivalve (Bi) and cirripede (C) (barnacle) fragments (Figure 47a), except in the few cases mentioned earlier where the carbonate content is low along the proposed palaeochannel of the Kleinriver and the sediments are dominated by lithic rock fragments.

The microscopic analyses of the sand fractions of the Facies 3 sediments (Figure 47b) showed that both relict and modern calcareous biogenic components occur in varying proportions. The $CaCO_3$ content averages 54% of the total weight of the samples and the calcareous components consist mainly of fragments of gastropod (G) and bivalve (Bi) shells and cirripede (C) fragments (Figure 47b). Echrinoid spines, sponge spicules, benthic foraminifera and ahermatypic coral debris also commonly occur. Astracods, bryozoa and brachiopods were observed as minor constituents.

The terrigenous component normally consists of quartz as the major constituent, calcarenite from the Waenhuiskrans Formation, Bokkeveld shale fragments and occasional grains of authigenic phosphorite and glauconite.

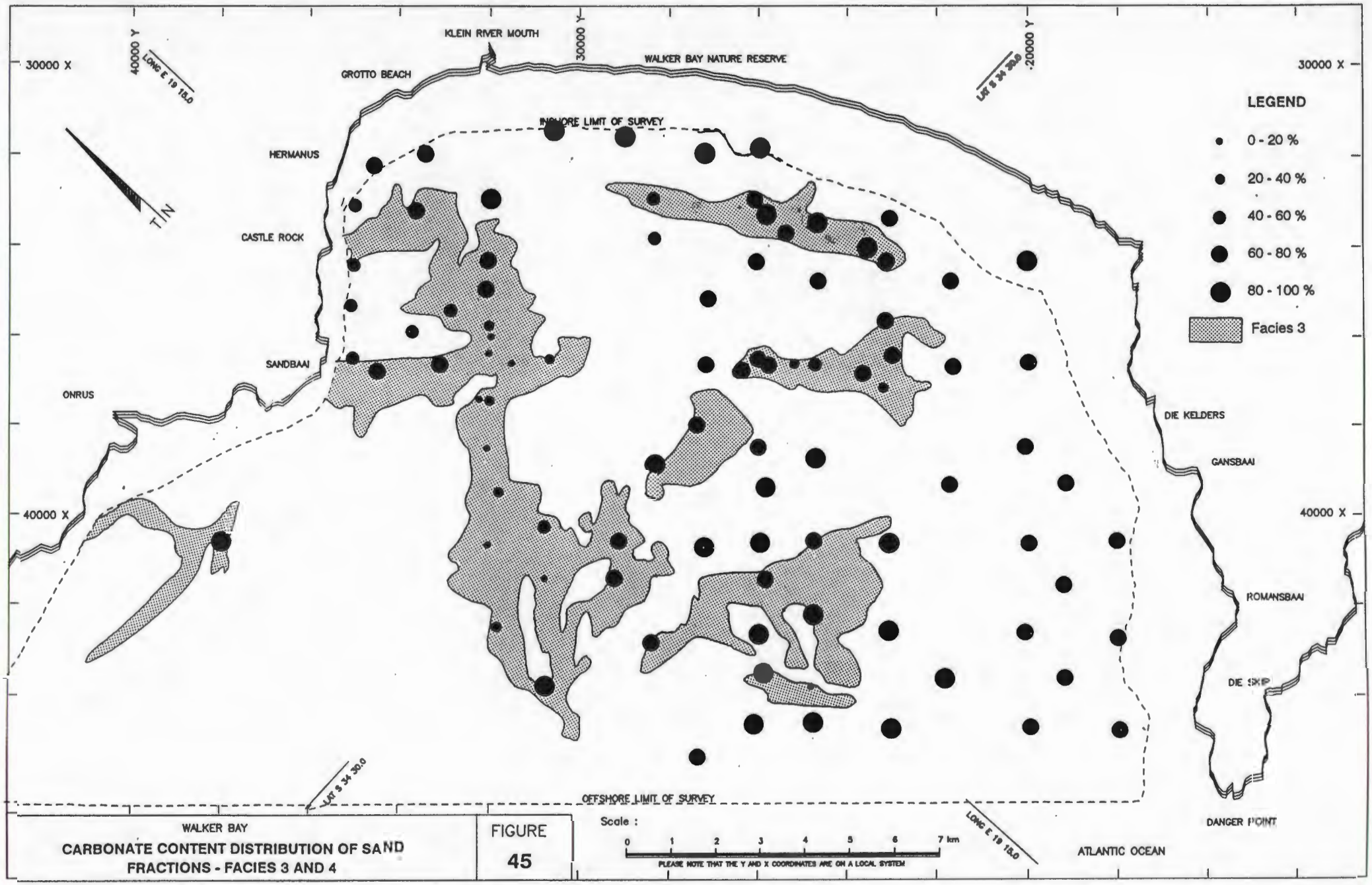

WALKER BAY

CARBONATE CONTENT DISTRIBUTION OF SAND FRACTIONS - FACIES 3 AND 4

FIGURE **45**

Background grid = 1mm

WALKER BAY

MICROGRAPH OF TERRIGENOUS FACIES 3 SEDIMENT.
SAMPLE 12/90, GRAVEL FRACTION.

FIGURE

46

(C) = Cirripede
(G) = Gastropod
(Bi) = Bivalve

(a)

Background grid = 1mm

(b)

WALKER BAY

MICROGRAPHS OF FACIES 3 SEDIMENT.

SAMPLE 19/90.

(a) GRAVEL FRACTION; (b) SAND FRACTION.

FIGURE

47

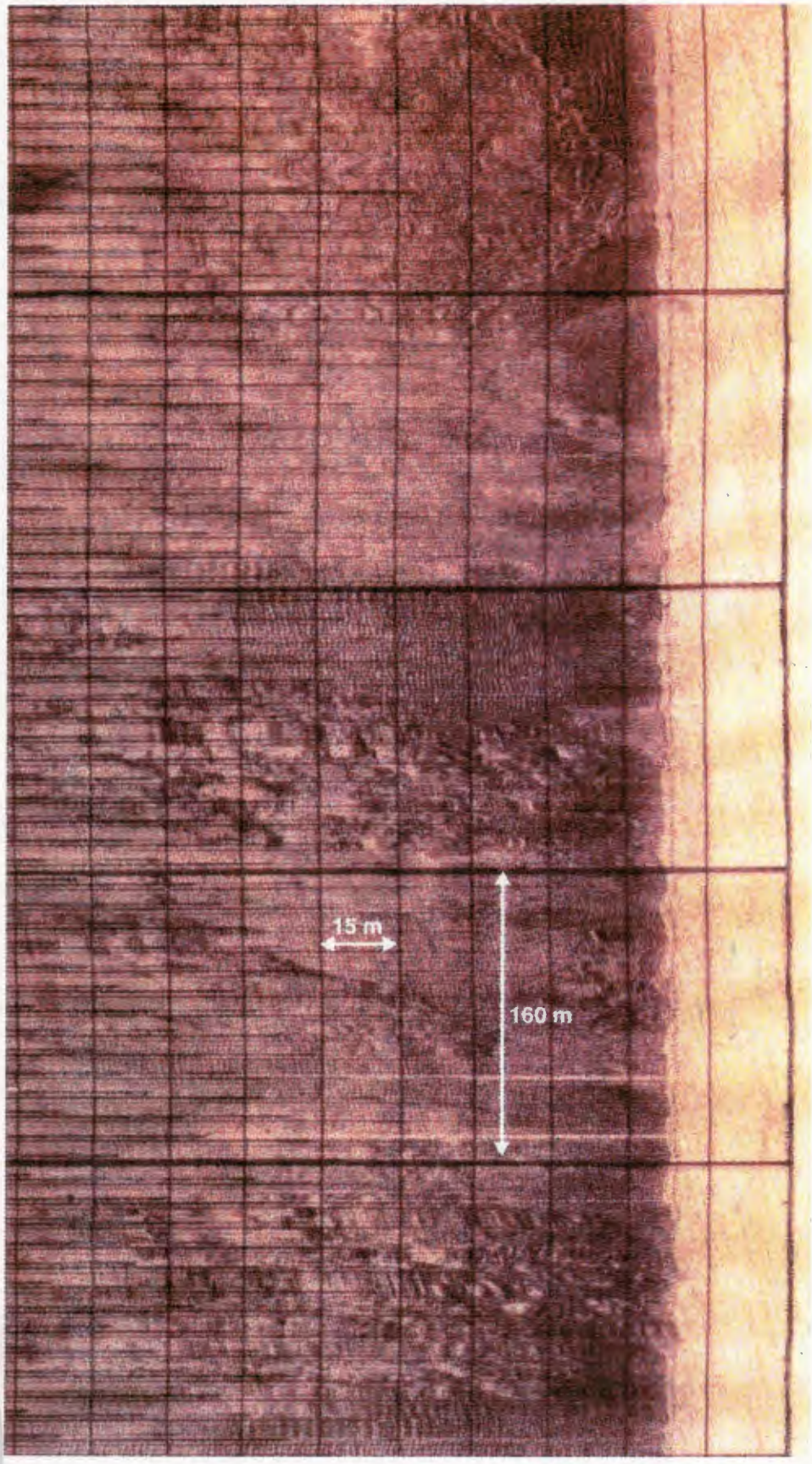

WALKER BAY

SONOGRAPH EXAMPLE - FACIES 2
LOCATION 35004 X; 31009 Y. LINE 11
100kHz

FIGURE

35

The video recording (Figure 36) at site number 3 off Hermanus (Figure 30) again confirmed the sonograph interpretation of Facies 2. Figure 36 shows an isolated rock pinnacle in the foreground (height approximately 1,5 m) and a low-lying area in the background, covered with what appears to be small boulders with an average diameter of 300 to 400mm. Marine growth appears to be similar to Facies 1, but is less abundant.

Facies 3 (Medium to high reflectivity megarippled patches)

Facies 3 occurs in irregularly shaped and scattered areas throughout the area. It clearly represents unconsolidated seabed material, as evidenced by the seismic profiles, but the reflectivity patterns are quite distinctive. Large "patches" occur where the seafloor is highly reflective due to well developed, long crested bedforms, typically spaced at 1,5 metres and with a trough-to-crest height of approximately 30 centimetres. Ashley (1990) recommended a large-scale bedform classification scheme based on first, second and third order descriptors. According to this scheme, the Facies 3 bedforms in Walker Bay are classed as "small subaqueous dunes". For the purpose of this study, however, the more concise term "megaripple" will be used throughout the text, mainly to avoid possible confusion with the small-scale ripples of Facies 4, which will be discussed later.

The megarippled patches are mostly elliptical with a large variation in size, typically 150 to 200 metres in diameter and generally elongated in a NE-SW orientation. Individual megarippled patches are separated by apparently smooth, featureless sandy seafloor with a low reflectivity. The boundaries of the rippled areas are very well defined with almost no change in megaripple characteristics towards the boundaries. Figures 37, 38, 39 and 40 show typical examples of Facies 3. The apparent seafloor undulations in Figure 37 were caused by changing the depth of the towfish and do not reflect changes in the seafloor topography. The "zig-zag" nature of the megaripple crests is also an artifact, caused by pitching and yawing of the side-scan towfish. Note the bifurcation of mega-ripple crests (Figure 40), a common phenomenon cited in numerous studies (e.g. Inman, 1957).

Video recordings of Facies 3 at sites 1, 4 and 8, (Figure 20) off the Walker Bay Nature Reserve, Sandbaai and Castle Rock respectively, show that the megaripples are

Facies 4 (Low reflectivity, apparently featureless sediment)

Facies 4 mainly occur in the southeastern half of the study area and the sonographs indicate featureless sediment with low reflectivity. An example is shown in Figure 48. Video recordings in the Facies 4 area, however, showed the seafloor to be covered with small-scale bedforms too small to be resolved by the sidescan sonar. Figures 49 and 50, taken at sites 2 and 7 (Figure 20) off the Walker Bay Nature Reserve and off Castle Rock, show a complex pattern of short-crested, randomly orientated ripples. Crest lengths vary between a few centimetres and up to 1,0m. Crest heights are typically between 10 and 20 centimetres.

All the Facies 4 sediment samples, with the exception of sample 17/87, were texturally classified as sand (S) (Table 7).

The mean grain sizes of the Facies 4 sand fractions vary, with few exceptions, between 2,0 and 3,0 phi, i.e. fine sand (Figure 44). The mean grain size appears to decrease towards the east and off the Gansbaai coastline the mean grain sizes are consistently finer than 2,5 phi. The finer sand in this area can be ascribed to the prevailing low-energy wave regime which can be expected north of Danger Point, an aspect which will be discussed in more detail in the next chapter.

The percentage carbonate distribution for Facies 4 shows no apparent trend and the values vary generally between 40 and 90 percent (Figure 45).

The microscopic analyses of Facies 4 samples (Figure 51) revealed the same components as observed in the Facies 3 samples. The only difference between the two facies appears to be in the grain size statistics as shown earlier. The carbonate content of the Facies 4 samples averages 74 percent which is considerably higher than the average for Facies 3.

The characteristics and the formation of both the bedforms in Facies 3 and Facies 4 will be further discussed in Chapter 7.

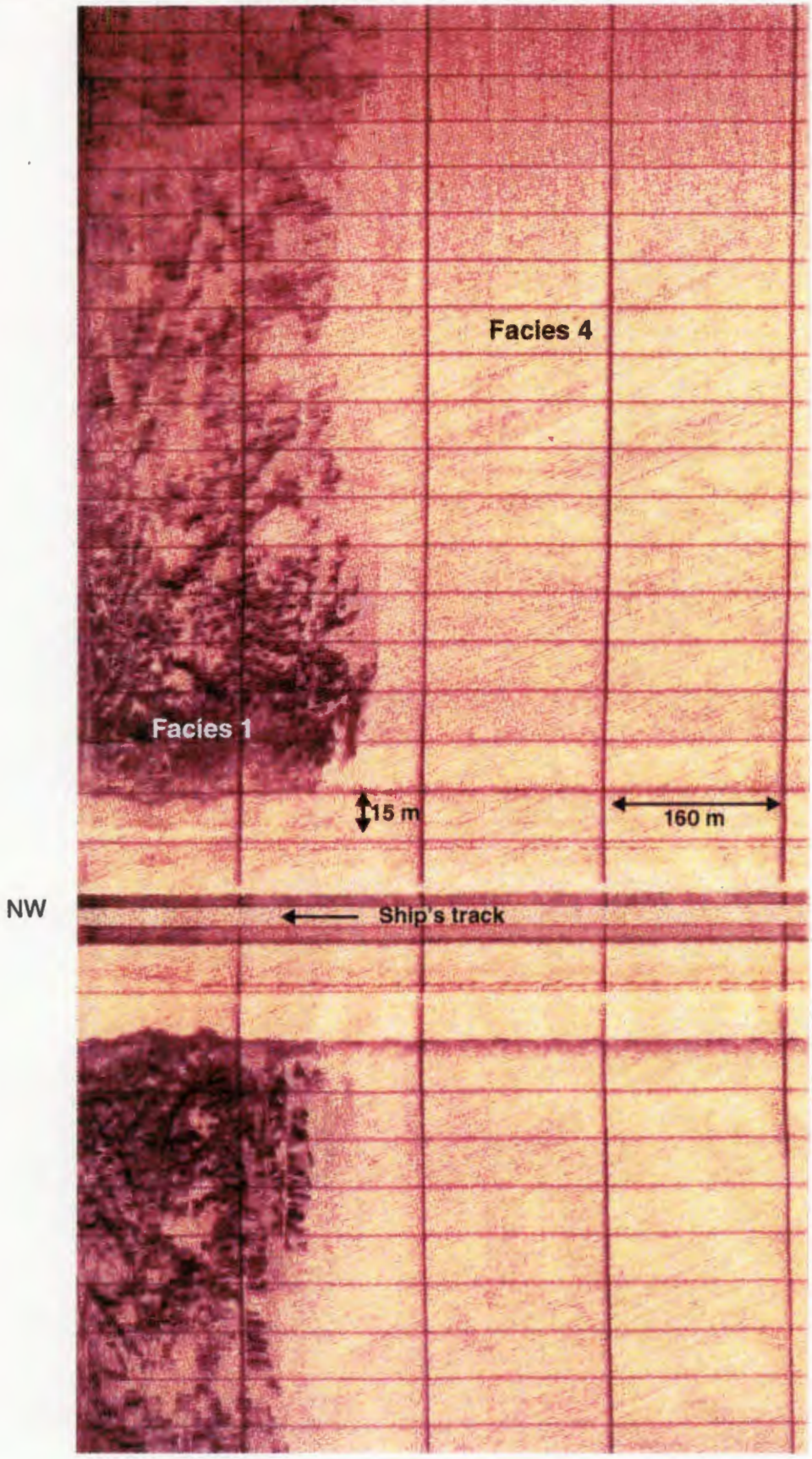

WALKER BAY

SONOGRAPH EXAMPLE - FACIES 1 & 4
LOCATION 46000 X; 24000 Y. LINE 42
100kHz

FIGURE

48

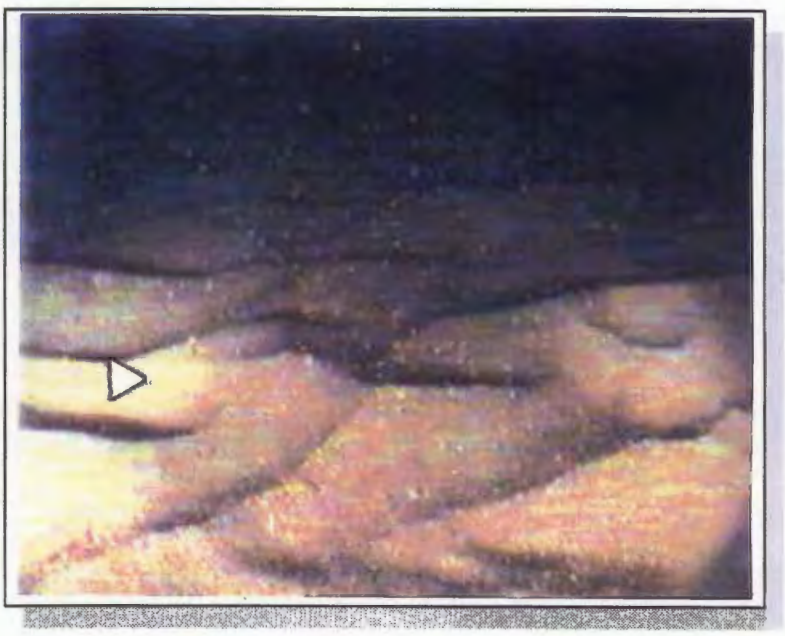

WALKER BAY

UNDERWATER PHOTOGRAPHS - FACIES 4
ROV SITE 2

FIGURE

49

ROV Site 2

ROV Site 7

WALKER BAY

UNDERWATER PHOTOGRAPHS - FACIES 4

FIGURE

50

Background grid = 1mm

WALKER BAY

MICROGRAPH OF FACIES 4 SEDIMENT.
SAMPLE 1/90

FIGURE

51

7. WAVE-GENERATED BEDFORM CHARACTERISTICS

7.1 General

The results of this study showed that wave-induced ripples and megaripples occur extensively over the sandy parts of the Walker Bay seafloor, i.e. the Facies 3 mega-ripples and the short-crested, randomly orientated ripples of Facies 4.

Although the survey methods used in Walker Bay did not allow detailed measurements to be made of the different bedform characteristics, it was nevertheless possible to extract, from the sidescan sonar and ROV data, estimates of the key parameters such as ripple orientations, wavelength and amplitude. Together with the known water-depths, wave heights and sediment grain sizes, such data could possibly supply the key to the fundamentals of bedform behaviour in Walker Bay.

Extensive literature exists on the generation of bedforms under wave action, e.g. Inman (1953), Manohar (1955), Horikawa and Watanabe (1967), Carstens *et al.* (1967), Dingler (1975), Miller and Komar (1980), Nielsen (1981), Boyd *et al* (1988) and Black and Healey (1988). Most of these studies deal with laboratory-obtained data under shallow-water conditions. Detailed field observations, especially in water depths outside the range of conventional scuba diving, are not common. Bedform analyses from sidescan sonar data are rarely done, due to the inherent inaccuracies involved.

In the following sections the characteristics of Facies 3 megaripples and Facies 4 ripples and their relationships with prevailing wave conditions will be discussed.

7.2 Local Wave Conditions

When incoming deep-sea generated waves approach shallower water with their crests moving at an angle to the depth contours, that part of the wave in deeper water will move faster than the part in the shallower water, causing the wave crest to bend toward alignment with the contours. These changes in the direction of wave propagation along

a wave front, known as wave refraction, result locally in either a convergence or divergence of wave energy which has a direct effect on the sediment dynamics and on the distribution of bedforms. Wave refraction is normally illustrated by means of wave orthogonals or wave rays, rather than the wave crests themselves. A wave ray can be defined as the path that a point on the wave crest will follow and as such shows the propagation direction of the wave. As two adjacent orthogonals converge or diverge, the energy concentration will increase or decrease.

The concept of wave refraction along an irregular coastline is illustrated schematically in Figure 52. Note how the orthogonals converge towards the headland and fan out in the bay as the wave crests align themselves with the coastline.

The wave height, H, of a shoaling wave at any point is expressed by the formula

$$\frac{H}{H_o} = k_s k_r$$

where H_o = deep water wave height
k_s = shoaling coefficient
k_r = refraction coefficient

The shoaling coefficient (k_s) describes the change in wave height as a wave moves into shallower water. It is a function of wavelength and water depth whereas the refraction coefficient (k_r) is a function of the relative spacing between the orthogonals. A detailed discussion of wave-refraction is given in CERC (1977).

An analysis of the regional wave conditions given in Section 2.2.1 (Figure 7 and Table 1) shows that the dominant incoming wave direction in Walker Bay is from the south-southwest. These deepwater swells have a dominant wave period (T) of 11,9 seconds and a representative deep-sea significant wave height (H_o) of 2,6 metres (Table 1). The transition from deepwater waves (i.e. no water particle movement at the seabed) to shallow-water waves (i.e. waves causing particle movement at the seabed) takes place when

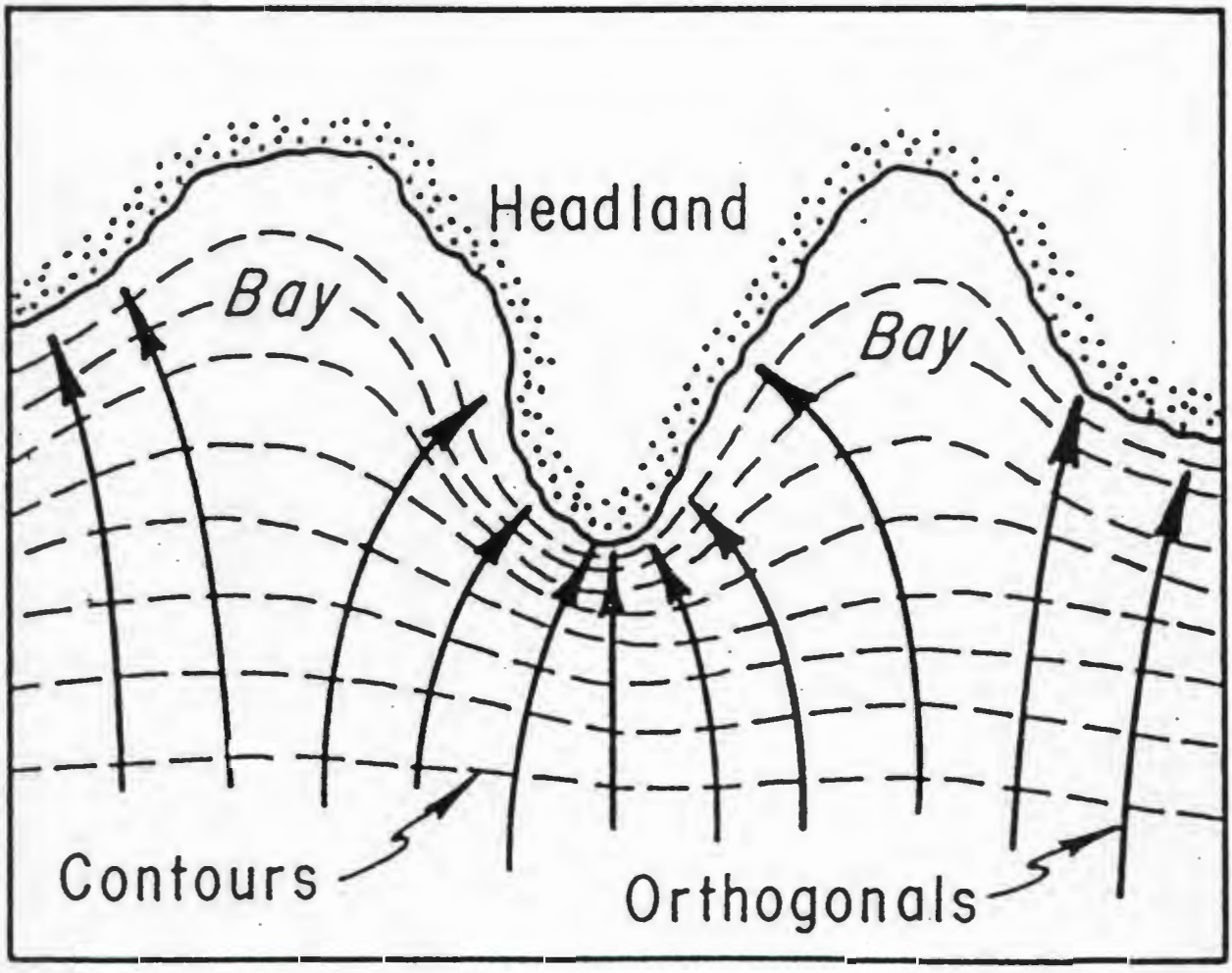

WALKER BAY

WAVE REFRACTION ALONG AN IRREGULAR SHORELINE.
(FROM CERC, 1977)

FIGURE

52

$$d = \frac{L_o}{2}$$

where d = water depth

L_o = $1{,}58\ T^2$ = deepwater wavelength

For the dominant wave conditions given above for Walker Bay, the transition from deepwater waves to shallow-water waves will therefore occur at a depth of approximately 111,0 metres. Since the maximum water depth in the study area is less than 111,0 metres (Figure 10), the dominant wave condition can be expected to influence sediment movement over the entire area although lower bottom orbital velocities will occur in shallower water with consequent less effect on bottom sediments.

Using these dominant values as input parameters, together with the water depths shown in Figure 10, basic wave-refraction calculations were done for Walker Bay in order to obtain an indication of the local wave pattern. A widely used computer-modelling program (RCP-WAVE), developed by the Coastal Engineering Research Centre of the United States Army Corps of Engineers, was used for the computations (CERC, 1986). A contoured plot of the distribution of the refraction coefficient (k_r) in Walker Bay is shown in Figure 53.

Figure 53 shows that in the centre of the bay the direction of the south-southwesterly swells is not significantly altered by the depth contours ($k_r > 0{,}8$). The waves proceed towards the beach without change in direction. Towards the east of the bay, the lower refraction coefficients ($k_r < 0{,}8$), indicate that the waves are refracted away from the incoming direction to become more perpendicular to the Gansbaai coastline. Off Castle Rock and Hermanus, another area of lower refraction coefficients indicates a divergence towards the north of the incoming wave direction.

Since the shoaling coefficient k_s is only a function of the water depth, and considering the fact that the shallower depth contours in Walker Bay (Figure 10) are generally

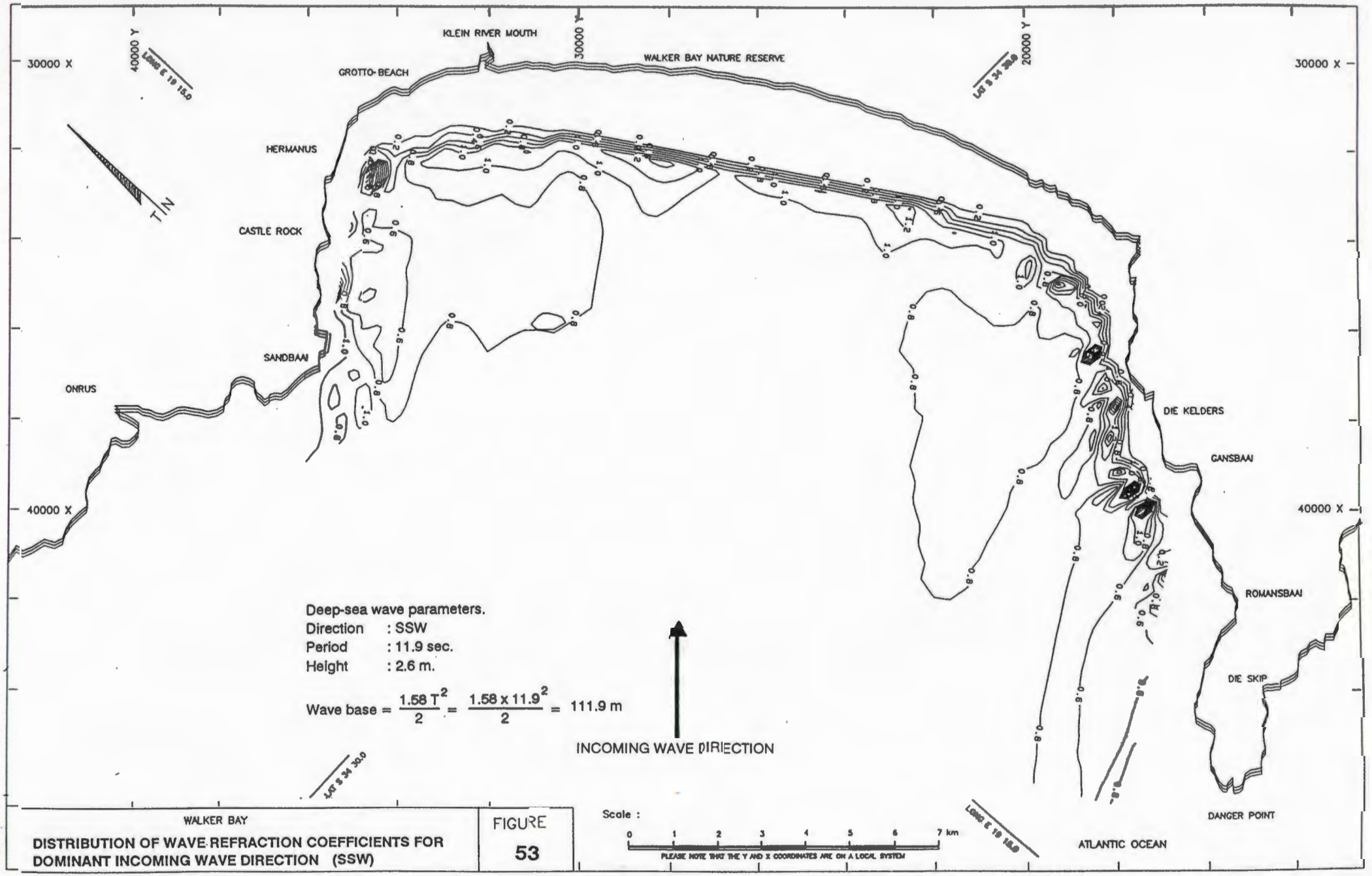

DISTRIBUTION OF WAVE REFRACTION COEFFICIENTS FOR DOMINANT INCOMING WAVE DIRECTION (SSW)

FIGURE 53

aligned with the coastline, Figure 53 can also be used to obtain basic information about the relative wave height distribution over the area for the dominant wave direction. In the central part of the bay the incoming wave is affected by shoaling only ($k_r = 1$) and relatively high waves can be expected. Towards the east and west relatively small waves can be expected due to the influence of refraction and the consequent divergence of the orthogonals.

7.3 Facies 3 Megarippled Patches

7.3.1 General characteristics

As defined earlier, sonograph Facies 3 consists of areas dominated by very discrete and well-defined patches of megarippled gravelly sand, flanked by smooth or small-scale rippled sand. Within Facies 3 the seafloor may therefore suddenly change from a megarippled state to a smooth or rippled state without any apparent change in water depth or hydraulic condition. A similar phenomenon is described by Langhorne *et al.* (1986) in a study of gravel bedforms in the tidal marine environment of the shallow (<20 m) West Solent area, off southern England, where they concluded that factors such as availability of mobile sediment and biological accretion may play a major part in the process. Langhorne *et al.* (1986) found no correlation between sediment characteristics (grain size distribution, shape and carbonate content) and bedform types.

7.3.2 Long-term stability

In order to assess the long-term stability of the Facies 3 megarippled patches, sidescan records from the 1986, 1988 and 1990 surveys were compared. For this purpose, a number of well-defined megaripple patch boundaries off Hermanus, along survey line 10 (Figure 18), were selected and plotted out in detail. Figure 54 shows an example of the sonograph images in this area. The results of the comparison is shown in Figure 55. Any attempt to compare individual crest lines was considered unfeasible, considering that the megaripple wave-lengths (1-2 metres) are of the same order of magnitude as the resolution of the sidescan sonar and less than the repeatability of the position fixing.

NW

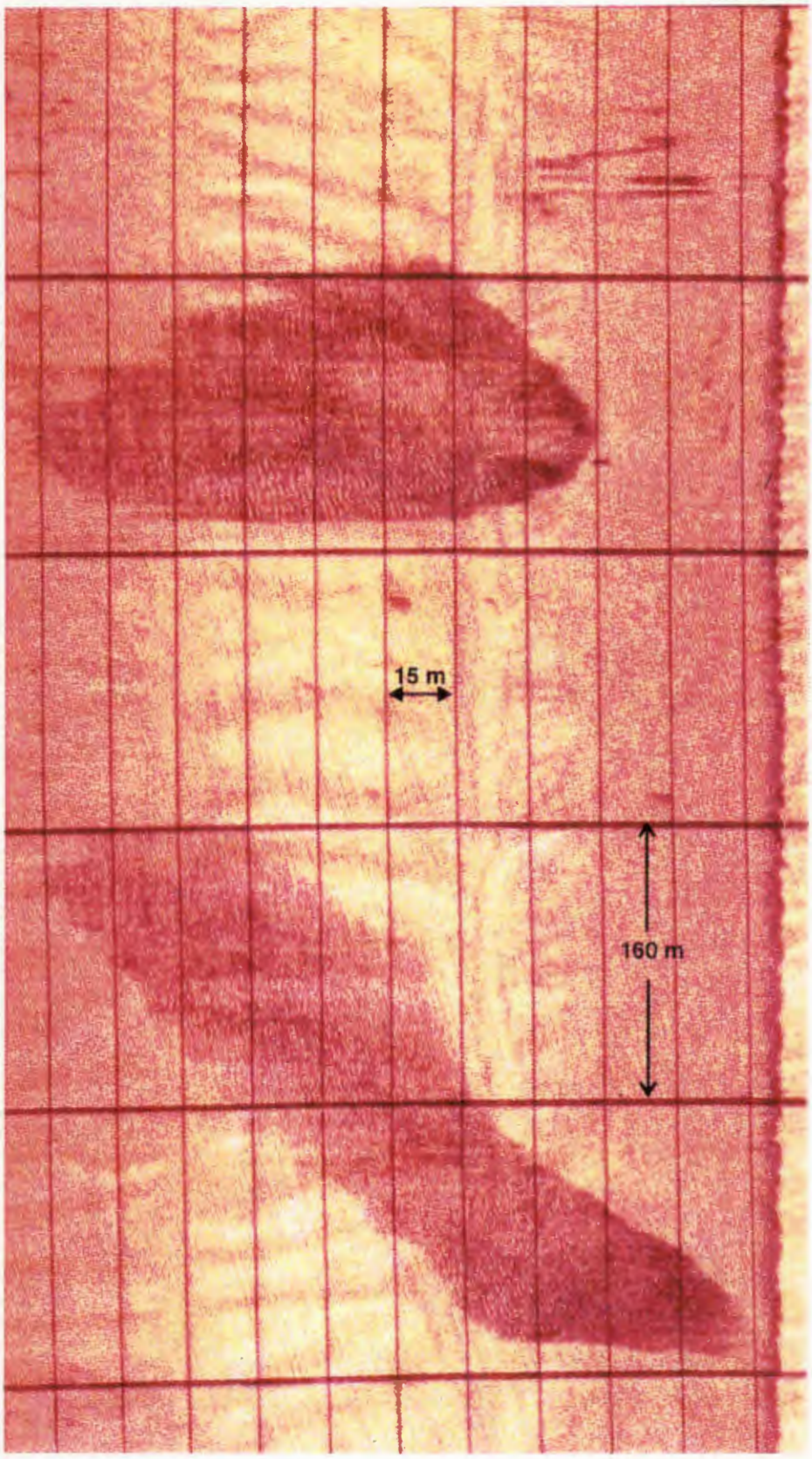

SE

WALKER BAY

SONOGRAPH EXAMPLE - FACIES 3 MEGARIPPLE PATCHES
LOCATION 34750 X; 34500 Y. LINE10
100kHz

FIGURE

54

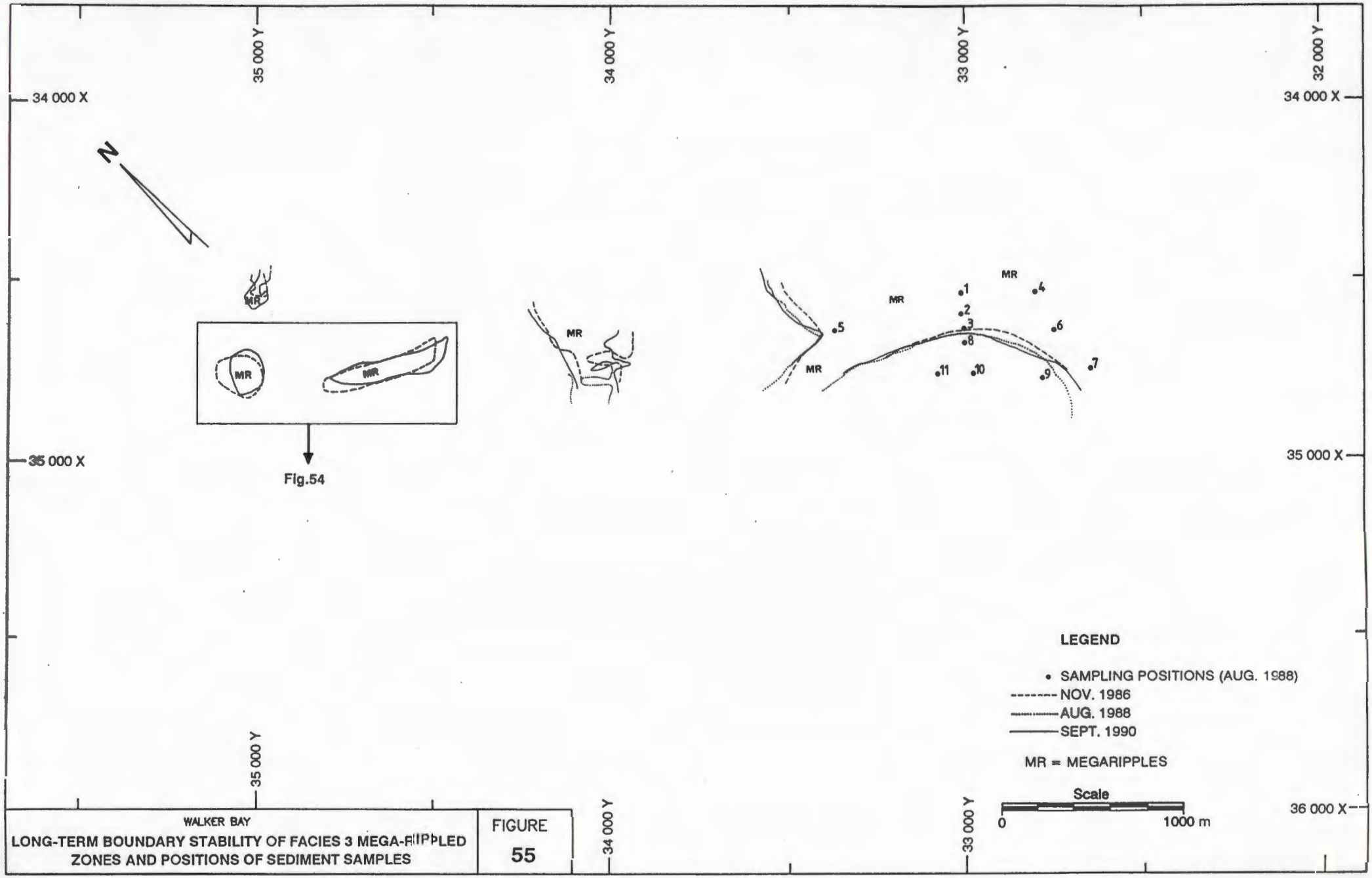

WALKER BAY

LONG-TERM BOUNDARY STABILITY OF FACIES 3 MEGA-RIPPLED ZONES AND POSITIONS OF SEDIMENT SAMPLES

FIGURE 55

Figure 55 shows that, given the inherent inaccuracies of survey methods and plotting techniques, no significant changes in the shape of the boundaries had taken place between the 3 surveys. A similar observation is reported by Langhorne *et al.* (1986). Although the shape of individual megarippled patches did not change, a discrepancy of up to 100m in the lateral position of individual boundaries is indicated by Figure 55. Since the lateral accuracy of the present survey is expected to be well below 100m, a proportion of these discrepancies must be ascribed to a seasonal or short-term change in the positions of the megarippled/rippled boundaries.

7.3.3 Grain size vs bedform dimensions

In his benchmark study on wave-generated ripples, as observed in the field, Inman (1957) states that the grain size of the sand is the single most important factor in determining the size of the ripple. In order to investigate the possible influence of sediment texture on the formation of Facies 3 megarippled patches, a total of 11 closely spaced sediment samples were collected at the same location along survey line 10. The positions of these samples are also shown on Figure 55, numbered 1 to 11. Samples 1 to 7 were retrieved from a megarippled patch whereas samples 8 to 11 are from the apparently smooth or small-scale rippled sand between the megarippled patches. These samples were analysed for textural characteristics only, using the procedure described in Chapter 4. The results are given in Table 10.

Table 10 illustrates a marked difference between the percentage gravel and the median grain diameters of the samples from the two environments, i.e. megarippled and rippled, within Facies 3. The average gravel component and median grain size of the sand fraction within the megarippled patch are 18 percent and 662µm (cS) respectively, whereas the corresponding values for the flanking small-scale rippled area are 0 percent and 276µm (mS). This is in accordance with the direct relationship between grain diameter and ripple size as shown by Inman (1957) and others, but in contrast with the study by Langhorne *et al.* (1986), who found no textural variation between the megarippled and smooth gravel zones in the West Solent.

TABLE 10: TEXTURAL CHARACTERISTICS - FACIES 3 SAMPLE SUITE, 1988

	Sample No	% Gravel	D50 (µm)	Average gravel %	Average D50 (µm)
Mega-rippled patches of gravelly sand	1	23	652 (cS)	18	662 (cS)
	2	21	618 (cS)		
	3	5	661 (cS)		
	4	35	709 (cS)		
	5	4	544 (cS)		
	6	34	721 (cS)		
	7	4	727 (cS)		
Surrounding rippled sand	8	0	303 (mS)	0	276 (mS)
	9	0	175 (fS)		
	10	0	311 (mS)		
	11	0	318 (mS)		

The results from Walker Bay indicate that very abrupt changes in median grain size and gravel content occur at the boundaries of Facies 3 megarippled patches and that the positions of these boundaries shift by up to 100 m on an annual time scale. The data do not, however, give a clear indication of the factors that control the formation and interannual location of megarippled patches. In addition, the mechanisms responsible for the shape of individual megarippled patches and the abrupt changes at their boundaries cannot be explained by the available data and are worthy of further research. Since the above spatial and textural analyses do not supply such information, the answers must rest with the near-bed hydraulic regime or the availability of coarse sediment within the Facies 3 area.

7.3.4 Influence of bedrock outcrops

The configuration of sonograph facies in Walker Bay (Figure 31) shows that Facies 3 megarippled patches always occur in the proximity of, and often on the landward side of bedrock outcrops (Facies 1 and 2) on the seafloor. These bedrock outcrops are the habitat for a wide variety of carbonate-producing organisms and as such they contribute largely to the predominantly shelly gravel component of the sediment in the area. One would therefore expect to find a gradual increase in grain size and gravel content towards bedrock outcrops, although the available data (Figure 44) are not sufficient to prove this hypothesis. The sudden increase in grain size and bedform dimensions at the boundary cannot, however, be related to sediment availability and may be explained in terms of nearbed orbital motion and the critical water velocities needed to move sediment particles of a given size.

For a given grain size and water depth, the character of wave-induced ripples is related to the horizontal amplitude and velocity of oscillatory water movement near the bottom. In order to initiate movement in sand of a given size, a minimum critical orbital velocity is required. No universally accepted relationship between grain size and critical orbital velocity, however, exists, mainly because the definition of the actual onset of movement is not clearcut. Earlier studies on the initiation of sand movement such as those of Bagnold (1946), Manohar (1955), Vincent (1959), Ishihara and Sawaragi (1962),

Carstens *et al.* (1967), Horikawa and Watanabe (1967), Rance and Warren (1968), Dingler (1975) and Davies and Wilkinson (1978) used different criteria for the initiation of movement. To complicate matters, sediment is often moved under the combined influence of waves and currents, requiring a different approach to the threshold condition (Kapdasli, 1991).

Using experimental data from various previous studies, however, the writer (Lenhoff, 1982) showed that the results are generally compatible and that the incipient motion of sediment particles under oscillatory flow can be estimated by the empirical curve shown in Figure 56 which was found to be very closely approximated by the following parabolic equation:

$$\log_{10} R_* = 0{,}092\,(\log_{10} D)^2 + 1{,}158\,\log_{10} D_* - 0{,}367$$

where $R_* = \frac{U_* D_{50}}{\nu}$ = shear Reynolds number

and $D_* = \left(\frac{\Delta_s g}{\nu}\right)^{1/3} D_{50}$

with U_* = shear velocity = $\left(\frac{\bar{\tau}}{\rho_w}\right)^{1/2}$

D_{50} = median grain size

ν = kinematic viscosity of fluid

$\bar{\tau}$ = mean shear stress = $1/4\ \rho_w f_w U_o^2$

ρ_s = density of sediment

ρ_w = density of fluid medium

Δ_s = relative buoyant sediment density = $(\rho_s - \rho_w)/\rho_w$

U_o = horizontal orbital velocity at the bed

f_w = wave friction factor = f (a_o/r)

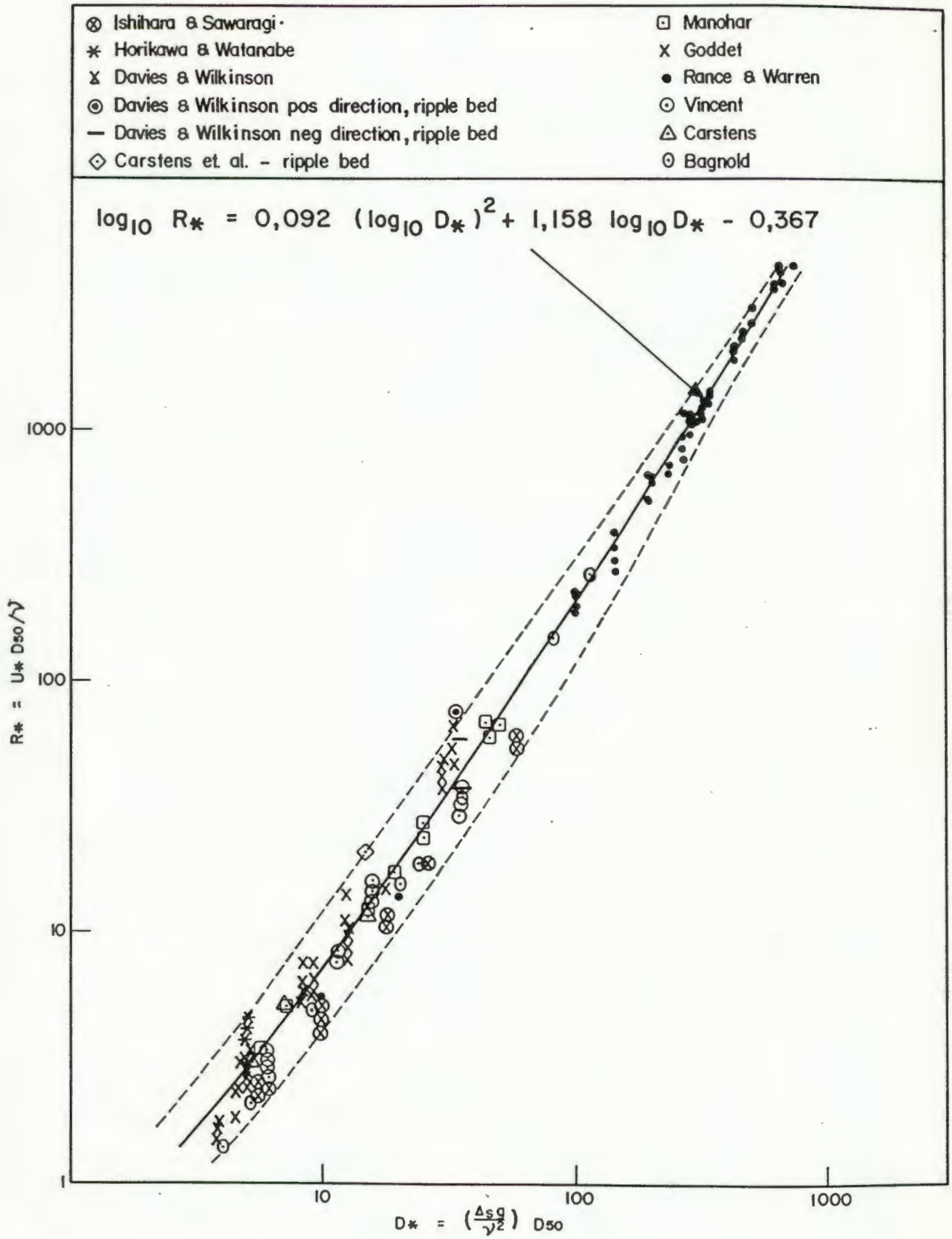

WALKER BAY

INCIPIENT MOTION OF SEDIMENT PARTICLES UNDER OSCILLATORY FLOW - FROM LENHOFF, 1982.

FIGURE

56

and a_o = maximum orbital excursion from mean position of the motion of water particles at the bed

r = bed roughness

It can be assumed that, given a smooth seabed and a constant water depth, the nearbed hydraulic regime caused by waves does not change rapidly over short distances. It is conceivable, however, that high-relief rock outcrops on the seabed (Facies 1 and 2) may significantly influence wave characteristics due to increased bed roughness and a consequent interference with the general refraction pattern. Local convergence of wave orthogonals landward of rock outcrops could lead to increased near-bed orbital velocities and amplitudes in certain areas, causing a change in bedform type. As the wave then progresses from a rocky area into a sandy area, a gradual change towards the original wave-form and refraction pattern may be expected. The resulting bedforms as observed in Facies 3 do not, however, follow a gradual change in characteristics, but an abrupt changeover. It would appear that when the moving forces at the seabed cross a critical threshold value, sudden changes in bedform characteristics can be expected. Figure 56, however, does not suggest any nick-points in the relationship between grain size and critical orbital velocity.

In Walker Bay (Figure 31) it would, therefore, appear that rock outcrops create specific environments on their landward sides, which are conducive to the formation of the large megaripples of Facies 3 and the removal of fine material. Once formed, the megaripples contribute further to the removal of finer sediment as the finer grains are placed in suspension by the vortex at the ripple crest and carried landward out of the area. When the entraining orbital velocities decline to a critical value the finer sediment settles and a sharp boundary between megarippled coarse sand and smooth or small-scale rippled finer sand is formed.

The factors finally influencing the configuration and shapes of the megarippled patches associated with the rock outcrops are most likely a complex combination of local wave diffraction and refraction phenomena, together with possible tidal influences. A further detailed discussion of these is beyond the scope of this study.

7.3.5 Megaripple wavelengths

Estimates of the wavelengths of Facies 3 megaripples were made from the sidescan sonar and are shown on Figure 57, together with the water depths at the specific locations. Figure 57shows that the wavelengths vary between 1,0 and 1,9 metres over water-depths of between 25 and 75 metres, with no obvious relationship between the two parameters. The shorter wavelengths do, however, appear to be more dominant in the eastern section of the area where, as discussed in Section 7.2, the waves are smaller off the Gansbaai coastline.

As discussed in Section 7.3.1, the mechanisms responsible for megaripple generation are complex and probably relate to the effect of a multitude of rock outcrops on the incoming waves. As such, the megaripple wavelength distribution is unlikely to reflect a simple wave pattern.

In general, the shorter megaripple-wavelengths appear to be associated with the shallower inshore areas, but no direct relationship can be concluded from the data.

7.3.6 Megaripple crest orientations

The distribution of Facies 3 megaripple crest orientations, as obtained from the sidescan sonar data, is also shown in Figure 57. Note that the crest orientations are illustrated schematically, showing the average crest orientation at a given locality. A comparison of the 1986, 1987 and 1990 surveys revealed no significant interannual variation in crest orientation.

Figure 57 shows that the directions of megaripple orthogonals range over approximately 20 degrees, between 210° and 255°, with the vast majority of values between 210° and 230°. (To aid comparison with wave directions (Figure 53), the orientation of the megaripple orthogonals is defined as the seaward bearing normal to the megaripple crest).

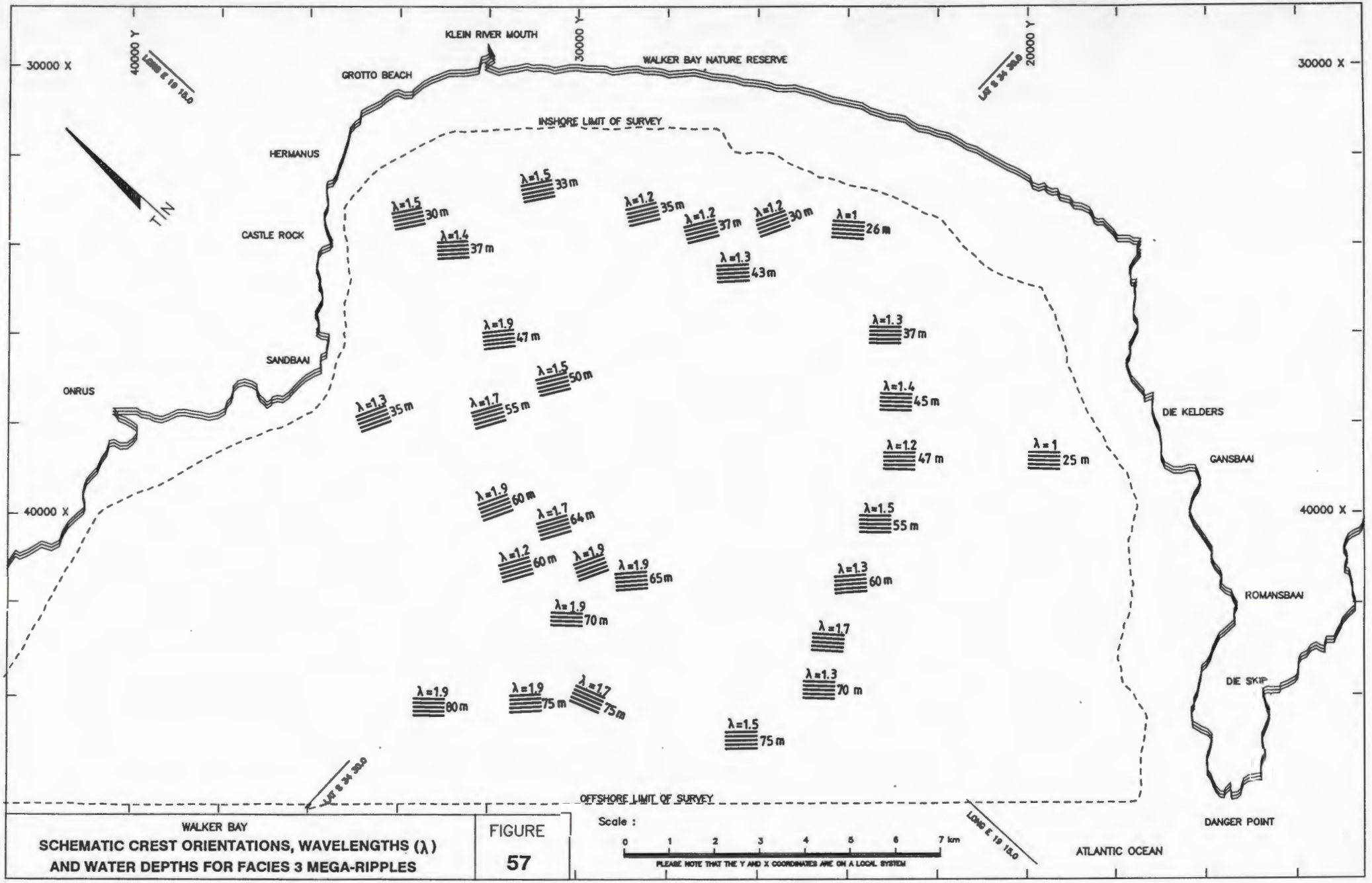

WALKER BAY

SCHEMATIC CREST ORIENTATIONS, WAVELENGTHS (λ) AND WATER DEPTHS FOR FACIES 3 MEGA-RIPPLES

FIGURE **57**

In the western section of the area, the orientations are centred in a narrow band around 210 degrees, whereas in the eastern section the mean orientation is 230 degrees. These orientations are suggestive of some wave refraction in the west, but they do not reflect the refraction off the Gansbaai coastline (Figure 53). Care should, however, be taken when megaripple-crest orientations are related to the incoming wave refraction patterns. Carter (1989) has shown that wave-reflection effects can also have a significant influence on megaripple-crest orientations, particularly when the incoming waves impinge obliquely onto the coastline, as is the case along the northern and southern shores of Walker Bay (Figure 53).

7.4 Facies 4 Ripples

The dimensions of the randomly orientated, short-crested Facies 4 ripples were too small to be resolved by the sidescan sonar and their existence was only revealed by the ROV observations (Figures 49 and 50). No quantitative data on their characteristics are available, other than the estimates previously mentioned.

Boyd *et al.* (1988) observed similar "chaotic" ripples in 10 m water depth, 1 km off Martinique Beach on the Atlantic coast of Nova Scotia. They are characterized by a confused irregular crest pattern and exhibit a wide range of wavelengths and shape indices. They typically exist only briefly during dramatic reorganizations of the bed and are associated with the initiation of higher-energy wave conditions.

The sedimentological data show that these ripples in Walker Bay are associated with fine sand, in contrast with the medium to coarse sand of the megaripples of Facies 3. Inman (1957) states that ripples in fine sand are more rapidly modified by changing wave conditions than ripples in coarse sand. As shown earlier, the directional wave spectrum for Walker Bay indicates significant wave energy flux from all directions within the southwestern quadrant (Figure 7). The Facies 4 ripples appear to respond quickly to these changing wave directions, giving rise to their chaotic nature. It could therefore be concluded that the Facies 4 ripples in Walker Bay represent ephemeral changes in wave direction and energy, whereas the Facies 3 megaripples are more stable and only become mobile during high-energy events.

8. ANALYSIS OF GRAIN SIZE PARAMETERS

8.1 General

In this chapter the grain size parameters of the Facies 3 and 4 sediment samples as obtained by settling tube will be discussed in more detail. Possible trends in mean size, sorting, skewness and kurtosis will be highlighted in an attempt to get a better perspective on the factors responsible for the present distribution of unconsolidated sediment in Walker Bay.

The distribution of sediment samples collected from Facies 3 and 4 is shown in Figure 58. Figure 59 shows the same data but with the grain size frequency curve and its graphic measures (mean size (M), sorting (S), skewness (Sk) and kurtosis (K)) added for each sample. The original settling-tube data are contained in Appendices A and B.

To avoid unnecessary congestion on Figure 59, samples taken within one kilometre of each other from the same facies **and** having similar grain size parameters are represented by a single data set. A small number of samples are therefore not shown on Figure 59 but are represented by a close neighbour instead. It was assumed that this procedure would have little influence on the validity of possible trends which may be detected as well as on the final conclusions.

Grain size trends of surficial sediments result from sediment transport processes and may therefore assist in identifying sediment pathways and transport mechanisms (Gao *et al.*, 1994). According to Gao and Collins (1992), any grain size trend which has a significantly higher probability of occurrence in the direction of net transport than in any other direction can be used to determine the nett transport pattern.

In Chapter 7 it was concluded that the clear-cut definition in the areal distribution of Facies 3 and 4 in Walker Bay can be attributed to the direct influence of rock outcrops on the incoming waves and hence the sediment entrainment forces on the seabed. As

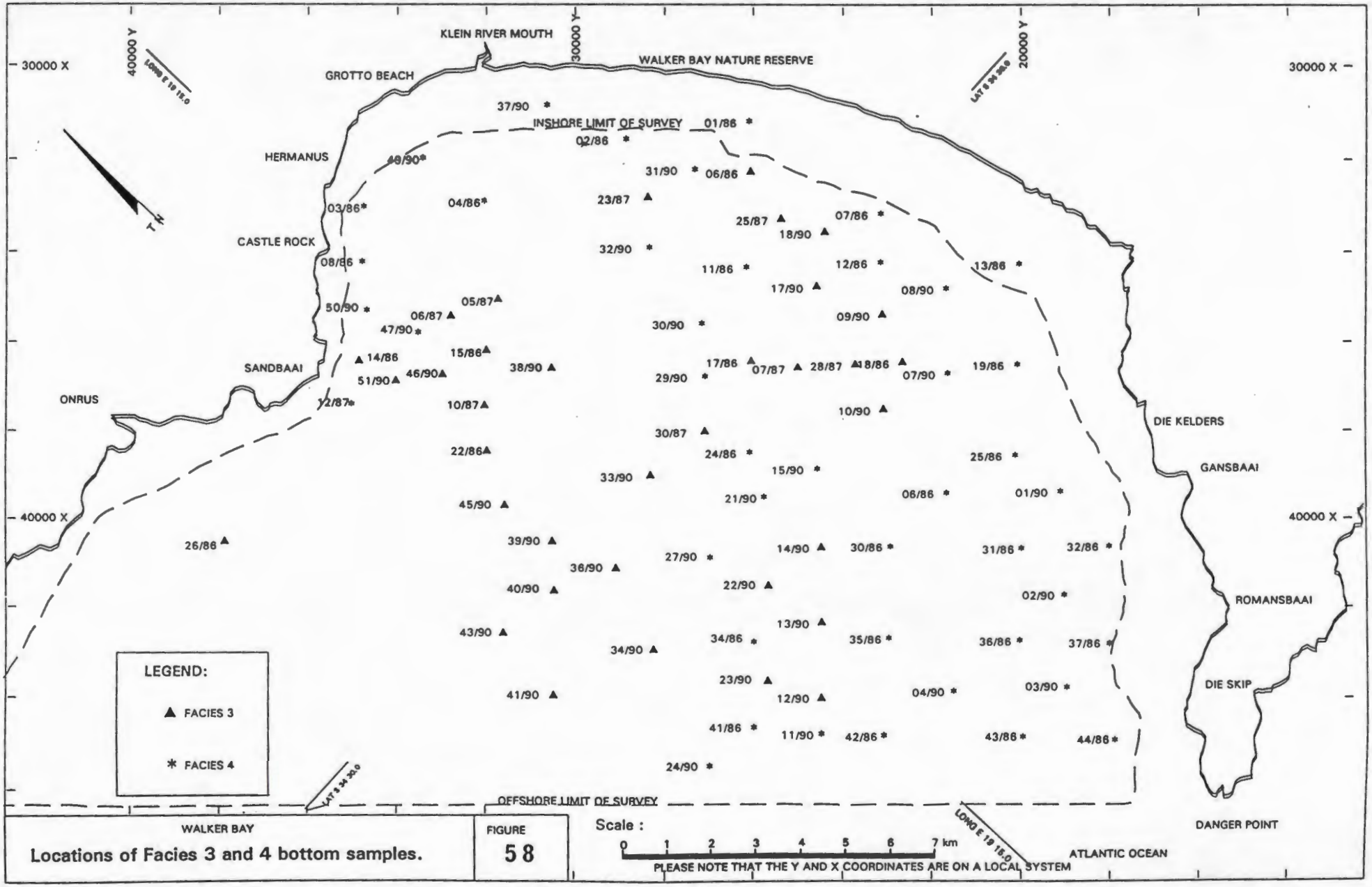

FIGURE 58

Locations of Facies 3 and 4 bottom samples.

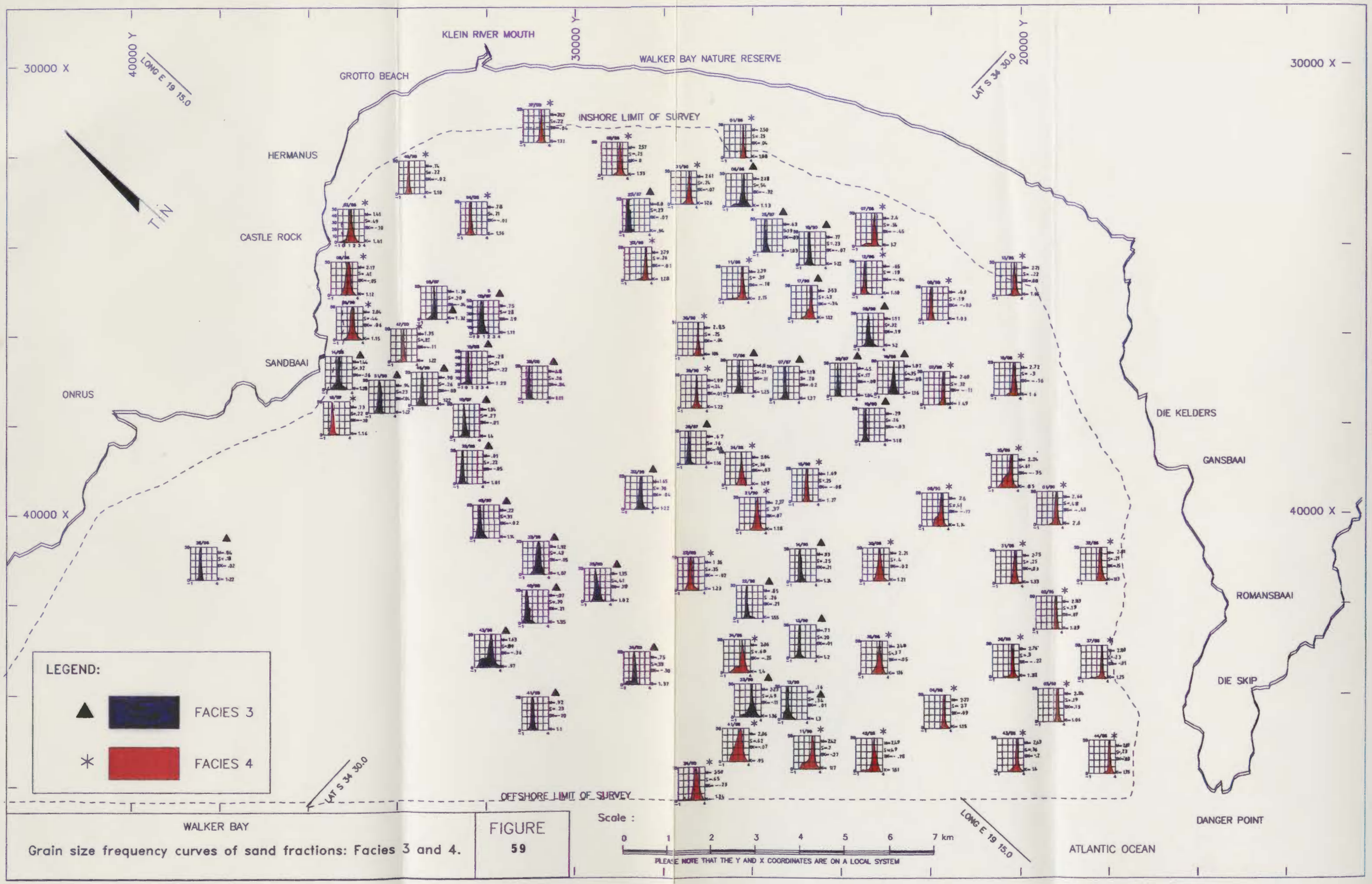

Grain size frequency curves of sand fractions: Facies 3 and 4.

FIGURE 59

such, typical sedimentological trends are unlikely to emerge due to the complex nature of the transport mechanisms. Sagga (1992) states that when analysing textural parameters the morphology of the environment should be considered, as the hydrodynamic conditions of sedimentation can be modified by the various morphological elements. The increased bed roughness due to exposed high relief rock outcrops in Walker Bay is considered as an example of such morphological elements.

In the following sections the modality, mean size, sorting, skewness and kurtosis of the samples within each facies will be compared and discussed.

8.2 Grain Size Distribution Modality

Most of the samples from both facies show a unimodal grain size distribution. Bimodal distributions do, however, occur in 7 samples from Facies 4, scattered throughout the area. In all these cases the secondary mode is not very pronounced and occurs on the coarse side of the primary mode.

The Facies 3 results show more deviations from the general unimodal trend and polymodal distributions commonly occur, with secondary modes both finer and coarser than the primary. The secondary modes are again not pronounced and no progressive mixing of populations is evident. The polymodal occurrences in Facies 3 can be attributed to the relatively high content of skeletal material which are derived from the mechanical breakdown of marine organisms on the nearby rock outcrops. Figure 59 and Table 8 show that bi- and polymodality generally occur in samples with a high carbonate content. Graf (1976) proposed that unimodal distributions are produced by the influence of the largest waves on the bottom material whereas bimodal distributions result from smaller waves. The modality trends in Walker Bay do not, however, show any obvious correlation with the dominant wave-energy pattern (Figure 53). Blackley and Heathershaw (1982) attributed polymodality to the influence of shoaling waves, which may explain the bimodal and polymodal occurrences in Walker Bay, considering the dominance of waves as transporting mechanisms.

In the following discussion of mean size, sorting, skewness and kurtosis only samples with a unimodal distribution were considered.

8.3 Mean Grain Size

The distribution of mean grain sizes was discussed earlier (Figure 44) and will only be briefly reviewed here.

The Facies 4 sediments in the southern section of the bay tend to be significantly finer than those in the northern corner off Hermanus. In the inshore area, off the sandy beach along the Walker Bay Nature Reserve, the Facies 4 samples display remarkably similar mean grain size characteristics (average 2.5 phi (fine sand)). These samples most likely belong to the nearshore sand prism and are subject to the dynamic processes typically associated with a sandy coastline under normally incident wave attack. Off the Gansbaai coastline the Facies 4 sediments also display very similar mean grain sizes (average 2,70 phi (fine sand)), indicating a relatively low energy environment, sheltered from the southerly swells by the headland at Danger Point. No obvious trends in mean grain size perpendicular to the coastline are evident.

The mean grain sizes within Facies 3 vary considerably, with an average of 0,96 ϕ. Along the submarine extension of the Klein River valley, discussed earlier (Figure 29), the relict terrigenous sediment appears to coarsen slightly in an offshore direction. This trend may be due to post-depositional reworking by processes associated with an advancing shoreline.

8.4 Sorting

In discussing sediment sorting, the following categories will be used, after Folk (1974):

< 0,35 ϕ	very well sorted
0,35 - 0,50 ϕ	well sorted
0,50 - 0,71 ϕ	moderately well sorted
0,71 - 1,00 ϕ	moderately sorted

1,00 - 2,00 ϕ	poorly sorted
2,00 - 4,00 ϕ	very poorly sorted
> 4,00 ϕ	extremely poorly sorted

The Facies 3 sediments are generally very well sorted with an overall average of 0,25 ϕ. Strong sorting therefore appears to take place in the areas where the incoming waves are affected by high relief outcrops on the seabed, i.e. areas dominated by Facies 3 sediments. On a regular sloping sandy seabed without the effect of rock outcrops, shoaling waves are believed to be responsible for poorly sorted sediments (Graf, 1976). This again illustrates the important effect of morphological irregularities on the entrainment criteria at the seabed.

Facies 4 also falls within the very well sorted category with an overall average of 0,31 ϕ which is slightly higher than the average for Facies 3 (0,25 ϕ). The samples from the nearshore sand prism collected off the Walker Bay Nature Reserve consistently show very low sorting values (average 0,23 ϕ) again emphasizing their common hydrodynamic environment as pointed out earlier. No obvious sorting trends within the Facies 4 samples were observed in any specific direction.

8.5 Skewness

The following verbal terms and their corresponding skewness limits are used in the discussion below (after Folk, 1974):

Strongly fine skewed	+1,00 to +0,30
Fine skewed	+0,30 to +0,10
Near-symmetrical	+0,10 to -0,10
Coarse skewed	-0,10 to -0,30
Strongly coarse skewed	-0,30 to -1,00

Sediment samples taken from Facies 3 have skewness values ranging from -0,18 (coarse skewed) to +0,21 (fine skewed) with an average of +0,01 (near symmetrical).

Approximately equal numbers of positively and negatively skewed distributions occur with almost 70 per cent of the samples falling in the near symmetrical category (+0,10 to -0,10). No significant trends were detected.

Facies 4 show skewness values ranging from -0,41 (strongly coarse skewed) to +0,15 (fine skewed) with an average of -0,05 (near symmetrical). The relatively wide variation in negative skewness seems to indicate that Facies 4 (i.e. chaotic small-scale rippled sediment) is more sensitive to fluctuations in wave energy levels than the coarser, megarippled Facies 3 (cf. Sagga, 1992).

8.6 Kurtosis

Facies 3 show kurtosis values (Folk, 1974) ranging between 1,0 and 1,6 (mesokurtic to very leptokurtic) with an average of 1,2 (leptokurtic). For Facies 4 the values range between 1,0 and 2,6 (mesokurtic to very leptokurtic) with an average of 1,3 (leptokurtic).

The kurtosis values for both Facies 3 and 4 appear to display no significant pattern.

8.7 Conclusions

The above analysis of grain size distributions in Walker Bay does not fully succeed in revealing the dominant sediment transport mechanisms responsible for the observed distribution of Facies 3 and 4 sediments. In many instances it serves as an illustration of the complexities involved in defining the processes of entrainment and deposition through grain size analyses. The results do, however, significantly contribute towards a better understanding of certain key factors controlling sediment dynamics in the bay. These may be briefly summarized as follows:

(i) The occurrences of bi- and polymodal distributions can be correlated with high carbonate content, derived from the mechanical breakdown of the calcareous skeletons of marine organisms, e.g. bivalves, on the nearby rock outcrops.

(ii) Homogeneous, well sorted fine sand (2,7 ϕ) of Facies 4 off the Gansbaai coastline underlines the important sheltering effect of the Danger Point headland.

(iii) The homogeneous, well sorted fine sand (2,5 ϕ) collected off the Walker Bay Nature Reserve probably belongs to the nearshore sand prism and show very similar characteristics.

(iv) The coarser Facies 3 sediments (average 0,96 ϕ) are subject to strong sorting mechanisms which are associated with the influence of nearby rock outcrops on incoming waves.

(v) The wide variation in negative skewness indicates that Facies 4 is more sensitive to fluctuations in wave energy than the coarser, megarippled Facies 3.

9. CONCLUSIONS

9.1 Seafloor Geology

The surficial shoreface geology of Walker Bay as investigated by seismic profiling, sidescan sonar, ROV photography and sediment sampling was described in terms of sonograph facies 1, 2, 3 and 4.

Facies 1 consists of high-relief Bokkeveld Group outcrops with the primary bedding striking NE-SW. Sediment-filled strike gullies, up to 100 m in width, commonly occur and an ENE-WSW orientated joint set was observed, intersecting the primary bedding.

Facies 2 consists of low-relief Bokkeveld Group outcrops and occurs as an eastward and shallower landward extension of Facies 1. These relatively flat outcrops are often covered with a thin veneer of unconsolidated sediment and lineaments are rarely visible. Loose cobbles and boulders commonly occur. Both Facies 1 and 2 outcrops are covered with abundant marine growth and serve as the main source of the carbonate content of unconsolidated sediments in the bay.

Pre-Mesozoic bedrock outcrops (Facies 1 and 2) occupy approximately 45% of the study area. In the remaining area the bedrock is overlain by unconsolidated sediment which was, based on surficial bedform characteristics, defined as Facies 3 and 4.

Facies 3 represents areas dominated by well defined and discrete megarippled gravelly sand patches, separated by small-scale rippled sand. These patches are typically 150 to 200 m in diameter and irregularly shaped. The mean size of the sand in Facies 3 varies between 0 and 2,0 phi, i.e. coarse to medium sand. The overall carbonate content generally varies between 40 and 60 percent and the components consist mainly of fragments of gastropod and bivalve shells and cirripede fragments. Echinoid spines, sponge spicules, benthic foraminifera and ahermatypic coral debris also commonly occur. The terrigenous component normally consists of quartz as the major constituent, calcarenite from the Waenhuiskrans Formation, Bokkeveld shale fragments and

occasional grains of authigenic phosphorite and glauconite. Toward the west, in an area southeast of Sandbaai and Onrus, the Facies 3 sediments are characterized by a very high lithic component. Here the rocky seafloor is trough-shaped, orientated NE-SW and the sediments are likely to be of fluvial origin, deposited in a paleo-channel of the Kleinrivier during sea-level lowstands.

Facies 4 occurs mainly in the southeastern half of the study area and consists exclusively of small-scale rippled sand. The mean size varies between 2,0 and 3,0 phi, i.e. fine sand. The mean grain size decreases towards the east and off the Gansbaai coastline the mean size is consistently finer than 2,5 phi. The carbonate content of Facies 4 sand averages 74 percent with no apparent trend. A microscopic analysis of the Facies 4 samples revealed similar components as mentioned above for Facies 3.

9.2 Wave-Generated Bedforms

The Facies 3 and 4 sediments in Walker Bay display distinctly different bedform characteristics, i.e. the megarippled patches of Facies 3 and the small-scale "chaotic" ripples of Facies 4.

Facies 3 megaripples

The long-term stability of the Facies 3 megaripples was assessed by comparing sidescan sonar data from surveys conducted over a period of 4 years. The results showed that although the shape of individual patches remained essentially unaltered, the positions of the boundaries shifted laterally by up to 100 m between the surveys, indicating short-term seasonal change.

Detailed sediment sampling along a traverse across a megaripple patch boundary showed that the gravel content and mean grain size values within the megarippled patch are considerably greater than those for the flanking small-scale rippled area. No change in components was detected.

The available data indicate that the formation of Facies 3 megarippled patches is closely related to the influence of bedrock outcrops on the local wave-refraction pattern. Local convergence of wave orthogonals landward of rock outcrops could lead to increased near-bed orbital velocities and amplitudes in specific areas, causing the formation of megarippled patches. The present data, however, do not offer a clearcut explanation for the sharp and well-defined boundaries of the megarippled patches. Commonly used sediment-entrainment criteria do not readily suggest sudden changes in bedform characteristics over very short distances. A detailed analysis of the mechanisms responsible for Facies 3 megaripples would require accurate long-term measurements of the orbital water velocities and amplitudes at the seabed on either side of a boundary, as well as the variations of these parameters due to changing wave conditions.

The megaripple crest orientations appear, broadly, to reflect the wave-refraction pattern in Walker Bay. The megaripple-wavelength distribution, however, does not show an obvious trend other than a slight decrease towards the shallower inshore areas.

Facies 4 ripples

The Facies 4 "chaotic" ripples could only be resolved by underwater photography and no quantitative data on their dimensions are available. It is concluded that they represent ephemeral changes in wave direction and energy.

In conclusion, this study once again emphasizes the importance of groundtruth information in geophysical seabed mapping. The use of a video-equipped R.O.V., in particular, proved to be highly effective in resolving small-scale seabed features which would otherwise have gone unnoticed, especially in depths beyond the range of normal scuba diving. In detailed seabed mapping projects the collection of groundtruth data should be considered an integral part of the survey rather than a mere complement to side-scan and seismic data, as is often the case.

9.3 Grain Size Distributions

Grain size distribution analyses of Facies 3 and 4 sediments contributed marginally towards the detailed documentation of transport mechanisms but succeeded in highlighting and confirming certain key factors controlling the sediment dynamics in Walker Bay.

REFERENCES

ANDERSEN, N.J.B. and ANDREOLI, M.A.G. 1990. The structural evolution of the coastal area between Danger Point and Struisbaai in the southern Cape Fold Belt, with implications for the siting of a nuclear power station. *S. Afr. J. Sci., 86 : 499-511.*

ASHLEY, G.M., CHAIRPERSON AND OTHERS 1990. Research Symposium; "Classification of Large-Scale Subagueous Bedforms: A new look at an old problem". Jour. Sed. Pet., 60: pp. 160-172.

BAGNOLD, R.A. 1946. Motion of waves in shallow water-interaction between waves and sand bottoms. *Proc. R. Soc. A187 : 1-18.*

BIRCH, G.F. 1978. "Nearshore Quaternary Sedimentation off the South Coast of South Africa. (Cape Town to Port Elizabeth). Bull. Jt. Geol. Surv./Univ. Cape Town Mar. Geosc. Unit, Tech. Rep 11, pp. 127-146.

BLACK, K.P. and HEALEY, T.R. 1988. Formation of ripple bands in a wave-convergence zone. *Jour. Sed. Pet., 58 : 195-207.*

BLACKLEY, M.W.L. and HEATHERSHAW, A.D. 1982. "Wave and tidal - current sorting of sand and a wide surf-zone beach. Mar. Geol., 49: 345-356.

BOYD, R., FORBES, D.L. and HEFFLER, D.E. 1988. Time-sequence observations of wave-formed sand ripples on an ocean shoreface. *Sedimentology, 35 : 449-464.*

BREMNER, J.M. 1978. "The Planimetric Shape of Algoa Bay". Bull. Jt. Geol. Surv./Univ. Cape Town Mar. Geosc. Unit, Tech. Rep. 11, pp. 107-117.

BREMNER, J.M. 1987. Continental margin bathymetry - Kleinmond to Cape Agulhas. *Geol. Surv. S. Afr. internal report, 4p and 17 bathymetry maps at 1:50 000 scale.*

BREMNER, J.M. and MALAN, J.A. 1990. 1:250 000 onshore/offshore map series, Geological Survey of South Africa. Coastal-zone morphology and geology, Hermanus.

BRINK, V.D.S. and ROGERS, J. 1985. Rapid granulometry of sand using a computer-linked settling-tube. *Tech. Rep. Jt. Geol. Surv./Univ. Cape Town Mar. Geosc. Unit, 15: 73-125.*

CARSTENS, M.R., NIELSON, F.M. and ALTINBILEK, H.D. 1967. An analytical and experimental study of bed forms under water waves. *Georgia Ins. Tech., Final Rep. Proj. A-798.*

CARTER, T.G. 1989. Formation of ripple bands in a wave-convergence zone - discussion. *Jour. Sed. Pet., 59 : pp. 346-348.*

C.E.R.C. 1977. Shore Protection Manual. Vol. 1. U.S. Army Coastal Engineering Research Centre, 468pp.

C.E.R.C. 1986. Regional Coastal Processes Numerical Modelling System, Rep. 1-RCPWAVE - A linear wave propagation model for engineering use. U.S. Army Corps of Engineers, Techn. Rep. CERC-86-4, 71 pp.

CSIR 1986. Mossel Bay Offshore Development Project Environmental Data for Design, Vol. 2 : Wave data. *CSIR Rep. C/SEA 8643/2, 39pp.*

CSIR 1990. Environmental Data for the Design and Operation of the Mossel Bay SPM. *CSIR Rep. EMA-C 90108, 33pp.*

DAVIES, A.G. and WILKINSON, R.H. 1978. Sediment motion caused by surface water waves. *Proc. 16th Conf. Coast. Eng., Vol. 1 : 1577-1595.*

DINGLE, R.V. and SCRUTTON, R.A. 1974. Continental breakup and the development of Post-Paleozoic sedimentary basins around southern Africa. *Geol.Soc. Am. Bull., 85 : 1467-1474.*

DINGLER, J.R. 1975. *Wave formed ripples in nearshore sands.* Unpubl. Ph.D. Thesis, Univ. of Calif., San Diego, Calif., 136 pp.

DU PLESSIS, A. and GLASS, J.G. 1991. The Geology of False Bay. *Trans. R. Soc. S. Afr., Parts 4 and 5 : 495-517.*

FLEMMING, B.W. 1976b. Side-scan sonar: A practical guide. *Int. Hydrogr. Rev. 53: 65-92.*

FOLK, R.L. 1974. "Petrology of Sedimentary Rocks", Hemphill, Austin, Tex., 92 pp.

FOX, W.T. and DAVIES, R.A. (Jr) 1976. Weather patterns and coastal processes. In: Davis, J.R. and Ethington, R.L. (Ed.) Beach and Nearshore Sedimentation. *Soc. Econ. Pal. Min. Spec. Publ. 24 : 1-23.*

FROMME, G.A.W. 1977. Establishment of a standard relationship between settling velocity and grain size of coastal sand. *CSIR Rep. SEA.I.R. 72 pp, CSIR, Stellenbosch, South Africa.*

GAO, S. and COLLINS, M. 1992. Net sediment transport patterns inferred from grain-size trends, based upon definition of "transport vectors". *Sediment. Geol.*, 81: 47-60

GAO, S., COLLINS M.B., LANCKNEUS, J., DE MOOR, G. and VAN LANCHER, V. 1994. "Grain size trends associated with net sediment transport patterns: An example from the Belgian continental shelf". Mar. Geol. 121: 171-185.

GRAF, J.B. 1976. "Composition of measured and predicted nearshore sediment grain-size distribution patterns, Southwestern Lake Michigan, USA", Mar. Geol., 22: 253-270.

GENTLE, R.I. 1987. The geology of the Inner Continental Shelf and Agulhas Arch: Cape Town to Port Elizabeth. *Bull. Jt. Geol. Surv./Univ. Cape Town Mar. Geosc. Unit, 20, 129pp.*

HÄLBICH, I.W. 1983. A geodynamic model of the Cape Fold Belt. In: Geodynamics of the Cape Fold belt, In: Söhnge, A.P.G. and Hälbich, I.W. (Ed.) *Geodynamics of the Cape Fold Belt. Geol. Soc. S. Afr.: 177-184.*

HEYDORN, A.E.F. and TINLEY, K.L. 1980. Estuaries of the Cape, Part 1: Synopsis of the Cape Coast. CSIR Res. Rep. 380, 96pp.

HORIKAWA, K. and WATANABE, A. 1967. A study on sand movement due to wave action. *Coast. Eng. Japan, Vol. X : 39-58.*

INMAN, D.L. 1957. Wave-generated ripples in nearshore sands. *U.S. Army Corps of Engineers, Tech, Mem., 100 : 65pp.*

ISHIHARA, T and SAWARAGI, T. 1962. Fundamental studies of sand drifts. *Coast. Eng. Japan, Vol 5 : 59-65.*

KAPDASLI, M.S. 1991. Threshold condition of sand particles under codirectional combined wave and current flew. In: Soulsby, R. and Bettes, R. (eds) *Sand Transport in Rivers, Estuaries and the Sea. A.A. Balkema, Rotterdam, pp. 31-36.*

KOMAR, P.D. 1976. Beach processes and sedimentation. *Prentice-Hall Inc., Englewood Cliffs, New Jersey, 429 pp.*

LANGHORNE, D.N., HEATHERSHAW A.D. and READ, A.A. 1986. Gravel Bedforms in the West Solent, Southern England. *Geo-Marine Letters, 5 : 225-230.*

LENHOFF, L. 1981. Comparison of settling tube results. *Unpublished CSIR project, Stellenbosch, South Africa.*

LENHOFF, L. 1982. Incipient motion of particles under oscillatory flow. *Proc. 18th Coast. Eng. Conf., 2 : 1555-1568.*

MALAN, J. 1987. The Bredasdorp Group in the area between Gans Bay and Mossel Bay. *S. Afr. J. Sci. 83 : 506-307.*

MANOHAR, M. 1955. Mechanics of bottom sediment due to wave action. *U.S. Army Corps of Engineers, Beach Erosion Board Tech. Mem. 75, 101*pp.

McQUILLIN, R., BACON, M. and BARCLAY, W. 1979. An Introduction to Seismic Interpretation. *Graham and Trotman Ltd, London, U.K., 199 pp.*

MILLER, M.C. and KOMAR, P.D. 1980. A field investigation of the relationship between oscillation ripple spacing and the near-bottom water orbital motions. *Jour. Sed. Pet., 50 : 183-191.*

MUNRO, J. 1988. *Die geomorfologiese verandering van die Walkerbaai-kuslyn.* Hons. Report, Dept. of Geography, Univ. of Stellenbosch, Stellenbosch, 40pp.

NIELSEN, P. 1981. Dynamics and geometry of wave-generated ripples. *J. Geophys. Res., 86 : 6467-6472.*

RAMSEY, P.J. and MASON, T.R. 1990. Development of a Type Zoning Model for Zululand Coral Reefs, Sodwana Bay, South Africa. *Jour. of Coast. Res., 6(4): 829-852.*

RANCE, P.J. and WARREN, N.F. 1968. The threshold of movement of coarse material in oscillatory flow. *Proc. 11th Conf. Coast. Eng., 1 : 487-494.*

ROGERS, J. 1985. Geomorphology, offshore bathymetry and Quaternary lithostratigraphy around the Bot River Estuary. Trans. R. Soc. S.A. 45: 211-237.

ROSSOUW, J. 1989. *Design waves for the South African coastline.* P.hD. Thesis, Dept. of Civil Engineering, Univ. of Stellenbosch, 130pp.

SAGGA, A.M.S. 1992. "The use of textural parameters of sand in studying the characteristics and depositional processes of coastal sediments south of Jeddah, Saudi Arabia". Mar. Geol., 104: 179-186.

SHEPPARD, F.P. 1950. Longshore bars and longshore troughs. *U.S. Army Corps of Engineers. Beach Erosion Board Tech. Mem. 15 : 1-31.*

SÖHNGE, A.P.G. 1983. The Cape Fold belt - Perspective. In: Söhnge A.P.G. and Hälbich, I.W. (eds), *Geodynamics of the Cape Fold Belt, Geol. Soc. of S. Afr., pp. 1-6.*

SWART, D.H. 1986. Walker Bay Regional Coastal Processes Site. *Symposium Handbook and abstracts of papers, 6th Nat. Oceanogr. Symp. p. B5.*

TANKARD, A.J. and SCHWEITZER, F.R. 1976. Textural analysis of cave sediments: Die Kelders, Cape Province, South Africa. In: Davidson, D.A. and Shackley, M.L. (eds.) *Geoarcheology - Earth Science and the Past.*

TERHORST, A. 1987. *The seafloor environment off Simon's Town in False Bay, revealed by side-scan sonar, bottom sampling, diver observations and underwater photography.* Unpublished M.Sc. Thesis, Dept. of Geol., Univ. of Cape Town.

TYSON, P.D. 1969. Atmospheric circulation and precipitation over South Africa. *Univer. of Witwatersrand, Johannesburg. Environ. Studies Occ. Pap. 2 :1 - 11.*

VINCENT, G.E. 1958. Contribution to the study of sediment transport on a horizontal bed due to wave action. *Proc. 6th Conf. Coastal Eng., Vol. 3(1) : 326-355.*

VON VEH, M.W. 1988. A structural investigation of the Escom Southern Cape Project area. Atomic Energy Corp. of South Africa. *Rep. Atomic Energy Corp. of South Africa, GEA-842, PIN-1122 (B/R).*

WADDEL, E. 1973. Dynamics of swash and its implications to beach response. *Tech. Rep., Louisiana State Univ. Coastal Stud. Inst., 139 : 1-49.*

WALDRON, M. 1986. *The Importance of Water Levels in the Management of the Klein River estuary, Hermanus.* Unpublished M.Sc. Thesis, Dept. of Environmental Studies, Univ. of Cape Town.

WRIGHT, L.D. and SHORT, A.P. 1983. Morphodynamics of beaches and surf zones in Australia. In: Komar, P.D. (ed), *Handbook of Coastal Processes and Erosion. CRC Press, 35-64.*

WRIGHT, L.D. SHORT, A.D. and GREEN M.O. 1985. Short-term changes in the morphodynamic states of beaches and surf zones: an empirical predictive model. *Marine Geology, 62 : 339-364.*

APPENDIX A

FACIES 3 SETTLING-TUBE RESULTS

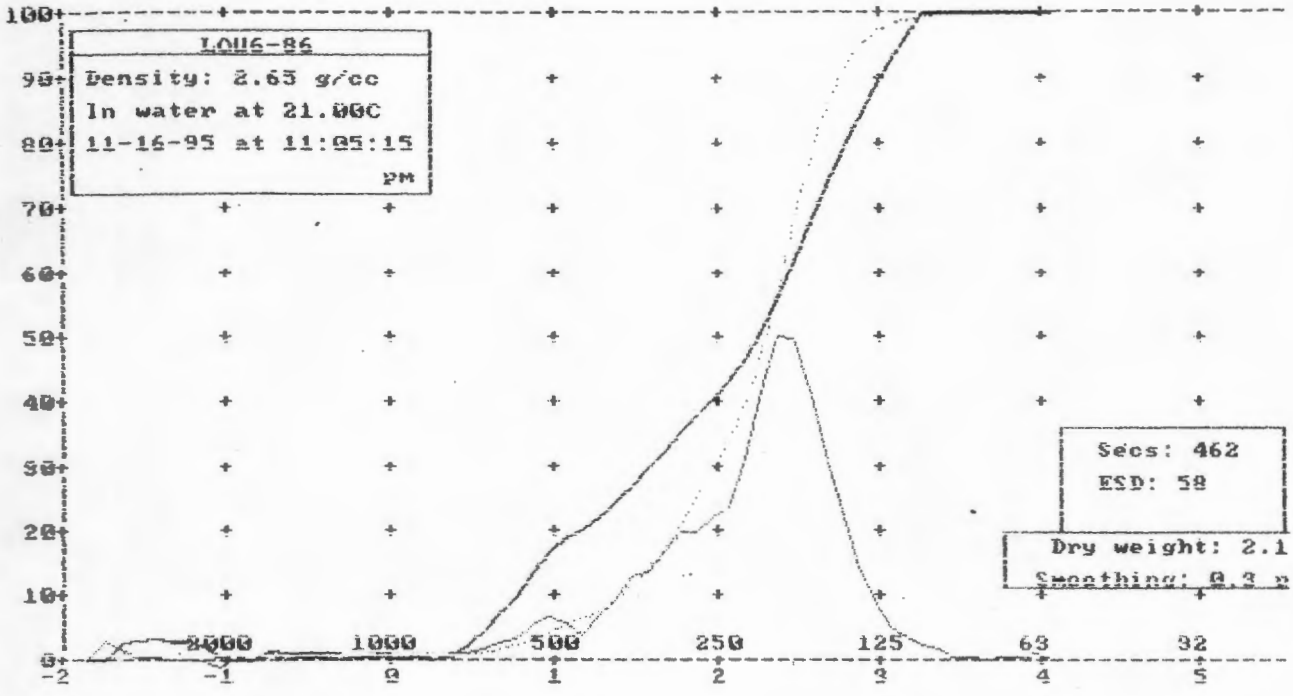

Moment statistics:
  Mean = 2.15 phi = 225.17u
  Std dev = 0.63 phi Skewness = -2.08 Kurtosis = 13.00

Graphical values (F&W):
  Mean = 2.18 phi = 219.96u
  Median (phi50) = 2.28 phi = 205.30u
  Sorting = 0.54 phi Skewness = -0.32 Kurtosis = 1.13

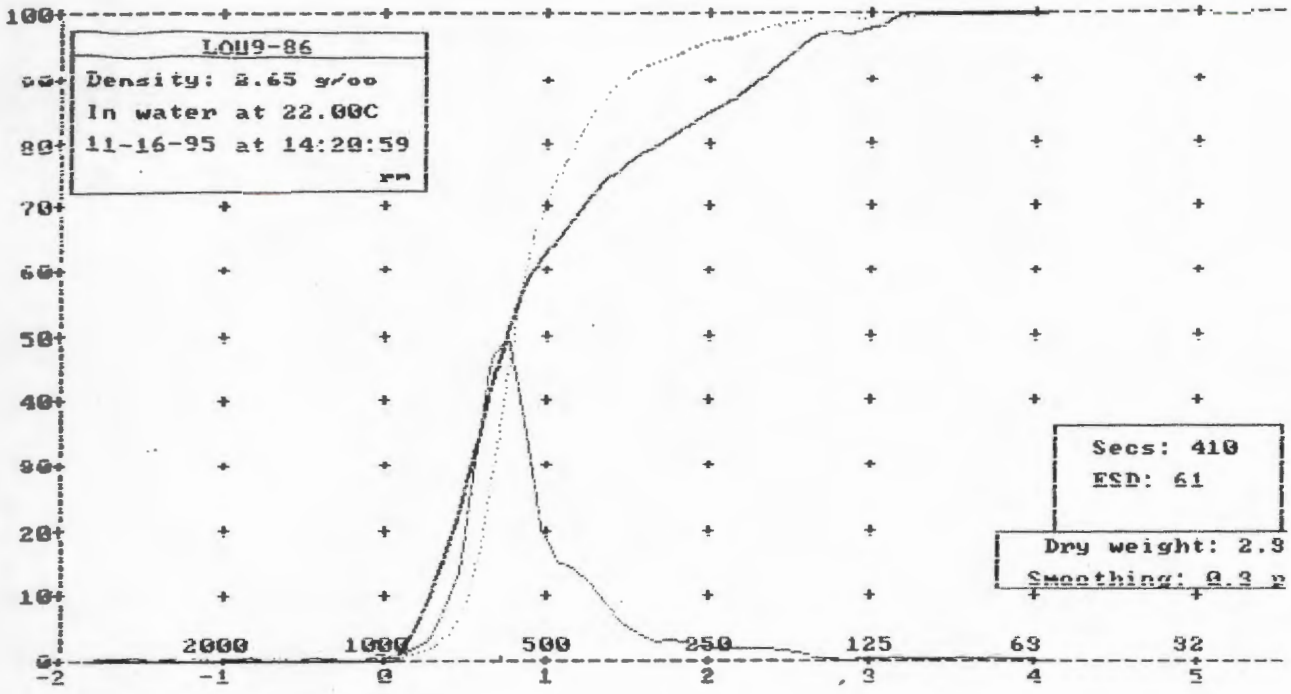

Moment statistics:
  Mean = 0.91 phi = 532.84u
  Std dev = 0.50 phi Skewness = 1.64 Kurtosis = 10.89

Graphical values (F&W):
  Mean = 0.87 phi = 547.02u
  Median (phi50) = 0.79 phi = 579.60u
  Sorting = 0.40 phi Skewness = 0.43 Kurtosis = 1.45

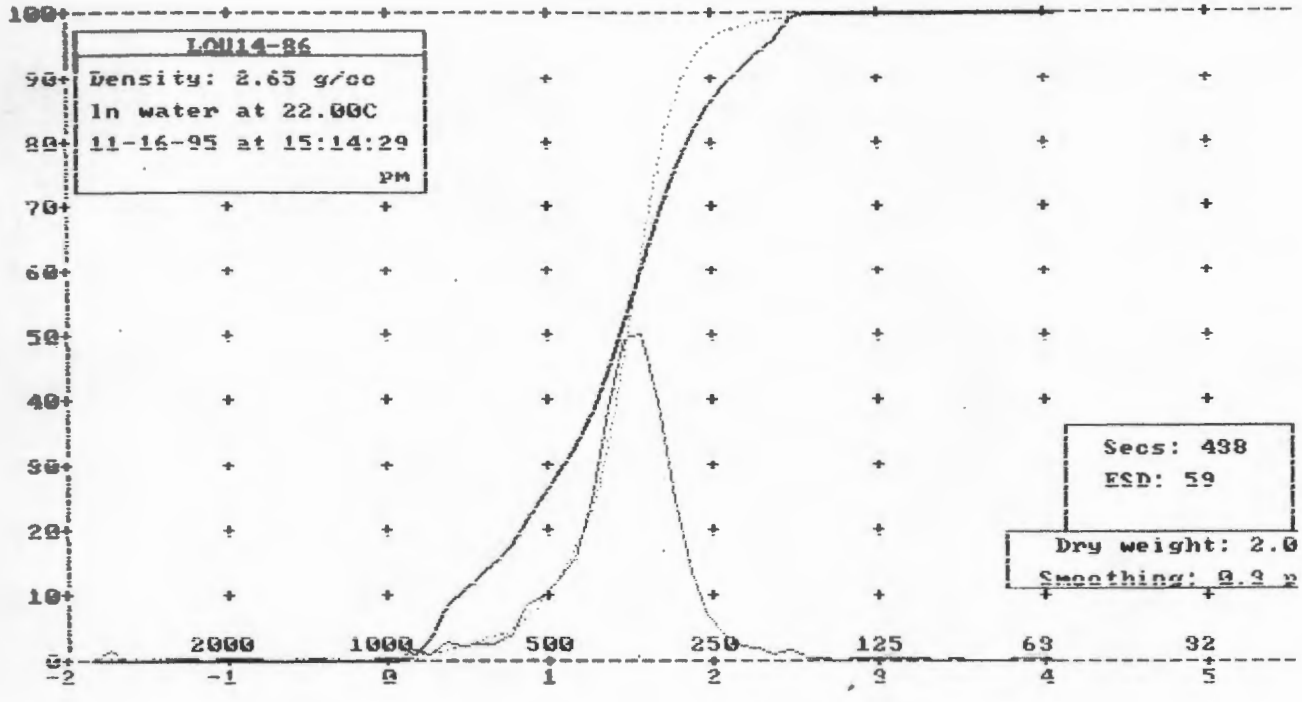

Moment statistics:
  Mean = 1.43 phi = 370.03u
  Std dev = 0.42 phi Skewness = -1.05 Kurtosis = 17.03

Graphical values (F&W):
  Mean = 1.44 phi = 368.20u
  Median (phi50) = 1.47 phi = 360.57u
  Sorting = 0.32 phi Skewness = -0.16 Kurtosis = 1.28

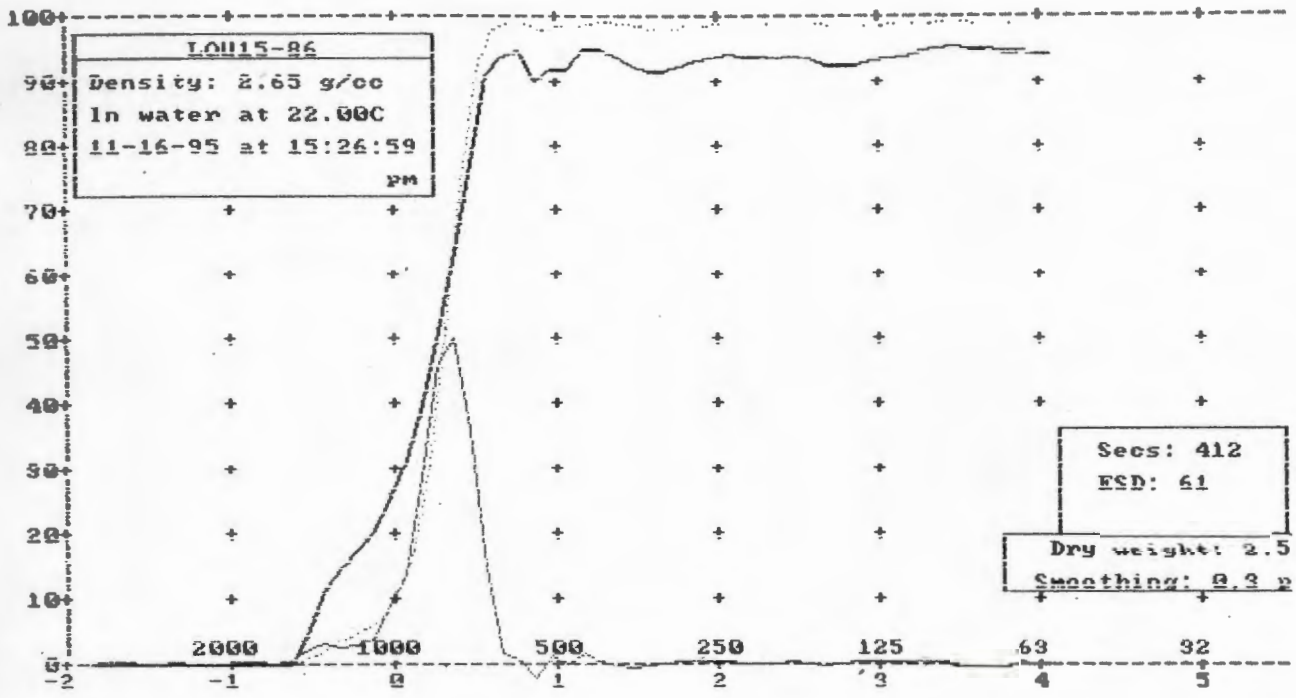

Moment statistics:
  Mean = 0.25 phi = 838.96u
  Std dev = 0.27 phi Skewness = 1.22 Kurtosis = 30.77

Graphical values (F&W):
  Mean = 0.28 phi = 825.18u
  Median (phi50) = 0.29 phi = 815.91u
  Sorting = 0.21 phi Skewness = -0.22 Kurtosis = 1.29

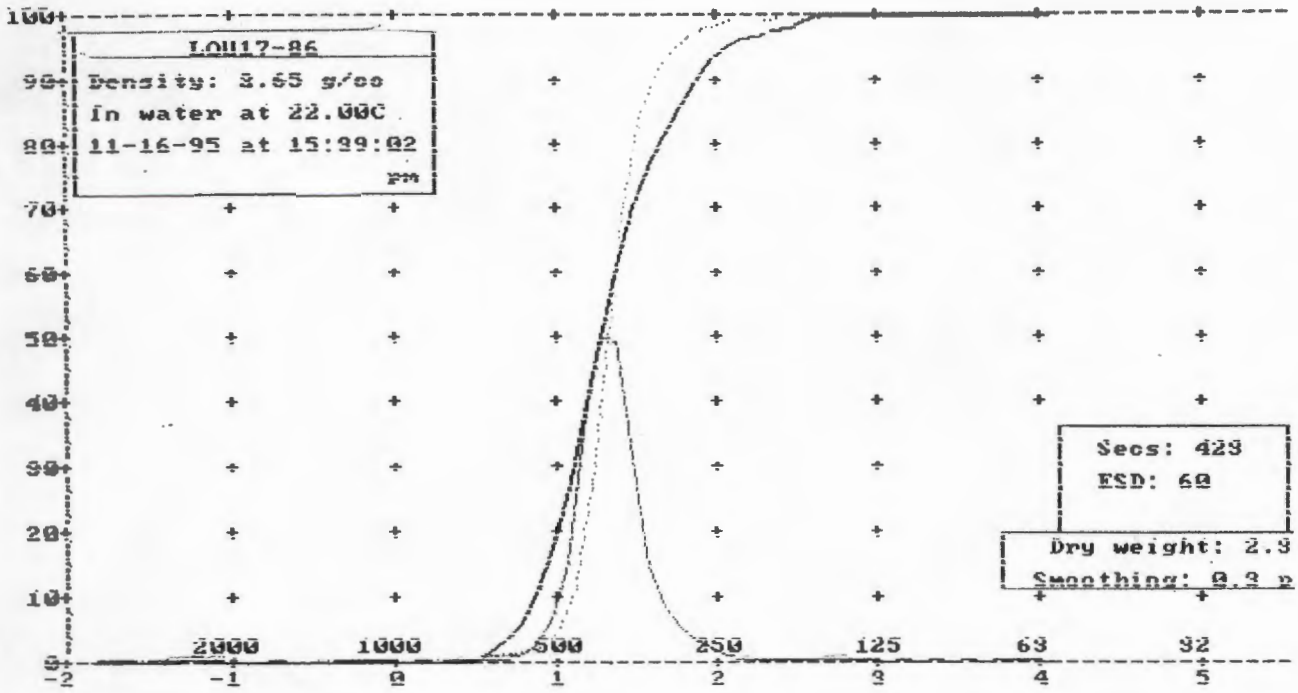

Moment statistics:
  Mean = 1.32 phi = 400.19u
  Std dev = 0.33 phi   Skewness = -1.37   Kurtosis = 39.07

Graphical values (F&W):
  Mean = 1.31 phi = 403.07u
  Median (phi50) = 1.30 phi = 404.82u
  Sorting = 0.21 phi   Skewness = 0.11   Kurtosis = 1.25

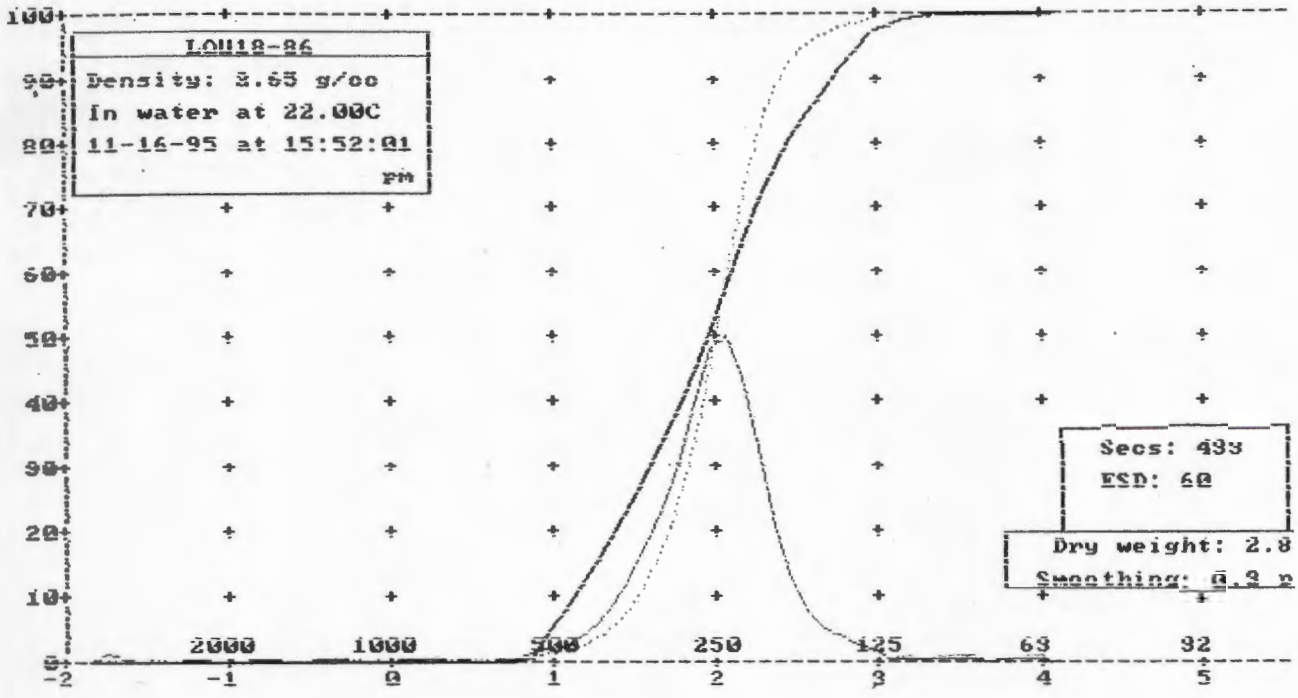

Moment statistics:
  Mean = 1.97 phi = 255.66u
  Std dev = 0.42 phi   Skewness = -1.47   Kurtosis = 19.74

Graphical values (F&W):
  Mean = 1.97 phi = 255.78u
  Median (phi50) = 1.99 phi = 252.19u
  Sorting = 0.35 phi   Skewness = -0.08   Kurtosis = 1.16

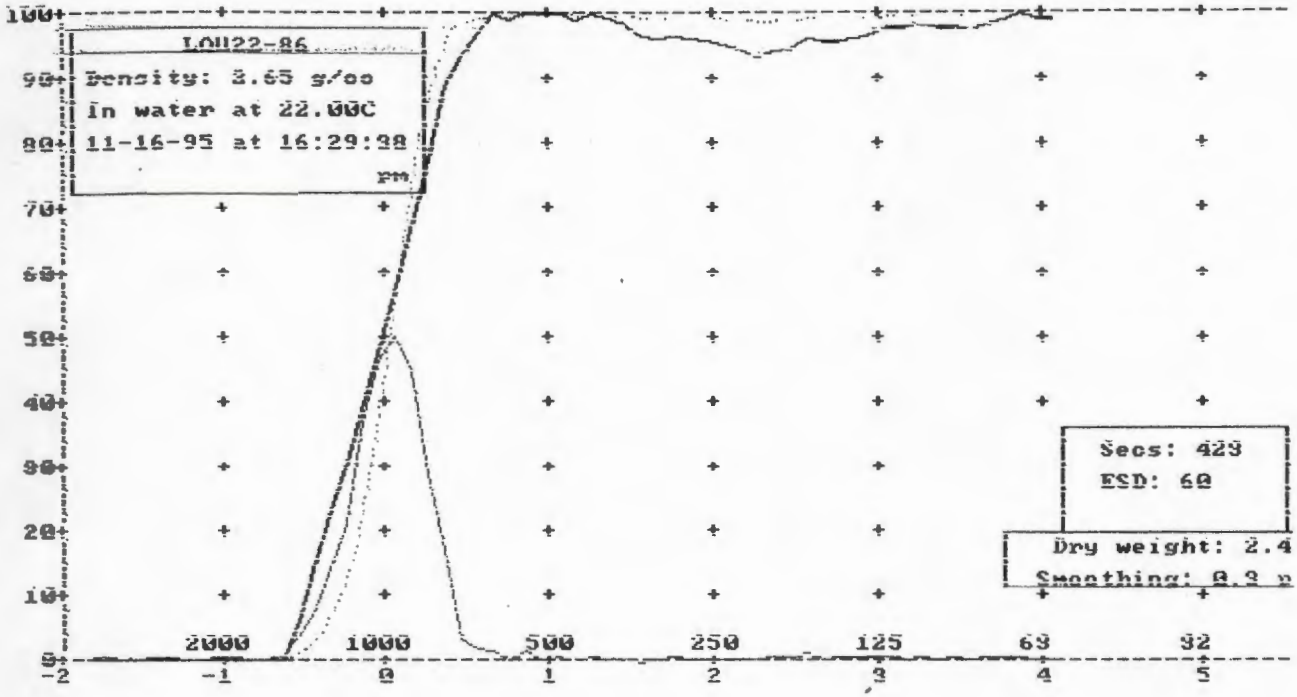

Moment statistics:

Mean = 0.01 phi = 991.30u
Std dev = 0.30 phi Skewness = 5.27 Kurtosis = 69.42

Graphical values (F&W):

Mean = 0.01 phi = 990.18u
Median (phi50) = 0.02 phi = 986.82u
Sorting = 0.22 phi Skewness = -0.05 Kurtosis = 1.01

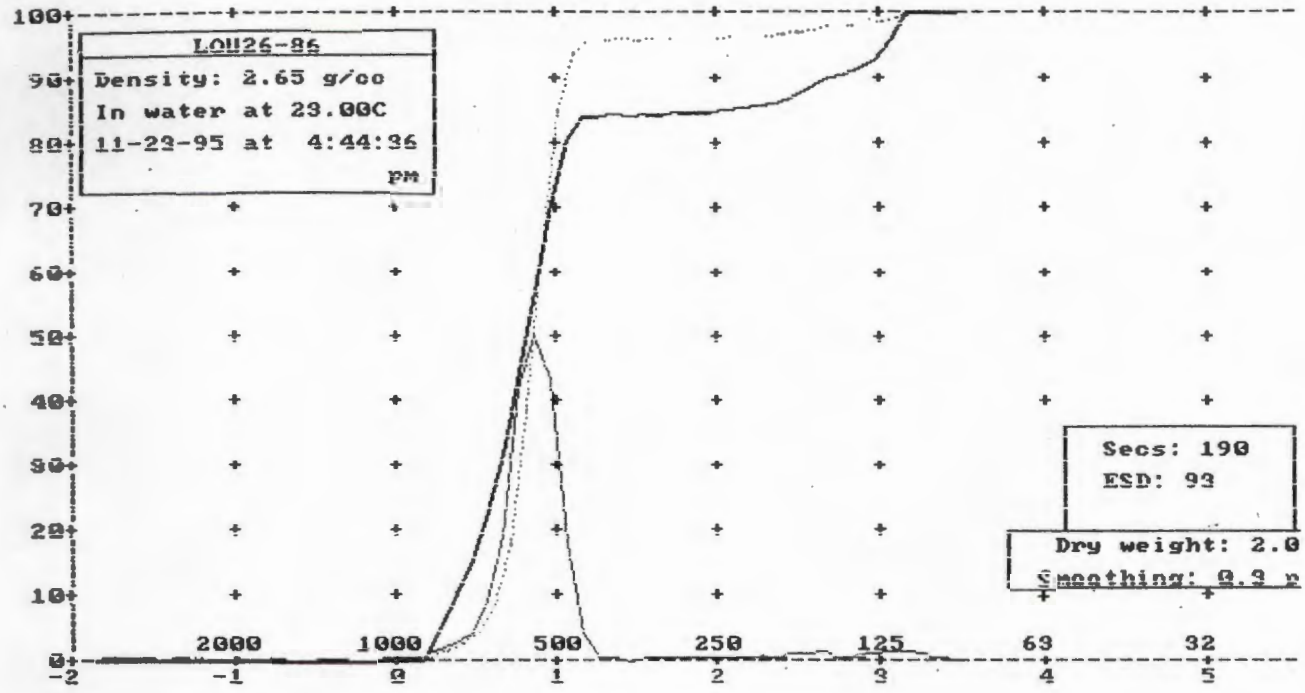

Moment statistics:
  Mean = 0.90 phi = 534.72u
  Std dev = 0.46 phi   Skewness = 2.86   Kurtosis = 18.35

Graphical values (F&W):
  Mean = 0.84 phi = 557.94u
  Median (phi50) = 0.85 phi = 556.08u
  Sorting = 0.18 phi   Skewness = -0.02   Kurtosis = 1.22

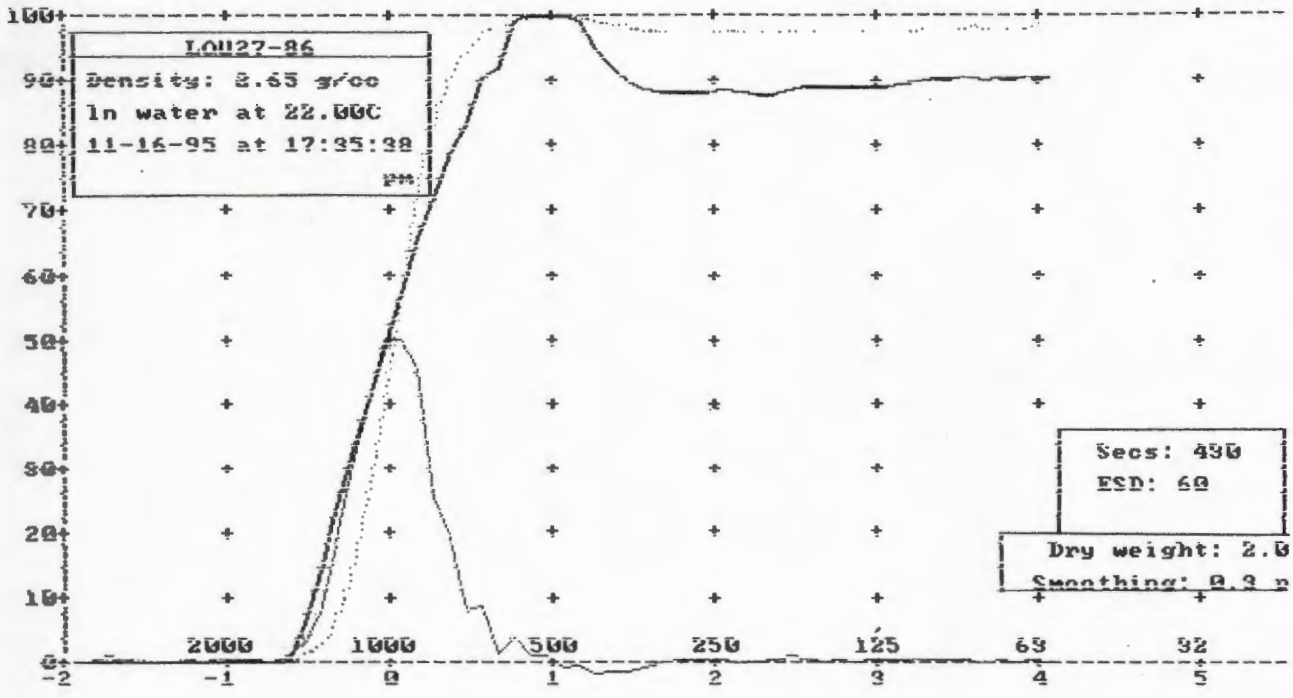

Moment statistics:
  Mean = 0.01 phi = 994.80u
  Std dev = 0.30 phi. Skewness = 5.21 Kurtosis = 75.00

Graphical values (F&W):
  Mean = 0.02 phi = 987.68u
  Median (phi50) = 0.01 phi = 989.98u
  Sorting = 0.26 phi Skewness = 0.06 Kurtosis = 1.08

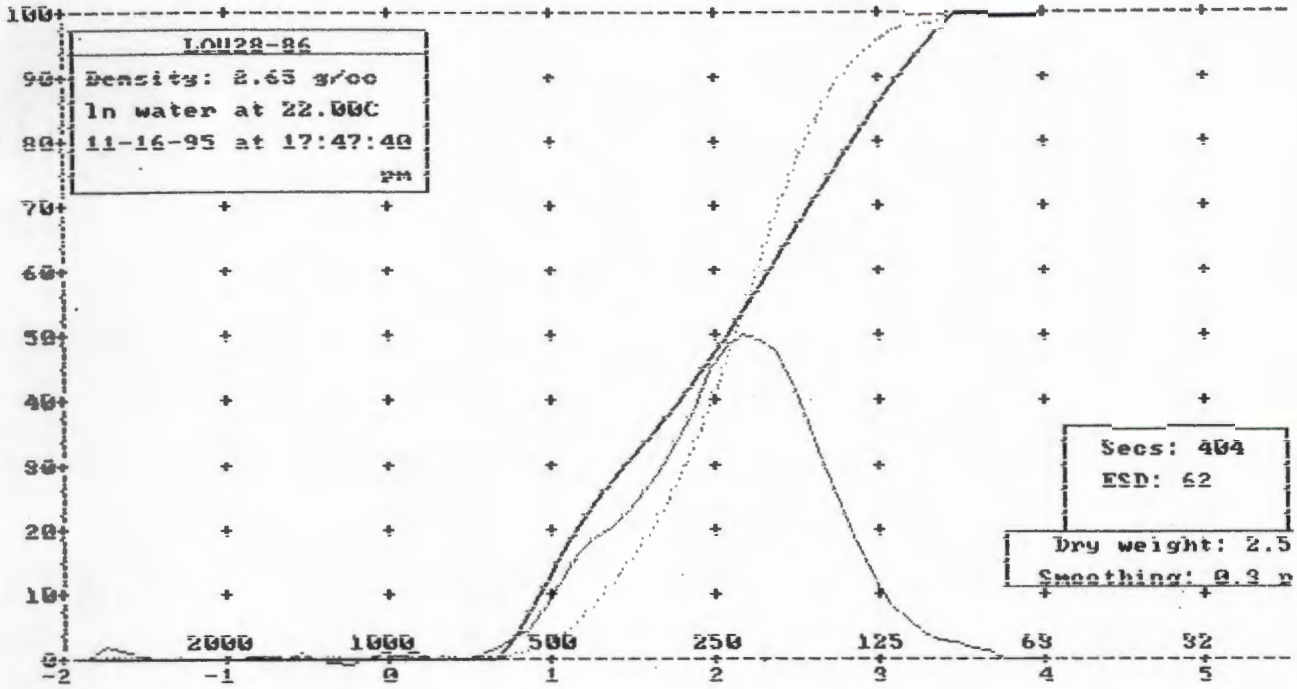

Moment statistics:
  Mean = 2.06 phi = 239.54u
  Std dev = 0.59 phi   Skewness = -0.98   Kurtosis = 8.50

Graphical values (F&W):
  Mean = 2.07 phi = 237.91u
  Median (phi50) = 2.11 phi = 231.70u
  Sorting = 0.56 phi   Skewness = -0.09   Kurtosis = 1.01

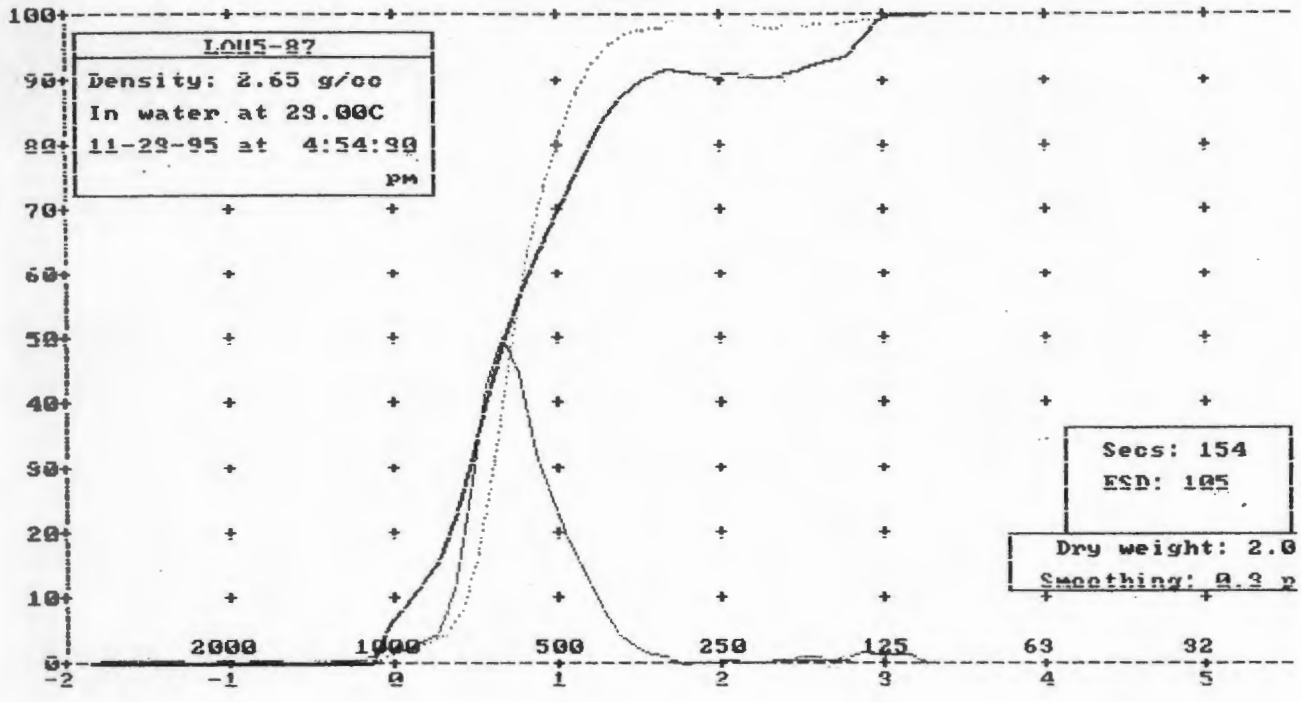

Moment statistics:
  Mean = 0.77 phi = 585.85u
  Std dev = 0.44 phi Skewness = 1.77 Kurtosis = 16.03

Graphical values (F&W):
  Mean = 0.75 phi = 595.19u
  Median (phi50) = 0.72 phi = 608.97u
  Sorting = 0.28 phi Skewness = 0.19 Kurtosis = 1.11

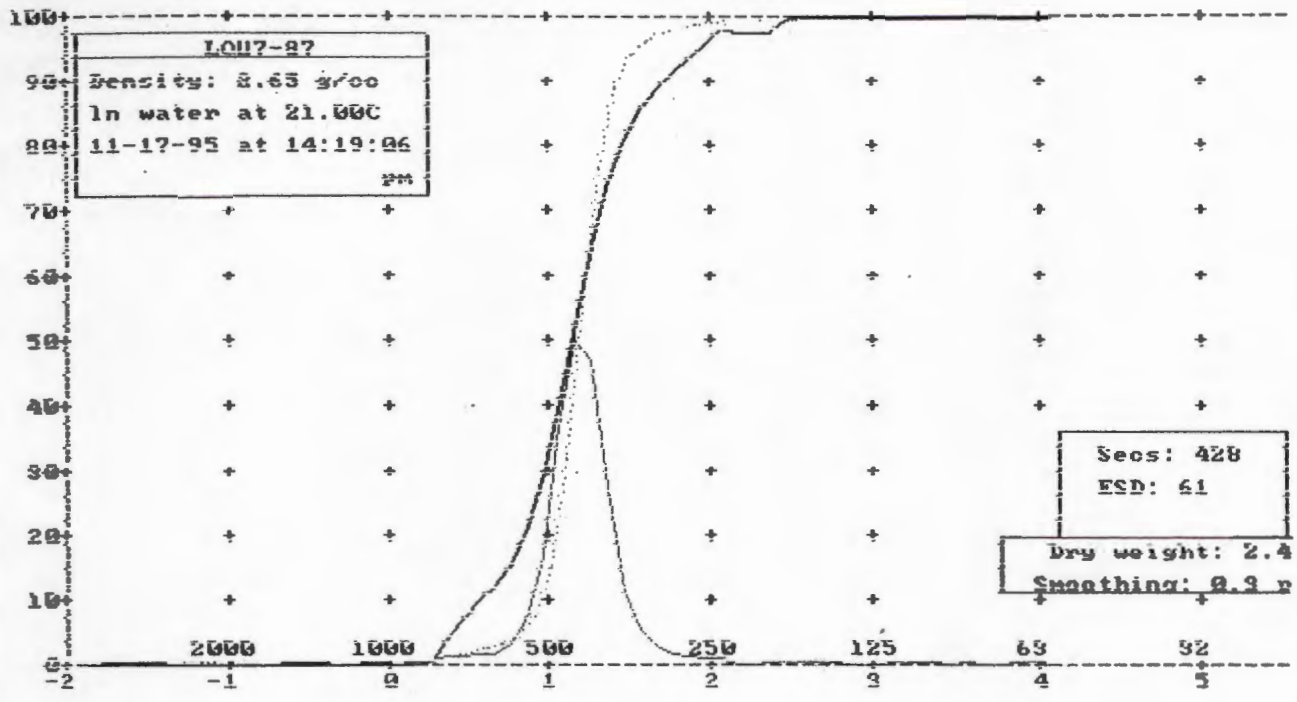

Moment statistics:
  Mean = 1.18 phi = 440.71u
  Std dev = 0.32 phi   Skewness = -0.21   Kurtosis = 34.70

Graphical values (F&W):
  Mean = 1.18 phi = 440.62u
  Median (phi50) = 1.18 phi = 441.57u
  Sorting = 0.20 phi   Skewness = 0.02   Kurtosis = 1.27

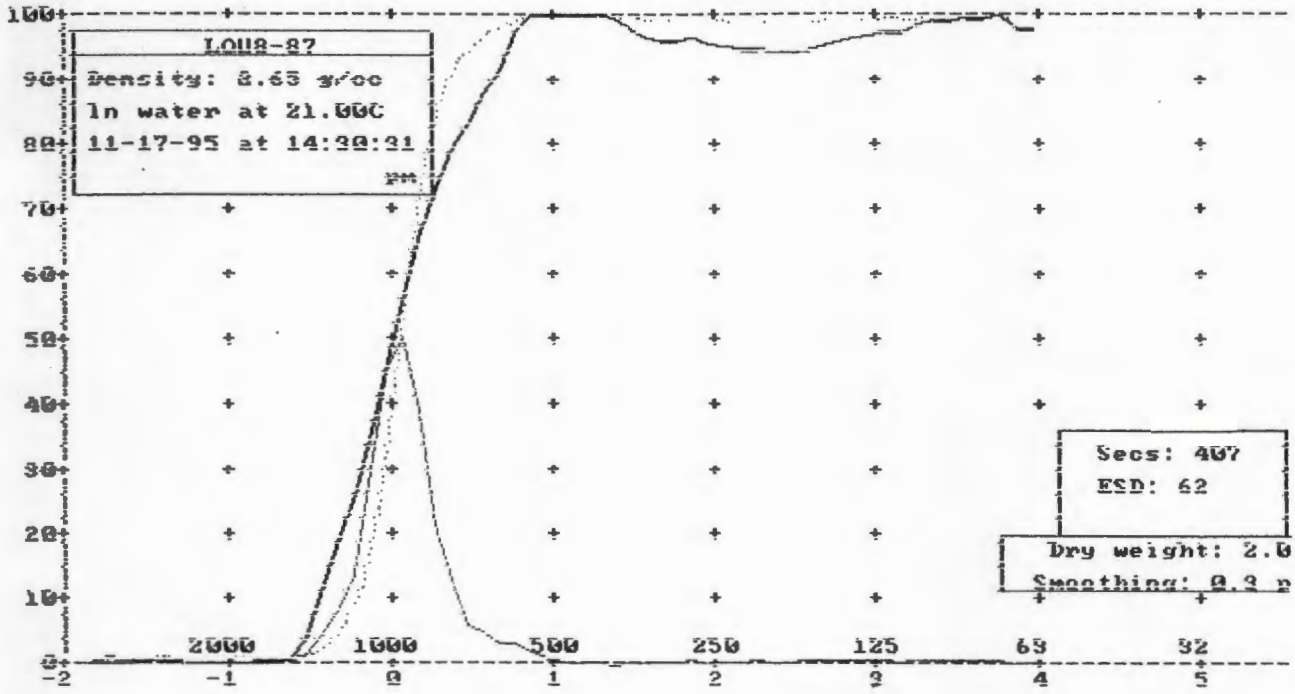

Moment statistics:
  Mean = 0.04 phi = 972.97u
  Std dev = 0.28 phi   Skewness = 0.53   Kurtosis = 23.98

Graphical values (F&W):
  Mean = 0.04 phi = 969.39u
  Median (phi50) = 0.04 phi = 974.29u
  Sorting = 0.23 phi   Skewness = 0.08   Kurtosis = 1.26

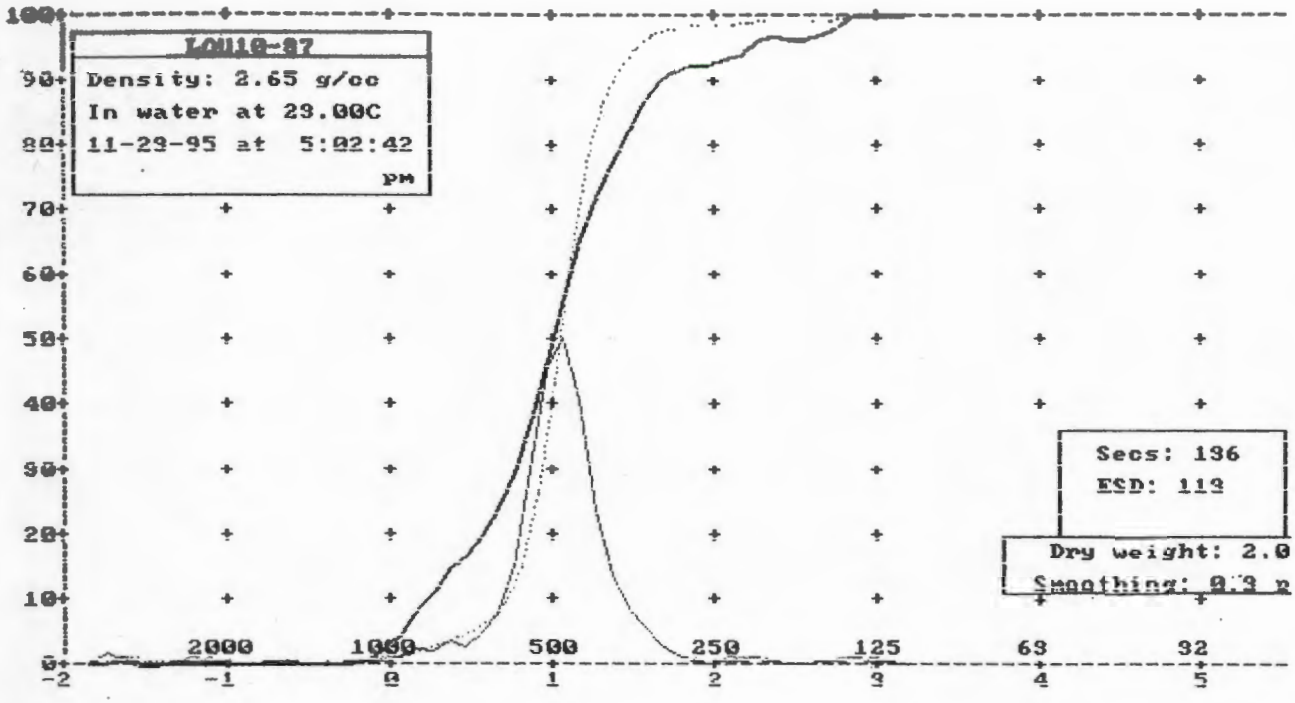

Moment statistics:
  Mean = 1.02 phi = 491.44u
  Std dev = 0.37 phi Skewness = -1.13 Kurtosis = 19.52

Graphical values (F&W):
  Mean = 1.04 phi = 486.24u
  Median (phi50) = 1.04 phi = 487.55u
  Sorting = 0.27 phi Skewness = -0.01 Kurtosis = 1.40

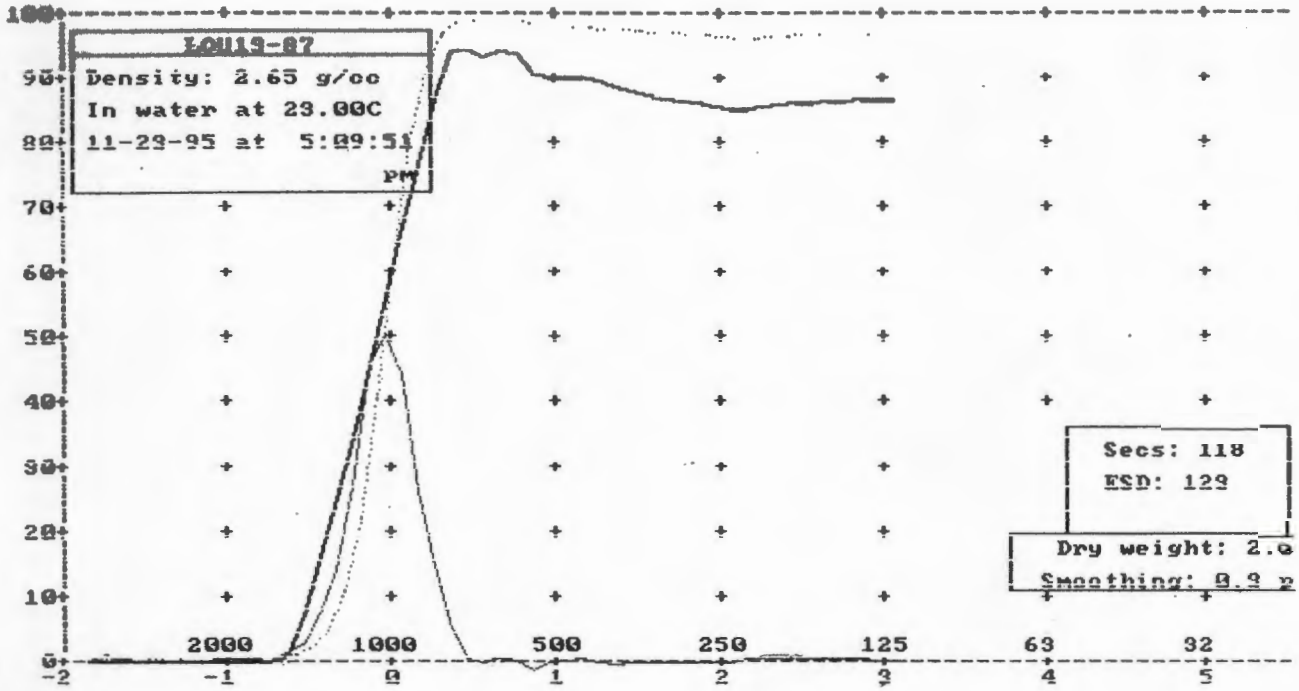

Moment statistics:
  Mean = -0.09 phi = 1061.15u
  Std dev = 0.15 phi Skewness = -2.05 Kurtosis =234.59

Graphical values (F&W):
  Mean = -0.05 phi = 1038.44u
  Median (phi50) = -0.05 phi = 1037.84u
  Sorting = 0.20 phi Skewness = -0.01 Kurtosis = 1.07

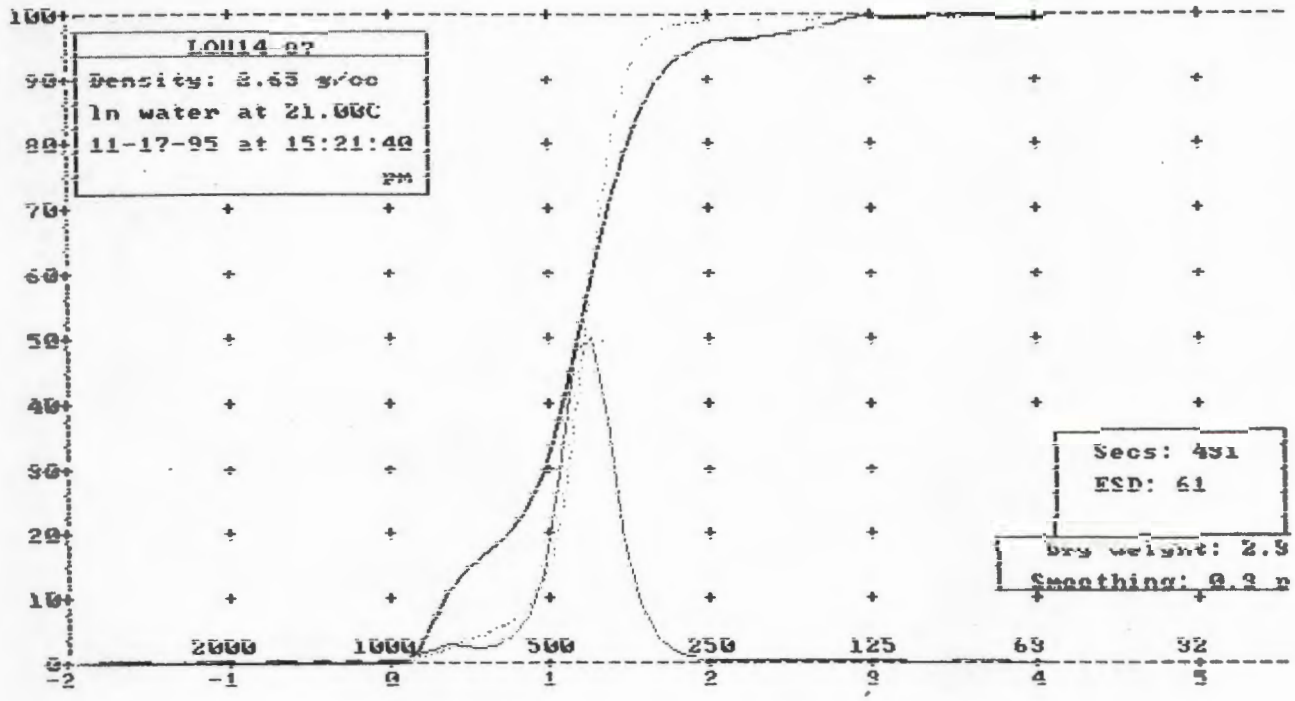

Moment statistics:
  Mean = 1.19 phi = 439.20u
  Std dev = 0.34 phi   Skewness = -0.52   Kurtosis = 22.36

Graphical values (F&W):
  Mean = 1.20 phi = 433.98u
  Median (phi50) = 1.21 phi = 431.99u
  Sorting = 0.24 phi   Skewness = -0.13   Kurtosis = 1.44

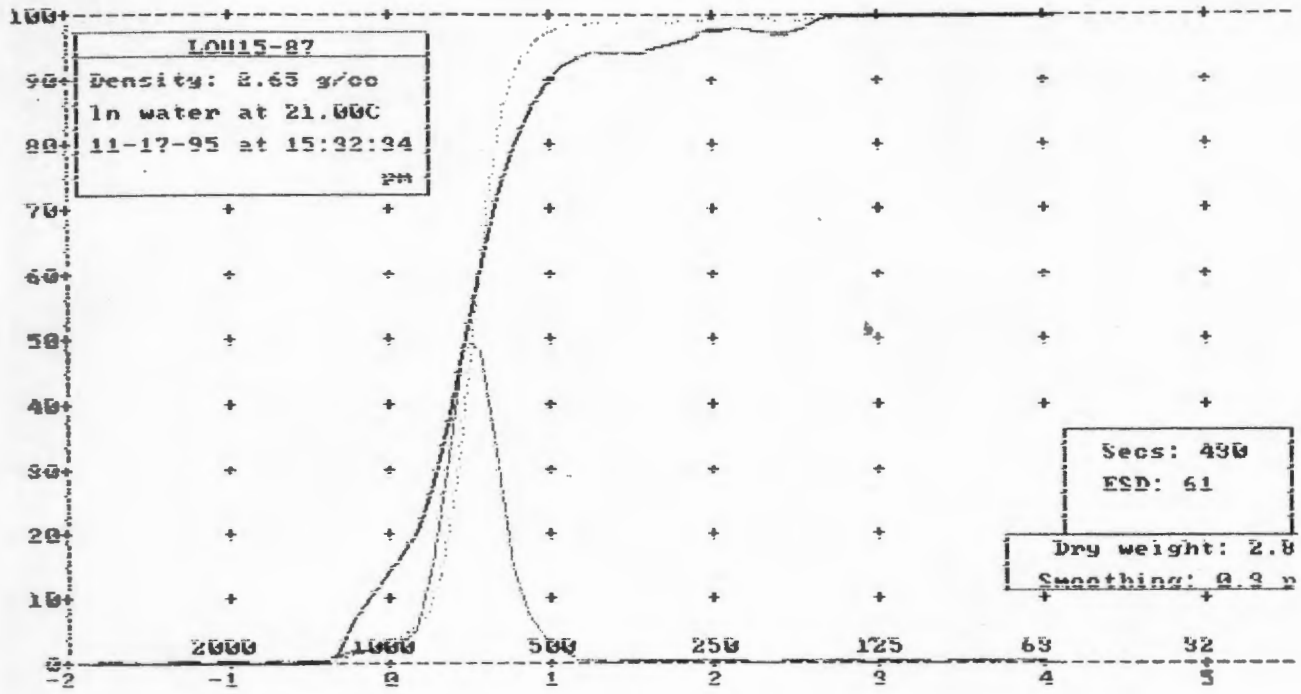

Moment statistics:
  Mean = 0.52 phi = 698.21u
  Std dev = 0.37 phi   Skewness = 4.00   Kurtosis = 39.46

Graphical values (F&W):
  Mean = 0.50 phi = 706.66u
  Median (phi50) = 0.50 phi = 707.34u
  Sorting = 0.21 phi   Skewness = 0.00   Kurtosis = 1.27

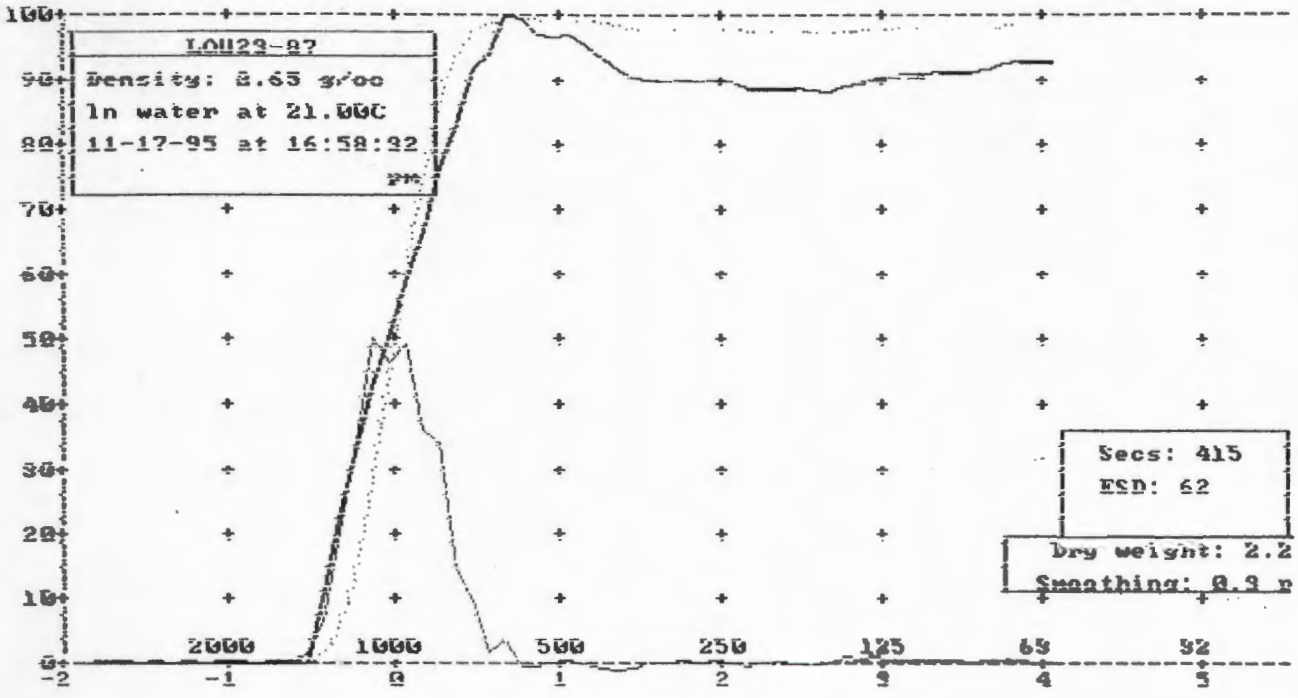

Moment statistics:
  Mean = -0.00 phi = 1001.39u
  Std dev = 0.35 phi Skewness = 6.56 Kurtosis = 73.80

Graphical values (F&W):
  Mean = -0.00 phi = 1001.75u
  Median (phi50) = -0.01 phi = 1007.77u
  Sorting = 0.24 phi Skewness = 0.07 Kurtosis = 0.94

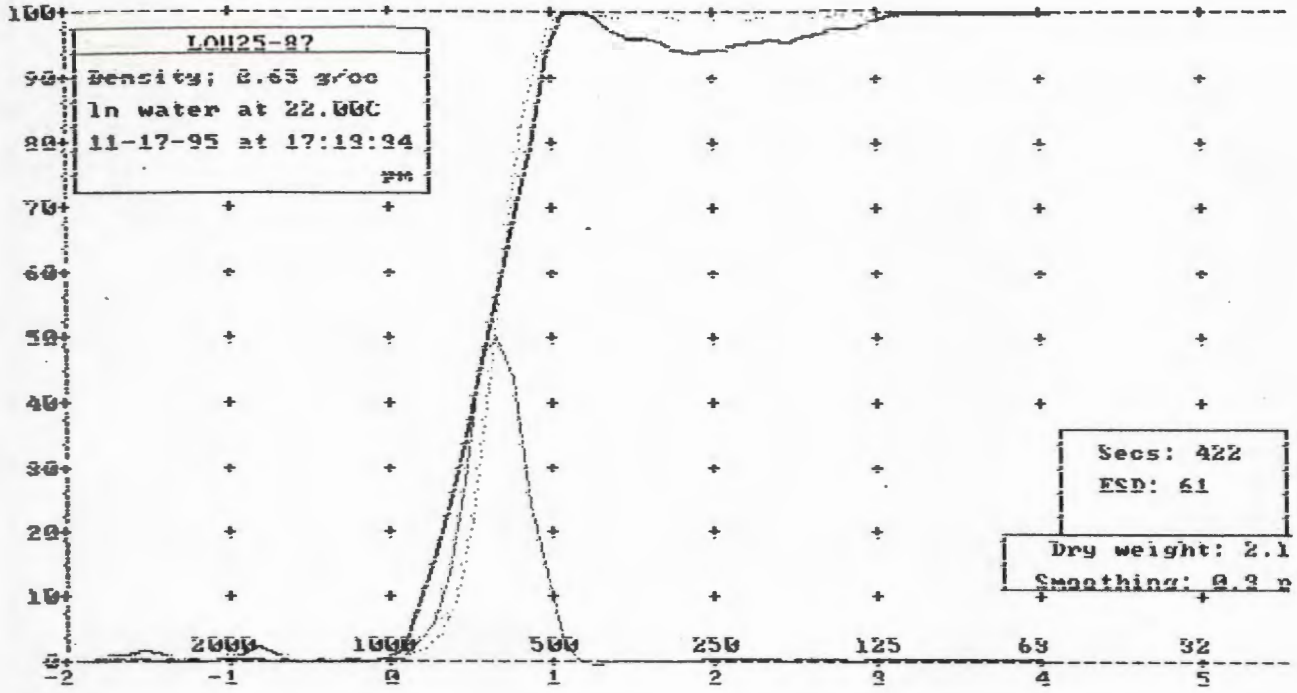

Moment statistics:
  Mean = 0.64 phi = 640.35u
  Std dev = 0.37 phi   Skewness = 2.36   Kurtosis = 40.30

Graphical values (F&W):
  Mean = 0.63 phi = 644.10u
  Median (phi50) = 0.64 phi = 642.94u
  Sorting = 0.19 phi   Skewness = -0.03   Kurtosis = 1.04

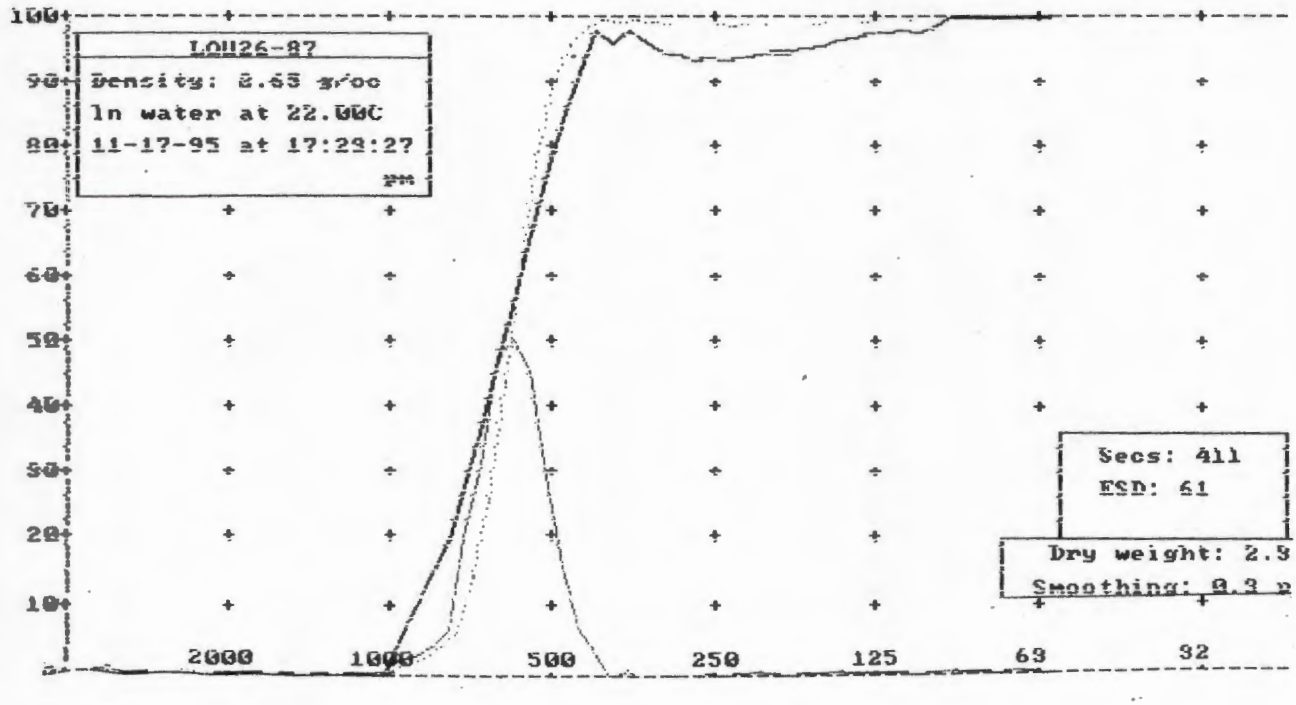

Moment statistics:
  Mean = 0.74 phi = 600.60u
  Std dev = 0.35 phi Skewness = 2.11 Kurtosis = 35.70

Graphical values (F&W):
  Mean = 0.73 phi = 601.54u
  Median (phi50) = 0.74 phi = 600.50u
  Sorting = 0.22 phi Skewness = -0.03 Kurtosis = 1.08

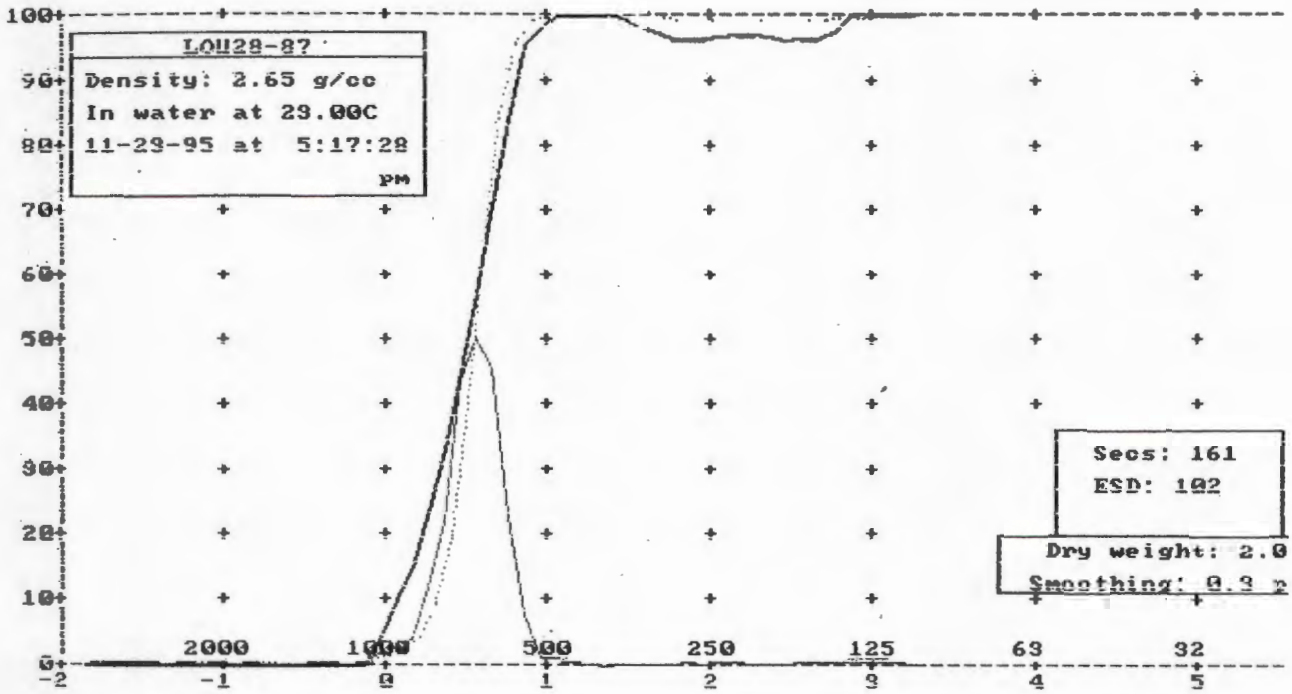

Moment statistics:
  Mean = 0,54 phi = 685,59u
  Std dev = 0.32 phi Skewness = 3.12 Kurtosis = 43.39

Graphical values (F&W):
  Mean = 0.54 phi = 689.87u
  Median (phi50) = 0.54 phi = 686.20u
  Sorting = 0.17 phi Skewness = -0.09 Kurtosis = 1.04

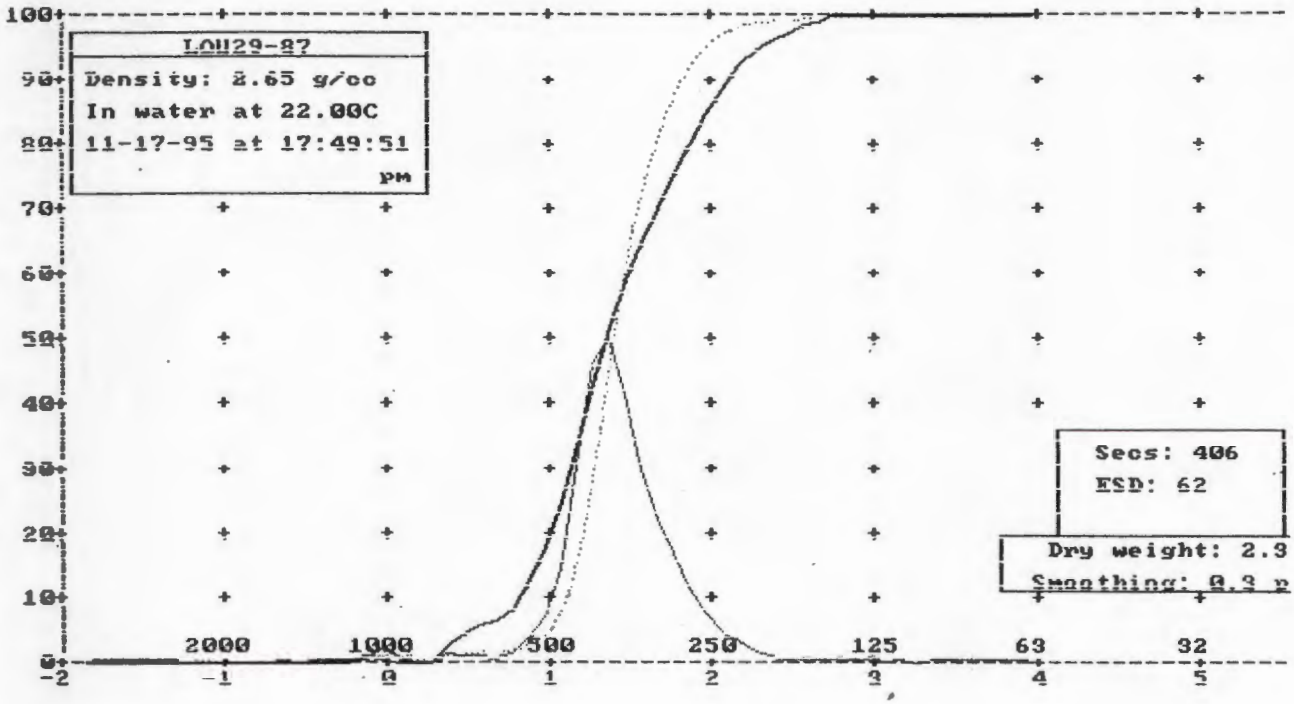

Moment statistics:
  Mean = 1.42 phi = 374.26u
  Std dev = 0.39 phi   Skewness = -0.56   Kurtosis = 20.58

Graphical values (F&W):
  Mean = 1.42 phi = 374.81u
  Median (phi50) = 1.38 phi = 382.82u
  Sorting = 0.28 phi   Skewness = 0.18   Kurtosis = 1.13

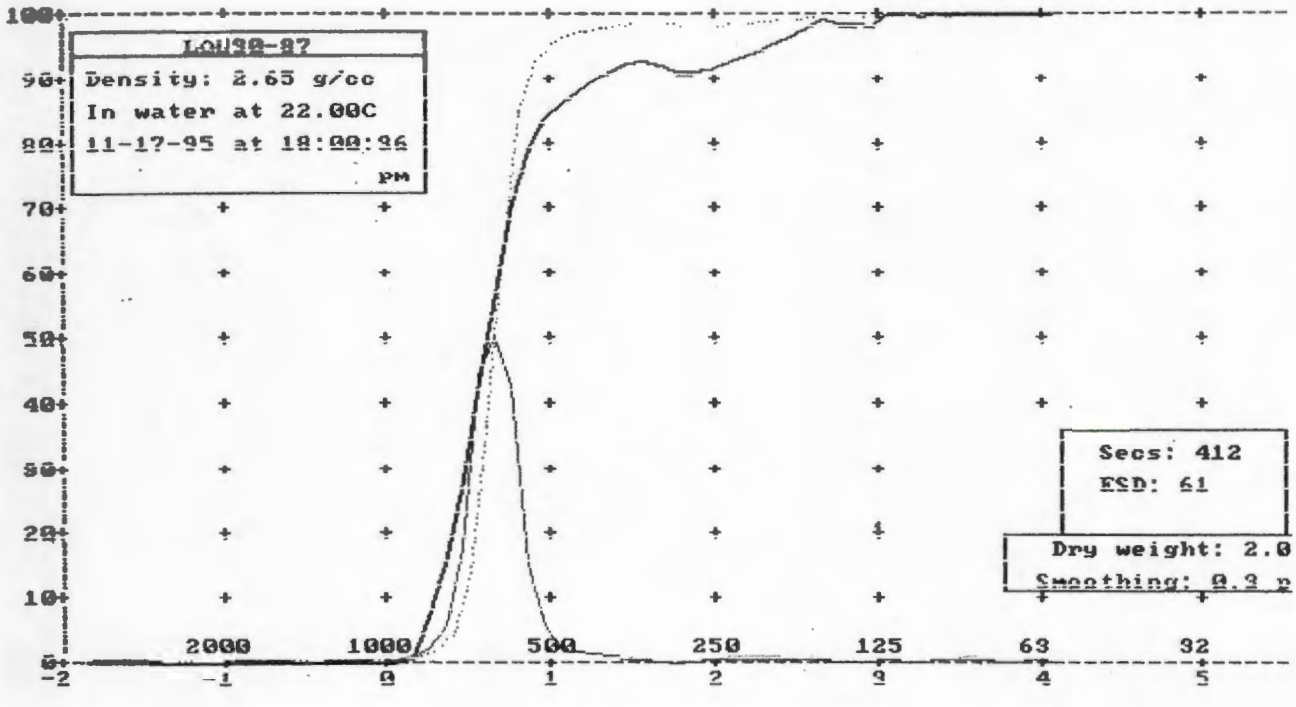

Moment statistics:
  Mean = 0.69 phi = 620.34u
  Std dev = 0.37 phi   Skewness = 3.71   Kurtosis = 37.44

Graphical values (F&W):
  Mean = 0.65 phi = 635.84u
  Median (phi50) = 0.65 phi = 636.43u
  Sorting = 0.16 phi   Skewness = 0.08   Kurtosis = 1.16

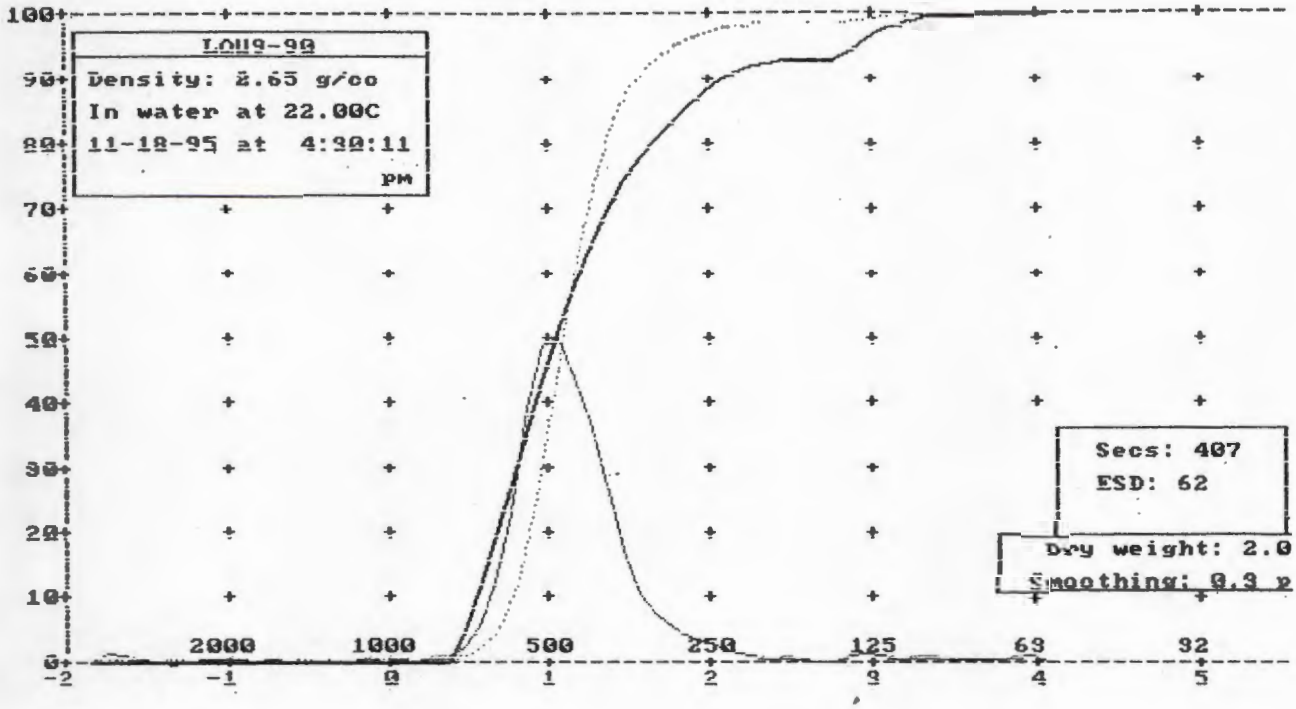

Moment statistics:
  Mean = 1.14 phi = 453.63u
  Std dev = 0.45 phi Skewness = 1.27 Kurtosis = 17.74

Graphical values (F&W):
  Mean = 1.11 phi = 464.64u
  Median (phi50) = 1.08 phi = 472.31u
  Sorting = 0.32 phi Skewness = 0.19 Kurtosis = 1.20

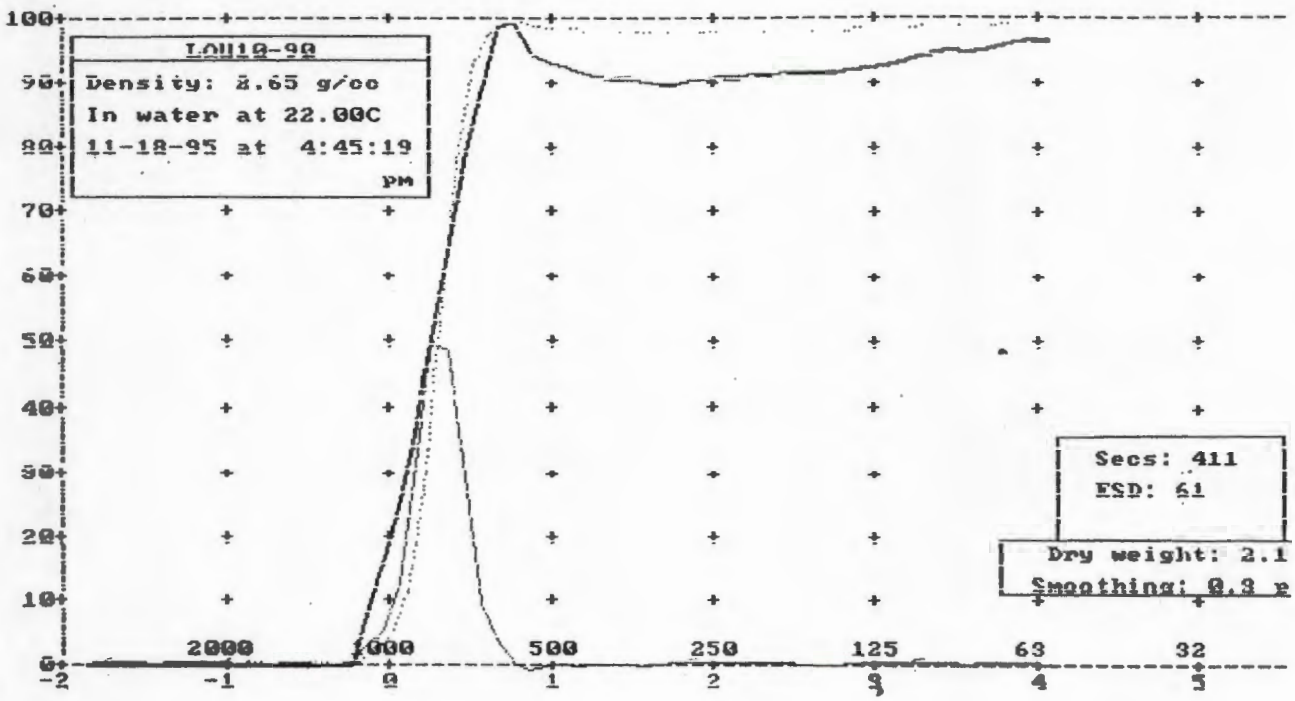

Moment statistics:
  Mean = 0.30 phi = 813.11u
  Std dev = 0.36 phi Skewness = 5.91 Kurtosis = 59.67

Graphical values (F&W):
  Mean = 0.29 phi = 819.17u
  Median (phi50) = 0.29 phi = 818.35u
  Sorting = 0.16 phi Skewness = -0.03 Kurtosis = 1.10

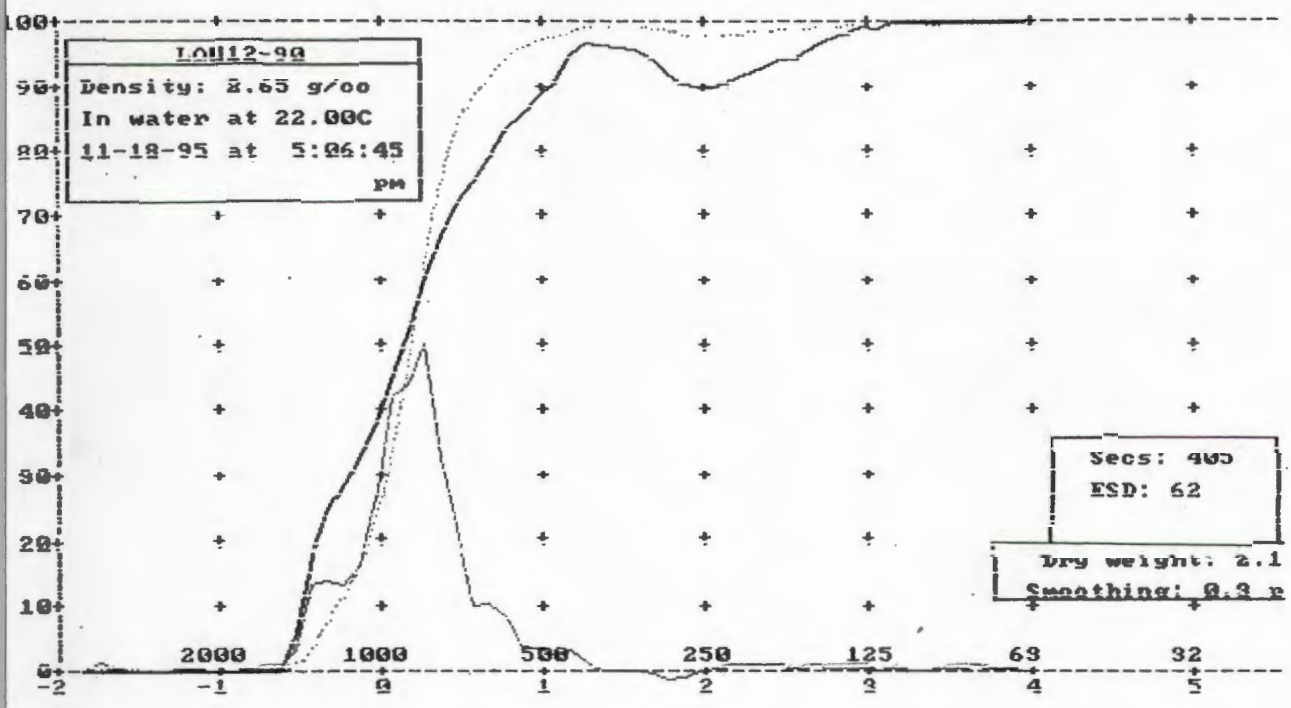

oment statistics:
Mean = 0.20 phi = 868.20u
Std dev = 0.50 phi Skewness = 3.06 Kurtosis = 21.02

raphical values (F&W):
Mean = 0.16 phi = 895.09u
Median (phi50) = 0.17 phi = 887.40u
Sorting = 0.34 phi Skewness = -0.01 Kurtosis = 1.30

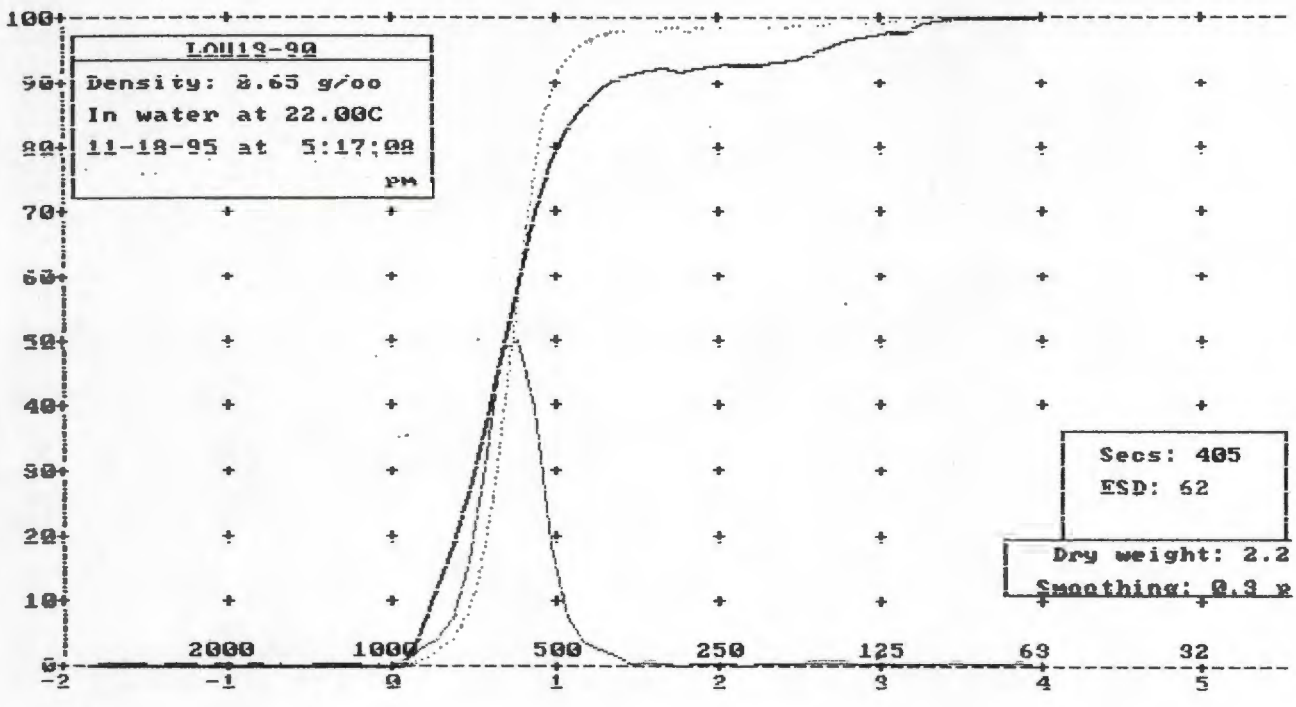

Moment statistics:
  Mean = 0.75 phi = 593.34u
  Std dev = 0.39 phi Skewness = 4.01 Kurtosis = 32.46

Graphical values (F&W):
  Mean = 0.71 phi = 609.22u
  Median (phi50) = 0.72 phi = 607.76u
  Sorting = 0.20 phi Skewness = 0.01 Kurtosis = 1.20

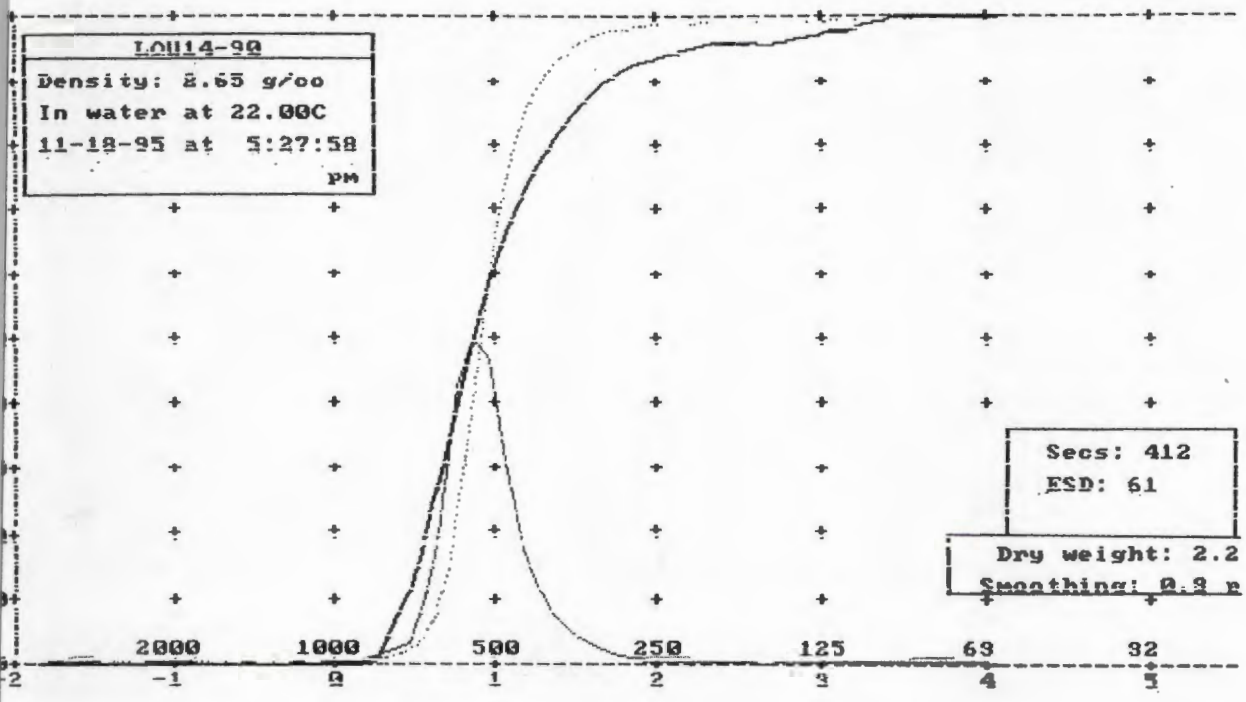

ent statistics:
ean = 0.95 phi = 516.27u
td dev = 0.40 phi Skewness = 2.54 Kurtosis = 26.15

phical values (F&W):
ean = 0.93 phi = 526.20u
edian (phi50) = 0.90 phi = 535.35u
orting = 0.25 phi Skewness = 0.21 Kurtosis = 1.24

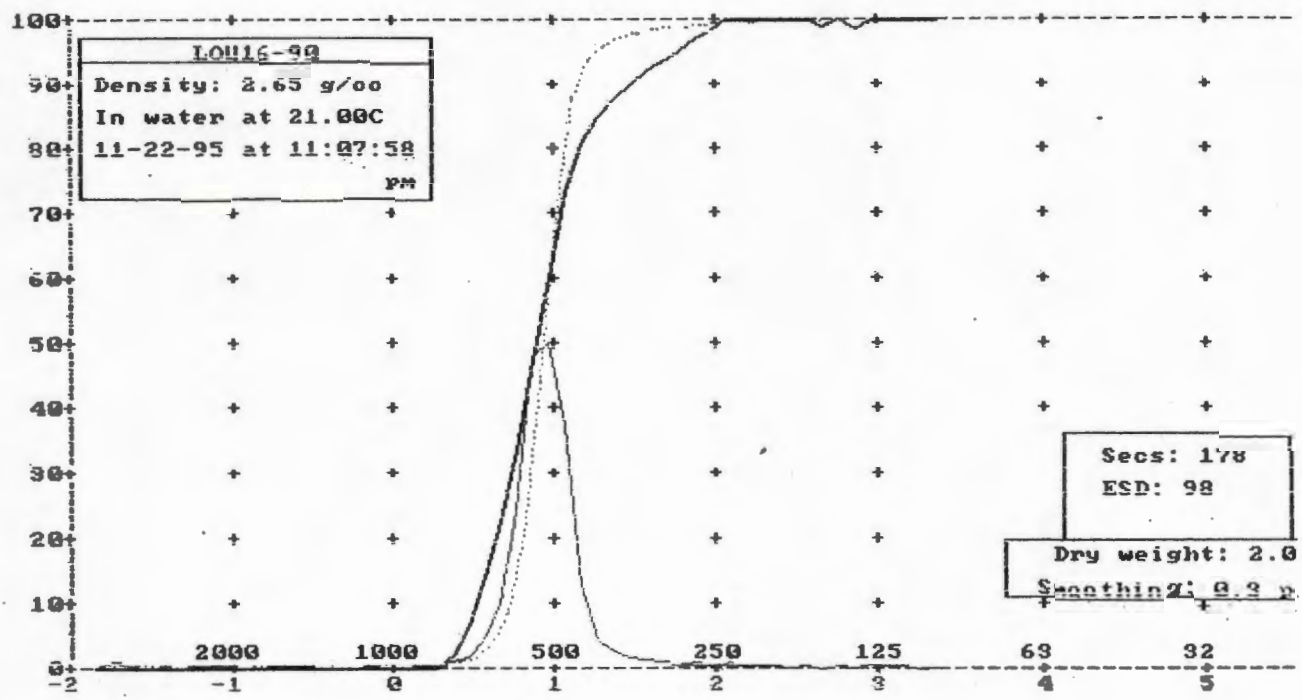

Moment statistics:
  Mean = 0.92 phi = 529.46u
  Std dev = 0.25 phi Skewness = -3.65 Kurtosis = 42.16

Graphical values (F&W):
  Mean = 0.92 phi = 527.37u
  Median (phi50) = 0.92 phi = 527.06u
  Sorting = 0.18 phi Skewness = 0.03 Kurtosis = 1.22

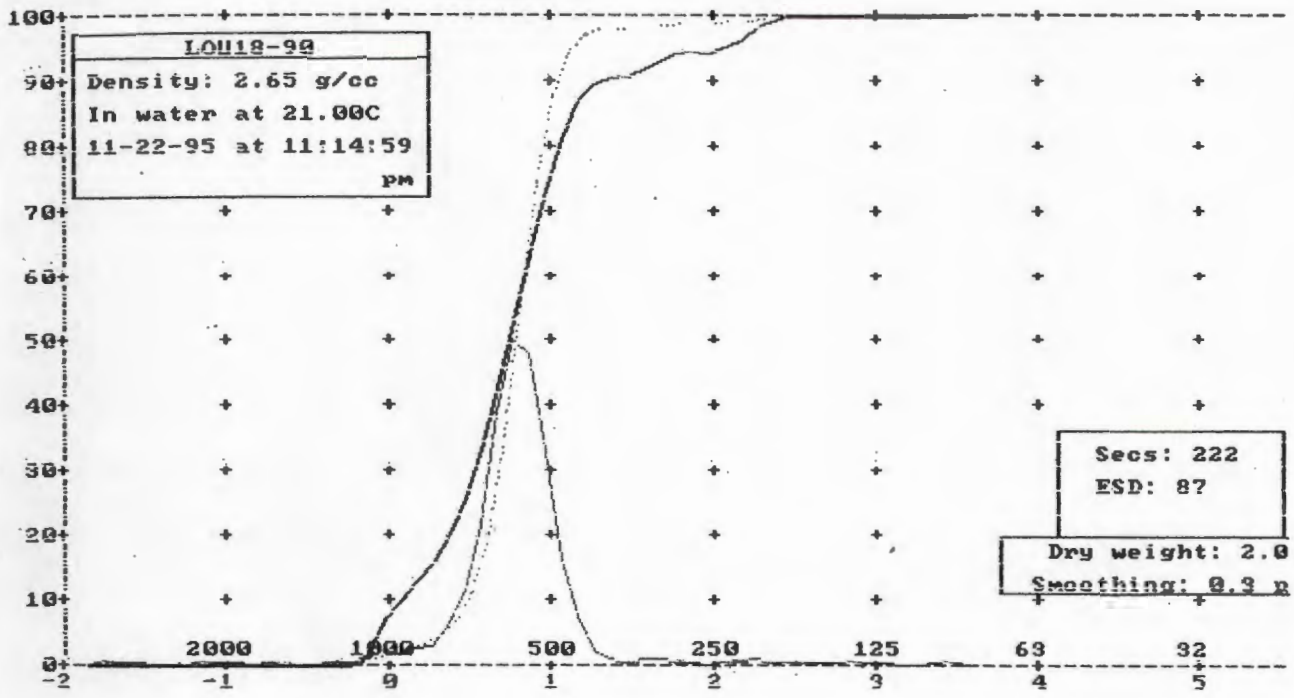

Moment statistics:
  Mean = 0.78 phi = 584.19u
  Std dev = 0.34 phi Skewness = 1.02 Kurtosis = 20.31

Graphical values (F&W):
  Mean = 0.77 phi = 587.01u
  Median (phi50) = 0.77 phi = 584.76u
  Sorting = 0.23 phi Skewness = -0.07 Kurtosis = 1.22

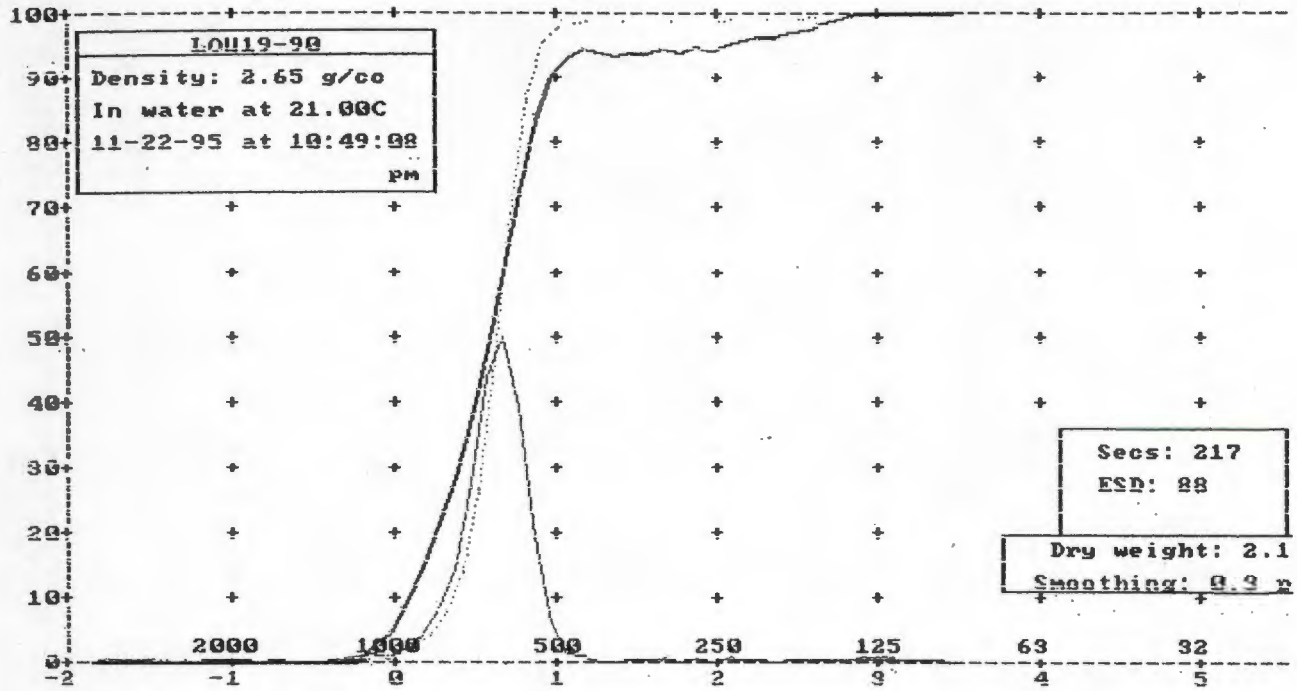

Moment statistics:
  Mean = 0.62 phi = 650.34u
  Std dev = 0.34 phi   Skewness = 2.74   Kurtosis = 30.26

Graphical values (F&W):
  Mean = 0.61 phi = 656.66u
  Median (phi50) = 0.62 phi = 651.90u
  Sorting = 0.19 phi   Skewness = -0.12   Kurtosis = 1.11

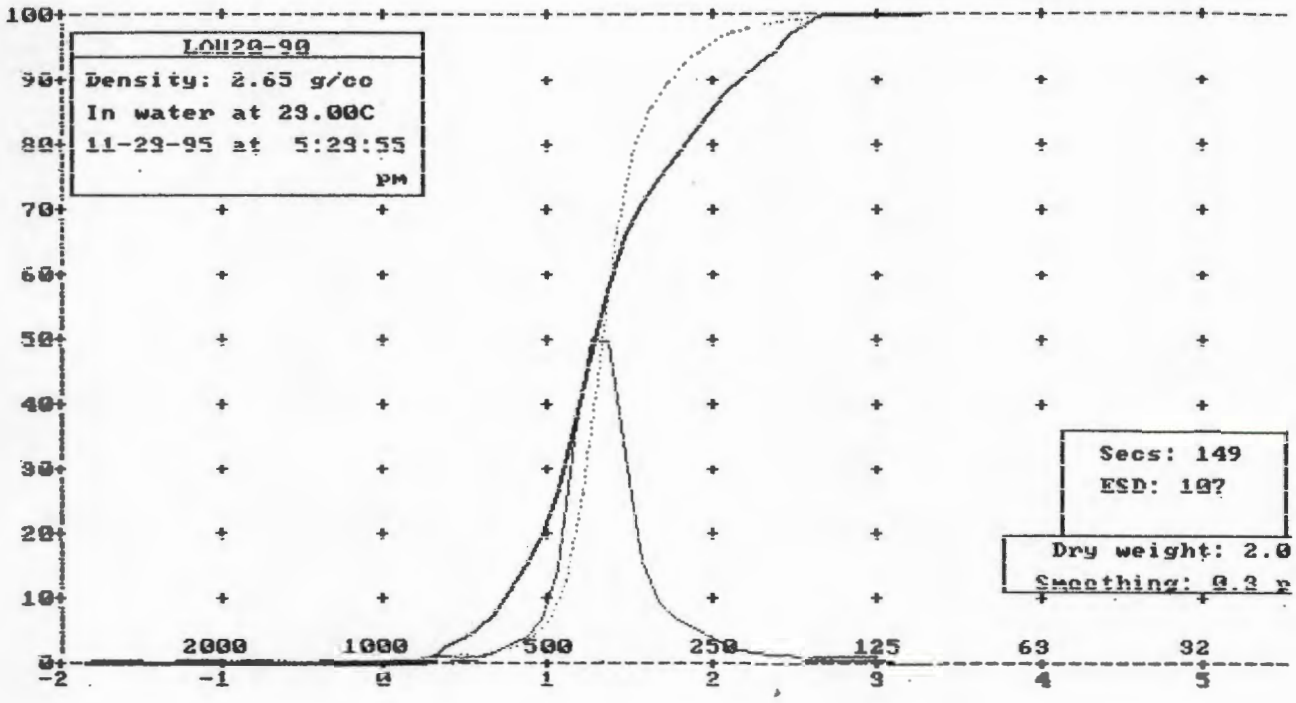

Moment statistics:
  Mean = 1.35 phi = 392.39u
  Std dev = 0.35 phi Skewness = -0.84 Kurtosis = 20.13

Graphical values (F&W):
  Mean = 1.34 phi = 394.92u
  Median (phi50) = 1.32 phi = 400.99u
  Sorting = 0.26 phi Skewness = 0.20 Kurtosis = 1.50

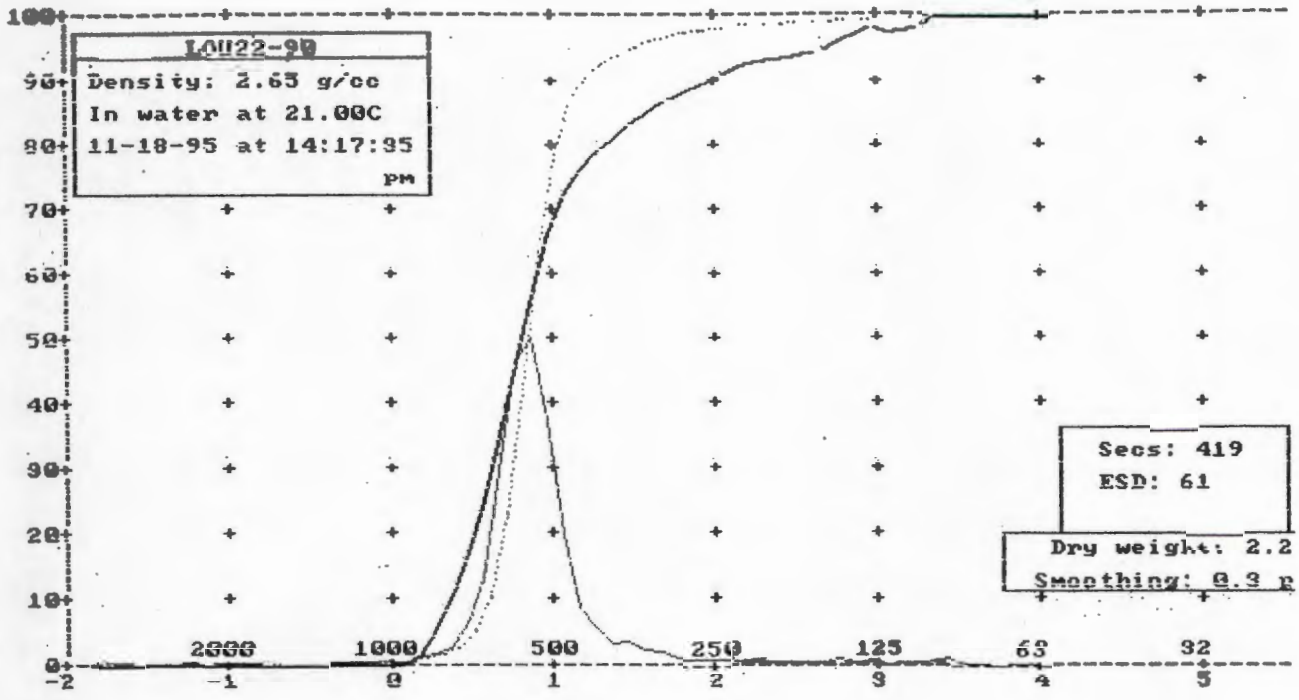

Moment statistics:
  Mean = 0.90 phi = 537.63u
  Std dev = 0.41 phi Skewness = 2.57 Kurtosis = 21.05

Graphical values (F&W):
  Mean = 0.85 phi = 554.19u
  Median (phi50) = 0.84 phi = 559.05u
  Sorting = 0.26 phi Skewness = 0.21 Kurtosis = 1.55

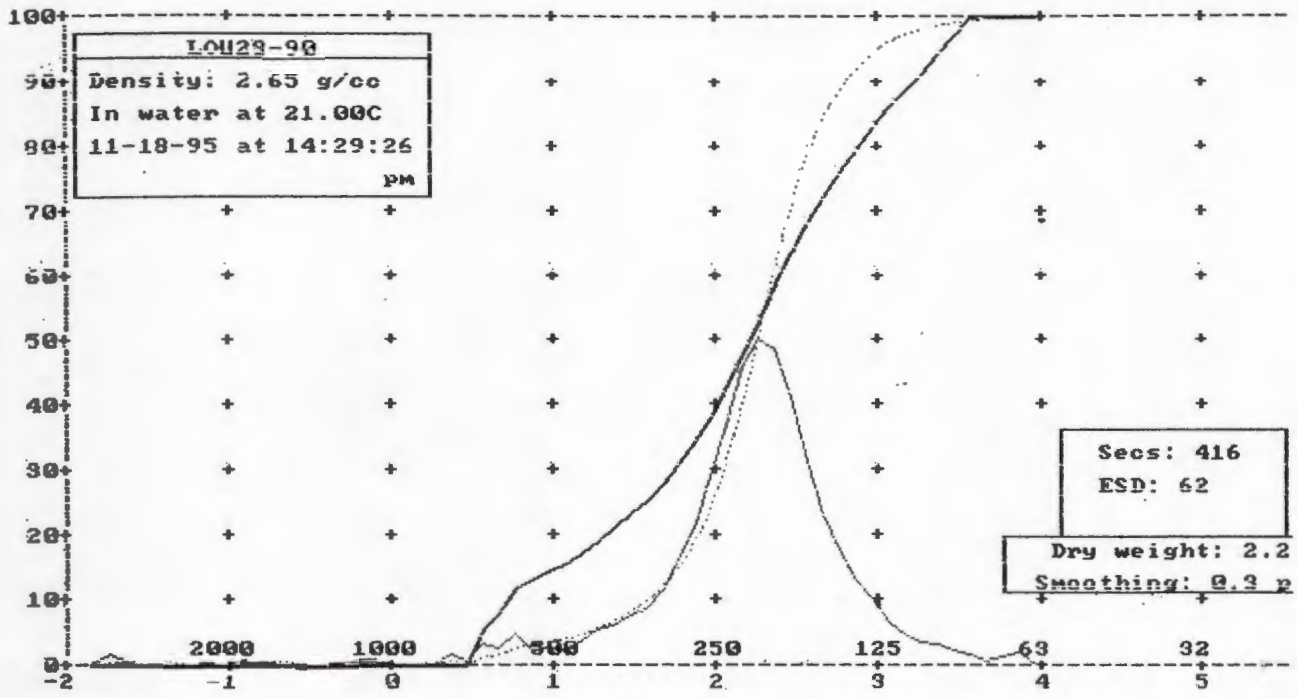

Moment statistics:
  Mean = 2.20 phi = 216.89u
  Std dev = 0.56 phi Skewness = -1.29 Kurtosis = 10.13

Graphical values (F&W):
  Mean = 2.23 phi = 213.00u
  Median (phi50) = 2.25 phi = 210.29u
  Sorting = 0.49 phi Skewness = -0.11 Kurtosis = 1.36

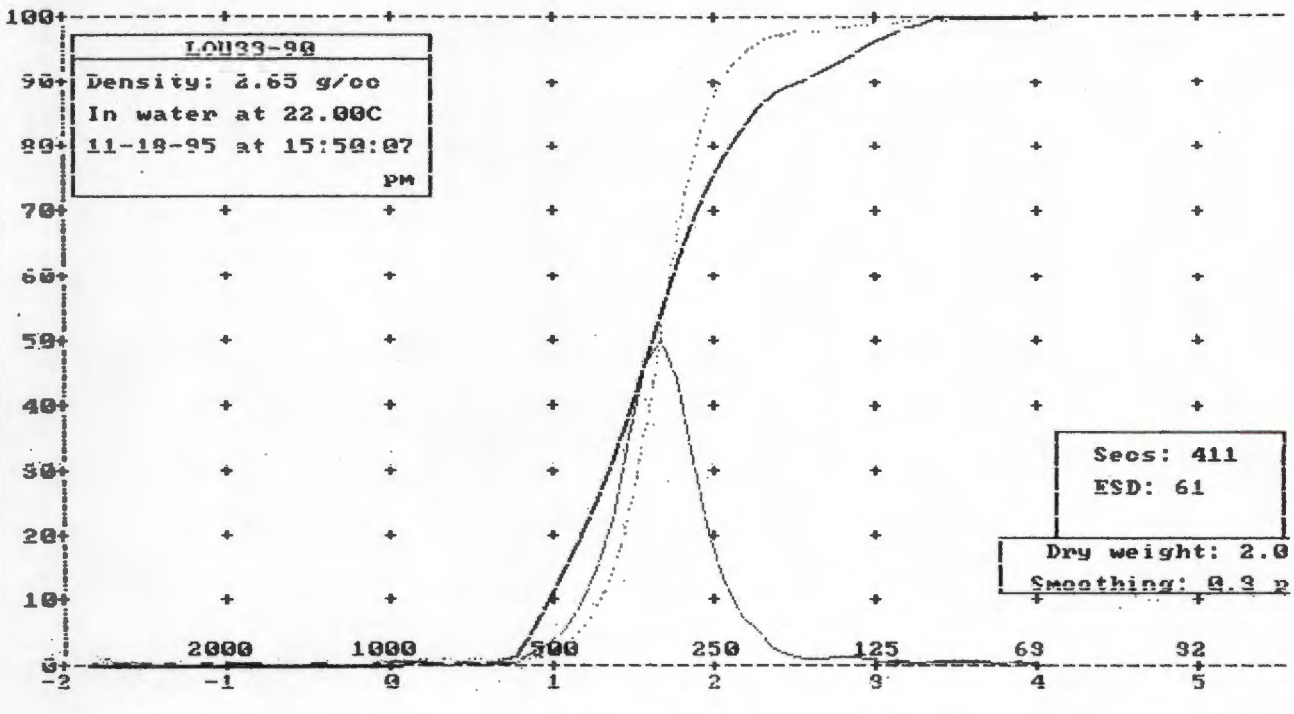

Moment statistics:
  Mean = 1.66 phi = 317.54u
  Std dev = 0.43 phi   Skewness = -1.13   Kurtosis = 22.13

Graphical values (F&W):
  Mean = 1.65 phi = 319.28u
  Median (phi50) = 1.64 phi = 320.03u
  Sorting = 0.30 phi   Skewness = 0.04   Kurtosis = 1.22

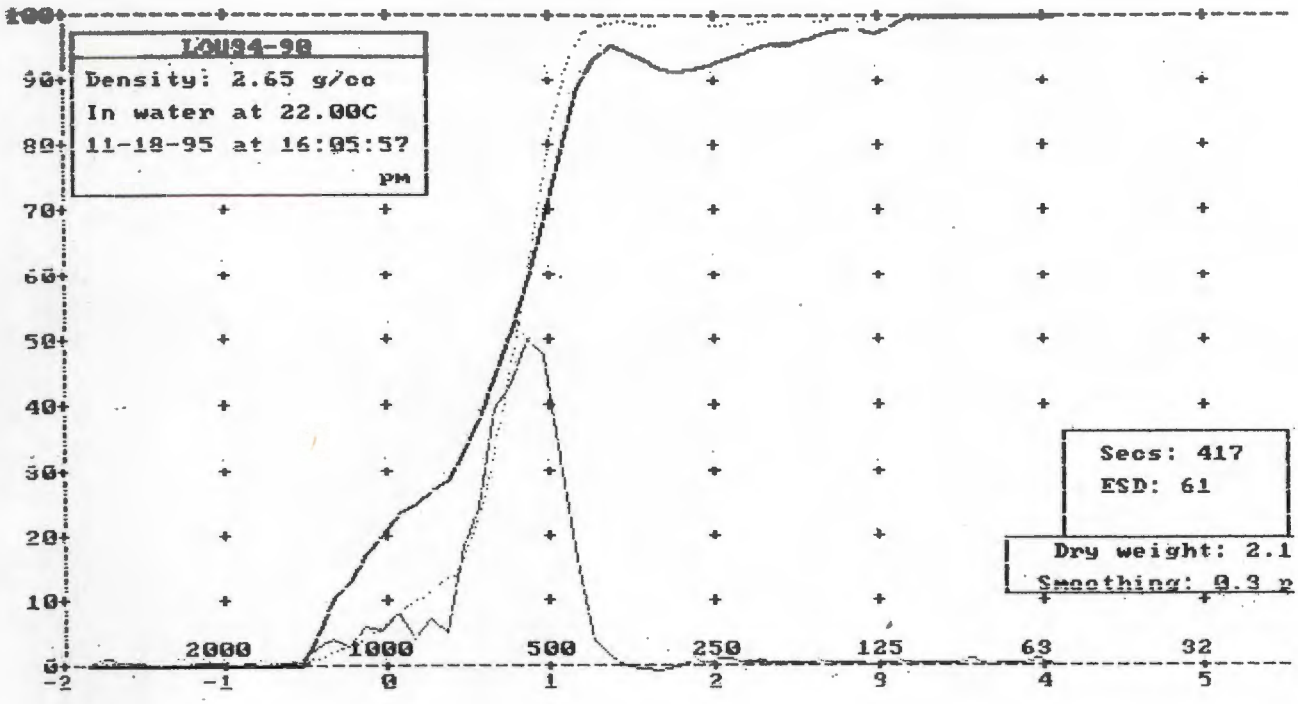

Moment statistics:
  Mean = 0.73 phi = 601.36u
  Std dev = 0.48 phi Skewness = 1.10 Kurtosis = 15.99

Graphical values (F&W):
  Mean = 0.75 phi = 596.27u
  Median (phi50) = 0.78 phi = 581.30u
  Sorting = 0.33 phi Skewness = -0.30 Kurtosis = 1.37

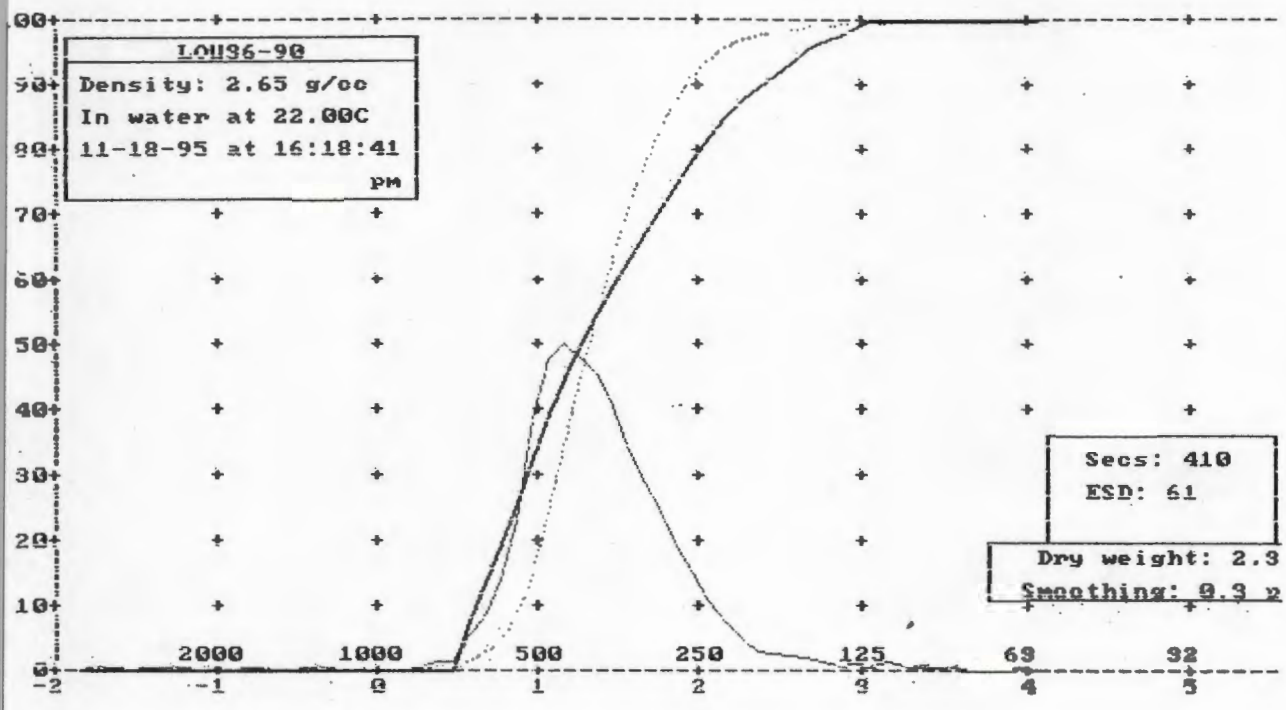

pment statistics:
Mean = 1.36 phi = 388.82u
Std dev = 0.46 phi Skewness = 0.28 Kurtosis = 8.75

raphical values (F&W):
Mean = 1.35 phi = 392.50u
Median (phi50) = 1.31 phi = 404.00u
Sorting = 0.41 phi Skewness = 0.18 Kurtosis = 1.02

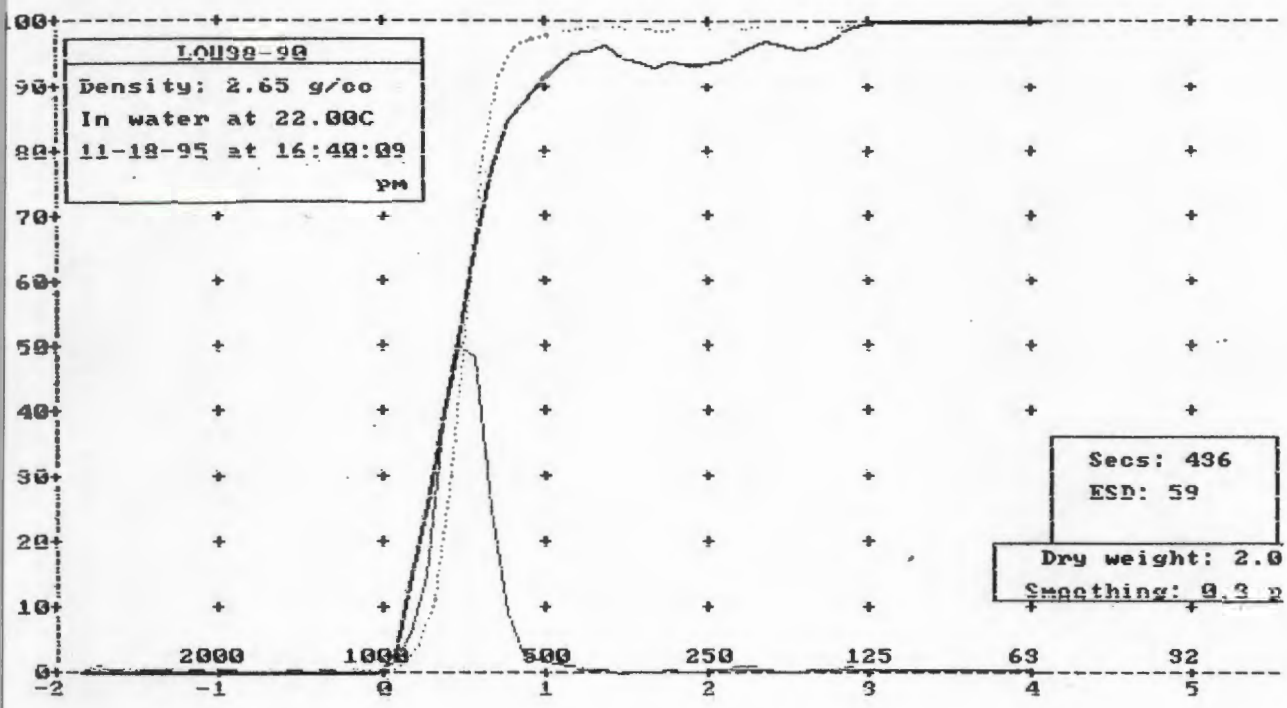

oment statistics:
Mean = 0.51 phi = 702.31u
Std dev = 0.37 phi Skewness = 4.06 Kurtosis = 42.32

raphical values (F&W):
Mean = 0.48 phi = 715.62u
Median (phi50) = 0.48 phi = 716.71u
Sorting = 0.16 phi Skewness = 0.04 Kurtosis = 1.11

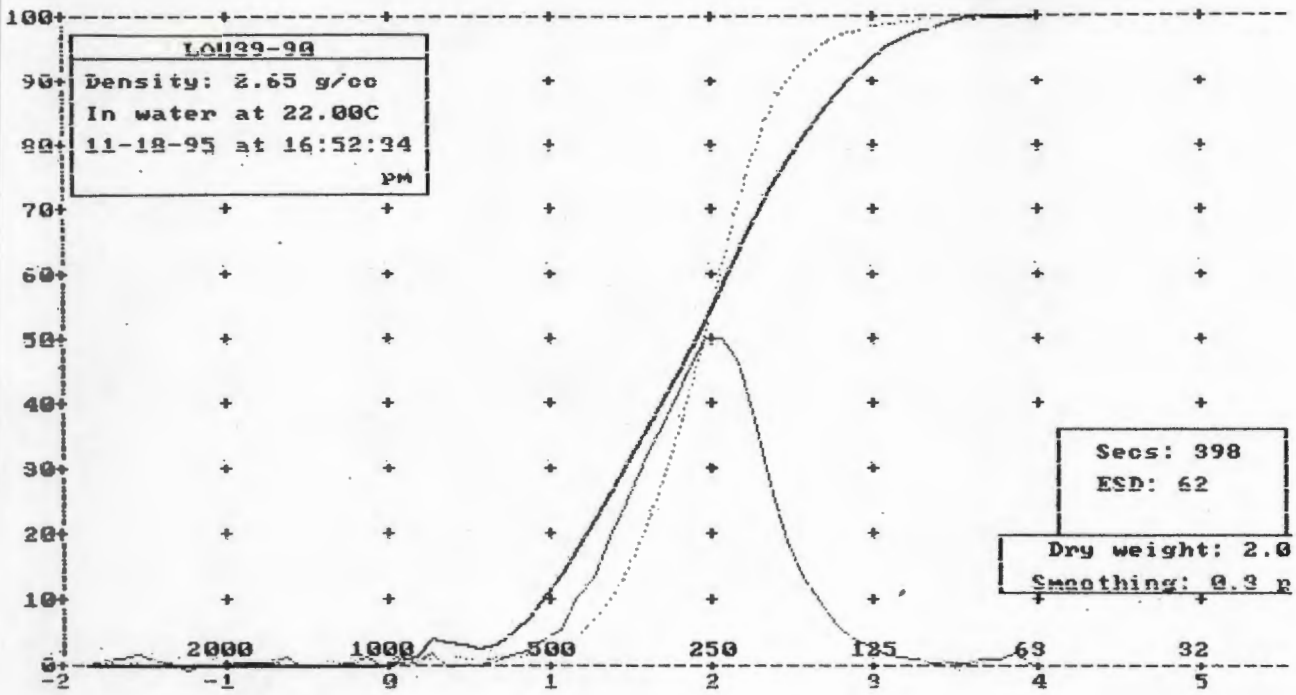

Moment statistics:
Mean = 1.92 phi = 265.04u
Std dev = 0.52 phi Skewness = -1.12 Kurtosis = 12.29

Graphical values (F&W):
Mean = 1.92 phi = 264.52u
Median (phi50) = 1.94 phi = 261.06u
Sorting = 0.43 phi Skewness = -0.05 Kurtosis = 1.07

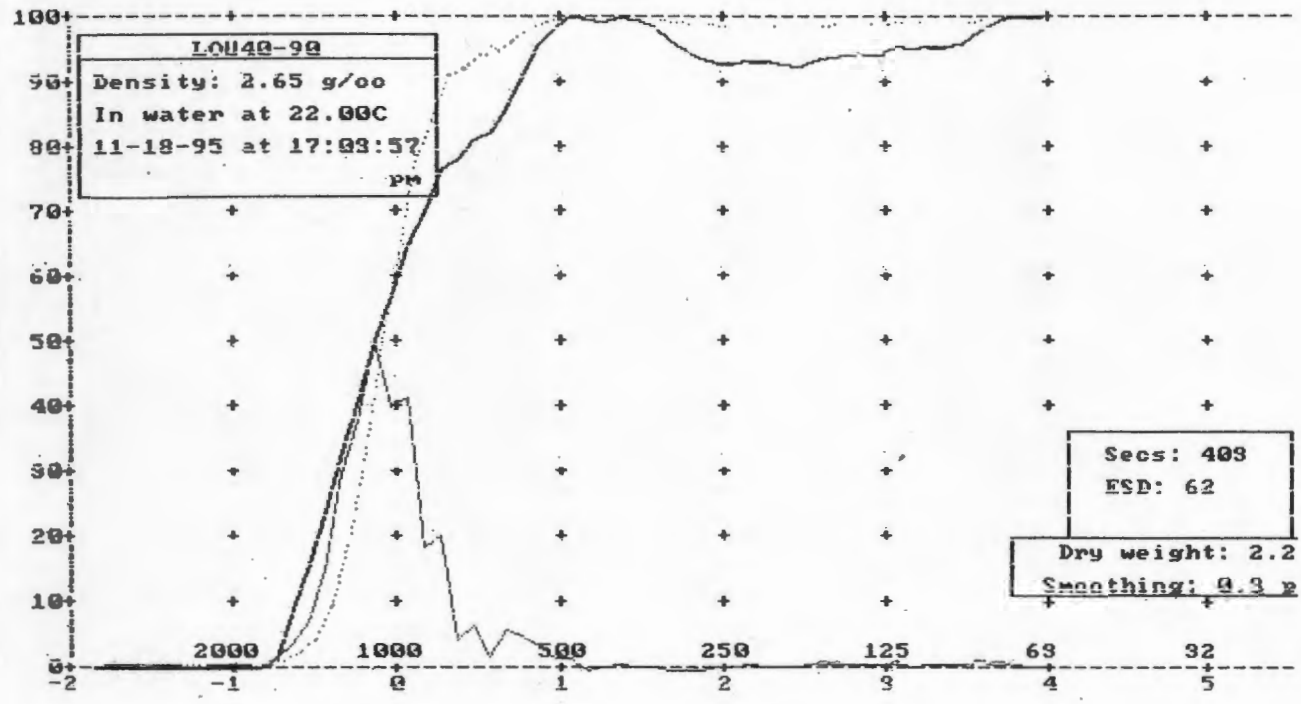

Moment statistics:
  Mean = -0.04 phi = 1031.22u
  Std dev. = 0.44 phi Skewness = 4.60 Kurtosis = 40.40

Graphical values (F&W):
  Mean = -0.07 phi = 1052.64u
  Median (phi50) = -0.10 phi = 1068.99u
  Sorting = 0.30 phi Skewness = 0.21 Kurtosis = 1.35

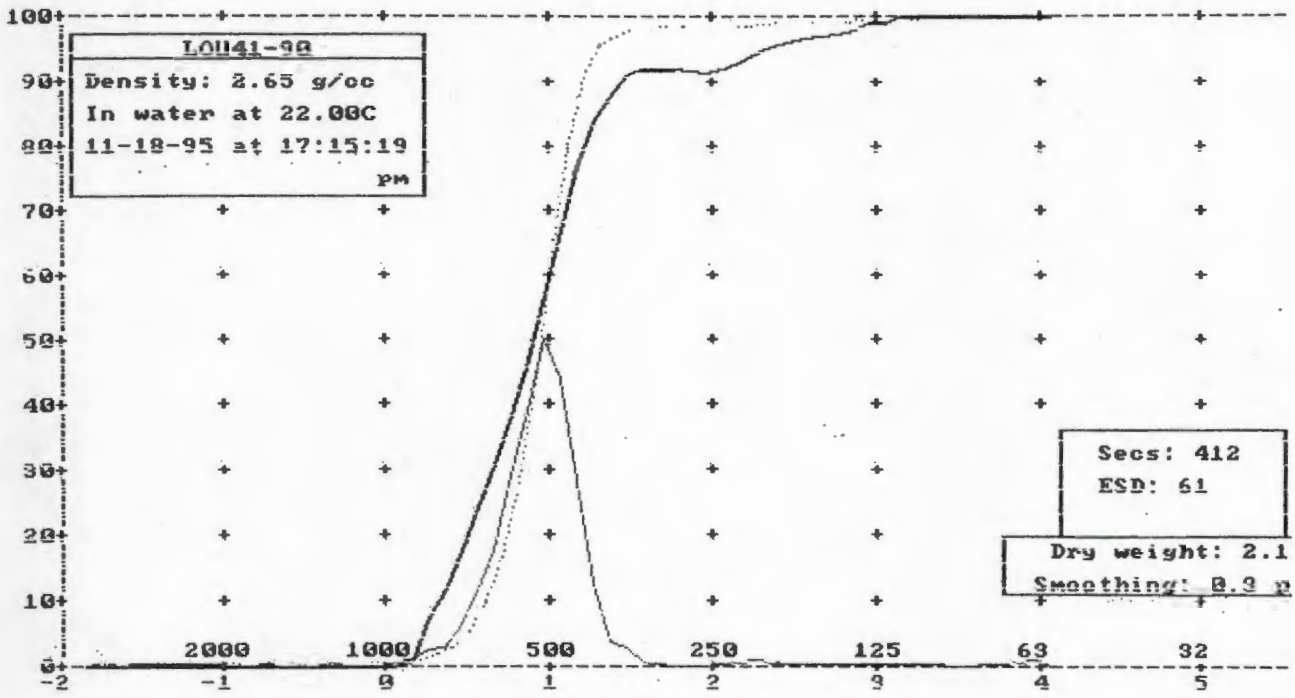

Moment statistics:
  Mean = 0.94 phi = 520.74u
  Std dev = 0.40 phi Skewness = 2.28 Kurtosis = 27.77

Graphical values (F&W):
  Mean = 0.92 phi = 526.97u
  Median (phi50) = 0.94 phi = 522.41u
  Sorting = 0.23 phi Skewness = -0.10 Kurtosis = 1.10

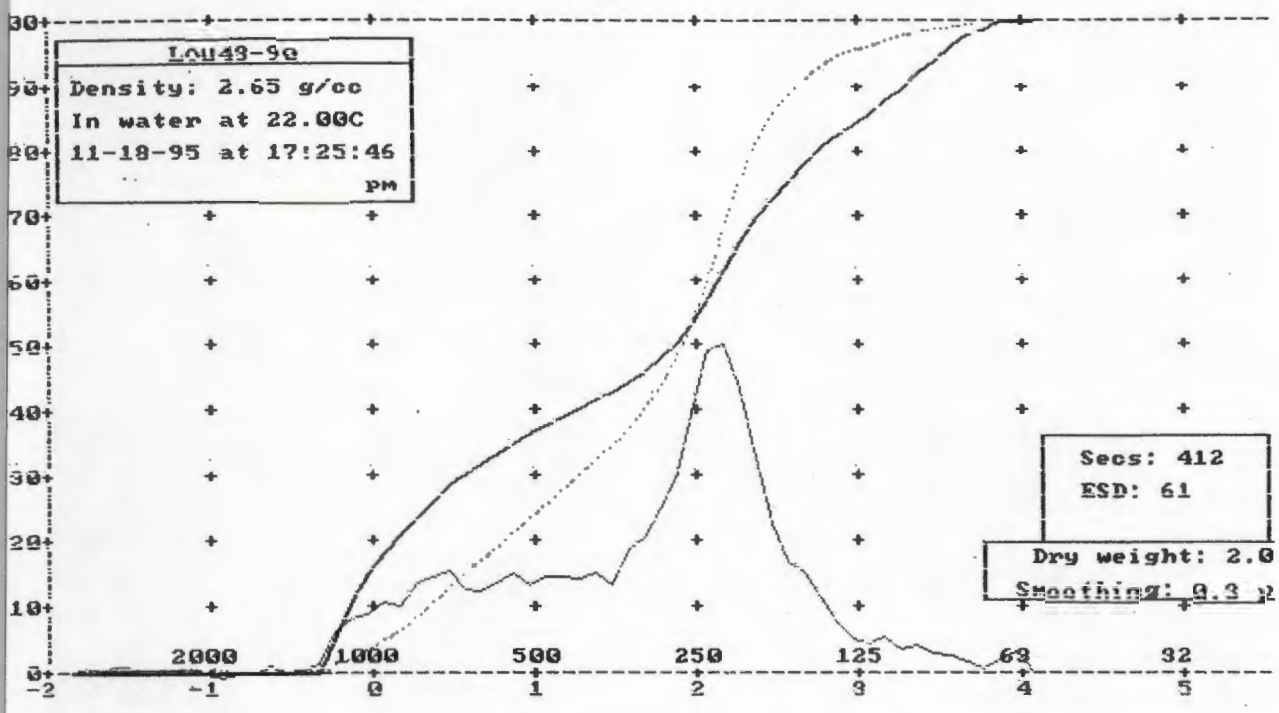

ment statistics:
Mean = 1.67 phi = 313.36u
Std dev = 0.89 phi Skewness = -0.40 Kurtosis = 2.94

aphical values (FRW):
Mean = 1.64 phi = 320.14u
Median (phi50) = 1.90 phi = 267.37u
Sorting = 0.89 phi Skewness = -0.36 Kurtosis = 0.97

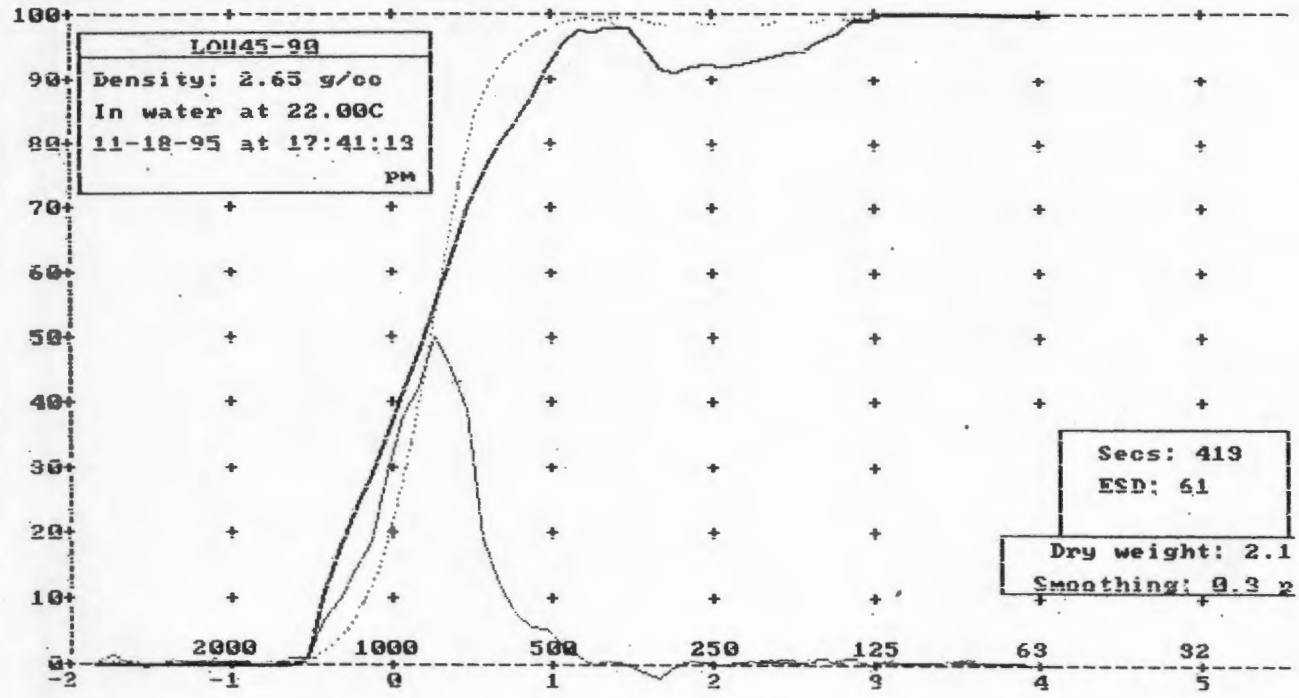

Moment statistics:
Mean = 0.25 phi = 842.49u
Std dev = 0.45 phi Skewness = 2.94 Kurtosis = 21.76

Graphical values (F&W):
Mean = 0.22 phi = 861.20u
Median (phi50) = 0.23 phi = 852.75u
Sorting = 0.31 phi Skewness = -0.02 Kurtosis = 1.14

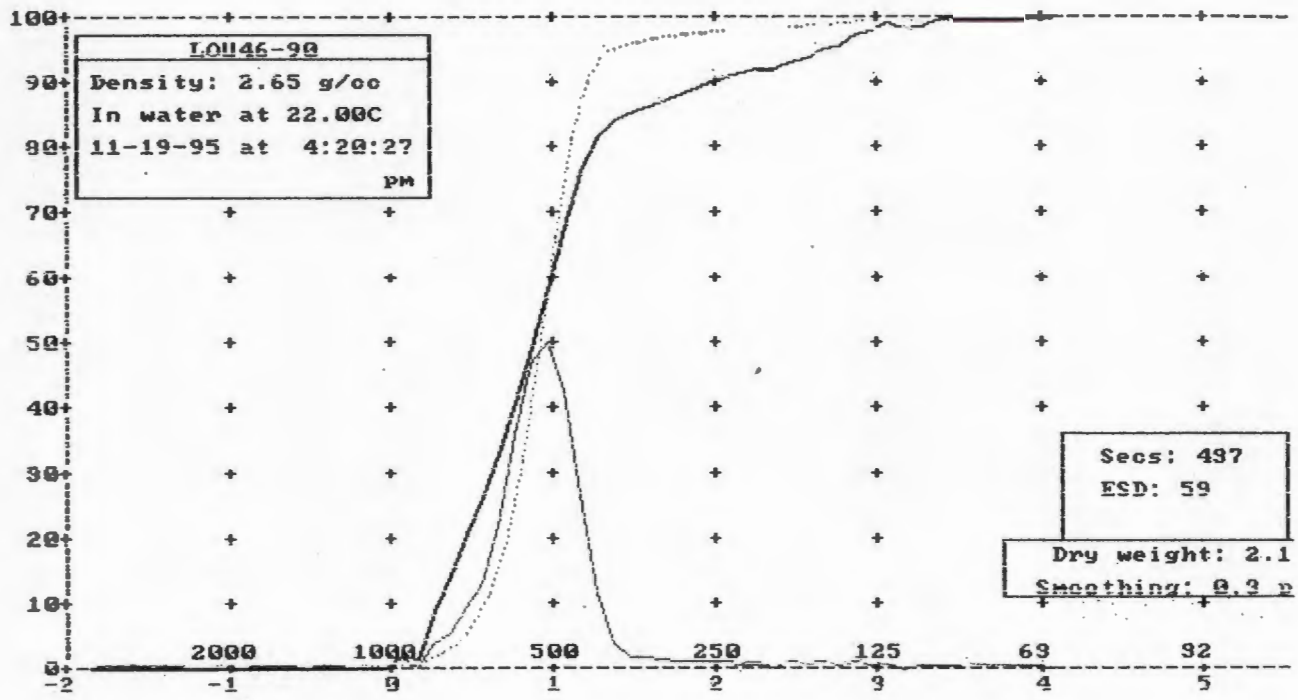

Moment statistics:
  Mean = 0.93 phi = 523.76u
  Std dev = 0.44 phi Skewness = 1.88 Kurtosis = 21.16

Graphical values (F&W):
  Mean = 0.90 phi = 535.16u
  Median (phi50) = 0.91 phi = 531.74u
  Sorting = 0.26 phi Skewness = -0.03 Kurtosis = 1.22

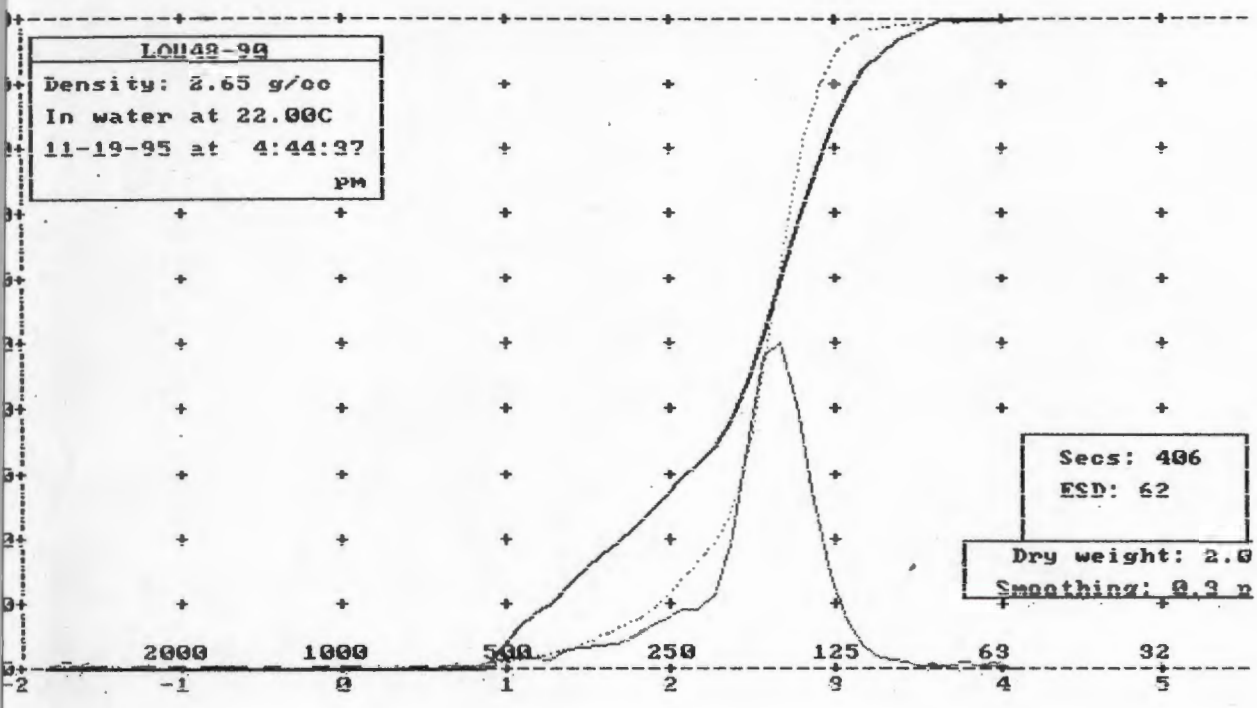

ent statistics:
ean = 2.49 phi = 178.33u
td dev = 0.49 phi Skewness = -2.80 Kurtosis = 21.52

phical values (F&W):
ean = 2.52 phi = 174.93u
edian (phi50) = 2.58 phi = 167.29u
orting = 0.39 phi Skewness = -0.34 Kurtosis = 1.52

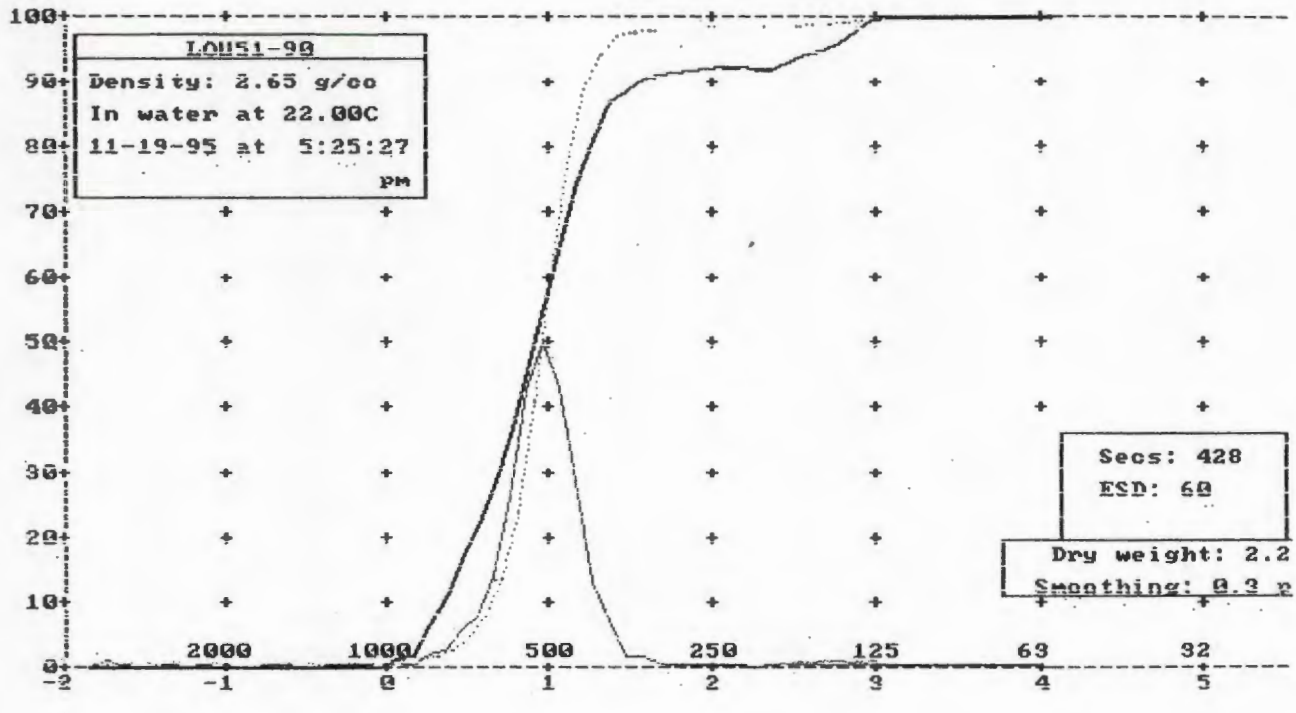

Moment statistics:
  Mean = 0.96 phi = 513.01u
  Std dev = 0.39 phi Skewness = 1.69 Kurtosis = 24.44

Graphical values (F&W):
  Mean = 0.94 phi = 519.51u
  Median (phi50) = 0.95 phi = 518.26u
  Sorting = 0.23 phi Skewness = -0.04 Kurtosis = 1.22

APPENDIX B

FACIES 4 SETTLING-TUBE RESULTS

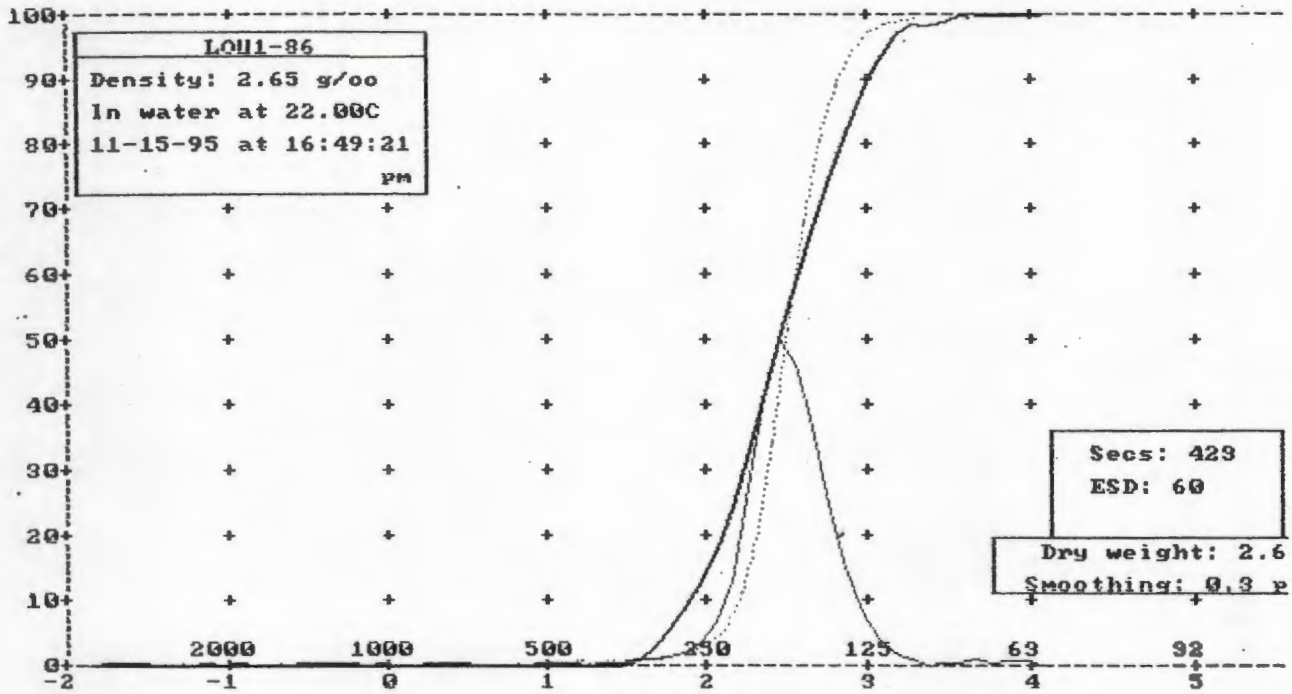

Moment statistics:
  Mean = 2.49 phi = 177.54u
  Std dev = 0.33 phi Skewness = -3.18 Kurtosis = 44.80

Graphical values (F&W):
  Mean = 2.50 phi = 176.83u
  Median (phi50) = 2.49 phi = 177.80u
  Sorting = 0.25 phi Skewness = 0.04 Kurtosis = 1.08

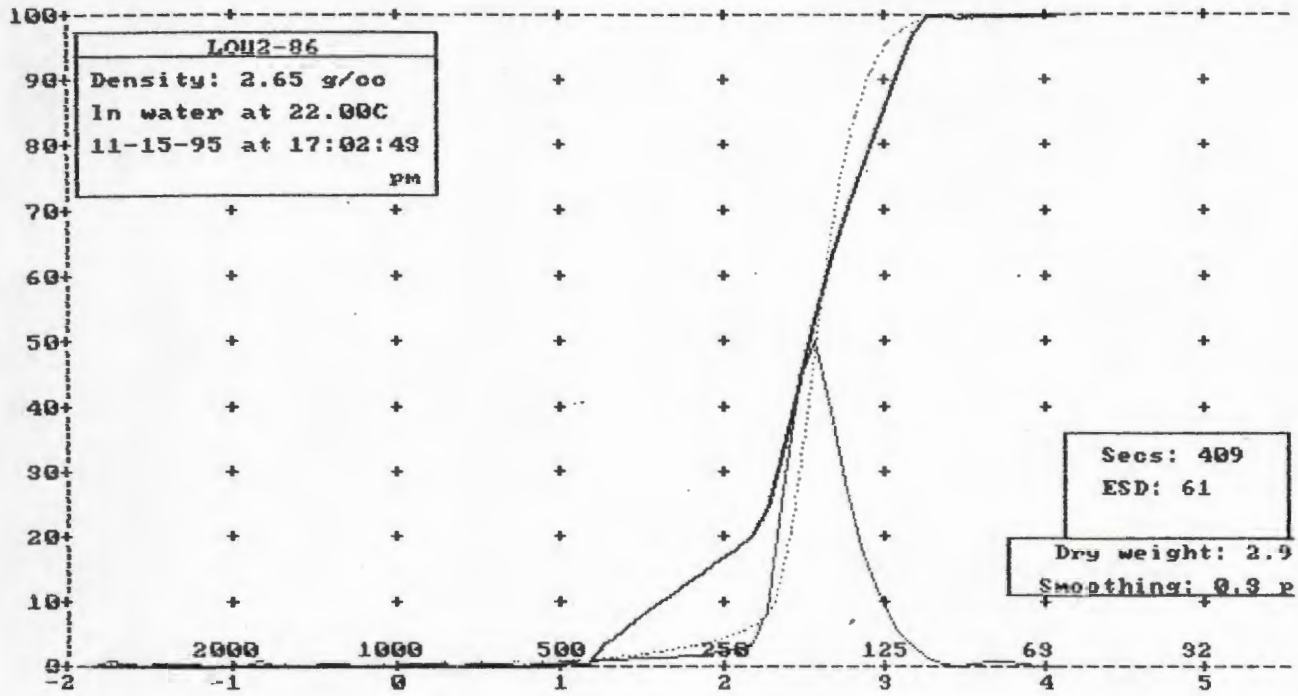

Moment statistics:
  Mean = 2.54 phi = 171.63u
  Std dev = 0.37 phi Skewness = -4.19 Kurtosis = 45.29

Graphical values (F&W):
  Mean = 2.57 phi = 168.25u
  Median (phi50) = 2.56 phi = 169.58u
  Sorting = 0.25 phi Skewness = 0.00 Kurtosis = 1.33

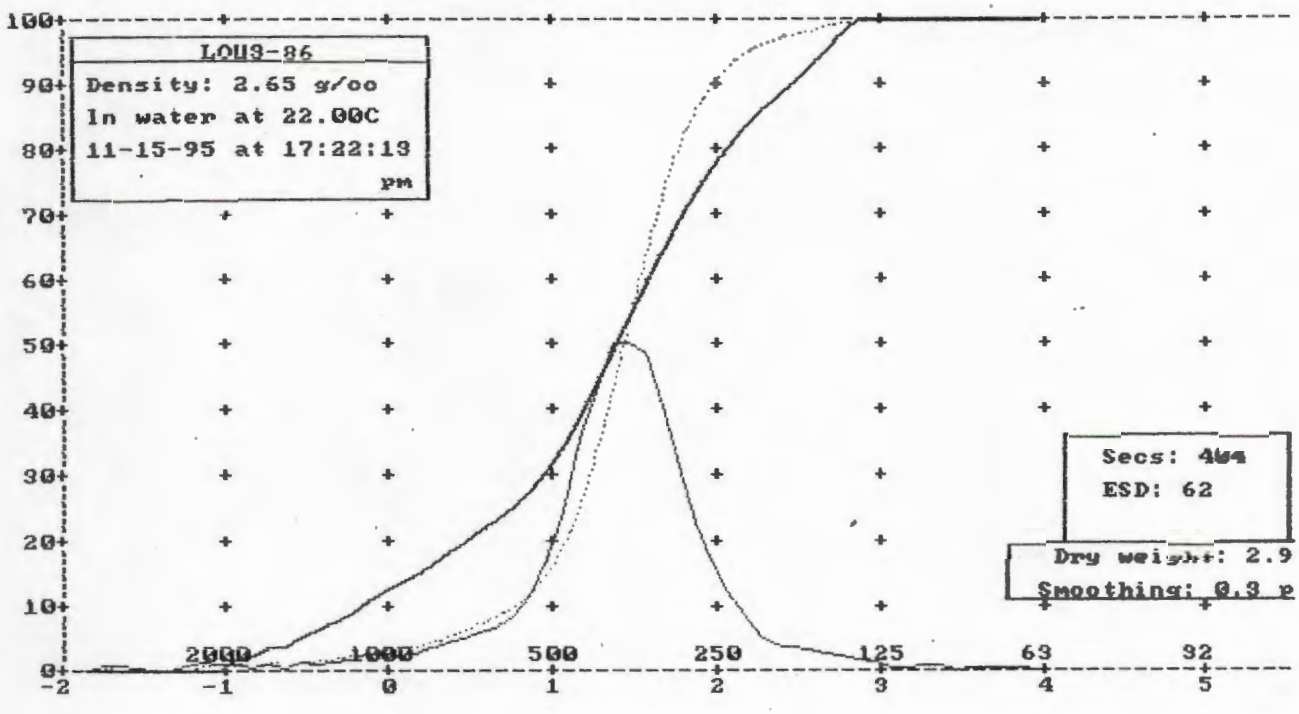

Moment statistics:
  Mean = 1.38 phi = 383.87u
  Std dev = 0.58 phi   Skewness = -0.99   Kurtosis = 7.19

Graphical values (F&W):
  Mean = 1.41 phi = 375.46u
  Median (phi50) = 1.42 phi = 373.10u
  Sorting = 0.49 phi   Skewness = -0.10   Kurtosis = 1.41

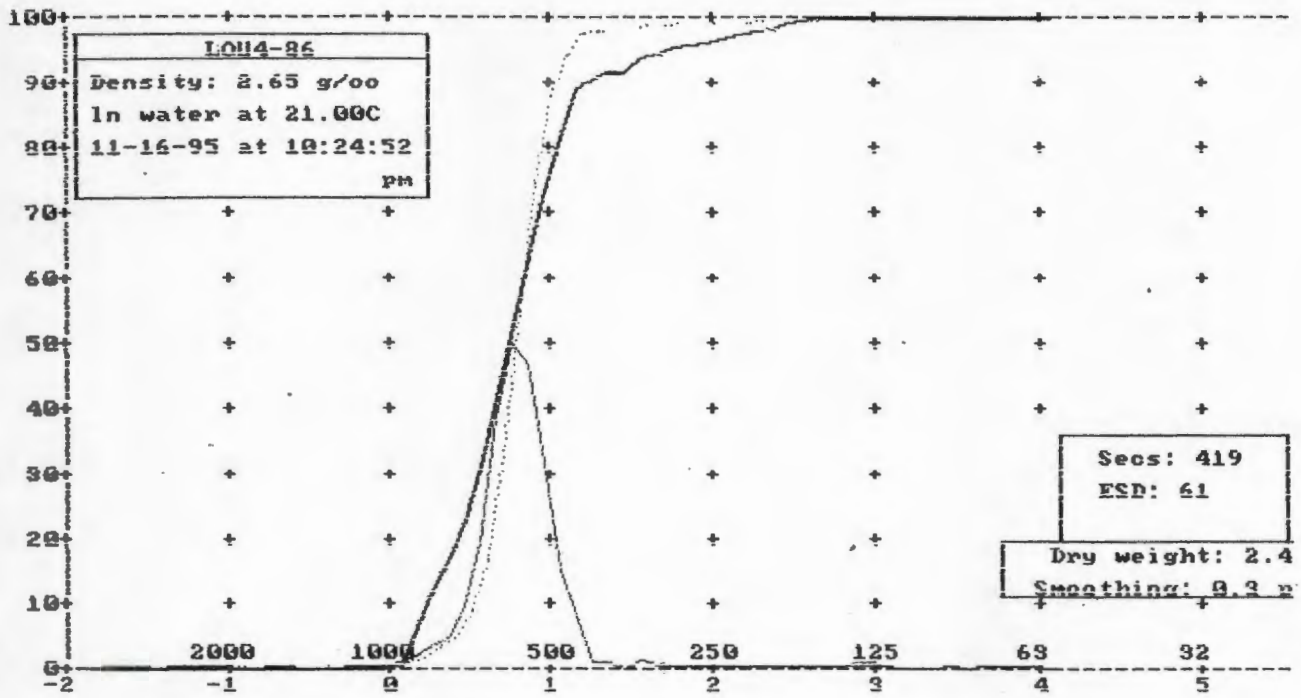

Moment statistics:
  Mean = 0.79 phi = 579.38u
  Std dev = 0.32 phi Skewness = 1.96 Kurtosis = 33.80

Graphical values (F&W):
  Mean = 0.78 phi = 582.14u
  Median (phi50) = 0.78 phi = 582.81u
  Sorting = 0.21 phi Skewness = -0.01 Kurtosis = 1.16

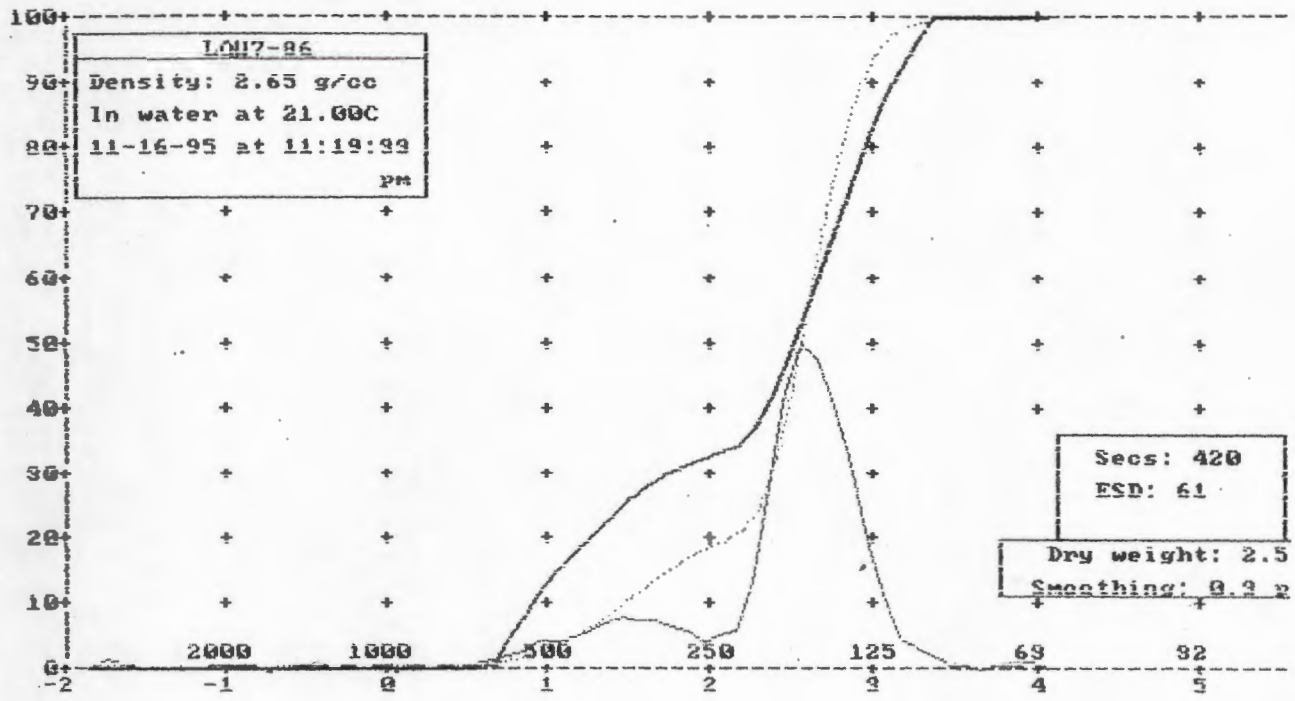

Moment statistics:
  Mean = 2.40 phi = 189.52u
  Std dev = 0.60 phi Skewness = -2.10 Kurtosis = 11.87

Graphical values (F&W):
  Mean = 2.40 phi = 189.38u
  Median (phi50) = 2.55 phi = 170.81u
  Sorting = 0.54 phi Skewness = -0.45 Kurtosis = 1.70

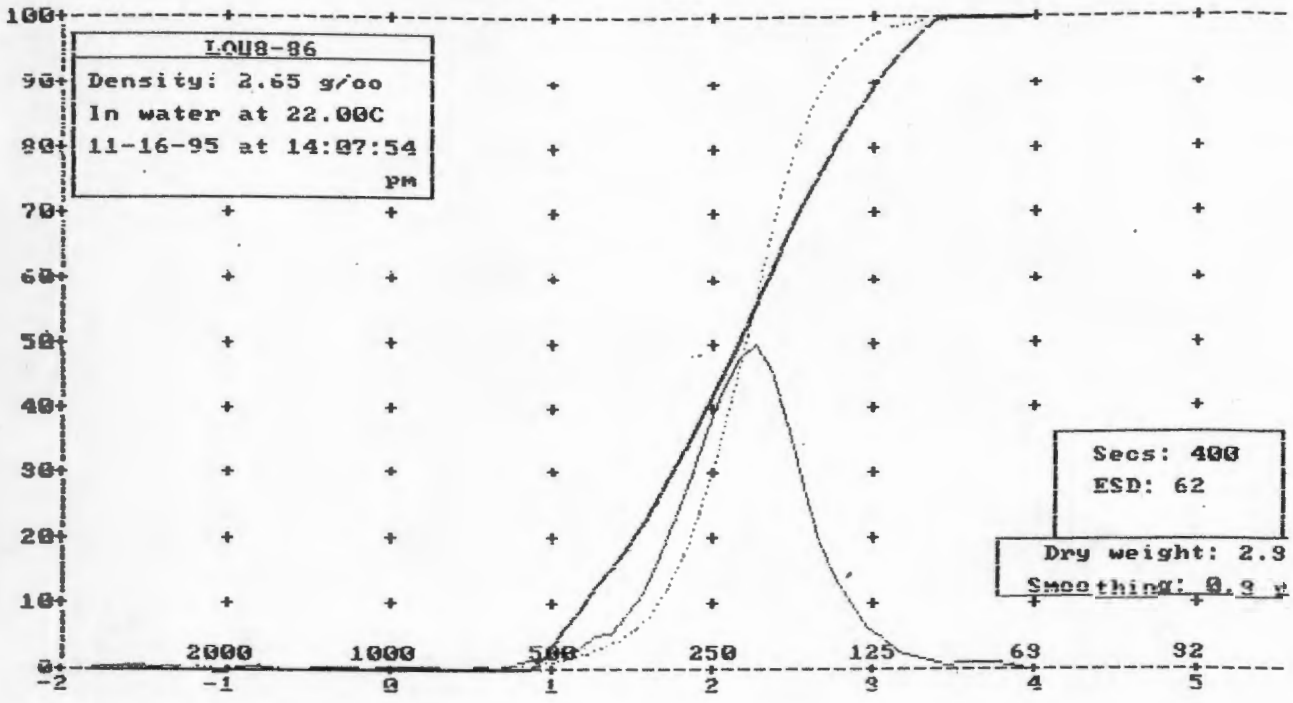

Moment statistics:
  Mean = 2.17 phi = 222.55u
  Std dev = 0.47 phi Skewness = -1.41 Kurtosis = 15.27

Graphical values (F&W):
  Mean = 2.17 phi = 221.57u
  Median (phi50) = 2.19 phi = 219.61u
  Sorting = 0.41 phi Skewness = -0.05 Kurtosis = 1.12

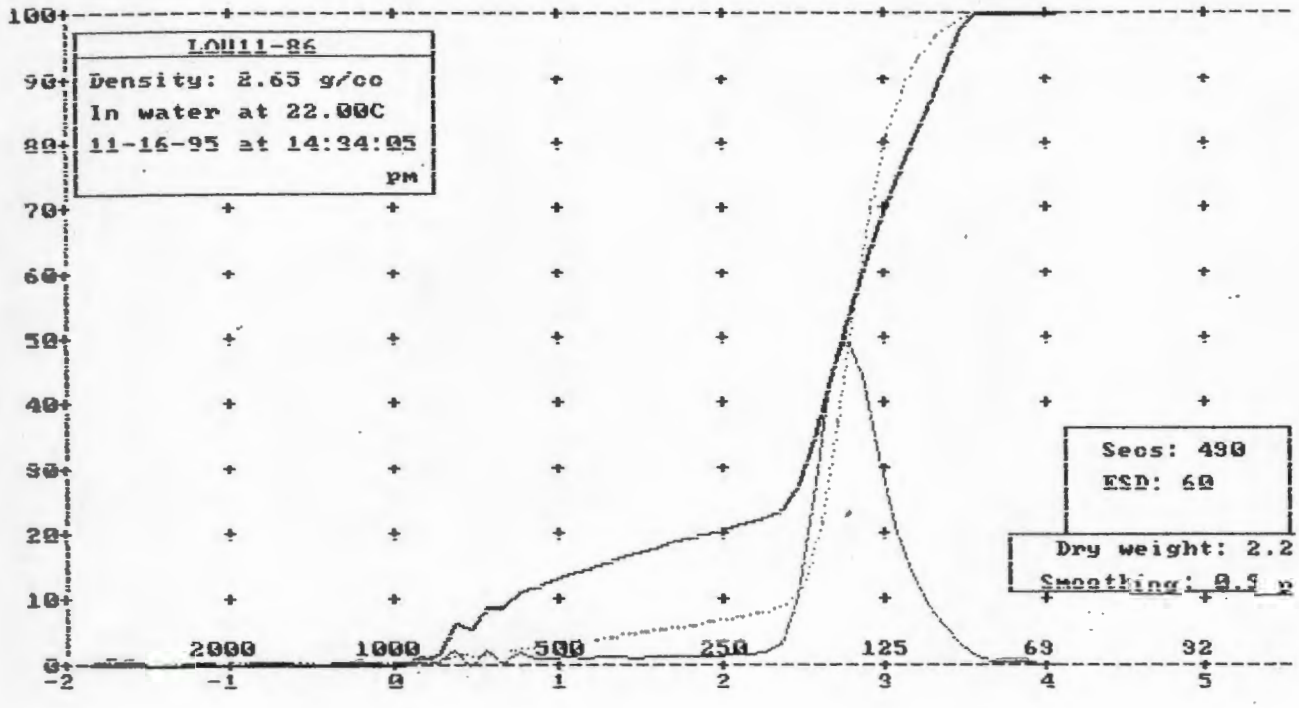

Moment statistics:
  Mean = 2.69 phi = 154.88u
  Std dev = 0.56 phi Skewness = -3.38 Kurtosis = 19.92

Graphical values (F&W):
  Mean = 2.79 phi = 144.99u
  Median (phi50) = 2.78 phi = 146.01u
  Sorting = 0.39 phi Skewness = -0.18 Kurtosis = 2.15

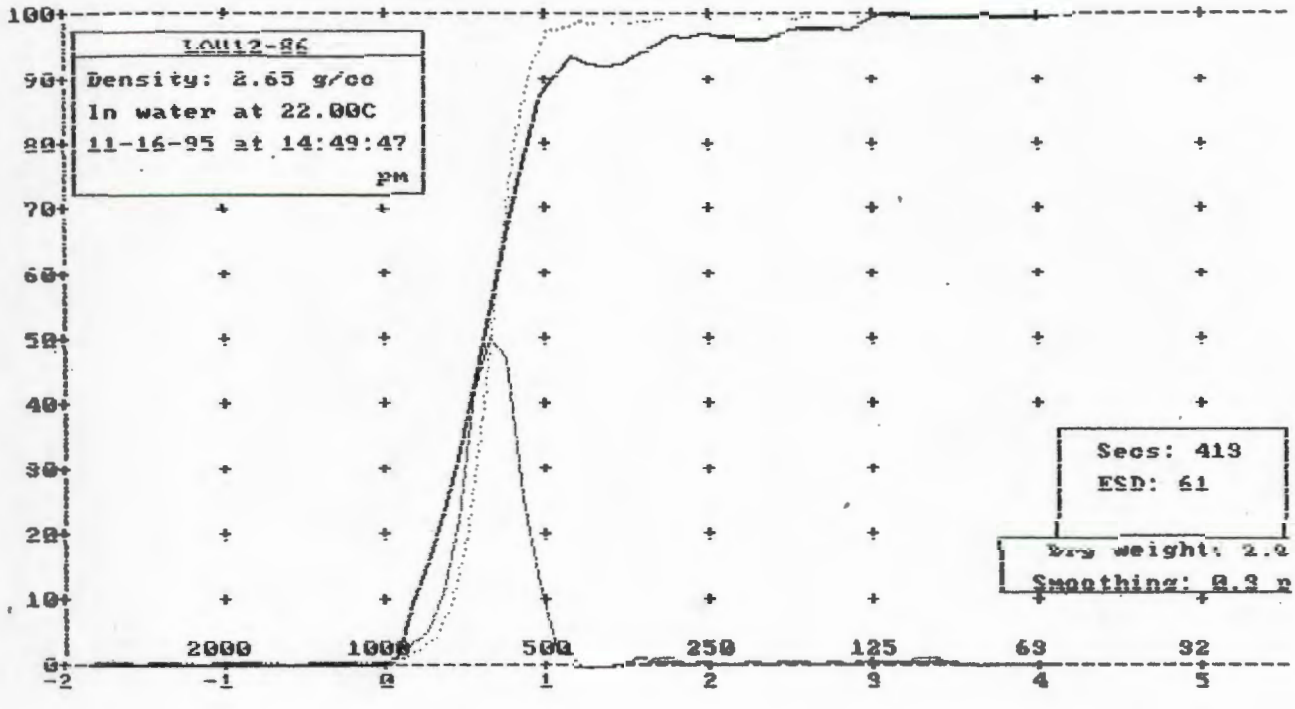

Moment statistics:
  Mean = 0.66 phi = 635.04u
  Std dev = 0.28 phi   Skewness = 0.42   Kurtosis = 23.41

Graphical values (F&W):
  Mean = 0.65 phi = 639.65u
  Median (phi50) = 0.66 phi = 634.19u
  Sorting = 0.19 phi   Skewness = -0.04   Kurtosis = 1.10

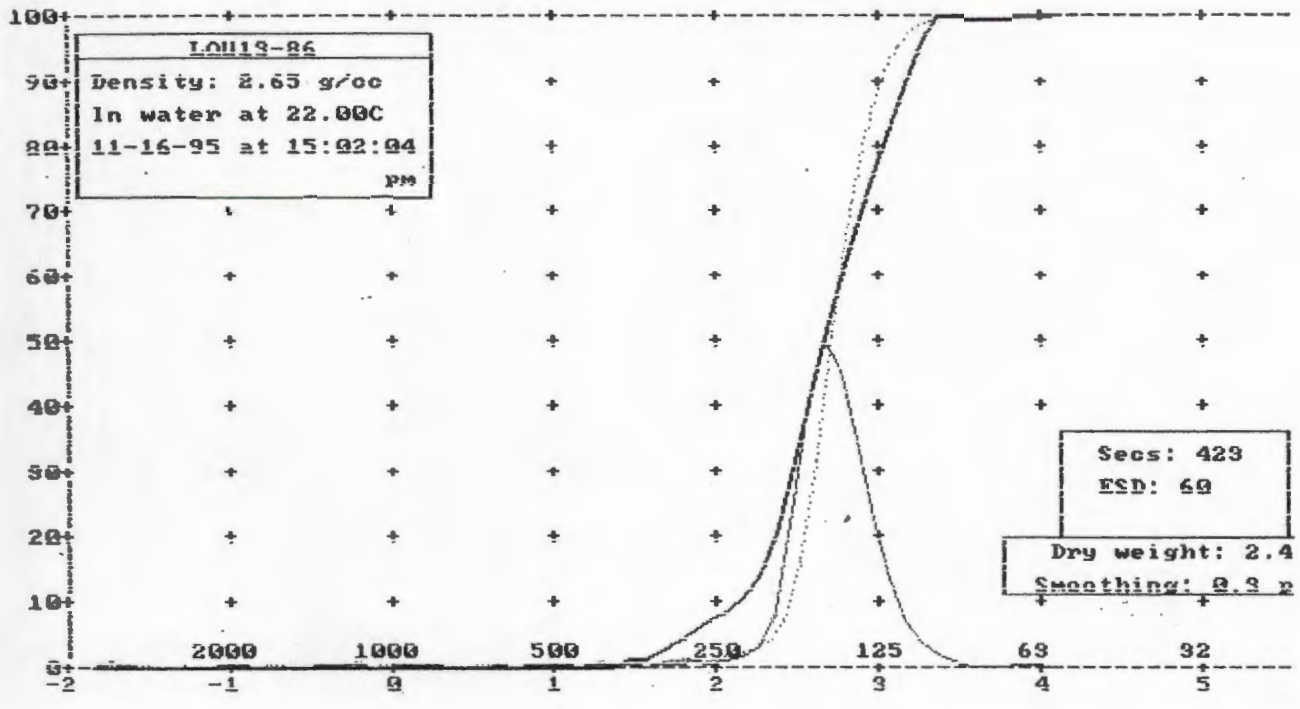

Moment statistics:
  Mean = 2.69 phi = 155.09u
  Std dev = 0.35 phi Skewness = -6.25 Kurtosis = 78.60

Graphical values (F&W):
  Mean = 2.71 phi = 152.75u
  Median (phi50) = 2.70 phi = 154.10u
  Sorting = 0.22 phi Skewness = 0.08 Kurtosis = 1.06

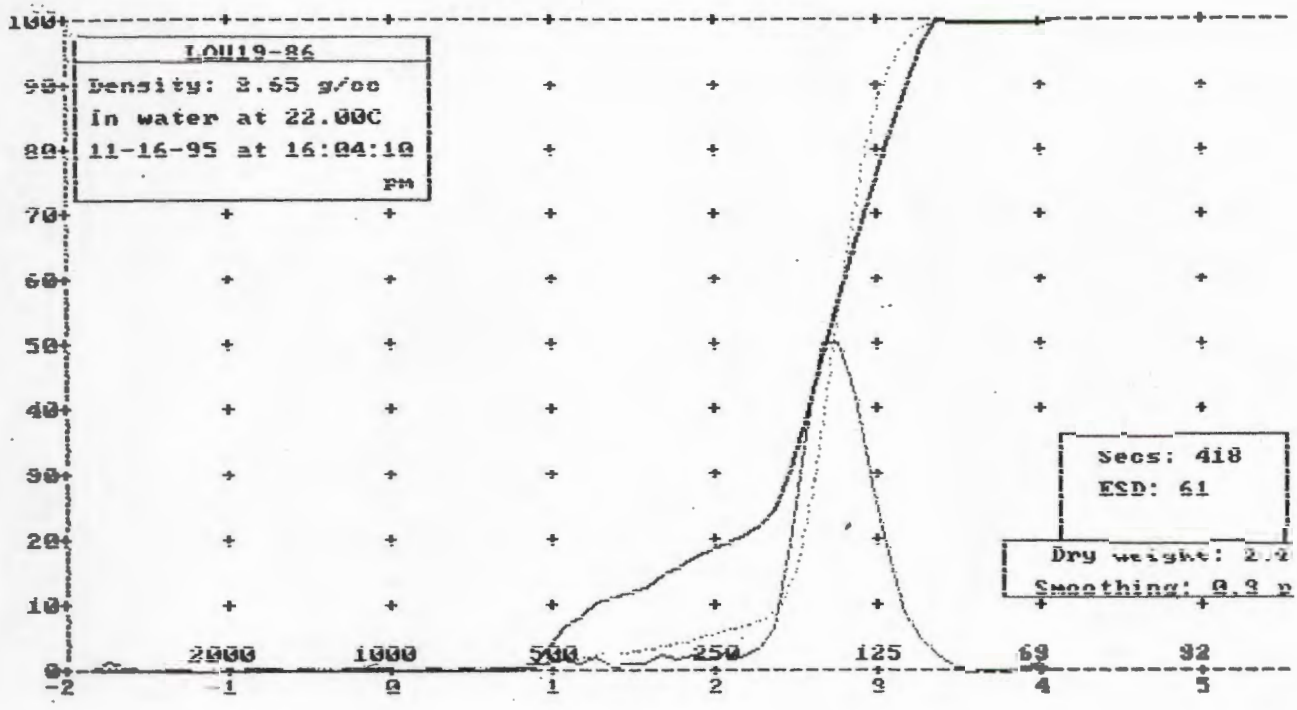

Moment statistics:
  Mean = 2.66 phi = 157.79u
  Std dev = 0.46 phi   Skewness = -4.54   Kurtosis = 38.83

Graphical values (F&W):
  Mean = 2.72 phi = 151.37u
  Median (phi50) = 2.72 phi = 151.68u
  Sorting = 0.30 phi   Skewness = -0.16   Kurtosis = 1.60

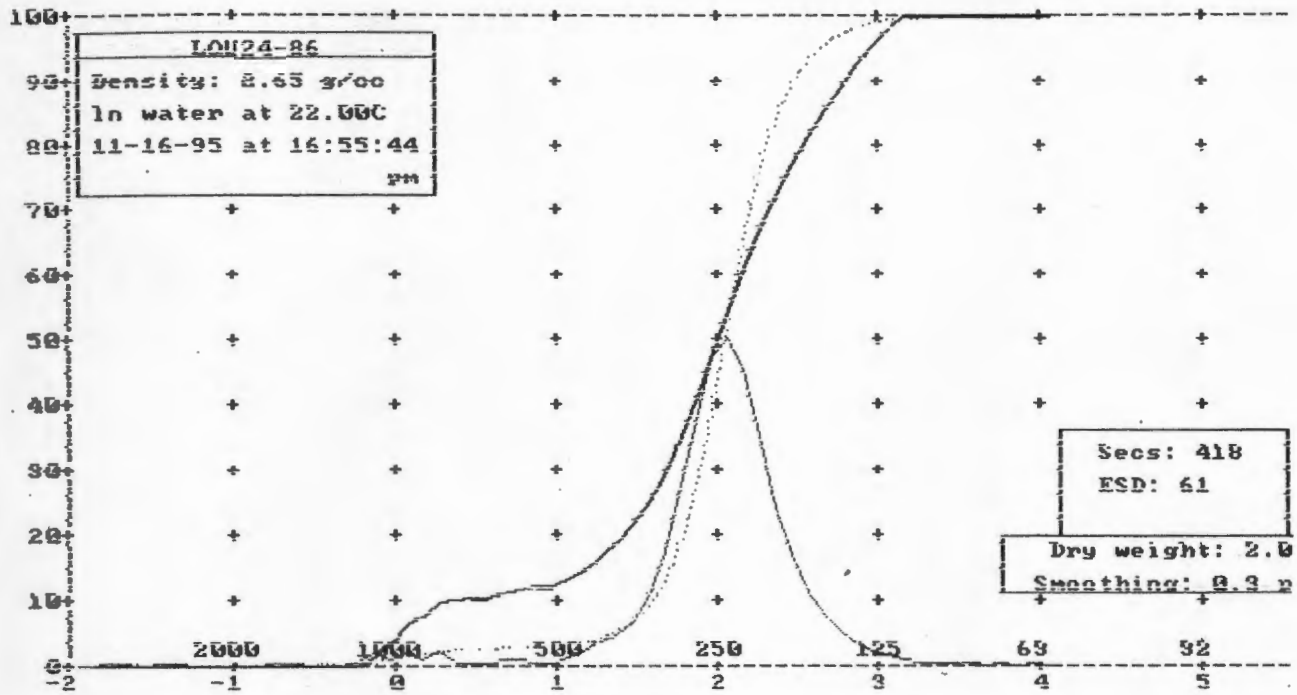

Moment statistics:
  Mean = 2.00 phi = 250.23u
  Std dev = 0.49 phi   Skewness = -2.07   Kurtosis = 14.18

Graphical values (F&W):
  Mean = 2.04 phi = 243.60u
  Median (phi50) = 2.04 phi = 243.68u
  Sorting = 0.36 phi   Skewness = -0.03   Kurtosis = 1.29

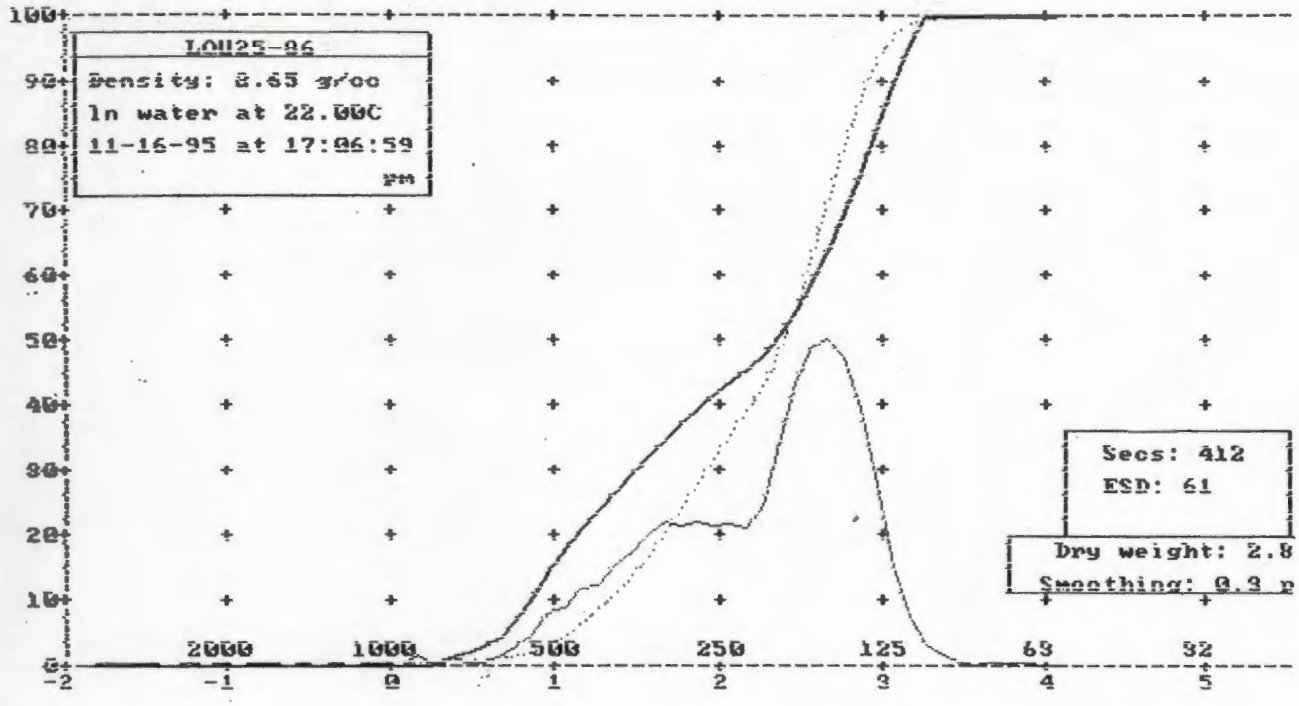

Moment statistics:
  Mean = 2.22 phi = 215.37u
  Std dev = 0.64 phi   Skewness = -1.02   Kurtosis = 5.23

Graphical values (F&W):
  Mean = 2.24 phi = 211.32u
  Median (phi50) = 2.39 phi = 190.90u
  Sorting = 0.61 phi   Skewness = -0.35   Kurtosis = 0.85

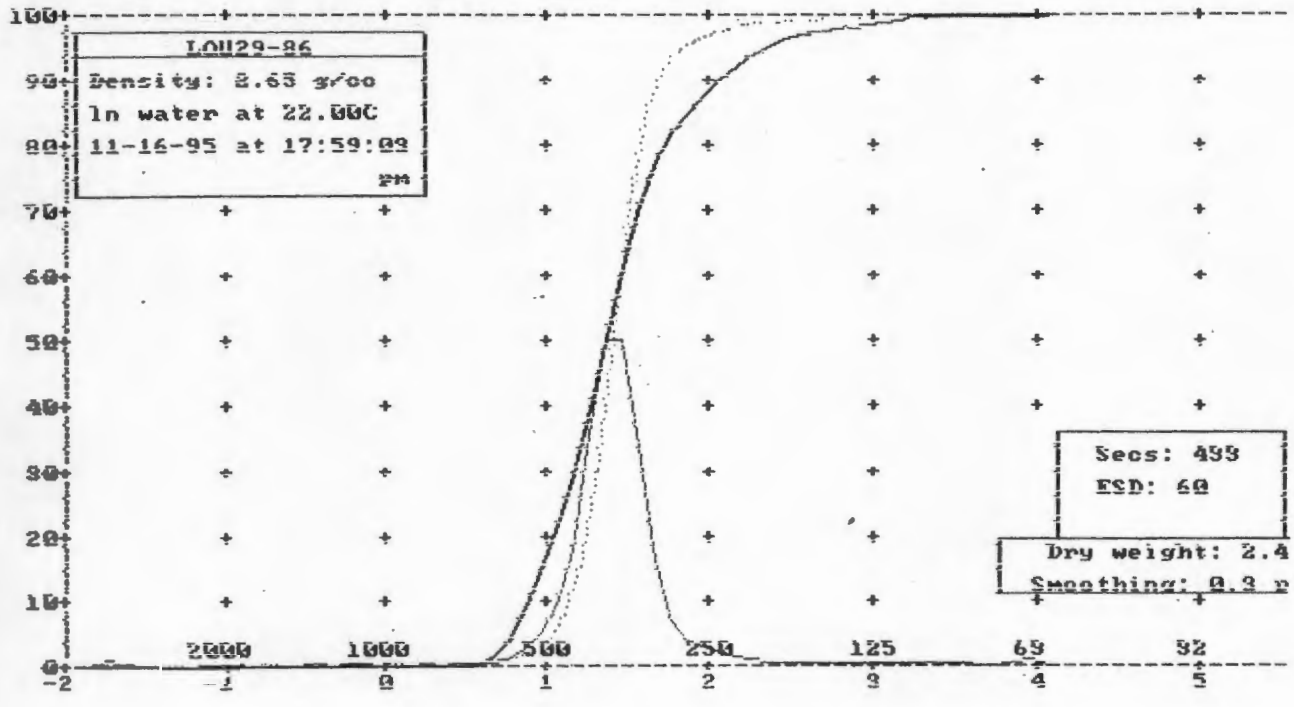

Moment statistics:
  Mean = 1.41 phi = 375.16u
  Std dev = 0.36 phi Skewness = 0.03 Kurtosis = 33.60

Graphical values (F&W):
  Mean = 1.40 phi = 379.06u
  Median (phi50) = 1.40 phi = 379.31u
  Sorting = 0.22 phi Skewness = 0.05 Kurtosis = 1.29

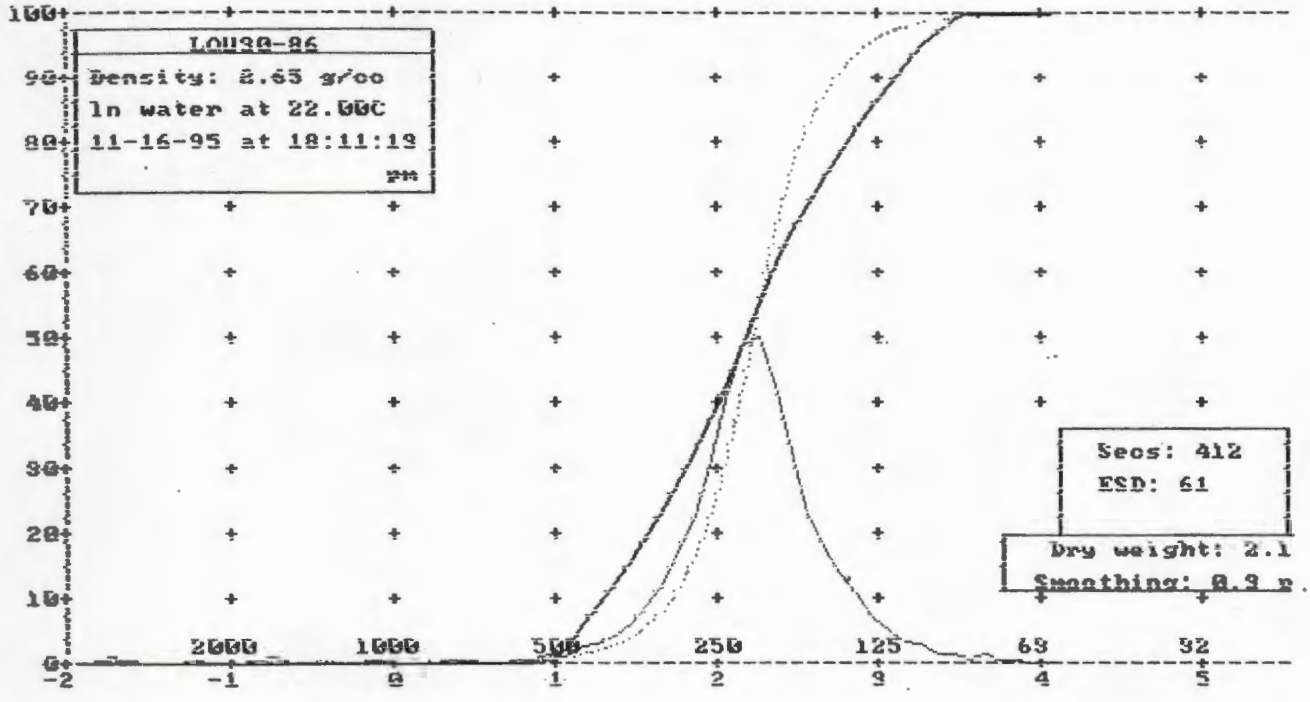

Moment statistics:
  Mean = 2.20 phi = 218.10u
  Std dev = 0.45 phi   Skewness = -1.35   Kurtosis = 15.77

Graphical values (F&W):
  Mean = 2.21 phi = 215.47u
  Median (phi50) = 2.21 phi = 216.00u
  Sorting = 0.40 phi   Skewness = 0.02   Kurtosis = 1.21

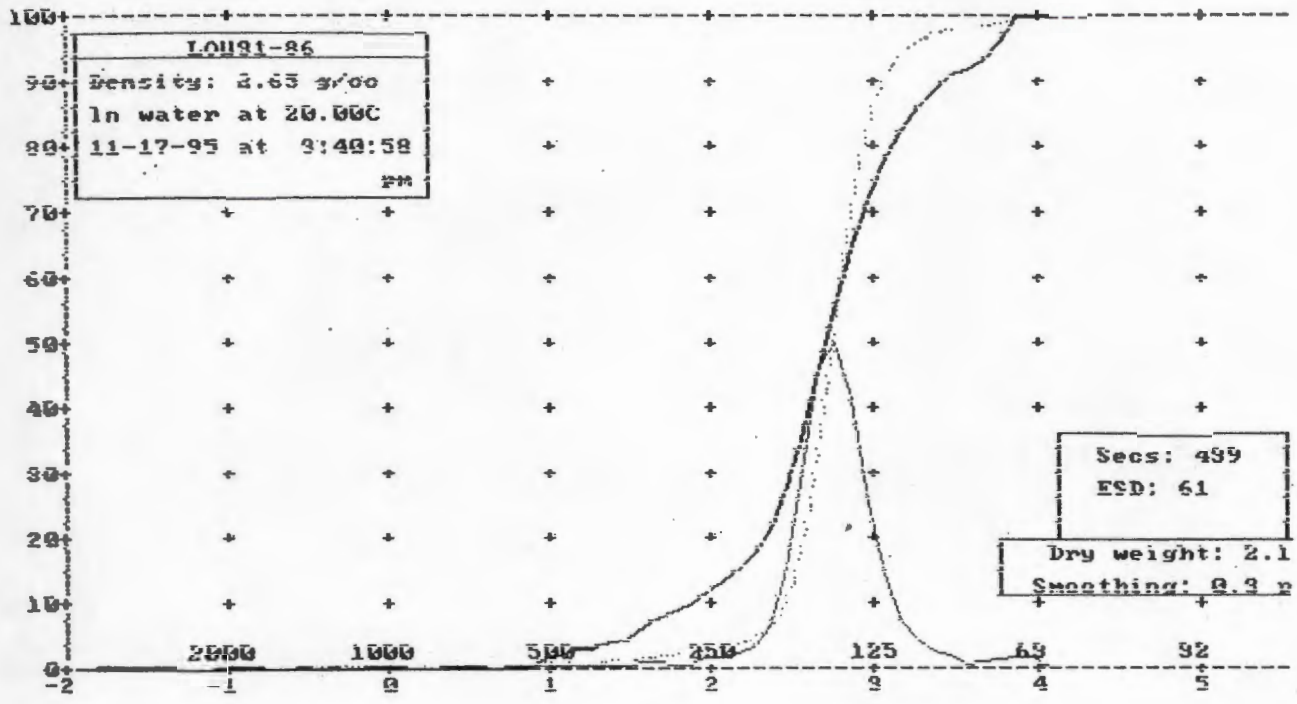

Moment statistics:
  Mean = 2.73 phi = 151.17u
  Std dev = 0.44 phi Skewness = -4.65 Kurtosis = 48.83

Graphical values (F&W):
  Mean = 2.75 phi = 149.02u
  Median (phi50) = 2.74 phi = 149.57u
  Sorting = 0.25 phi Skewness = 0.03 Kurtosis = 1.33

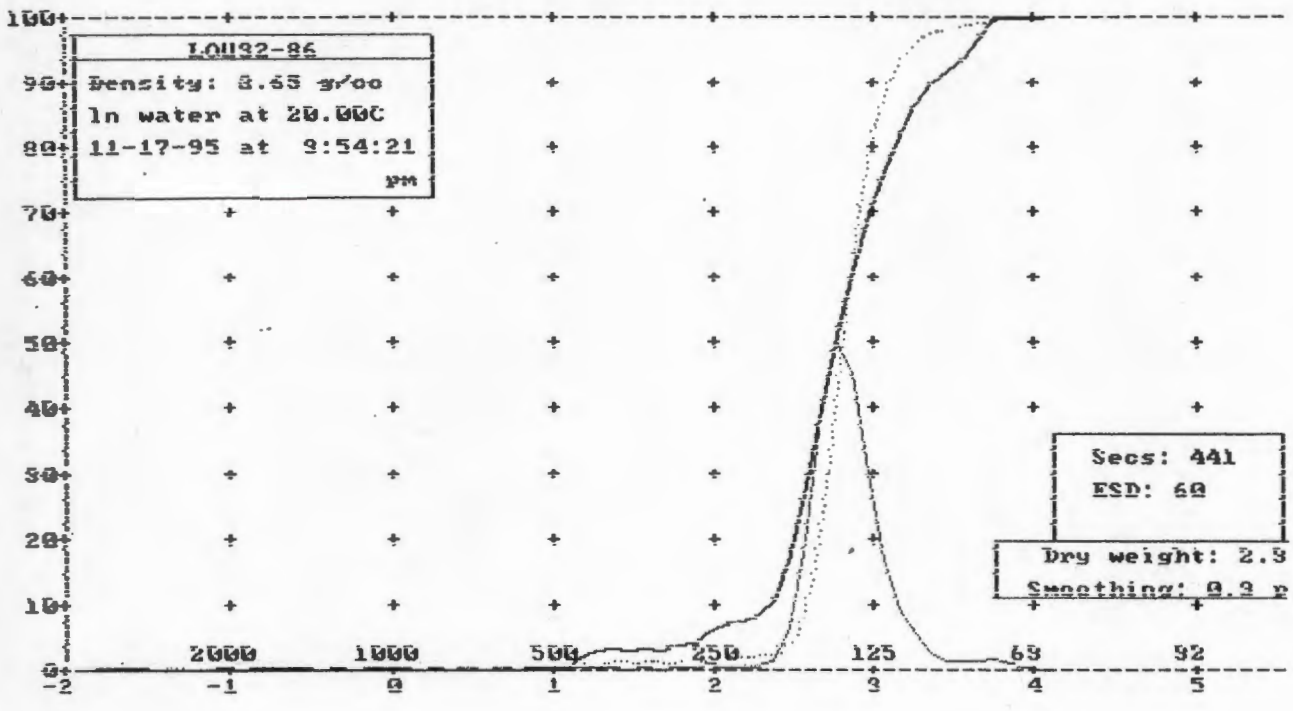

Moment statistics:
  Mean = 2.80 phi = 143.99u
  Std dev = 0.38 phi Skewness = -5.64 Kurtosis = 65.01

Graphical values (F&W):
  Mean = 2.81 phi = 142.89u
  Median (phi50) = 2.79 phi = 144.20u
  Sorting = 0.21 phi Skewness = 0.15 Kurtosis = 1.13

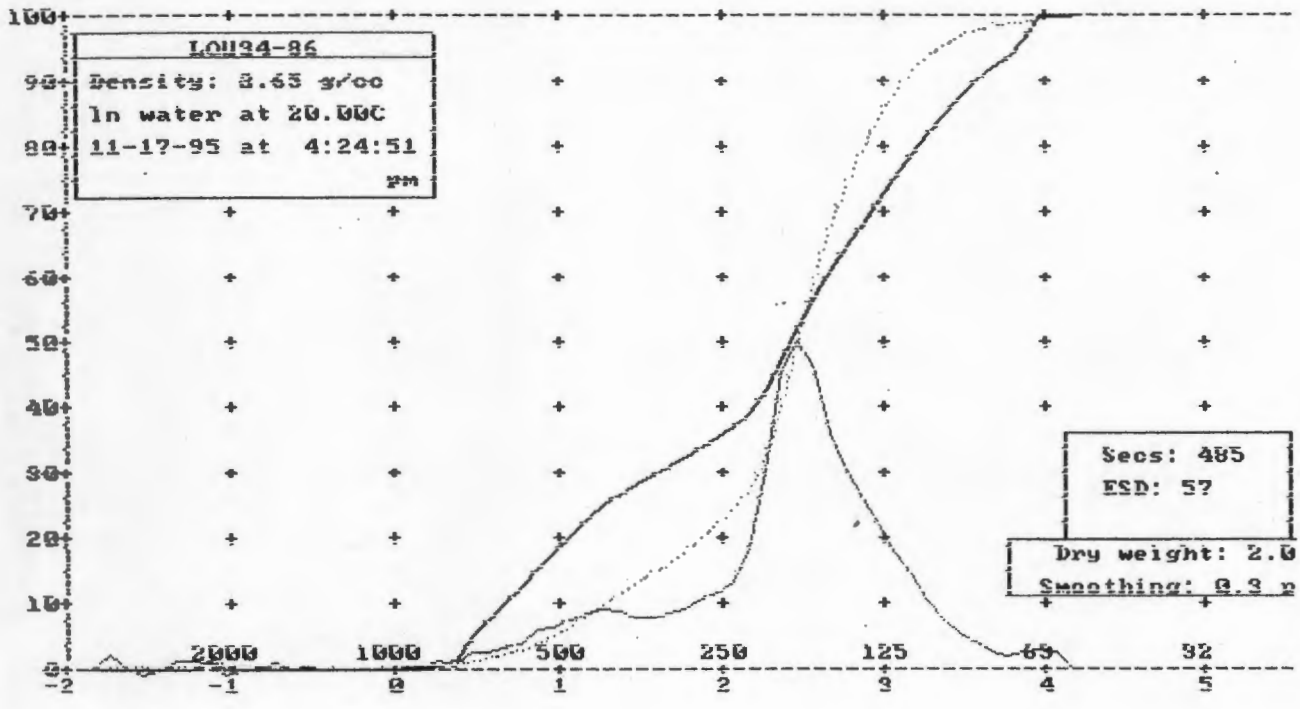

Moment statistics:
  Mean = 2.35 phi = 196.23u
  Std dev = 0.73 phi   Skewness = -1.19   Kurtosis = 6.79

Graphical values (F&W):
  Mean = 2.36 phi = 195.28u
  Median (phi50) = 2.46 phi = 181.86u
  Sorting = 0.68 phi   Skewness = -0.25   Kurtosis = 1.40

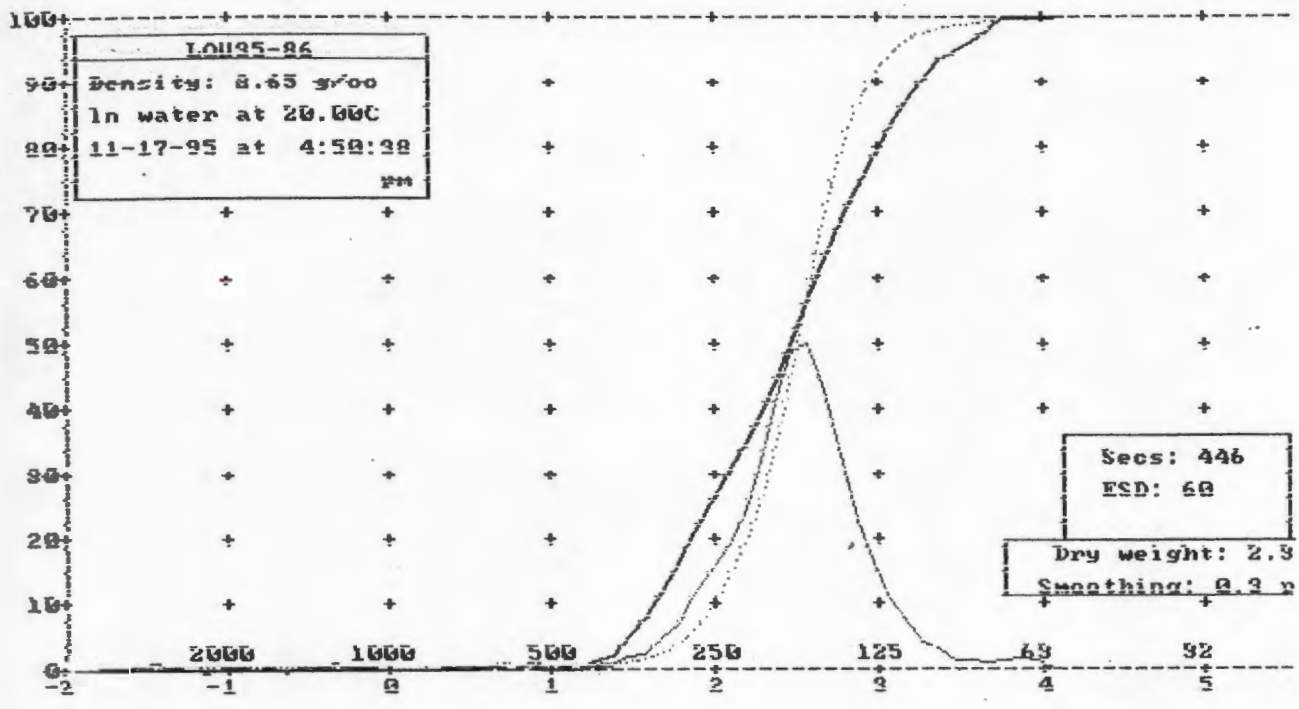

Moment statistics:
  Mean = 2.47 phi = 180.57u
  Std dev = 0.47 phi Skewness = -2.31 Kurtosis = 22.90

Graphical values (F&W):
  Mean = 2.48 phi = 179.67u
  Median (phi50) = 2.49 phi = 177.86u
  Sorting = 0.37 phi Skewness = -0.05 Kurtosis = 1.16

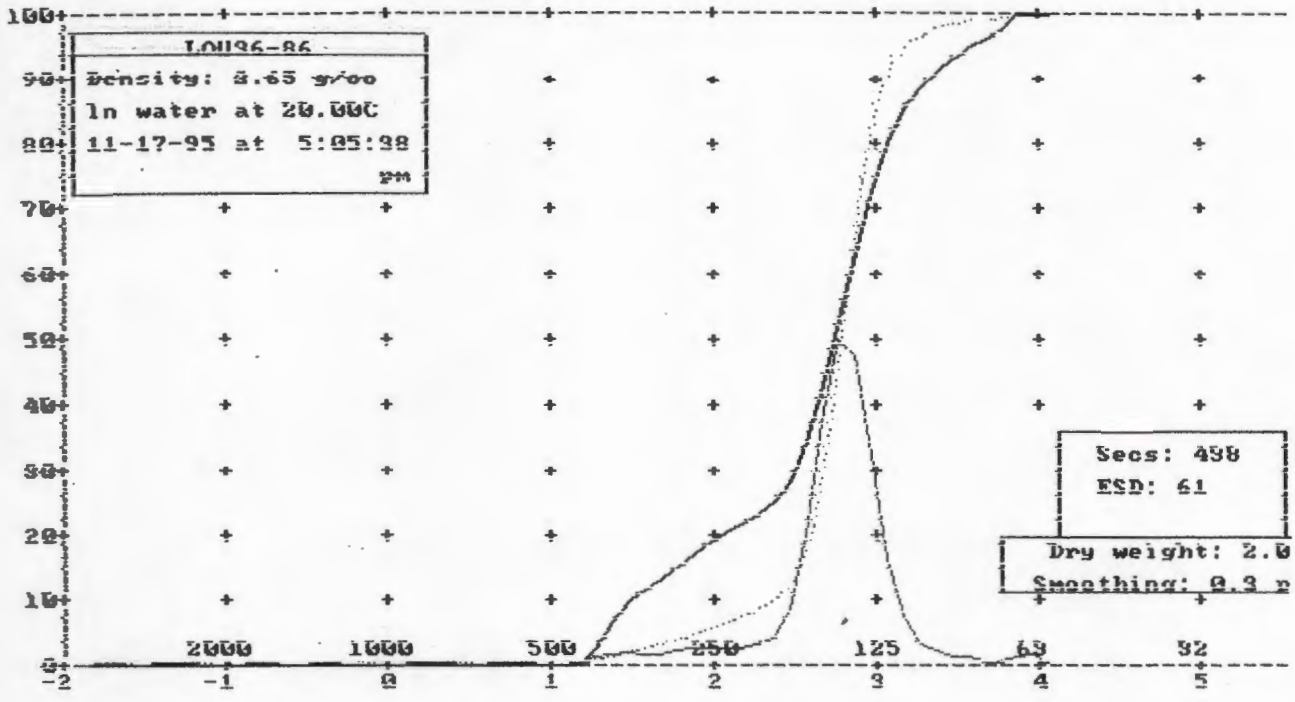

Moment statistics:
  Mean = 2.72 phi = 152.10u
  Std dev = 0.43 phi   Skewness = -3.54   Kurtosis = 32.75

Graphical values (F&W):
  Mean = 2.76 phi = 147.59u
  Median (phi50) = 2.77 phi = 146.43u
  Sorting = 0.30 phi   Skewness = -0.22   Kurtosis = 1.82

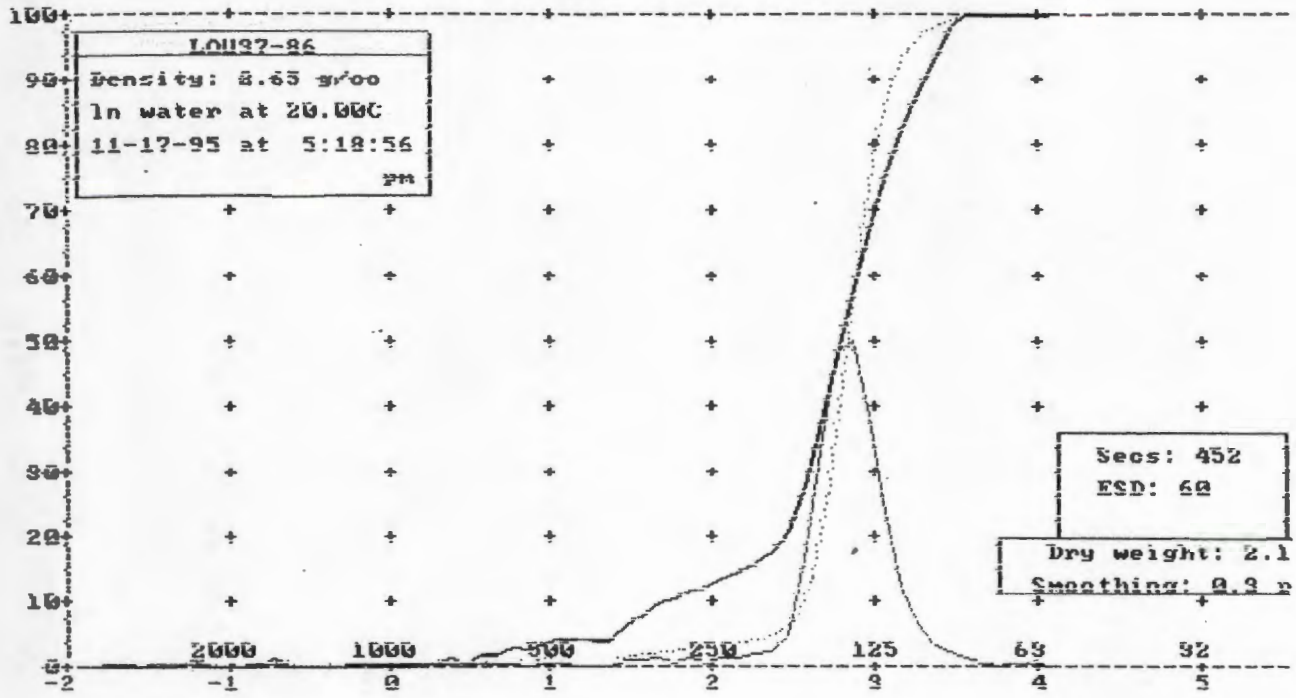

Moment statistics:
  Mean = 2.79 phi = 145.06u
  Std dev = 0.45 phi   Skewness = -5.54   Kurtosis = 50.40

Graphical values (F&W):
  Mean = 2.83 phi = 140.87u
  Median (phi50) = 2.82 phi = 141.31u
  Sorting = 0.23 phi   Skewness = -0.01   Kurtosis = 1.25

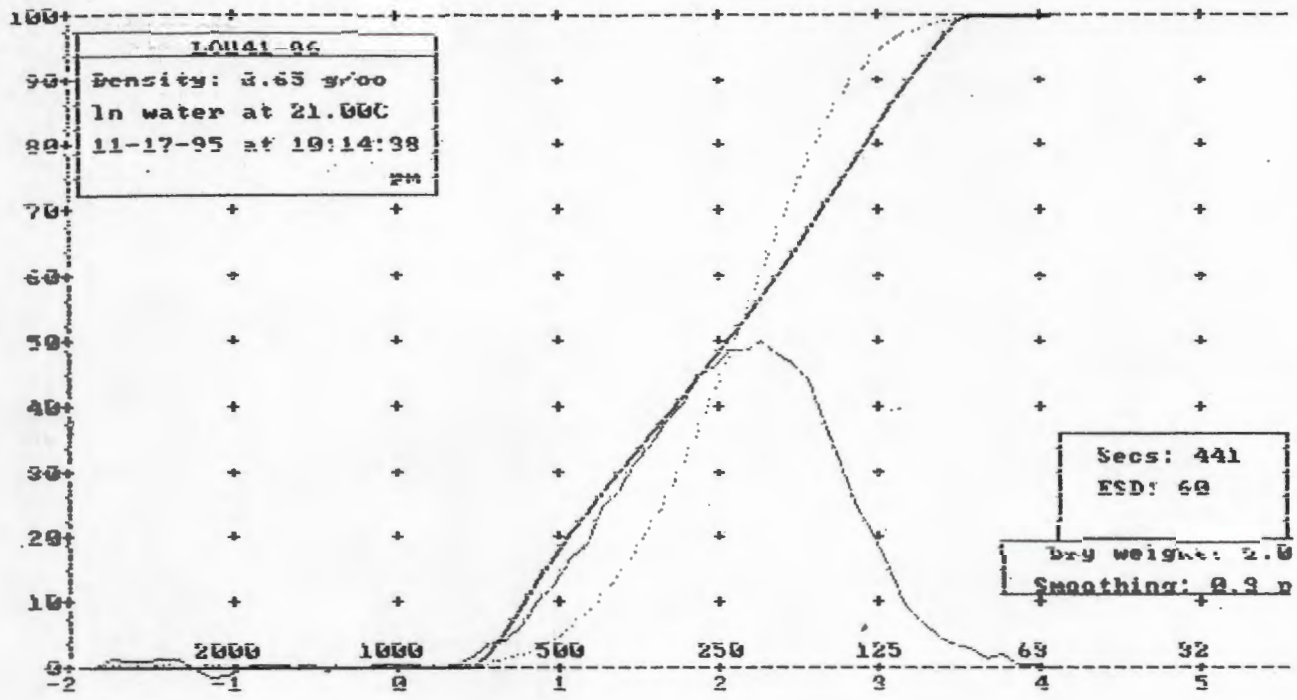

Moment statistics:
  Mean = 2.06 phi = 240.64u
  Std dev = 0.64 phi   Skewness = -0.58   Kurtosis = 5.53

Graphical values (F&W):
  Mean = 2.06 phi = 239.82u
  Median (phi50) = 2.09 phi = 235.17u
  Sorting = 0.62 phi   Skewness = -0.07   Kurtosis = 0.95

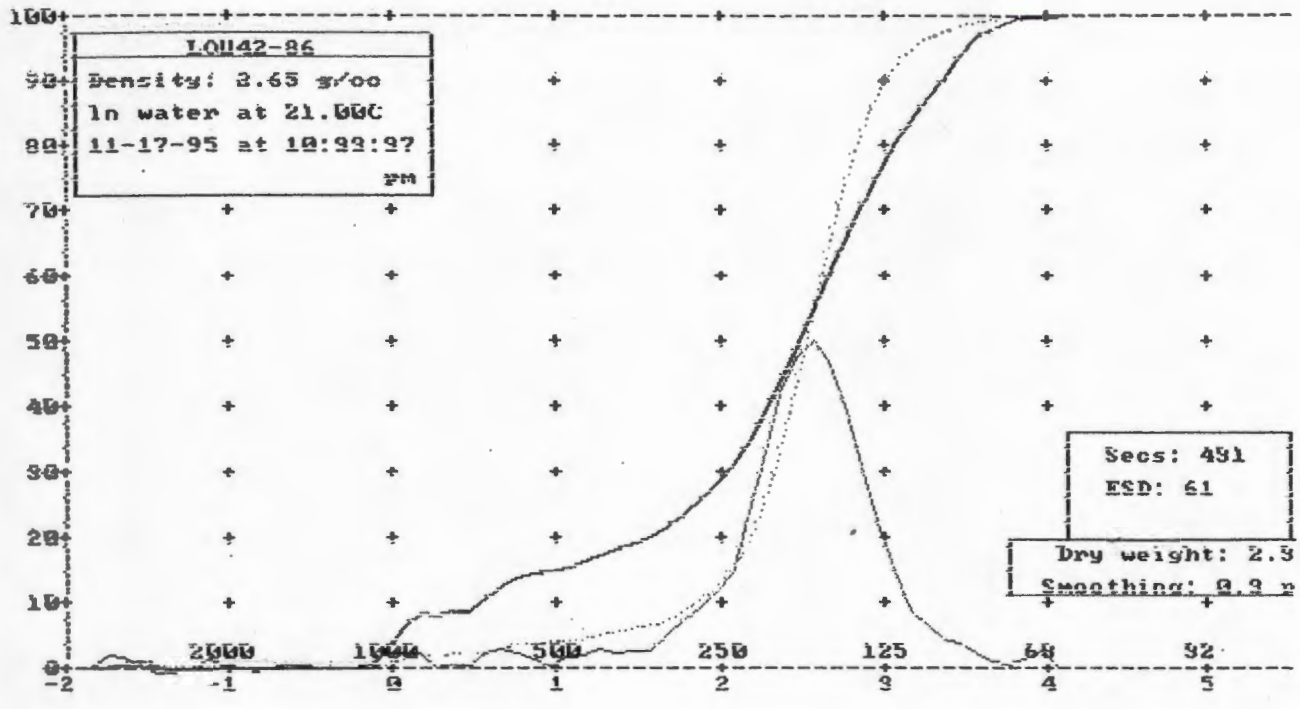

Moment statistics:
  Mean = 2.42 phi = 186.55u
  Std dev = 0.64 phi   Skewness = -2.32   Kurtosis = 13.43

Graphical values (F&W):
  Mean = 2.49 phi = 178.47u
  Median (phi50) = 2.51 phi = 175.84u
  Sorting = 0.49 phi   Skewness = -0.18   Kurtosis = 1.51

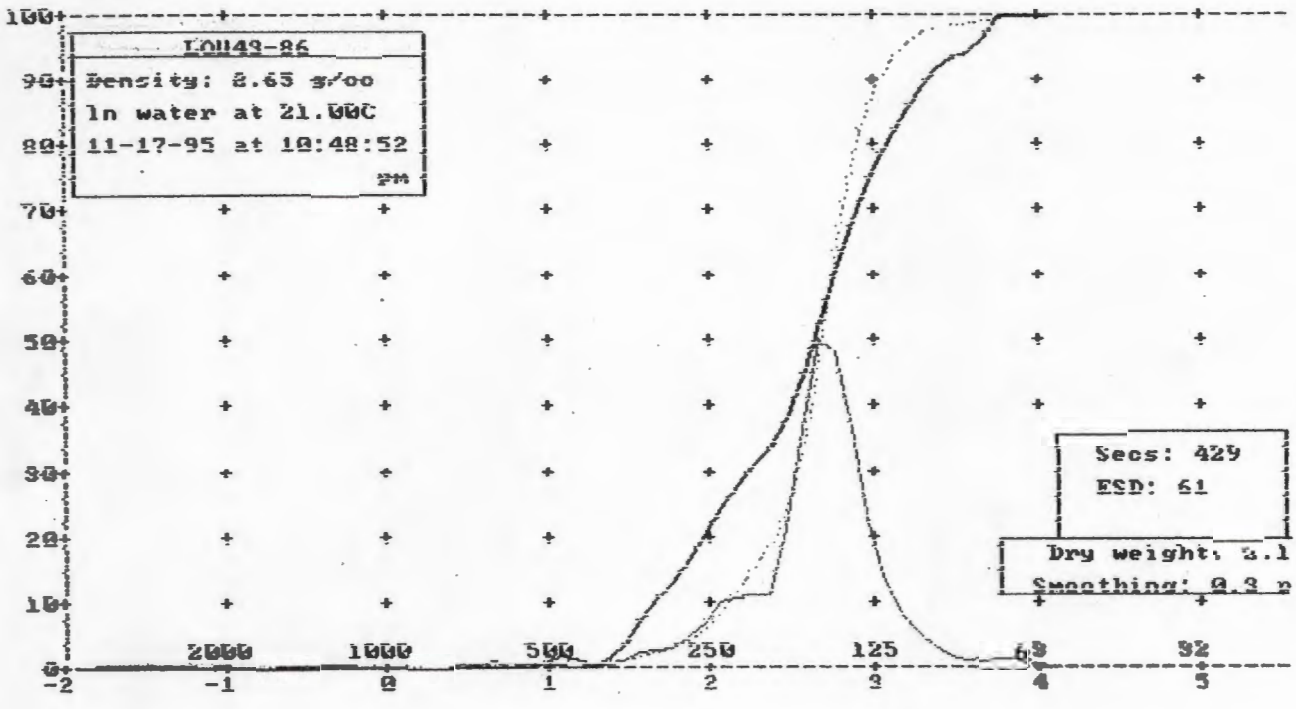

Moment statistics:
  Mean = 2.62 phi = 162.76u
  Std dev = 0.46 phi   Skewness = -2.95   Kurtosis = 28.04

Graphical values (F&W):
  Mean = 2.63 phi = 161.82u
  Median (phi50) = 2.67 phi = 156.97u
  Sorting = 0.36 phi   Skewness = -0.20   Kurtosis = 1.40

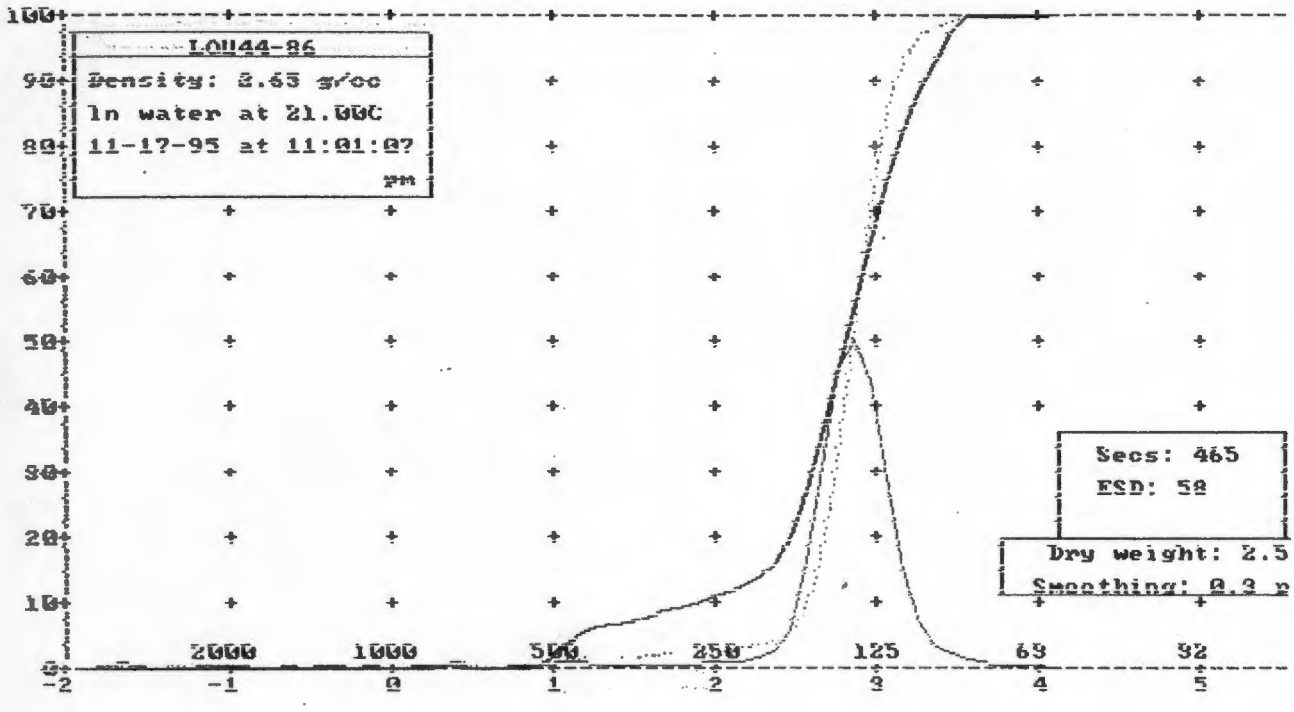

Moment statistics:
  Mean = 2.81 phi = 142.90u
  Std dev = 0.42 phi   Skewness = -5.67   Kurtosis = 55.92

Graphical values (F&W):
  Mean = 2.84 phi = 139.41u
  Median (phi50) = 2.84 phi = 139.39u
  Sorting = 0.23 phi   Skewness = -0.03   Kurtosis = 1.15 .

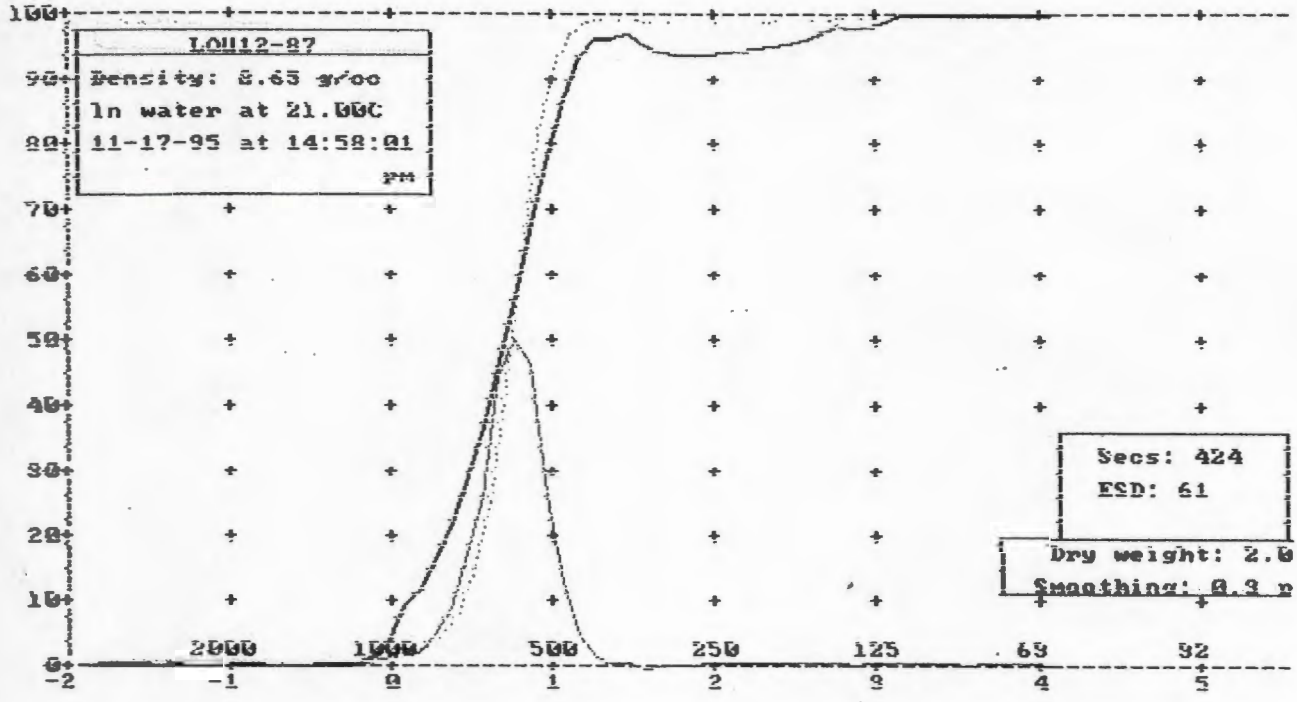

Moment statistics:
  Mean = 0.74 phi = 598.60u
  Std dev = 0.38 phi   Skewness = 3.32   Kurtosis = 33.95

Graphical values (F&W):
  Mean = 0.73 phi = 604.86u
  Median (phi50) = 0.74 phi = 600.27u
  Sorting = 0.22 phi   Skewness = -0.10   Kurtosis = 1.16

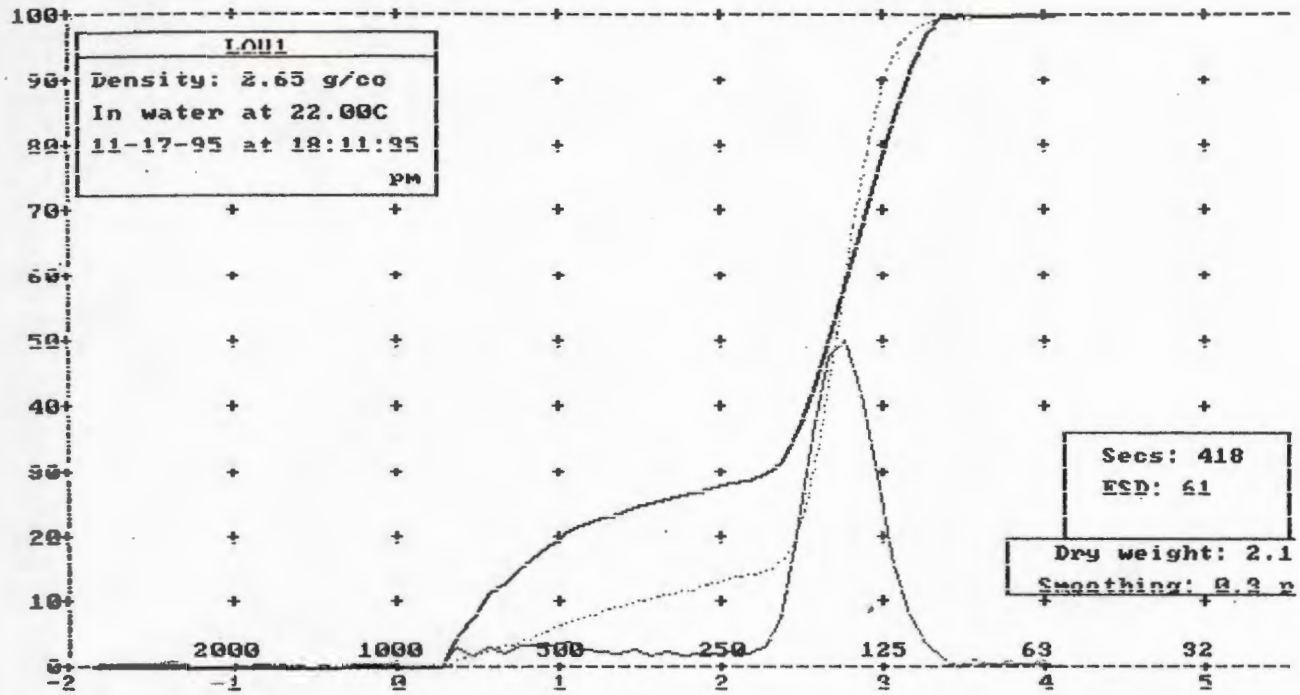

Moment statistics:
  Mean = 2.52 phi = 174.38u
  Std dev = 0.66 phi Skewness = -2.44 Kurtosis = 10.62

Graphical values (F&W):
  Mean = 2.66 phi = 158.31u
  Median (phi50) = 2.69 phi = 154.45u
  Sorting = 0.48 phi Skewness = -0.41 Kurtosis = 2.60

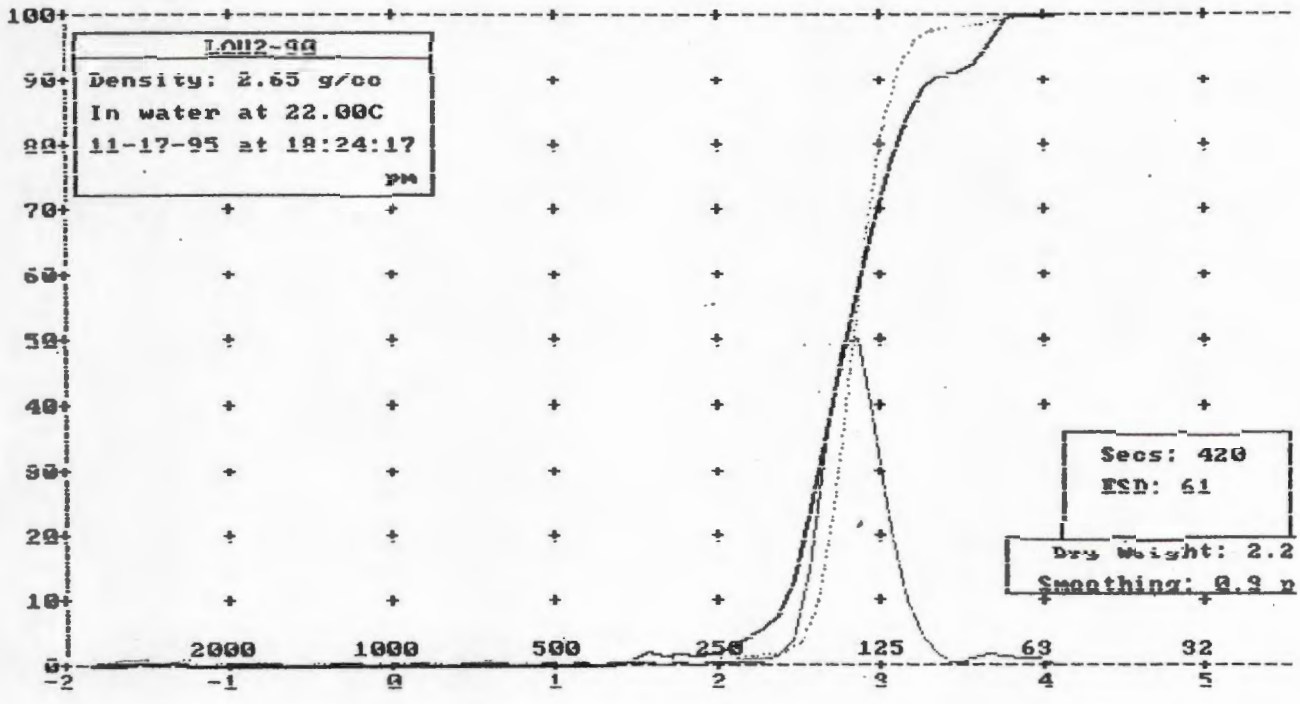

Moment statistics:
  Mean = 2.82 phi = 141.65u
  Std dev = 0.38 phi Skewness = -7.27 Kurtosis = 92.28

Graphical values (F&W):
  Mean = 2.83 phi = 140.84u
  Median (phi50) = 2.82 phi = 141.39u
  Sorting = 0.19 phi Skewness = 0.07 Kurtosis = 1.09

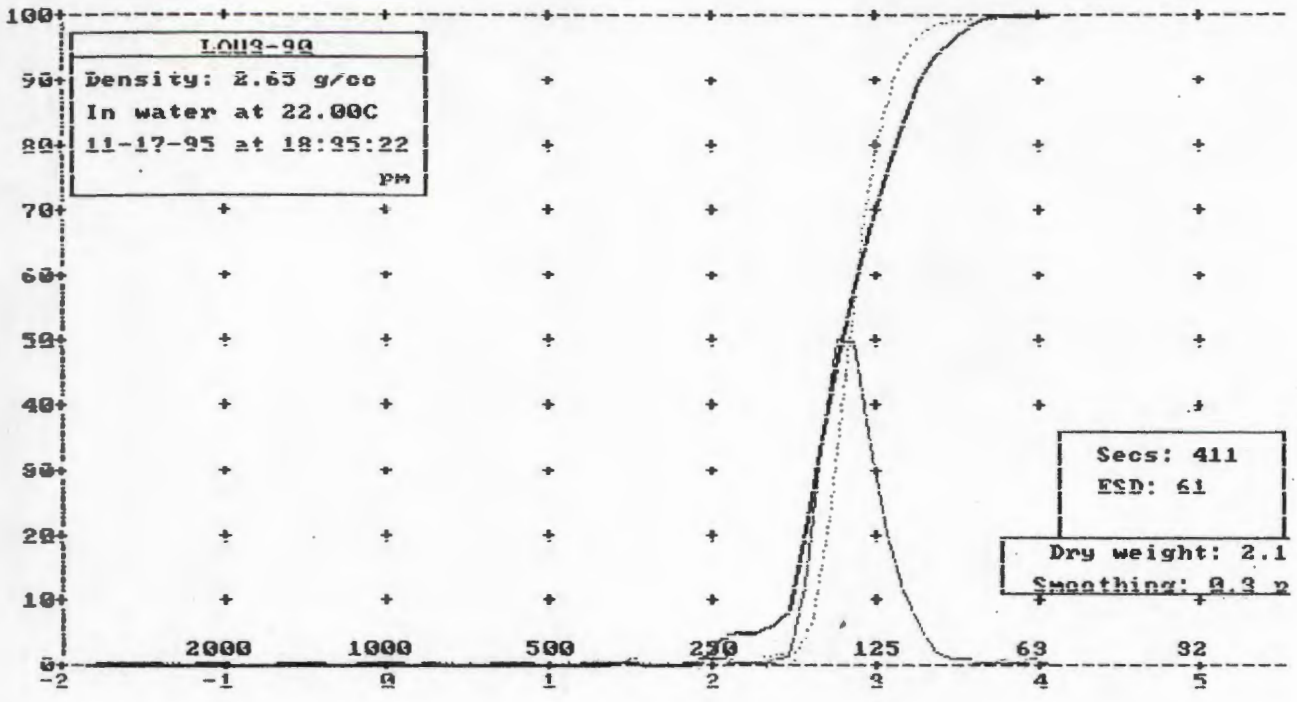

Moment statistics:
  Mean = 2.83 phi = 140.20u
  Std dev = 0.31 phi Skewness = -6.63 Kurtosis =100.07

Graphical values (F&W):
  Mean = 2.84 phi = 139.70u
  Median (phi50) = 2.83 phi = 140.96u
  Sorting = 0.19 phi Skewness = 0.13 Kurtosis = 1.06

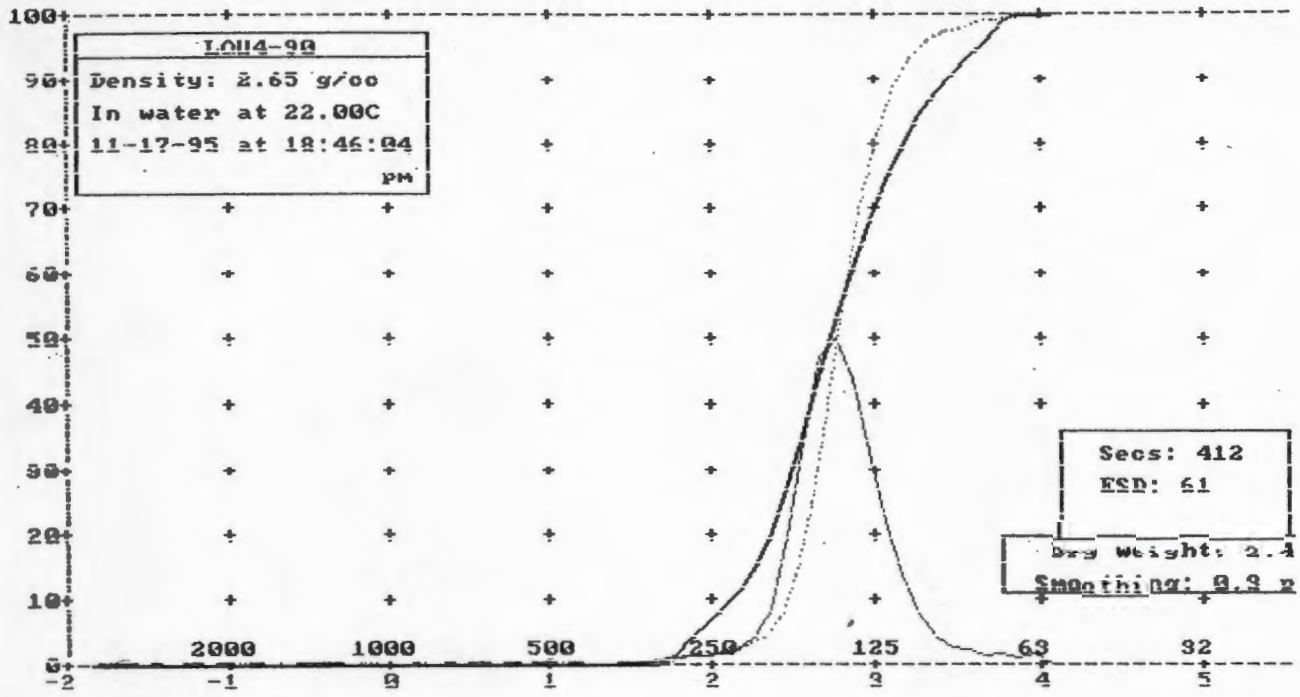

Moment statistics:
  Mean = 2.77 phi = 146.81u
  Std dev = 0.38 phi Skewness = -4.19 Kurtosis = 54.47

Graphical values (F&W):
  Mean = 2.77 phi = 146.22u
  Median (phi50) = 2.76 phi = 147.49u
  Sorting = 0.27 phi Skewness = 0.09 Kurtosis = 1.15

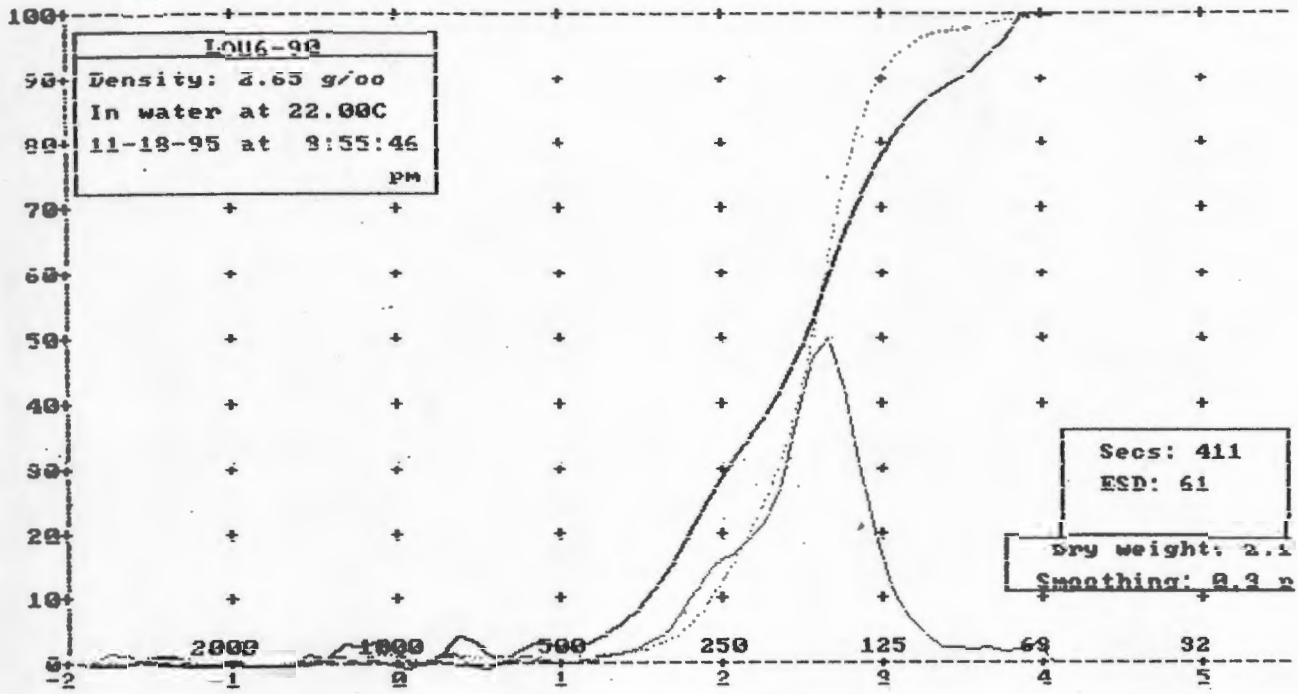

Moment statistics:
  Mean = 2.49 phi = 177.84u
  Std dev = 0.55 phi Skewness = -2.69 Kurtosis = 22.57

Graphical values (F&W):
  Mean = 2.50 phi = 176.97u
  Median (phi50) = 2.55 phi = 170.24u
  Sorting = 0.41 phi Skewness = -0.17 Kurtosis = 1.14

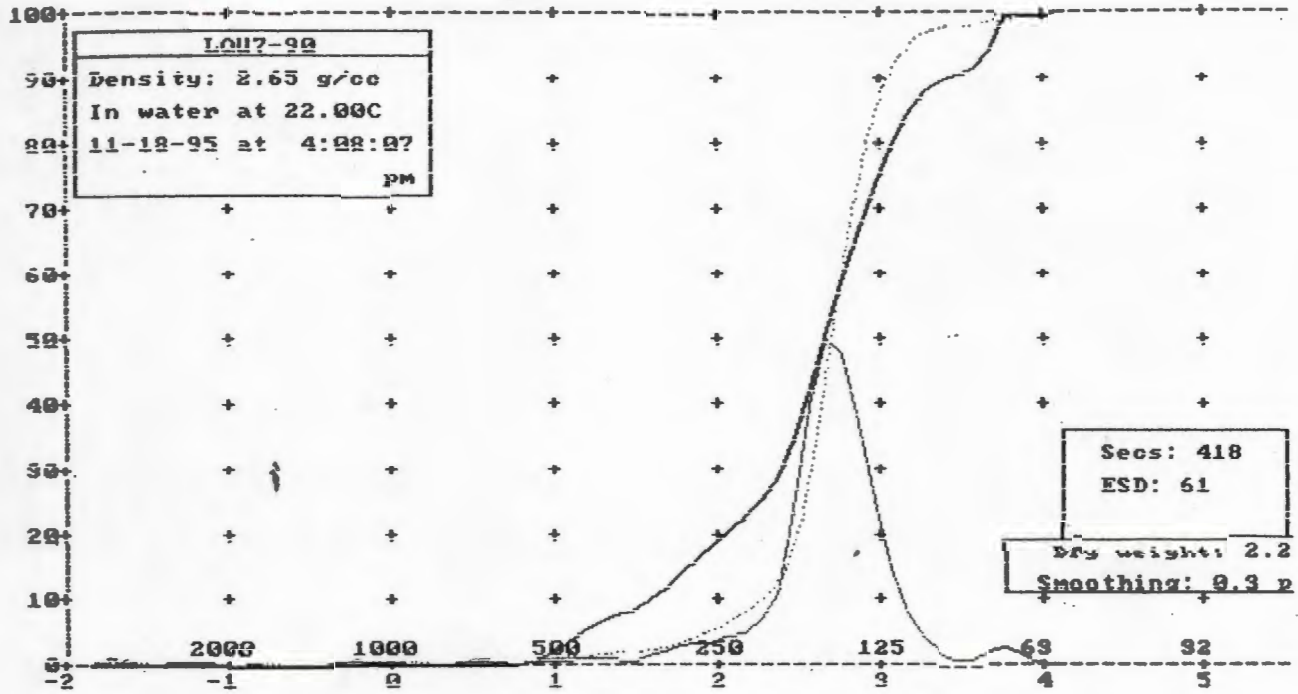

Moment statistics:
  Mean = 2.65 phi = 159.66u
  Std dev = 0.45 phi Skewness = -3.29 Kurtosis = 31.13

Graphical values (F&W):
  Mean = 2.69 phi = 155.33u
  Median (phi50) = 2.69 phi = 155.10u
  Sorting = 0.32 phi Skewness = -0.11 Kurtosis = 1.49

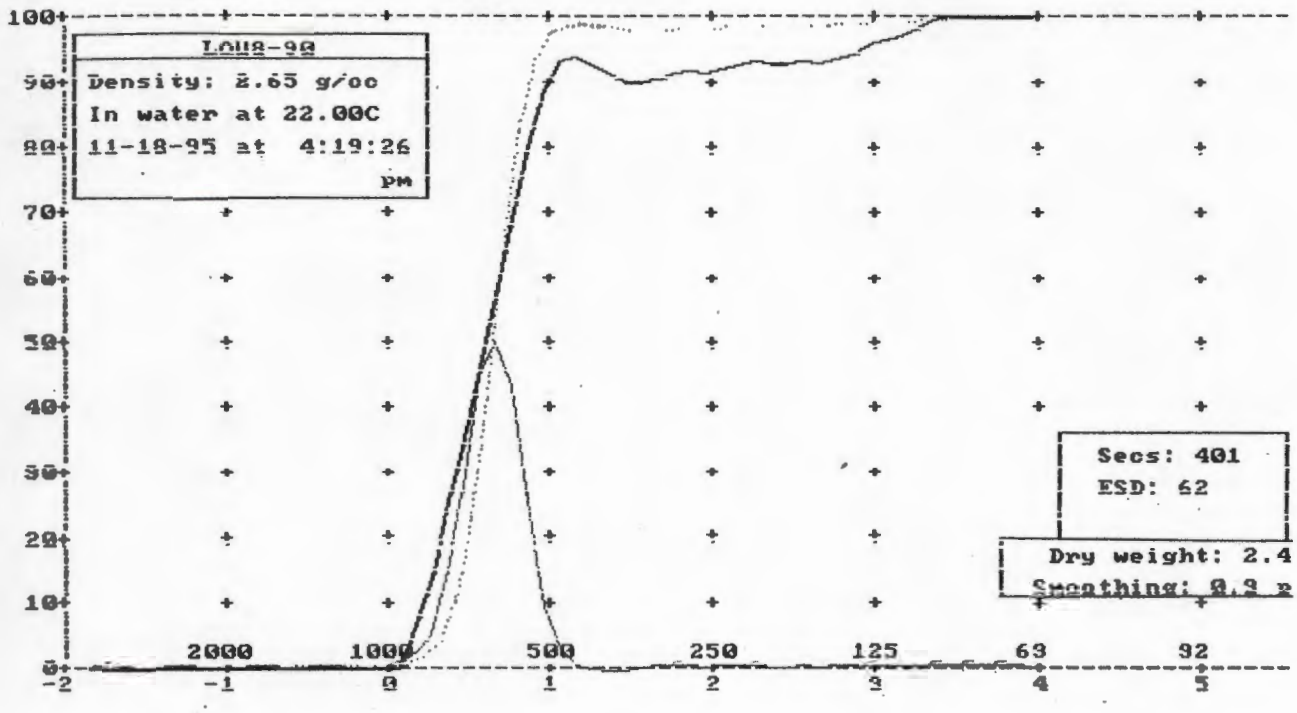

Moment statistics:
  Mean = 0.67 phi = 629.39u
  Std dev = 0.42 phi Skewness = 3.70 Kurtosis = 33.07

Graphical values (F&W):
  Mean = 0.63 phi = 644.59u
  Median (phi50) = 0.64 phi = 642.76u
  Sorting = 0.19 phi Skewness = -0.03 Kurtosis = 1.03

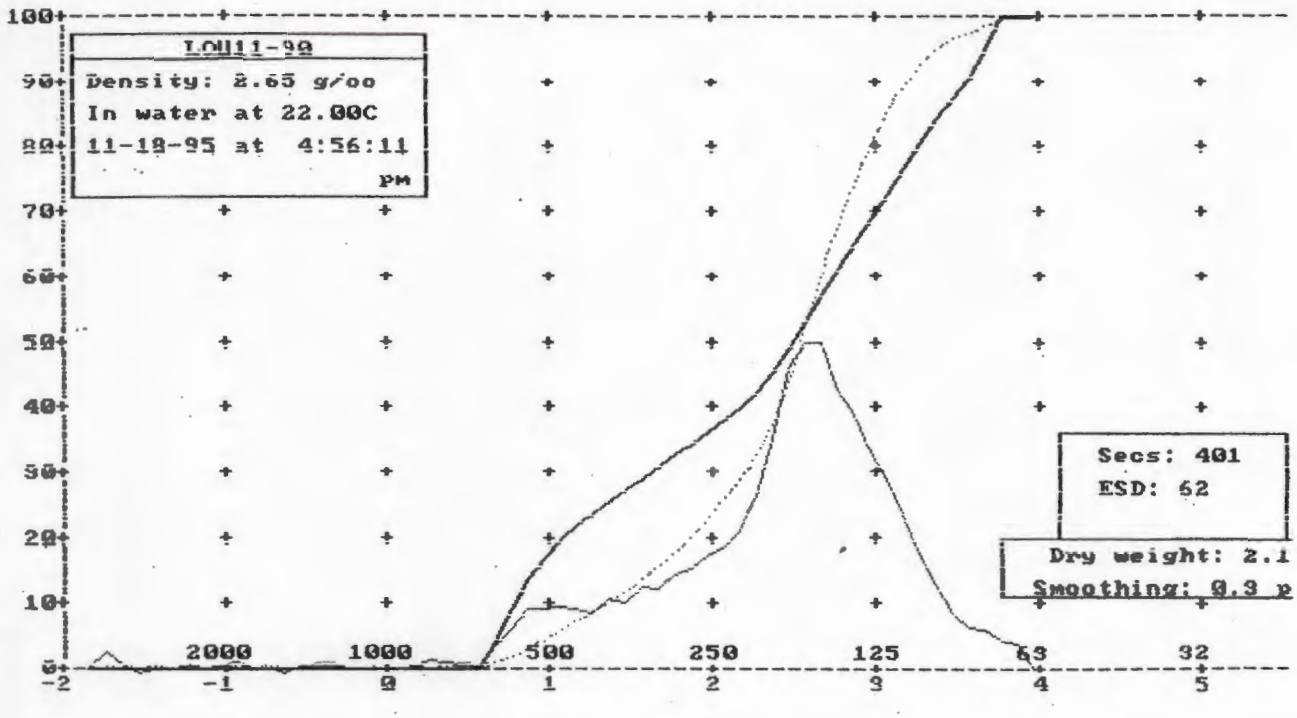

Moment statistics:
  Mean = 2.40 phi = 189.01u
  Std dev = 0.71 phi Skewness = -1.02 Kurtosis = 5.63

Graphical values (F&W):
  Mean = 2.42 phi = 187.34u
  Median (phi50) = 2.53 phi = 173.18u
  Sorting = 0.70 phi Skewness = -0.27 Kurtosis = 1.17

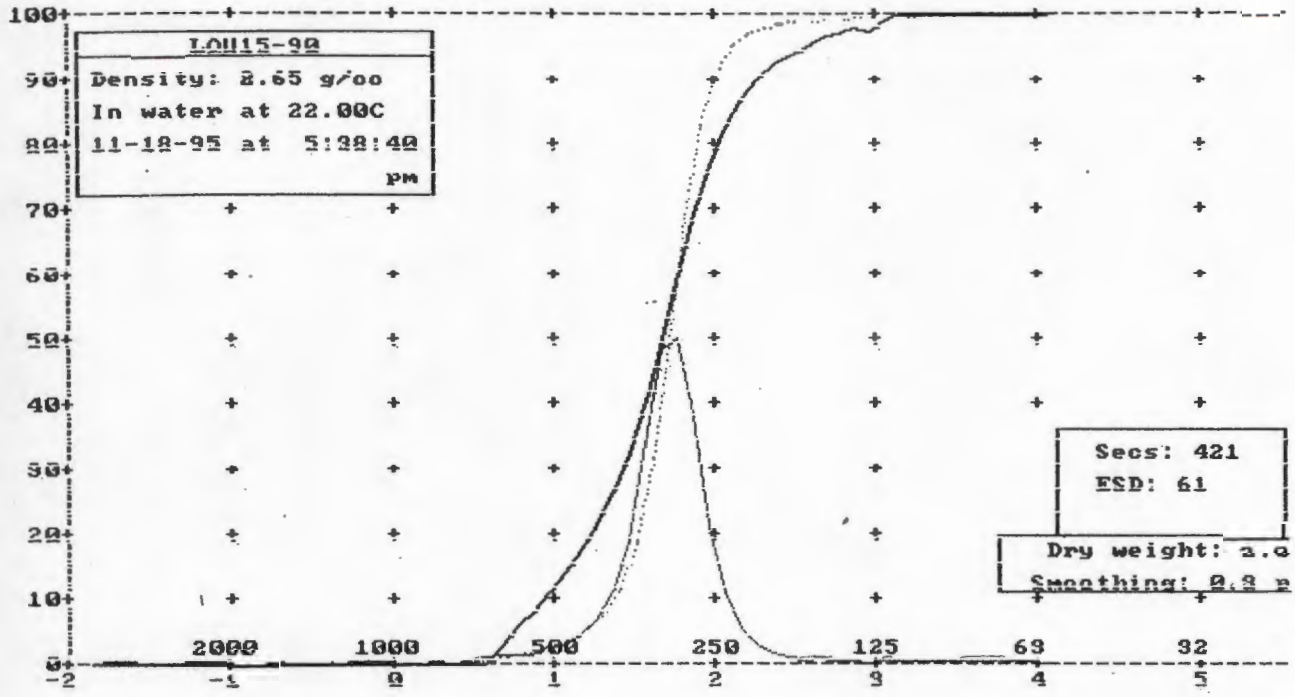

Moment statistics:
  Mean = 1.69 phi = 309.12u
  Std dev = 0.36 phi   Skewness = -0.71   Kurtosis = 23.72

Graphical values (F&W):
  Mean = 1.69 phi = 308.88u
  Median (phi50) = 1.70 phi = 307.06u
  Sorting = 0.25 phi   Skewness = -0.08   Kurtosis = 1.27

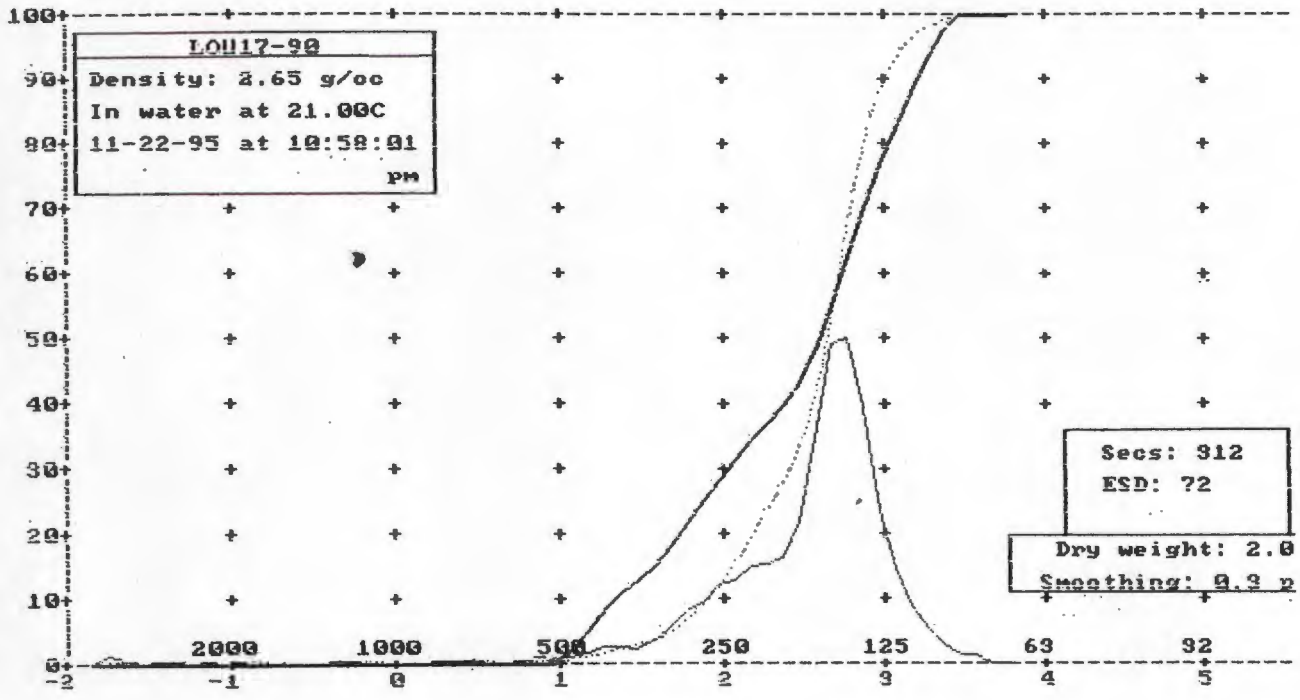

Moment statistics:
  Mean = 2.51 phi = 175.66u
  Std dev = 0.50 phi Skewness = -2.50 Kurtosis = 19.72

Graphical values (F&W):
  Mean = 2.53 phi = 172.83u
  Median (phi50) = 2.63 phi = 161.37u
  Sorting = 0.43 phi Skewness = -0.34 Kurtosis = 1.12

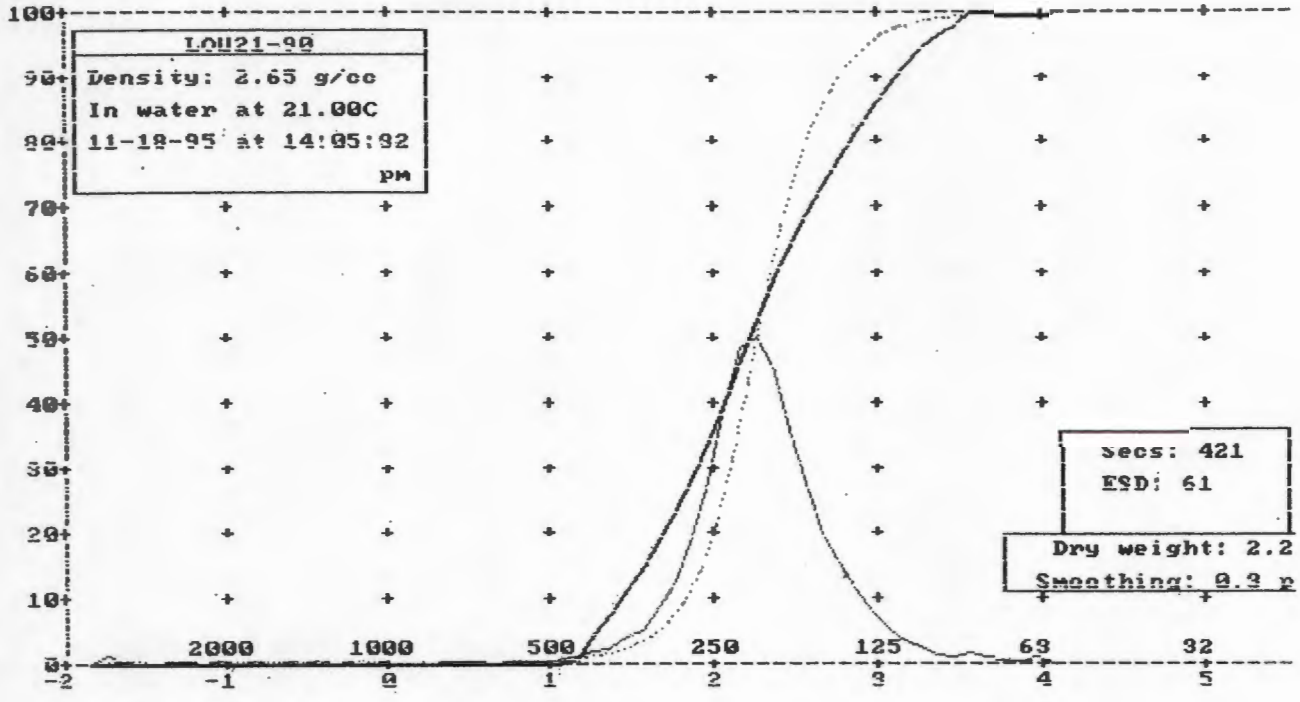

Moment statistics:
  Mean = 2.27 phi = 207.60u
  Std dev = 0.45 phi Skewness = -1.79 Kurtosis = 21.86

Graphical values (F&W):
  Mean = 2.27 phi = 207.05u
  Median (phi50) = 2.26 phi = 209.17u
  Sorting = 0.37 phi Skewness = 0.07 Kurtosis = 1.18

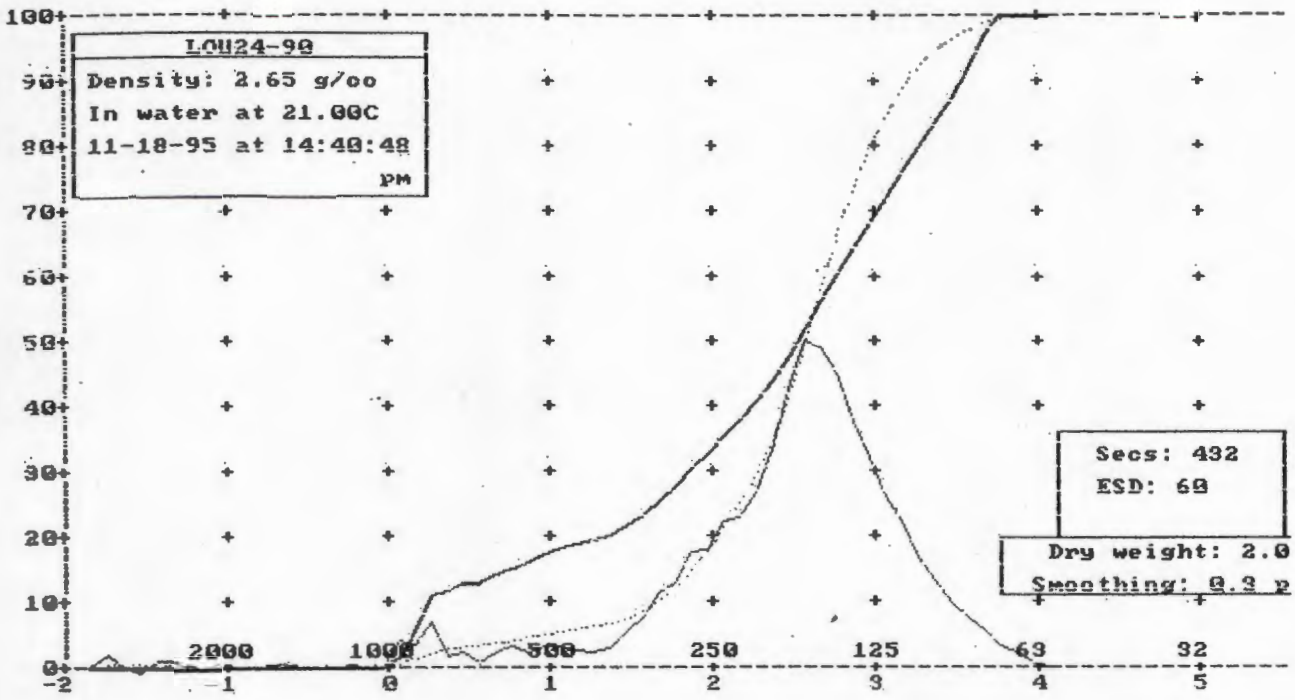

Moment statistics:
  Mean = 2.45 phi = 182.64u
  Std dev = 0.71 phi Skewness = -1.50 Kurtosis = 7.46

Graphical values (F&W):
  Mean = 2.50 phi = 176.19u
  Median (phi50) = 2.56 phi = 169.32u
  Sorting = 0.65 phi Skewness = -0.23 Kurtosis = 1.34

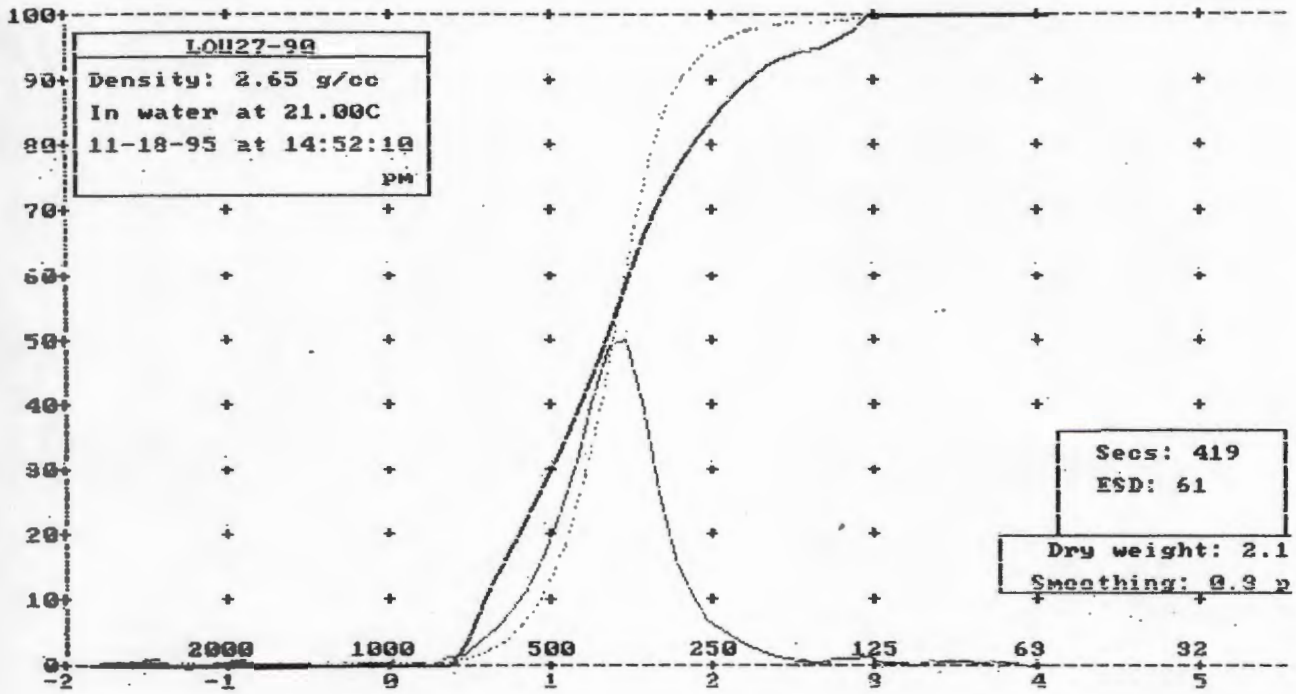

Moment statistics:
  Mean = 1.37 phi = 387.15u
  Std dev = 0.42 phi Skewness = -0.39 Kurtosis = 13.57

Graphical values (F&W):
  Mean = 1.36 phi = 388.94u
  Median (phi50) = 1.37 phi = 385.82u
  Sorting = 0.35 phi Skewness = -0.02 Kurtosis = 1.23

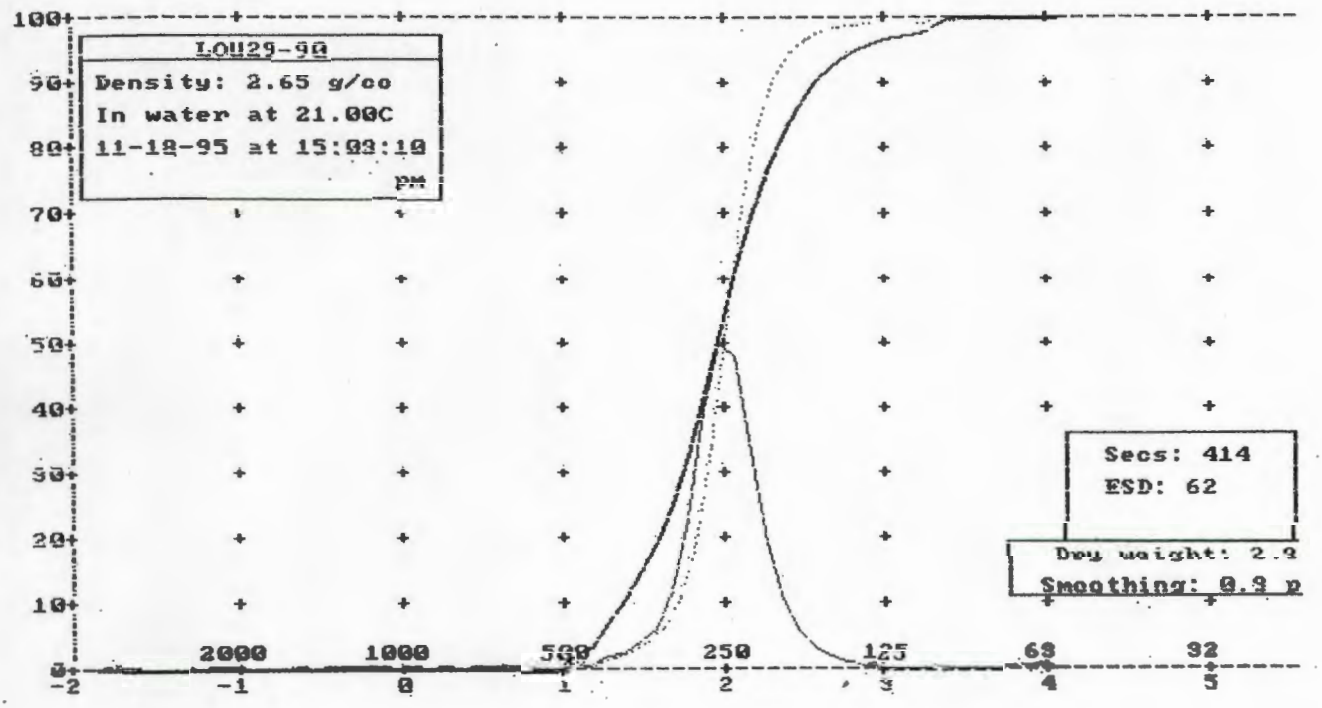

Moment statistics:
Mean = 1.99 phi = 251.80u
Std dev = 0.35 phi Skewness = -1.55 Kurtosis = 33.37

Graphical values (F&W):
Mean = 1.99 phi = 252.38u
Median (phi50) = 1.99 phi = 252.59u
Sorting = 0.24 phi Skewness = 0.01 Kurtosis = 1.22

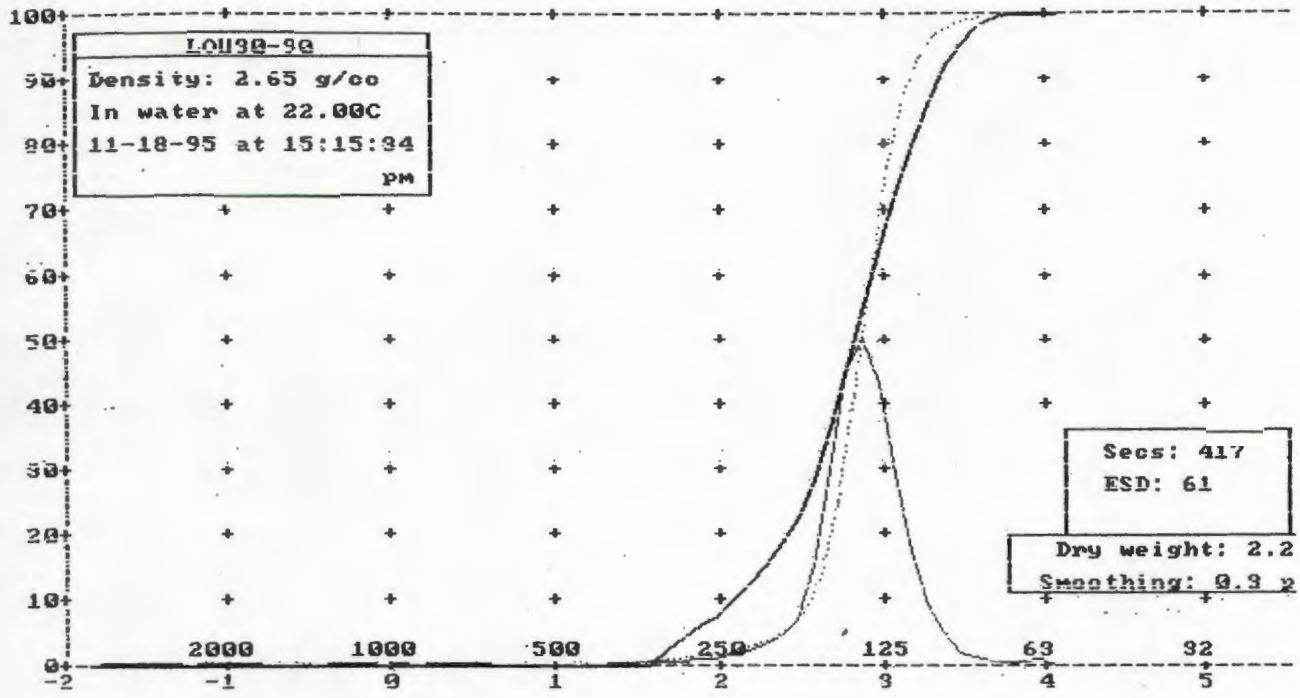

Moment statistics:
  Mean = 2.82 phi = 141.19u
  Std dev = 0.39 phi Skewness = -5.38 Kurtosis = 60.33

Graphical values (F&W):
  Mean = 2.85 phi = 138.94u
  Median (phi50) = 2.85 phi = 139.03u
  Sorting = 0.25 phi Skewness = -0.04 Kurtosis = 1.26

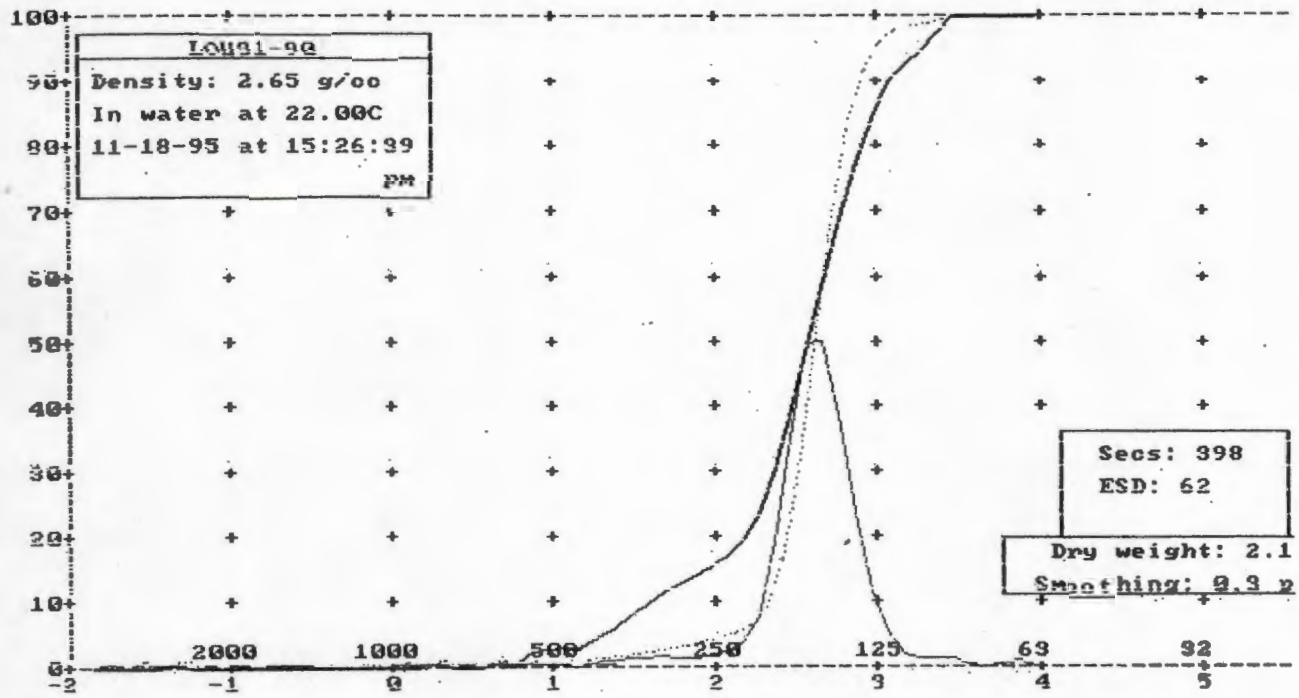

Moment statistics:
Mean = 2.57 phi = 168.15u
Std dev = 0.42 phi Skewness = -4.96 Kurtosis = 47.98

Graphical values (F&W):
Mean = 2.61 phi = 164.06u
Median (phi50) = 2.61 phi = 164.08u
Sorting = 0.24 phi Skewness = -0.07 Kurtosis = 1.26

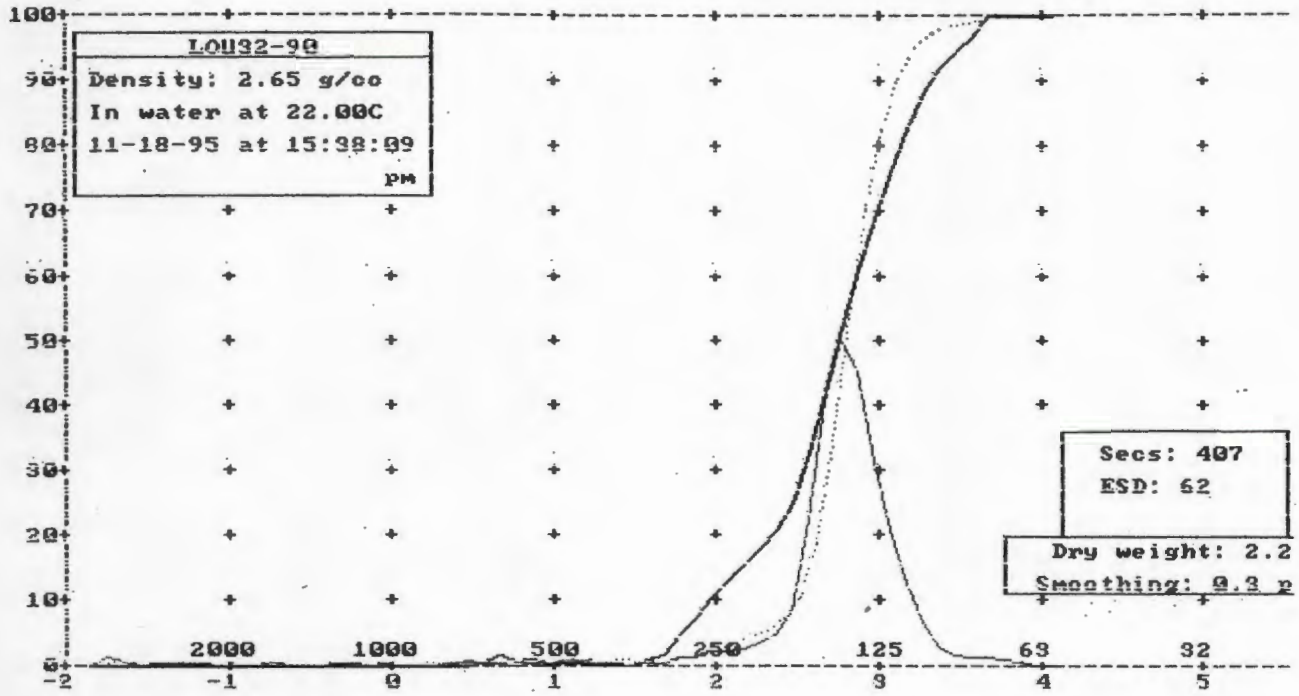

Moment statistics:
Mean = 2.75 phi = 148.23u
Std dev = 0.42 phi Skewness = -5.79 Kurtosis = 61.47

Graphical values (F&W):
Mean = 2.79 phi = 144.44u
Median (phi50) = 2.78 phi = 145.26u
Sorting = 0.26 phi Skewness = -0.01 Kurtosis = 1.28

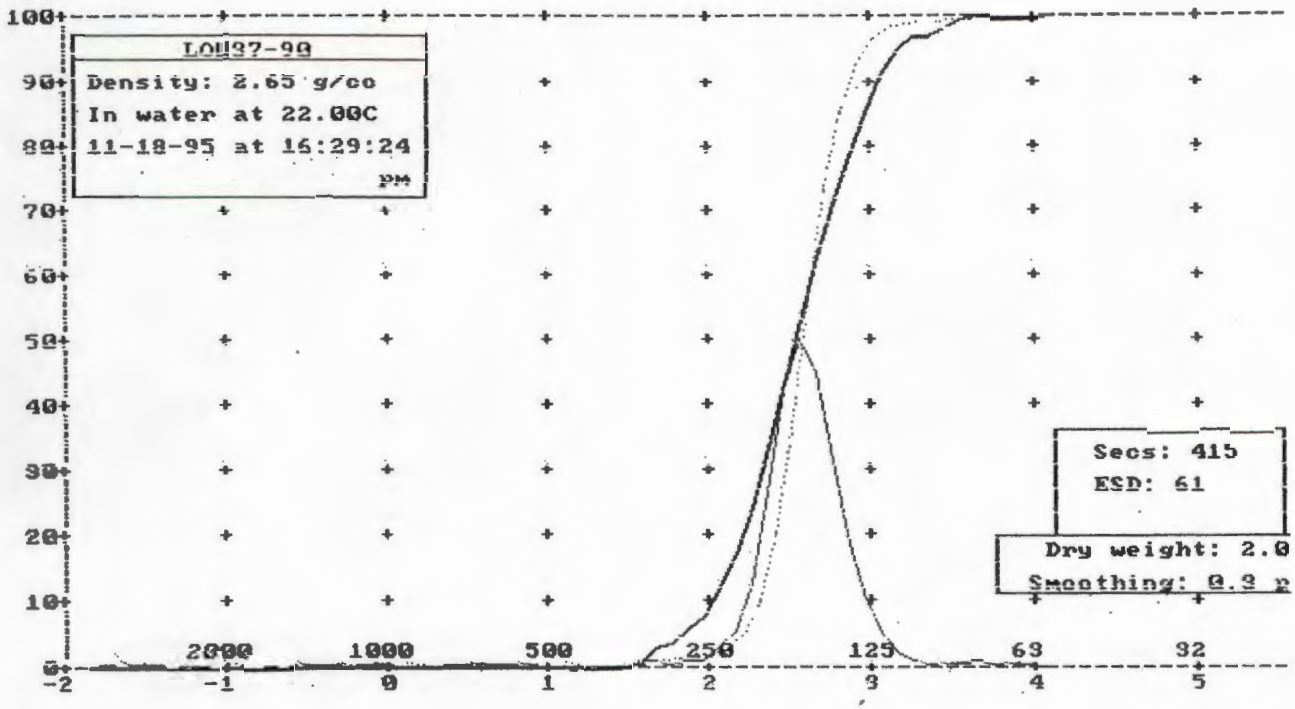

Moment statistics:
  Mean = 2.56 phi = 169.14u
  Std dev = 0.34 phi Skewness = -5.24 Kurtosis = 70.21

Graphical values (F&W):
  Mean = 2.58 phi = 167.79u
  Median (phi50) = 2.57 phi = 168.22u
  Sorting = 0.22 phi Skewness = 0.04 Kurtosis = 1.11

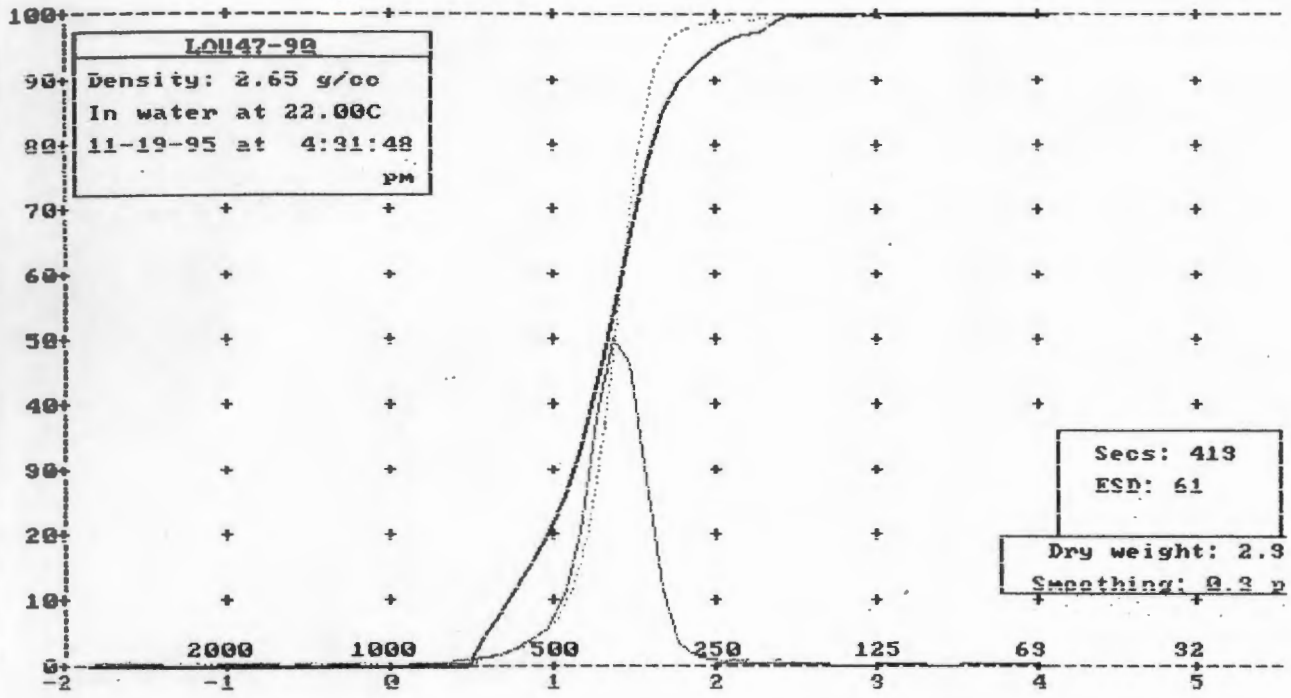

Moment statistics:
  Mean = 1.35 phi = 392.61u
  Std dev = 0.34 phi Skewness = -0.81 Kurtosis = 37.80

Graphical values (F&W):
  Mean = 1.35 phi = 391.76u
  Median (phi50) = 1.36 phi = 389.33u
  Sorting = 0.21 phi Skewness = -0.11 Kurtosis = 1.22

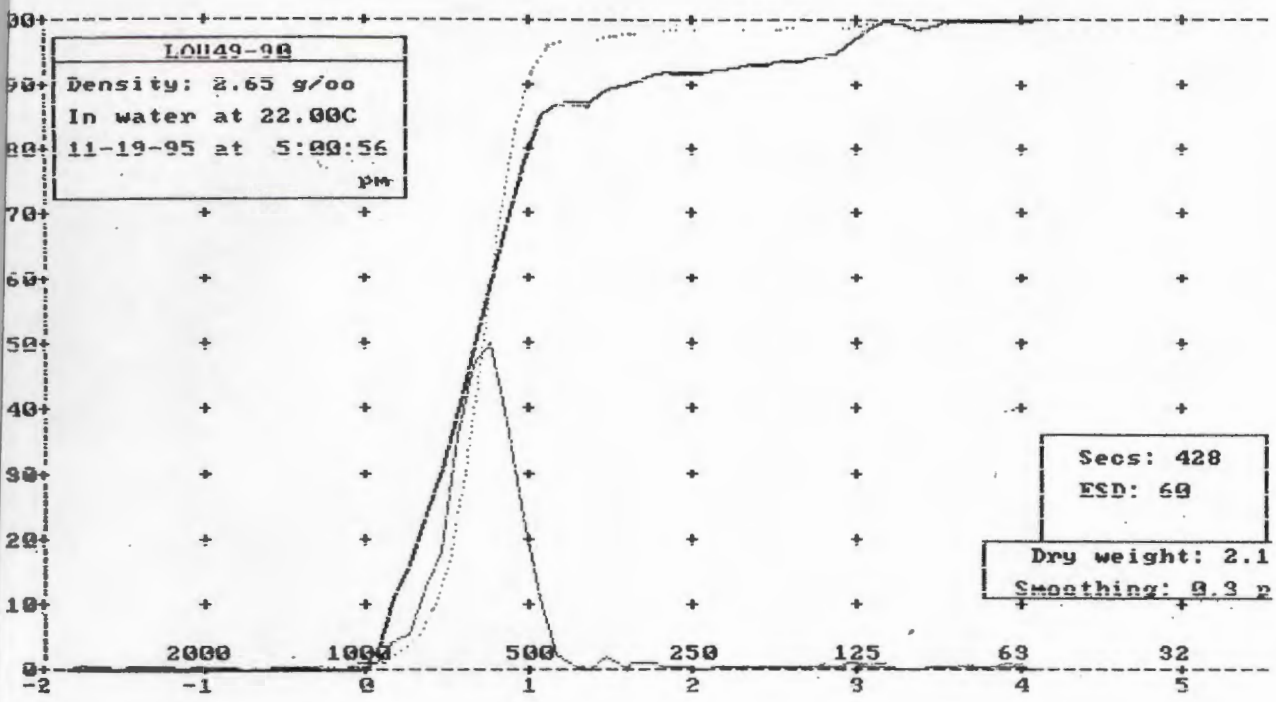

oment statistics:
Mean = 0.74 phi = 599.30u
Std dev = 0.43 phi Skewness = 3.46 Kurtosis = 27.90

raphical values (F&W):
Mean = 0.71 phi = 612.75u
Median (phi50) = 0.71 phi = 611.90u
Sorting = 0.22 phi Skewness = -0.02 Kurtosis = 1.10

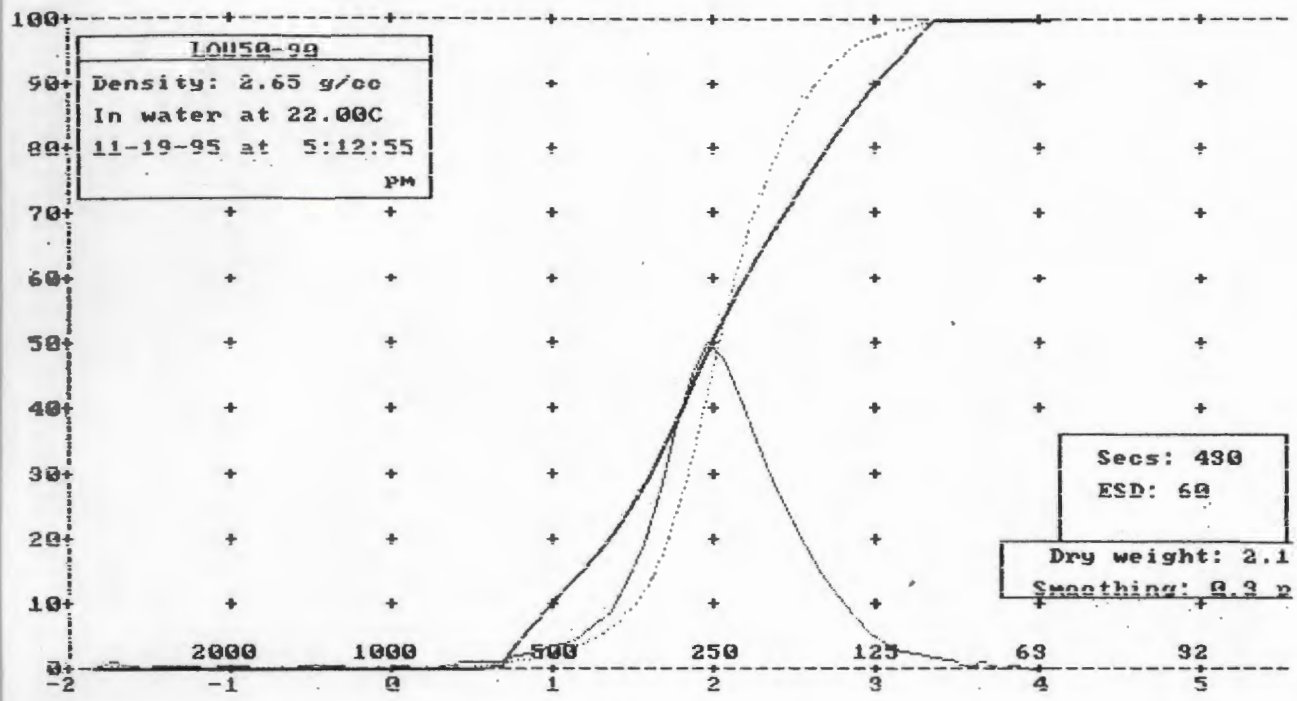

Moment statistics:
Mean = 2.03 phi = 245.56u
Std dev = 0.48 phi Skewness = -0.91 Kurtosis = 10.51

Graphical values (F&W):
Mean = 2.04 phi = 242.47u
Median (phi50) = 2.02 phi = 246.22u
Sorting = 0.44 phi Skewness = 0.06 Kurtosis = 1.15